MAX-PLANCK-INSTITUT
FÜR BIOANORGANISCHE CHEMIE

A Magneto-Structural Study on Polynuclear Metal Complexes

Dissertation for the degree of
Doktor der Naturwissenschaften
in the Fakultät für Naturwissenschaften
(Department Chemie)
at the Universität Paderborn

Presented by
Biplab Biswas

MÜLHEIM AN DER RUHR, 2008

To the memory of my father

This work was independently carried out between September 2005 and June 2008 at the **Max-Planck-Institut für Bioanorganische Chemie,** Mülheim an der Ruhr, Germany.

Submitted on: 25.07.2008 Examination: 12.09.2008

Papers published:

1. **A one-pot synthesis of a paramagnetic high-nuclearity nickel(II) cluster: an octadecanuclear $Ni^{II}_{16}Na^{I}_{2}$ metal aggregate**
Biplab Biswas, Sumit Khanra, Thomas Weyhermüller and Phalguni Chaudhuri, *Chem. Commun.* **2007**, 1057-1059

2. **A spin-frustrated star-shaped heterotetranuclear $Cr^{III}Mn^{II}_{3}$ species and its magnetic and HF-EPR measurements**
Sumit Khanra, **Biplab Biswas**, Christian Golze, Bernd Büchner, Vladislav Kataev, Thomas Weyhermüller and Phalguni Chaudhuri, *Dalton Trans*. **2007**, 481-487.

3. **Tridentate Facial Ligation of Tris(pyridine-2-aldoximato)nickel(II) and Tris(imidazole-2-aldoximato)nickel(II) To Generate $Ni^{II}Fe^{III}Ni^{II}$, $Mn^{III}Ni^{II}$, $Ni^{II}Ni^{II}$, and $Zn^{II}Ni^{II}$ and the Electrooxidized $Mn^{IV}Ni^{II}$, $Ni^{II}Ni^{III}$, and $Zn^{II}Ni^{III}$ Species: A Magnetostructural, Electrochemical, and EPR Spectroscopic Study**
Phalguni Chaudhuri, Thomas Weyhermüller, Rita Wagner, Sumit Khanra, **Biplab Biswas**, Eberhard Bothe, and Eckhard Bill, *Inorg. Chem.* **2007;** *46*(21) pp 9003 - 9016;

4. **Effect of the substituents on the spin coupling between iminosemiquinone π-radicals mediated by diamagnetic metal ions: l.s. Co(III) *vs* Ga(III)**
Phalguni Chaudhuri, Rita Wagner, Ulrich Pieper, **Biplab Biswas** and Thomas Weyhermüller, *Dalton Trans*. **2008**, 1286-1288.

5. **A Ferromagnetically Coupled Diiron(III) Complex with a m-Phenylenediamine Based Ligand**
Biplab Biswas, Sunita Salunke-Gawali, Thomas Weyhermüller, Vinzenz Bachler, Eckhard Bill and Phalguni Chaudhuri, *Eur. J. Inorg. Chem.* **2008**, 2391–2395.

6**. Radical-Ligand Derived C-N Coupling. Ga(III)-Radical vs. low-spin Co(III)-Radical Reactivity**

Phalguni Chaudhuri, Eckhard Bill, Rita Wagner, Ulrich Pieper, **Biplab Biswas** and Thomas Weyhermüller, *Inorg. Chem.* **2008**, *49*, 5549.

Examination Committee:

Prof. Dr. P. Chaudhuri

Prof. Dr. G. Henkel

Prof. Dr. K. Huber

Acknowledgements

I would like to acknowledge everyone who extended their invaluable support and help during the course of this work at the Max Planck Institute for Bioinorganic Chemistry, Muelheim an der Ruhr, Germany. My deep sense of gratitude goes to:

• Prof. Dr. P. Chaudhuri, who introduced me to the research area of coordination chemistry and taught me the way of scientific thinking. His constant guidance, hour-long invaluable discussions, perpetual inspiration with occasional reformatory thrashings always acted as motivating factors to my research works. He shared his wealth of experience in numerous occasions and this had provided me with a great learnig experience.

• Prof. Dr. K. Wieghardt for the opportunity of working in his research group, providing with all needed laboratory facilities and also for intricate scientific discussions and invaluable guidance.

• Dr. E. Bill for extending his warm hand for me in the field of Molecular Magnetism. Hour- long discussions with him on some intricate scientific issues infused a sense of confidence in me to complete this thesis.

• Dr. T. Weyhermüller and Mrs. H. Schucht for their elegant work with the X-ray crystallography.

• Dr. E. Bothe and Mrs. P. Höfer for their help during electrochemical measurements, discussions and fruitful suggestions.

• Dr. Vinzenz Bachler for DFT calculations.

• Dr. Sunita Salunke-Gawali for measurements and analysis of MCD.

• Mr. A. Göbels, Mr. F. Reikowski, and Mr. B. Mienert for discussions and measurements of EPR, SQUID, and Mössbauer.

• Mrs. R. Wagner and Mr. U. Pieper, for technical assistance in the laboratory and due to their suggestions.

• Mrs. U. Westhoff for skillfull GC analysis.

• Mr. J. Bitter and Mrs. K. Neurieder for skillfull NMR analysis.

• Mrs. Peters-Hahn and Mrs**.** B. Deckers for their helpfulness in general.

• Dr. Jennifer Shaw, Dr. Connie Lu and Dr. Geoff Spikes for their invaluable suggestion and correction to complete this thesis.

• Shaun Presow, Carsten Milsmann, Flavio Benedito, Dr. Marik Khusniyarov, Dr. Stephen Sproules, Dr. Corinna Hess, Dr. Chandan Mukherjee, Dr. John Berry, Dr. Krzysztof Chłopek, Dr. Prasanta Ghosh, Dr. Ruta Kapre, Dr. Kallol Ray, Dr. Peter

Larsen, Dr. Swarnalata Kokatam, Dr. Nicolleta Muresan, Dr. József Pap, Dr. Isabelle Sylvestre, Bram Pluijmaekers and Michael Nippe for a cordial working atmosphere and invaluable friendship.

- Dr. Santanu Mukherjee, Dr. Priyabrata Banerjee, Dr. Meenakshi Ghosh, Nabarun Roy, Dr. Rajkumar Halder, Dr. Subhas Chandra Pan, Prodipta Pal and many others for a nice homely atmosphere outside the laboratory and a wonderful friendship.
- Dr. Sumit Khanra and Mrs. Suchismita Sanyal for their inspiration and invaluable support.
- My mother and brothers for their constant inspiration and encouragement.
- Deutsche Forschungsgemeinschaft (DFG) and Max-Planck-Gesellschaft (MPG) for financial support.

Last but not the least in the list of my well wishers and aides, is the convoy of my research- mates in this Institute, my friends and fraternities outside, who stood by me in my weal and woe during my academic career in the Max Planck Institute for Bioinorganic Chemistry, Muelheim, Germany.

Contents

Abbreviations

Technical terms:

AF: antiferromagnetic

Ag / $AgNO_3$: reference electrode

av.: average

B: magnetic field

CT: charge transfer

D: zero-field splitting

deg: degree (°)

e^- : electron

E: total energy

exp.: experimental

F: ferromagnetic

fac.: facial

Fc^+/Fc: ferrocenium/ferrocene (internal electrochemical standard)

g: Landé factor

H: Hamiltonian

h.s: high spin

I: nuclear spin

IS: intermediate spin

J: coupling constant (cm^{-1})

KD: Kramer's doublet

LF: ligand field

m/z: mass per charge

$[M]^+$: molecular ion peak

M: molar magnetization

mer.: meridional

MP: melting point

PI: paramagnetic impurity

rt: room temperature (293K)

S: electron spin

sim: simulated

TIP: temperature independent paramagnetism

ZFS: zero-field splitting

Techniques:

CV: cyclic voltammetry

EA: elemental analysis

EI: electron ionization

EPR: electron paramagnetic resonance

ESI: electrospray ionization

IR: infrared spectroscopy

LC: liquid chromatography

MS: mass spectroscopy

NMR: nuclear magnetic resonance

SQUID: superconducting quantum interface device

MCD: Magnetic Circular Dichrosim

DFT: Density Functional Theory

SW: square wave voltammetry

UV-Vis: ultraviolet-visible spectroscopy

VTVH: Variable-temperature variable field

Units:

Å: angstrom (10^{-10} m)

cm: centimeter

emu: electromagnetic unit

G: Gauss

K: Kelvin

M : molar

mL : mililiter

mm : millimeter

nm : nanometer (10^{-9} m)

ppm: parts per million

s: second

T : tesla

V : volts

μ_B : Bohr magneton

Symbols:

λ: wavelength (nm)

ε: extinction coefficient ($M^{-1}cm^{-1}$)

IS: isomer shift (mms^{-1})

μ_{eff}: effective magnetic moment (μ_B)

ΔE_Q: quadrupole splitting (mm/s)

δ: isomer shift (mm/s)

Solvents and reagents:

NaOMe : sodiummethoxide

Et_3N: triethylamine

$TBAPF_6$: tetrabutylammonium hexafluorophosphate

TMS: tetramethylsilane

MeOH : methanol

MeCN : acetonitrile

DCM : dichloromethane

Et_2O : diethylether

Me_3Tacn: tmtacn = 1,4,7-trimethyl-1,4,7-triazacyclononane (**L'**)

Ligands used in this work:

^{H}**ImOx**: 1-H-2-imidazolealdoxime

^{Me}**ImOx**: 1-methylimidazole-2-aldoxime

$\mathbf{LH_2}$: *N*-methyldiethanolamine

$\mathbf{L''H_2}$: *N'N*-di(3,5-di-*tert*-butyl-salicylidene)-1,3-diaminobenzene

List of complexes synthesized with their numbers:

$[Na^{I}_{2}\{Ni^{II}_{4}(HL)_3(OOCCH_3)_5(HCOO)_{0.5}\}_4]\cdot 3CH_3CN\cdot 21H_2O$ (1)

$[NaL_6(V{=}O)_6](ClO_4)\cdot 2CH_3OH$ (2)

$[Mn^{III}_{2}(^{H}ImOx)_4(CH_3COO)_2]_n$ (3)

$[L''_2Fe^{III}_{2}(NO_3)_2]\cdot CH_2Cl_2\cdot$hexane (4)

$[C_6H_4(NH_2)_2][L''_2V^{III}_{2}V^{IV}_{2}(\mu\text{-}Cl)_6(Cl)_4]$ (5)

$[L'Fe^{III}Ni^{II}(^{Me}ImOx)_3](ClO_4)_2$ (6)

$[L'Fe^{III}Zn^{II}(^{Me}ImOx)_3](ClO_4)_2$ (7)

$[L'Ga^{III}Ni^{II}(^{Me}ImOx)_3](ClO_4)_2$ (8)

$[L'Fe^{III}Mn^{II}(^{Me}ImOx)_3](ClO_4)_2$ (9)

$[L'Fe^{III}Fe^{II}(^{Me}ImOx)_3](ClO_4)_2$ (10)

$[L'Fe^{III}Cu^{II}(^{Me}ImOx)_3](ClO_4)_2$ (11)

$[L'Co^{III}Fe^{II}(^{Me}ImOx)_3](ClO_4)_2$ (12)

$[L'Cr^{III}Ni^{II}(^{Me}ImOx)_3](ClO_4)_2$ (13)

$[L'Cr^{III}Zn^{II}(^{Me}ImOx)_3](ClO_4)_2$ (14)

Chapter 1

Introduction and Objectives

1.1 Introduction

Magnets have broad application in science, technology and domestic life while molecular and macromolecular systems are found in materials such as plastics, woven synthetics, display technology and optics. The development of molecular magnets is of great interest although it is a field which is still at an early stage. Currently the focus is on understanding the fundamental principles that govern magnetic behavior, in particular when moving from isolated molecules to three dimensional clusters.

Polynuclear metal clusters are of general interest as they are found in biological systems such as ferritin.[1,2] Metal clusters with high-spin ground states can act as supermagnets[3,4] and molecular magnets,[5,6,7] and can exhibit spin transition behavior.[8] Synthetically self-assembly can be used to build up beautiful molecular architectures,[7,10-15] which contain new configurations of paramagnetic ions, and endow unique properties on the materials.[16]

While the main aim for a magnetochemist is to synthesize new magnetic systems, presumably under mild conditions, (i.e. from solution at room temperature and pressure) and also to study how to synthesize new molecular magnetic systems with specific magnetic and electronic properties that might be suitable for future applications, it is important to consider the theoretical underpinning for such structures. The aim of this work is to obtain a deeper understanding of how electronic and molecular structures (spin density, band structure, anisotropy, etc) relate to the macroscopic physical (magnetic, electrical, optical, etc) properties.

1.2 Background and Objectives

Polynuclear Complexes

The development of molecule-based magnets[17] requires the specific alteration of magnetic properties by established organic or coordination chemistry techniques and the combination of magnetic properties with other mechanical, electrical and/or optical properties in harmony with simplicity of fabrication.[18] The past few years have witnessed significant interest in single-molecule magnets (SMMs)[19] along with an increased understanding of what is required in order for a system to be of use.

Single molecular magnets (SMMs) form a class of systems whose permanent magnetic moments stem from their molecular structure.[5,19c] Generally, SMMs are characterized by a large ground state spin number (S) and a relatively large uniaxial-type magnetic anisotropy (D_{St}). As a result, an energy barrier ($D_{St}\cdot S_t^2$) appears for switching the SMM's spin between the two stable spin states $| \pm S >$. At higher temperatures SMMs behave like paramagnetic or superparamagnetic particles with a large magnetic moment. When the temperature is lowered, the thermal energy is not sufficient to reverse the spin orientation of the molecule. Thus, the necessary requirements for better SMMs are a high spin ground state (S_t) and a large magnetic anisotropy (D_{St}). To rationally design polynuclear complexes with high S_t values, a control of the exchange couplings is highly desirable.

The main goal of this project is therefore to synthesize high-spin molecules. The different ligands used in this work for synthesizing polynuclear complexes are listed below:

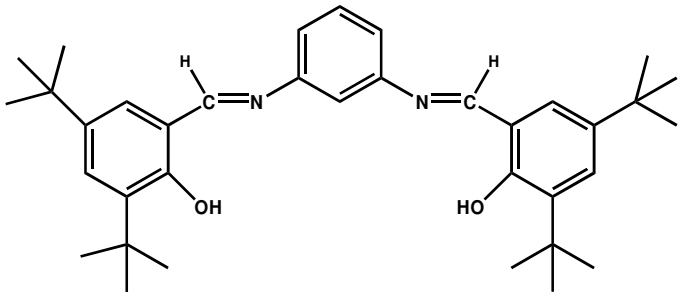

N'N-di(3,5-di-*tert*-butyl-salicylidene)-1,3-diaminobenzene
(**L''H$_2$**)

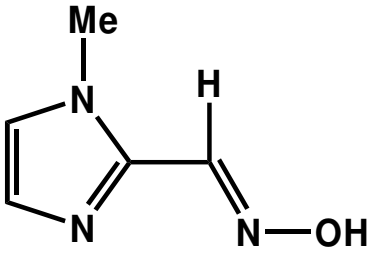

^{Me}ImOxH

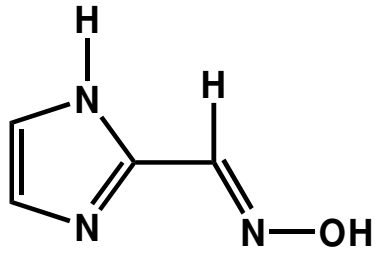

^{H}ImOxH

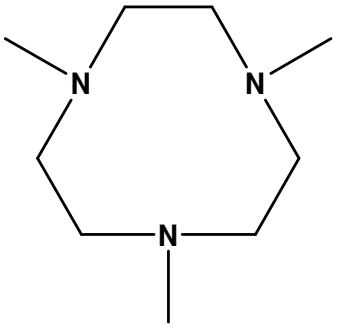

Me_3Tacn (L')

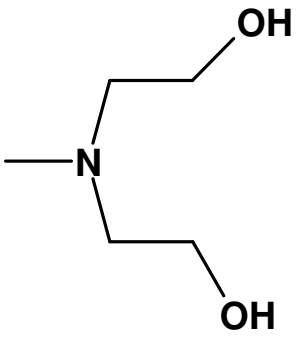

N-methyldiethanolamine (LH_2)

There is no obvious or general synthetic route to high nuclearity clusters.[20] Thus, polymetal cages are often self assembled, the assembly process sometimes being facilitated by alkali metal templates.[21] Consequently, the use of ligands containing good bridging groups, fostering the formation of polynuclear products, has become an active research area. In this field we have been exploring the hydroxy (-OH) group containing ligands[15] to influence the nuclearity and topology of metal complexes. *N*-methyldiethanolamine is an interesting ligand which has been reported in the literature. Depending on the reaction condtions, the hydroxy groups of this ligand can coordinate with the metal in protonated or deprotonated forms, while the N atom of the amine can also coordinate and hence the use of *N*-methyldiethanolamine in the synthesis of 3D polynuclear complexes. Since nickel(II) is known to have a large single-ion zero-field splitting and often gives rise to ferromagnetic coupling, we have focused our attention on polynuclear nickel complexes with the aim of obtaining “high-spin” molecules.

Metal oximates have previously proven to be versatile ligands in polynuclear complexes due to their ambidentate character with potential for nitrogen and/or oxygen coordination. [39-44] Some of the bonding modes observed for oximes modes are depicted in Figure 1.1 below:

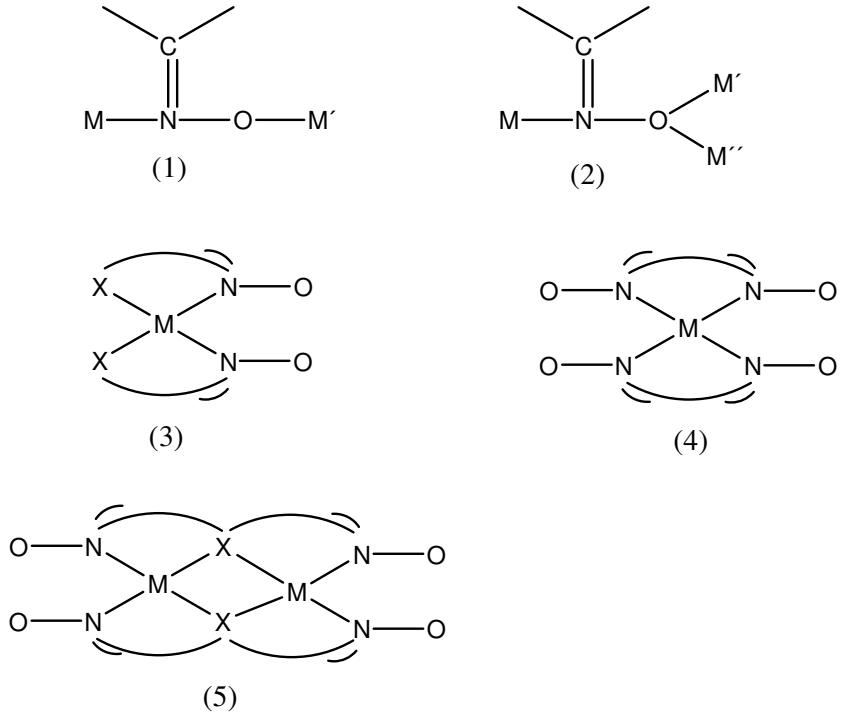

Figure 1.1 Bonding modes in oximes.

Due to this versatility in bonding, oximes are excellent bridging units in modular synthesis. The idea of synthesizing polynuclear complexes involving "metal oximates" as building blocks has become quite popular in the last few years. Modular preparation with oximato ligands enables the synthesis of linear symmetrical and asymmetrical cores containing two different metal ions.[22-25] Additionally, butterfly cores have also been achieved with the synthesis of asymmetric heterotrinuclear complexes with different oximes and end cap ligands. Diatomic N-O-bridging has been demonstrated by several series of isostructural complexes with different metal ions. Such isostructural series[22] are not available for any other bridging ligands.

The synthesis of homo and heteropolynuclear complexes incorporating the end-cap ligand 1,4,7-trimethyl-1,4,7-triazacyclononane, Me_3Tacn, with oximes is an approach developed in recent years.[22-24] Acyclic polyamines including di-, tri-, and tetra-amines and

bipyridine have been used as end cap ligands due to their commercial availability and the function of such ligands is to prevent undesired oligomerization processes. We have chosen to use Me_3Tacn since it is a facially coordinating tridentate nitrogen ligand and a significant number of both thermodynamically and kinetically stable complexes of these ligands are known.[22-24]

New exchange pathways can be expected for heteropolynuclear complexes where unusual sets of magnetic orbitals can be made to overlap with each other; hence an investigation of a series of heteropolynuclear complexes can be more informative than those of homopolynuclear complexes and serve as a source of fundamental information about exchange coupling in multinuclear assemblies. Another reason to study heterodinuclear metal complexes is that they may be used as building blocks for molecular based magnetic materials.

Among the variety of methodologies applied to synthesize polymetallic coordination compounds, the use of 'metaloligands', i.e. metal complexes as ligands, in which the ligands already bound to one metal have free coordination sites that can bind a second metal of the same or a different kind, has proven to be very successful; this route involving multinucleating ligands offers many potential advantages over the self-assembly route in that it enables more stringent control over the course of the reaction and upon the products that are formed. Regarding the 'metaloligands' concept: previously it has been shown by our group that pyridinealdoxime can be used successfully to synthesize a series of dinuclear complexes with predictable magnetic moment. We introduce here a new ligand 1-methyl-2-imidazolealdoxime (^{Me}ImOxH), designed to synthesize a series of dinuclear complexes. Our main aim is here the study of intramolecular exchange interactions between the paramagnetic transition metal ions as a function of their respective d^n electronic configurations and also to compare the ligation and σ donating properties of ^{Me}ImOxH ligand with the pyridinealdoxime ligand. Investigation and analysis of the electronic transitions using MCD is another aspect of this project. The basic principles of MCD is discussed later in this chapter.

We have already pointed out that zero-field splitting (*D*) is one of the important parameters for SMMs. Normally the Mn(III) (h.s.) ion is a potential candidate to show Jahn-Teller distortion. The Mn(III) is known to have a large single-ion zero-field

splitting. Additionally, Mn(III) ions often give rise ferromagnetic coupling, which is a necessary condition to generate a high-spin molecule. Moreover, Mn(III) complexes bridged only by oximate groups are quite rare, although complexes in the presence of other co-bridging ligands like oxo, hydroxo or carboxylate are not unprecedented. Polynuclear Mn(III) complexes with oximate bridges have been reported recently,[40b, 41j, 42] however the coexistence of the multibridging pathways precludes conclusions being drawn on the magnetic coupling via the oximate bridge only. To clarify the nature of the exchange interaction via an oximate pathway, the synthesis of such a compound is expected. Working towards this goal, we have introduced imidazolealdoxime as a ligand.

Spin-Polarization

The spin polarisation mechanism is of most interest in magnetic behavior. This mechanism arises from the molecular orbital model proposed by Longuet-Higgis for conjugated alternate hydrocarbons,[26] which results in ferromagnetic or antiferromagnetic coupling between two radicals depending nature of the bridge. When the radicals are separated by a m-phenylene bridge the are ferromagnetically coupled because two unpaired electrons reside in a pair of mutually orthogonal but degenerate SOMOs.[26a] A consequence of this molecular orbital behavior is the alternation of α and β spin density induced on the bridging atoms, which has actually been detected and measured in some cases.[26b,c] This simple principle has been behind the preparation of numerous polyradicals exhibiting a very high spin ground state.[26]

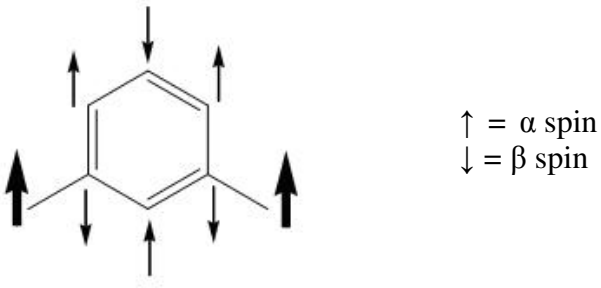

Figure 1.2 m-Phenylene based linkage with α and β spin distribution.

Though this mechanism is well known for organic polyradicals systems, it has received limited attention in the case of metal coordinated systems. We can apply this knowledge in our choice of ligands. The use of m-phenylene based linkages (Figure 1.2)

to achieve parallel spin coupling in transition metal complexes has indeed been successful in some cases[27] but anti ferromagnetic interactions have also been reported.[28]

To introduce this spin-polarization concept in our metal complex we have synthesized *N'N*-di(3,5-di-*tert*-butyl-salicylidene)-1,3-diaminobenzene (L"H_2). Using this ligand at first we have studied Fe(III) chemistry, as ferromagnetic interaction between the Fe(III) centers is very rare and still a matter of curiosity.

Low Valent Vanadium Cluster

The electronic configuration of the V(III) ion is d^2. So in an octahedral environment ground term for V(III) is ^3F and $^3T_{1g}$ is the ground electronic state. Because of this triplet state ($^3T_{1g}$), orbital contribution should occur leading to a significant amount of zero-field splitting. Literature shows that this d^2, $S = 1$ ion typically exhibits a large zero-field splitting (ZFS)[4] and, hence, is attractive as a building block towards magnetic materials such as SMMs. However, the literature is dominated by high-valent, V^{IV}/V^{V} chemistry[1] and there are very few low valent V^{III} or V^{III}/V^{IV} clusters reproted[2,3] due to the reducing nature of the V^{III} ion and the inherent stability of the $[V^{IV}O]^{2+}/[V^{V}O]^{3+}$ions. Some V^{III} or V^{III}/V^{IV} clusters are known either with carborxylate or with phosphate containing ligands.[2,3,5] Apart from these with carboxylate or phosphate groups, polynuclear V^{III} complexes with detailed analysis of magnetic properties are very rare.[6-10] Thus, we have introduced the L"H_2 ligand to synthesize low-valent vanadium complexes.

Evaluation of Coupling Constants

The evaluation of coupling constant in heteropolynuclear paramagnetic clusters is not a trivial task. The most important aspect in evaluating the coupling constants is to choose the correct spin-Hamiltonian for a particular system. For a polynuclear system the spin-Hamiltonian may be written as $H = -2 \Sigma J_{ij} S_i S_j$, where the sum is taken over all pairwise interactions of intensity J_{ij} between spins S_i and S_j in the molecule. This model of the isotropic interaction between the spin carriers is based on the concept of magnetic orbitals and overlap densities between pairs of such orbitals, and allows an analysis of the spin coupling. We are interested not only in the individual spins of the paramagnetic

centers, but also in the total spin of the whole cluster. Depending on the environment of the paramagnetic centers, the nature of the interactions can change from one cluster to another. There are three mathematical methods for calculating the magnetic susceptibilities of polynuclear complexes: (i) *Vector Coupling* (VC), (ii) *Full Matrix Diagonalization* (FMD) and (iii) *Irreducible Tensor Operator* (ITO).

VC was formulated by Kambe in 1950.[29] This method is the simplest and most used, however, it does have some limitations regarding the symmetry of the cluster. Since one has to be able to obtain the appropriate and unique solutions to multivariable problems, it can be used only for certain symmetries. Thus, to avoid such drawbacks FMD or ITO are more useful for evaluating the correct J values. FMD has a major drawback in that it can result in very large matrices requiring long diagonalization times, and thus long computation times. The ITO method[30] reduces the size of the matrices and computation times dramatically but it is difficult to set up and requires a considerable degree of sophisticated mathematics. It is also difficult to include single-ion effects such as zero-field splitting (ZFS) in ITO calculations which are easily included in FMD. Therefore FMD is the most commonly used method in this work.

Magnetizations at Different Fields

If a sample, containing 1 mol of a molecular compound within a homogeneous magnetic field, acquires a molar magnetization M, then $\partial M / \partial H = \chi$, where χ is the molar magnetic susceptibility. If the magnetic field is weak enough, then χ is independent of H (the applied magnetic field), such that it can be written as $M = \partial M / \partial H = \chi H$. The molar magnetization M, can be expressed in cm^3Gmol^{-1} or in $N\beta$ units, N being Avogadro's number and β the electronic Bohr magneton. Molar paramagnetic susceptibility characterizes the way in which the applied magnetic field (H) interacts with the angular momentum associated with the thermally populated states of a molecule. When a sample is perturbed by an external magnetic field, its magnetization is related to its energy variation through $M = - \partial E / \partial H$. To get the molar magnetization M, one can make a sum of the microscopic magnetizations weighted according to the Bolzman distribution law, which leads to, $M = [N\Sigma_n (\partial E_n / \partial H) \exp(-E_n / kT)] / \Sigma_n \exp(-E_n / kT)$, where T is the temperature of the sample and k is the Boltzman constant. Hence, from the above expression, molar

magnetic susceptibility varies as C/T, (where C is a constant, proportional to E_n/K) i.e. Currie's law. It is important to keep in mind that Currie's law is valid only when $H << kT$. Then molar magnetization M is linear in H. When $H >> kT$, M approaches the saturation value M_s, $M_s = Ng\beta S$.

Magnetic Circular Dichrosim (MCD)

MCD spectroscopy is an experimental technique that investigates the geometric and electronic structures of transition metal complexes. MCD is the differential absorption of left and right circularly polarized light in presence of a magnetic field. This technique provides information not only for the electronic ground states but also for the electronic excited states for both paramagnetic and non-paramagnetic centers. MCD is also site selective; when a system contains multiple chromophores, each chromophore generates a distinct absorption band making it possible to study the individual centers.

Paramagnetic substances in a magnetic field appear to be optically active, the relationship with natural optical activity is not straightforward. In both phenomena the same quantities are measured as a function of frequency, namely, the difference in the refractive indices for left and right circularly polarized light (which manifests itself as the angle of rotation of plane polarized light) or the difference in absorption coefficients for left and right circularly polarized light. The former is the optical rotatory dispersion (o.r.d.) and the latter is the circular dichroism (c.d.). In natural optical activity the dissymmetry of the molecules causes the electrons to move in a helical path on excitation which may then absorb left circularly polarized light to a greater or lesser extent than right depending upon the 'handedness' of the helix. In magnetic optical activity, left and right circularly polarized photons no longer interact equivalently with an absorbing medium in the presence of a magnetic field. Thus we should not anticipate the same direct relationship between magnetic optical activity and molecular stereochemistry which we find in natural optical activity.

MCD is a multidimensional spectroscopy. It has many experimental variables (*e.g.* wavelength of the incident radiation, temperature and magnetic field) which play a crucial role in characterizing the chromophore being examined. The MCD absorption (ΔA) for a transition from ground state to excited state is defined by:

$$\Delta A = A_{LCP} - A_{RCP} = \gamma\beta H[- (\partial f(E)/ \partial E)A + (B + C/KT)f(E)]dc \qquad \text{equation 1}$$

where γ is the spectroscopic constant, β is the Bohr magneton constant, H is the magnetic field, k is the Boltzman constant, f(E) is the line shape function (Gaussian), E is the energy of the incident radiation, d is the pathlength, c is the concentration of the molecular species.[32]

MCD is based on the Faraday effect, which describes how matter, in the presence of a magnetic field parallel to the direction of propagation of light, appears optically active.[31] The Faraday effect is however closely related to another well-known phenomenon which arises from the interaction of magnetic fields with matter, namely the Zeeman effect. As an illustration, we will consider here the Zeeman effect for a system with a spherically symmetric potential, *e.g.*, a single atom.

There are three additive terms A, B and C in equation 1. From the MCD spectra one can easily recognize the A, B and C-terms. The A-term originates from degenerate excited states. A simple example is given by the atomic transition ($^1S \rightarrow {}^1P$), where the excited states are degenerate (Figure 1.3). In the presence of a magnetic field, H, the excited states experience Zeeman splitting where the energy levels are $M_J = +1, 0, -1$. Both of the transitions, left circularly polarized (LCP) and right circularly polarized (RCP), would be equal in intensity, but vary in frequency resulting in a derivative shaped absorption band that is temperature independent (Figure 1.4).

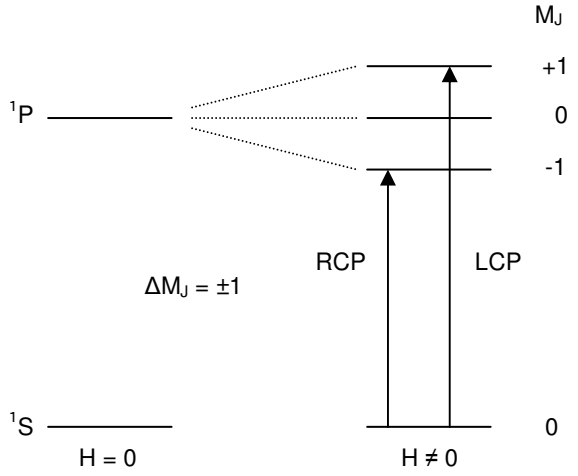

Figure 1.3 Example of the origin of the A-term for the atomic transition ($^1S \rightarrow {}^1P$).

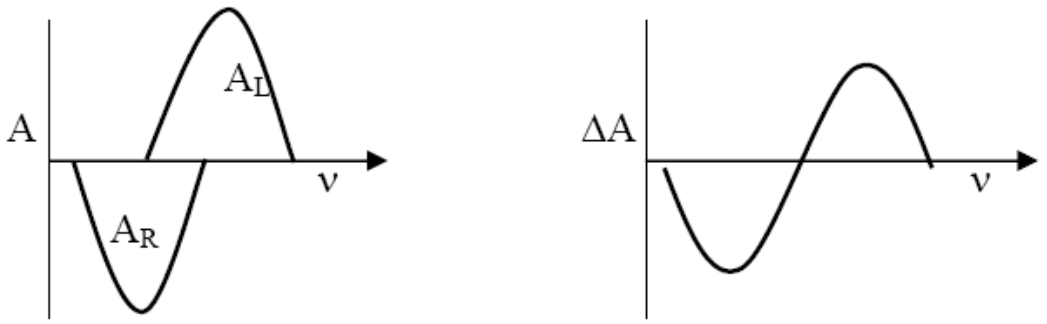

Figure 1.4 Absorption of left circularly polarized light (plotted positive) and right circularly polarised light (plotted negative) when ^1P excited state is split by the field (left hand side). Note that the two transitions occur with equal probability. Resultant magnetic circular dichroism curve (right hand side) showing Faraday A term line shape.

In type C spectra, MCD absorption is a consequence of the magnetic field breaking the degeneracy of the ground state of the optical absorption, as for the atomic transition $^1P \rightarrow {}^1S$ (Figure 1.5). The ground state experiences a Zeeman interaction where the Boltzman distribution has an affect on the population of the ground states. This changes the intensity of the left and right circularly polarized light according to temperature ultimately leading to a temperature dependent C-term (Figure 1.6). For samples exhibiting both A and C class spectra, taking the MCD as a function of temperature is a way to separate the relative contributions of these two effects.

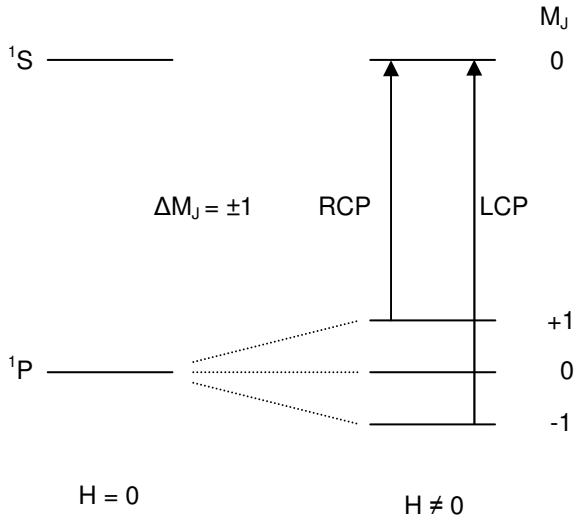

Figure 1.5 Example of the origin of the C-term for the atomic transition ($^1P \rightarrow {}^1S$).

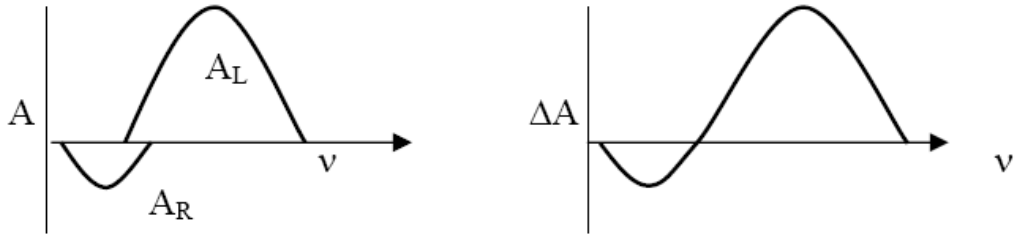

Figure 1.6 Absorption of left circularly polarised (plotted positive) and right circularly polarized (plotted negative) light in the presence of the field (left hand side). Note that the relative intensities of these depend on a Boltzmann factor which reflects the number of atoms in the $M_J = -1$ and $M_J = +1$ sublevels. Resultant magnetic circular dichroism (right hand side) showing Faraday C term line shape.

The B-term contribution to the MCD spectrum does not require degeneracy as it is the result of the mixing of electronic states. The B-term is induced by ground and excited states mixing with all other relatively close excited states. Thus, all molecules exhibit this effect, accounting for the universality of the Faraday effect. The B-term is temperature independent.

Magnetization curves monitor the saturation properties of discrete MCD bands as a function of increasing or decreasing the magnetic field or temperature. This provides information to resolve and assign electronic transitions such as estimations of the ground state spin state, g-factors, and zero field parameters (zfs).

In biology, metalloproteins are the most likely candidates for MCD measurements, as the presence of metals with degenerate energy levels leads to strong MCD signals.[33-38]

1.3 Scope of Thesis

This thesis mainly deals with the magneto-structural studies of homo- and heteropolynuclear metal complexes, with particular emphasis on the investigations of different exchange pathways. Different spectroscopic techniques (viz. MS, IR, NMR, UV-VIS, SQUID, EPR, MCD, etc) have been used to provide a complete picture as possible.

The work is divided into five main chapters. In Chapter 2 the use of hydroxyl-group containing ligands[15] to influence the nuclearity and topology of metal complexes is reported. Some other interesting developments regarding the magneto-structural chemistry of complexes incorporating this ligand are discussed. The aggregation of soft metal centers to form covalently bonded clusters is well known.[48] Hard metal cations do not readily form metal-metal bonds, and usually require bridging ligands such as carboxylate, oxide, or hydroxide ligands to induce aggregation.[15,45-47] Herein we report two interesting examples of metal–ligand frameworks which can be successfully self-assembled about an alkali metal cation template.

Polynuclear complexes with oximate bridges have been reported, however the coexistence of multiple bridging pathways preclude clear analysis of the magnetic coupling via oximate bridges only. To clarify the nature of exchange interactions via oximate ligands, the syntheis of new materials was necessary. Working towards this goal, the singly oximato-bridged $[Mn^{III}_2]_\alpha$ complex has been sucessfully synthesized and is disscussed in Chapter 3.

Chapter 4 concerns the synthesis and charecterization of a ferromagnetically coupled dinuclear ferric complex. Though the spin-polarization mechanism is well known for organic polyradical systems, it has received limited attention in case of metal coordinated systems. This system has also been studied using DFT. In Chapter 5 the synthesis and chracterization of a valence-traped tetranuclear $[V(III)V(IV)]_2$-complex, a rare example of a mixed-valent vanadium cluster without any carboxylate or phosphate ligands is reported.

Finally, in Chapter 6 a series of dinuclear homo- and heteropolynuclear complexes using *N*-methylimidazolealdoxime as a bridging group are reported. We have previously reported such series of complexes with pyridinealdoxime ligands. In this chapter we also show how this allows straightforward comparison of magnetic and coordination properties

between complexes of 1-methyl-2-imidazolealdoxime and pyridinealdoxime ligands with 3d-transition metals. MCD is an important analytical tool to investigate the geometric and electronic structures of transition metal complexes. Together with magnetostructural studies, Chapter 6 also concerns the MCD studies of $Fe^{III}Ni^{II}$, $Fe^{III}Zn^{II}$ and $Ga^{III}Ni^{II}$ complexes with the gound state S = 3/2, 5/2 and 1, respectively.

References

1. D. D. Awschalom, D. P. DiVincenzo, J. F. Smyth, *Science* **1992**, *258*, 414.

2. S. Gider, D. D. Awschalom, T. Douglas, S. Mann, M. Charpala, *Science* **1995**, 77, 267.

3. M. A. Bolcar, S. M. J. Aubin, K. Folting, D. N. Hendrickson, G. Christou, *Chem. Commun.* **1997**, 1485.

4. C. Delfs, D. Gatteschi, L. Pardi, R. Sessoli, K. Wieghardt, D. Hanke, *Inorg. Chem.* **1993**, *32*, 3099.

5. R. Sessoli, D. Gatteschi, A. Caneschi, M. A. Novak, *Nature* **1993**, *365*, 141.

6. L. Thomas, F. Lionti, R. Ballou, D. Gatteschi, R. Sessoli, B. Barbara, *Nature* **1996**, 383.

7. R. E. P. Winpenny, *J. Chem. Soc., Dalton Trans.* **2001**, 1.

8. M. Ruben, E. Breuning, J.-M. Lehn, V. Ksenofontov, F. Renz, P. GRtlich, G. B. M. Vaughan, *Chem. Eur. J.* **2003**, *9*, 4422.

9. a) A. Ardizzoia, M. A. Angarconi, G. LaMonica, F. Cariati, S. Cenini, M. Moret, N. Masciocchi, *Inorg. Chem.* **1991**, *30*, 4347; b) S. Parsons, J. M. Rawson, D. Reed, R. E. P.Winpenny, *J. Chem. Soc., Dalton Trans.* **1995**, 163.

10. P. N. W. Baxter, J.-M. Lehn, G. Baum, D. Fenske, *Chem. Eur. J.* **2000**, *6*, 4510.

11. a) M. Ruben, J. Rojo, F. J. Romero- Salguero, L. H. Uppadine, J.-M. Lehn, *Angew. Chem., Int. Ed.* **2004**, *43*, 3644; b) J. Rojo, J.-M. Lehn, G. Baum, D. Fenske, O. Waldmann, P. Müller, *Eur. J. Inorg. Chem.* **1999**, 517.

12. P. J. Van Koningsbruggen, E. MRller, J. G. Haasnoot, J. Reedijk, *Inorg. Chim. Acta* **1993**, *208*, 37.

13. M. Fujita, K. Umemoto, M. Yoshizawa, N. Fujita, T. Kusukawa, K. Biradha, *Chem. Commun.* **2001**, 509.

14. L. K. Thompson, *Coord. Chem. Rev.* **2002**, 193.

15. *a*) T. K. Paine, E. Rentschler, T. Weyhermüller and P. Chaudhuri, *Eur. J. Inorg. Chem.* **2003**, 3167; b) S. Khanra, T. Weyhermüller, E. Rentschler and P. Chaudhuri, *Inorg. Chem.* **2005**, *44*, 8176; and references therein.

16. O. Waldmann, J. Hassmann, P. Müller, G. S. Hanan, D. Volkmer, U. S. Schubert, J.-M. Lehn, *Phys. Rev. Lett.* **1997**, *78*, 3390.

17. O. Kahn, *Acc. Chem. Res.* **2000**, *33*, 647-657.

18. J. S. Miller, A. J. Epstein, *Angew. Chem., Int. Ed.* **1994**, *33*, 385.

19. a) G. Aromi, E. K. Brechin, *Struct. Bonding.* **2006***, 122*, 1; b) G. Christou, D. Gatteschi, D. N. Hendrickson, R. Sessoli, *MRS Bull.* **2000**, *25*, 66; c) D. Gatteschi, R. Sessoli, *Angew. Chem., Int. Ed.* **2003***, 42*, 268.

20. R. E. P. Winpenny, *Adv. Inorg. Chem.* **2001**, *52*, 1.

21. *a*) X. Lin, D. M. J. Doble, A. J. Blake, A. Harrison, C. Wilson and M. Schröder, *J. Am. Chem. Soc.* **2003**, *125*, 9476; *b*) D. M. J. Doble, C. H. Benison, A. J. Blake, D. Fenske, M. S. Jackson, R. D. Kay, Wan-Sheung Li and M. Schröder, *Angew. Chem., Int. Ed.* **2003**, *38*, 1915; *c*) G. Aromi, A. R. Bell, M. Helliwell, J. Raftery, J. Teat Simon, G. A. Timco, O. Roubeau, R. E. P. Winpenny, *Chem. Eur. J.* **2003**, *9*, 3024; *d*) E. K. Brechin, R. O. Gould, S. G. Harris, S. Parsons, R. E. P. Winpenny, *J. Am. Chem. Soc.* **1996**, *118*, 11293; *e*) A. Bell, G. Aromi, S. J. Teat, W. Wernsdorfer, R. E. P. Winpenny, *Chem. Commun.* **2005**, 2808; *f*) R. W. Saalfrank, T. Nakajima, N. Mooren, A. Scheurer, H. Maid, F. Hampel, C. Trieflinger, J. Daub, *Eur. J. Inorg. Chem.* **2005**, 1149; *g*) E. M. Rumberger, L. N. Zakharov, A. L. Rheingold, D. N. Hendrickson, *Inorg. Chem.* **2004**, *43*, 6531.

22. P. Chaudhuri, M. Winter, P. Fleischhauer, W. Haase, U. Flörke, H.-J. Haupt, *J. Chem. Soc., Chem. Commun*. **1990**, 1728.

22. P. Chaudhuri, *Coord. Chem. Rev*. **2003**, *243*, 143.

23. a) F. Birkelbach, U. Flörke, H-J. Haupt, C. Butzlaff, A.X. Trautwein, K. Wieghardt, P. Chaudhuri, *Inorg. Chem*. **1998**, *37*, 2000; b) D. Burdinsky, F. Birkelbach, T. Weyhermüller, U. Flörke, H-J. Haupt, M. Lengen, A. X. Trautwein, E. Bill, K. Wieghardt, P. Chaudhuri, *Inorg. Chem*. **1998**, *37*, 1009; c) P. Chaudhuri, M. Winter, B. P. C. D. Vedova, P. Fleischhauer, W. Hasse, U. Flörke, H-J. Haupt, *Inorg. Chem*. **1991**, *30*, 4777; d) P. Chaudhuri, M. Winter, B. P. C. D. Vedova, E. Bill, A. Trautwein, S. Gehring, P. Fleischhauer, B. Nuber, J. Weiss, *Inorg. Chem*. **1991**, *30*, 2148.

24. S. Ross, T. Weyhermüller, E. Bill, K. Wieghardt, P. Chaudhuri, *Inorg. Chem*. **2001**, *40*, 6656.

25. a) C. Krebs, Dissertation, Bochum, Germany, **1997**; b) C. Krebs, M. Winter, T. Weyhermüller, E. Bill, K. Wieghardt, P. Chaudhuri, *J. Chem. Soc., Chem Commun.* **1995**, 1913.

26. a) J. C. Longuet-Higgins, *J. Chem. Phys.* **1950**, *18*, 265 ; b) H. Iwamura, *Adv. Phys. Org. Chem.* **1990**, *26*, 179; c) A. Rajca, *Chem. Rev.* **1994**, *94*, 871; d) S. Rajca, A. Rajca, J. Am. Chem. Soc. **1995**, *117*, 9172; e) A. Rajca, S. Rajca, J. Am. Chem. Soc. **1996**, *118*, 8121.

27. a) V. A. Ung, A. M. W. Cargill Thompson, D. A. Bardwell, D. Gatteschi, J. C. Jeffery, J. A. McCleverty, F. Totti, M. D. Ward, *Inorg. Chem.* **1997**, *36*, 3447; b) T. Ishida, S. Mitsubori, T. Nogami, N. Takeda, M. Ishikawa, H. Iwamura, *Inorg. Chem.* **2001**, *40*, 7059; c) X. Ottenwaelder, J. Cano, Y. Journax, E. Riviére, C. Brennan, M. Nielrich, R. Ruiz-García, *Angew. Chem., Int. Ed.* **2004**, *43*, 850; d) M. Pascu, F. Lloret, N. Avarvari, M. Julve, M. Andruh, *Inorg. Chem.* **2004**, *43*, 5189; e) T. Glaser, M. Heidemeier, S. Grimme, E. Bill, *Inorg. Chem.* **2004**, *43*, 5192; f) F. Lloret, G. De Munno, J. Cano, R. Ruiz, A. Caneshi, *Angew. Chem., Int. Ed.* **1998**, *37*, 135; g) E. Pardo, K. Bernot, M. Julve, F. Lloret, J. Cano, R. Ruiz-García, F. S. Delgado, C. Ruiz-Perez, X. Ottenwaelder, Y. Journaux, *Angew. Chem., Int. Ed.* **2004**, *43*, 2768; h) E. Pardo, J. Faus, M. Julve, F. Lloret, M. C. Munoz, J. Cano, X. Ottenwaelder, Y. Journaux, R. Carrasco, G. Blay, I. Fernandez, R. Ruiz-Garcia, *J. Am. Chem. Soc.* **2003**, *125*, 10770; i) A. R. Paital, T. Mitra, D. Ray, W. T. Wong, J. Ribas-Arino, J. J. Nova, J. Ribas, G. Aromi, *Chem. Commun.* **2005**, 5172; j) I. Fernandez, R. Ruiz, J. Faus, M. Julve, F. Lloret, J. Cano, X. Ottenwaelder, Y. Journaux, M. Carmen Munoz, *Angew. Chem., Int. Ed.* **2001**, *40*, 3039.

28. a) E. F. Hasty, L. J. Wilson, D. N. Hendrickson, *Inorg. Chem.* **1978**, *17*, 1834; b) T. Ishida, T. Kawakami, S. Mitsubori, T. Nogami, K. Yamaguchi, H. Iwamura, *J. Chem. Soc., Dalton Trans.* **2002**, 3177; c) M. Matsushita, T. Yasuda, R. Kawano, T. Kawai, T. Iyoda, *Chem. Lett.* **2000**, 812; d) H. Torayama, T. Nishida, H. Asada, M. Fujiwara, T. Matushita, *Polyhedron*, **1997**, *16*, 3787; e) A. Dei, D. Gatteschi, C. Sangregorio, L. Sorace, M. G. F. Vaz, *Inorg. Chem.* **2003**, *42*, 1701; f) A. Mederos, S. Dominguez, R. Hernádez-Molina, J. Sanchiz, F. Brito, *Coord. Chem. Rev.* **1999**, *193-195*, 857 and references therein.

29. K. Kambe, *J. Phys. Soc., Jpn*. **1950**, *5*, 48.

30. D. Gatteschi, L. Pardi, *Gazz. Chim. Ita*. **1993**, *123*, 231.

31. P. N. Schatz, and A. J. McCaffery, The Faraday Effect. Quarterly Review of the Chemical Society **1969**, *25*, 552.

32. M. K. Johnson, *CD and MCD Spectroscopy of Metalloproteins*, in *Physical Methods in Bioinorganic Chemistry Spectroscopy and Magnetism*, L. Que, Editor. **2000**, 232.

33. K. E. Loeb, J. M. Zaleski, T. E. Westre, R. J. Guajardo, P. K. Mascharak, B. Hedman, K. O. Hodgson, E. I. Solomon, *J. Am. Chem. Soc.* **1995**, *117*, 4545.

34. J. W. Whittaker, E. I. Solomon, *J. Am. Chem. Soc.* **1988**, *110*, 5329.

35. P. A. Mabrouk, A. M. Orville, J. D. Lipscomb, E. I. Solomon, *J. Am. Chem. Soc.* **1991**, *113*, 4053.

36. E. G. Pavel, L. J. Martins, W. R. Jr. Ellis, E. I. Solomon, *Chem. Biol.* **1994**, *1*, 173.

37. M. A. Pavlosky, Y. Zhang, T. E. Westre, Q.-F. Gan, E. G. Pavel, C. Campochiaro, B. Hedman, K. O. Hodgson, E. I. Solomon, *J. Am. Chem. Soc.* **1995**, *117*, 4316.

38. K. E. Loeb, T. E. Westre, T. J. Kappock, N. Mitic, E. Glasfeld, J. P. Caradonna, B. Hedman, K. O. Hodgson, E. I. Solomon, *J. Am. Chem. Soc.* **1997**, *119*, 1901.

39. P. Chaudhuri, P. *Proc. Indian Acad. Sci*. **1999**, *111*, 397.

40. a) S. Khanra, T. Weyhermüller, E. Bill, P. Chaudhuri, *Inorg. Chem.* **2006**, *45*, 5911; b) P. Chaudhuri, T. Weyhermüller, R. Wagner, S. Khanra, B. Biswas, E. Bothe, E. Bill, *Inorg. Chem.* **2007**, *46*, 9003; c) S. Khanra, T. Weyhermüller, P. Chaudhuri, *Dalton Trans*. 2**007**, 4675; d) S. Khanra, B. Biswas, C. Golze, B. Büchner, V. Kataev, T. Weyhermüller, P.Chaudhuri, *Dalton Trans*. 2**006**, 481; e) T. Weyhermüller, R. Wagner, S. Khanra, P. Chaudhuri, *Dalton Trans*. **2005**, 2539.

41. a) F. Birkelbach, M. Winter, U. Florke, H.-J. Haupt, C. Butzlaff, M. Lengen, E. Bill, A. X. Trautwein, K. Wieghardt, P. Chaudhuri, *Inorg. Chem.* **1994**, *33*, 3990; b) F. Birkelbach, T. Weyhermüller, M. Lengen, M. Gerdan, A. X. Trautwein, K. Wieghardt, P. Chaudhuri, *J. Chem. Soc., Dalton Trans.* **1997**, 4529; c) C. N. Verani, E. Rentschler, T. Weyhermuller, E. Bill, P. Chaudhuri, *J. Chem. Soc., Dalton Trans.* **2000**, 4263; d) V. V. Pavlishchuk, F. Birkelbach, T. Weyhermüller, K. Wieghardt, P. Chaudhuri. *Inorg. Chem.* **2002**, *41*, 4405; e) P. Chaudhuri, E. Rentschler, F. Birkelbach, C. Krebs, E. Bill, T. Weyhermüller, U. Flörke, *Eur. J. Inorg. Chem.* **2003**, 541; f) S. Ross, T. Weyhermüller,

E. Bill, E. Bothe, U. Flörke, K. Wieghardt, P. Chaudhuri, *Eur. J. Inorg. Chem.*, **2004**, 984; g) C. N. Verani, E. Bothe, D. Burdinski, T. Weyhermüller, U. Flörke, P. Chaudhuri, *Eur. J. Inorg. Chem.* **2001**, 2161.

42. a) T. Afrati, C. Dendrinou-Samara, C. P. Raptopoulou, A. Terzis, V. Tangoulis, D. P. Kessissoglou, *Angew. Chem., Int. Ed.* **2002**, *41*, 2148; b) S. G. Sreerama, S. Pal, *Inorg. Chem.* **2002**, *41*, 4843; c) C. J. Milios, A. Vinslava, W. Wernsdorfer, S. Moggach, S. Parsons, S. P. Perlepes, G. Christou, E. K. Brechin. *J. Am. Chem. Soc.* **2007**, *129*, 2754; d) C. J. Milios, A. Vinslava, W. Wernsdorfer, A. Prescimone, P. A. Wood, S. Parsons, S. P. Perlepes, G. Christou, E. K. Brechin. *J. Am. Chem. Soc.* **2007**, *129*, 6547; e) C. J. Milios, A. Vinslava, P. A. Wood, S. Parsons, W. Wernsdorfer, G. Christou, S. P. Perlepes, E. K. Brechin. *J. Am. Chem. Soc.* **2007**, *129*, 8; f) T. C. Stamatatos, D. Foguet-Albiol, C. C. Stoumpos, C. P. Raptopoulou, A. Terzis, W. Wernsdorfer, S. P. Perlepes, G. Christou. G. *J. Am. Chem. Soc.* **2005**, *127*, 15380; g) Y-B. Jiang, H-Z. Kou, R-J. Wang, A-L. Cui, J. Ribas. *Inorg. Chem.* **2005**, *44*, 709; h) C. J. Milios, A. Prescimone, A. Mishra, S. Parsons, W. Wernsdorfer, G. Christou, S. P. Perlepes, E. K. Brechin, *Chem. Commun.* **2007**, 153.

43. S. Khanra, Ph. D. Thesis, University of Paderborn, **2005**.

44. a) H. Miyasaka, T. Nezu, K. Sugimoto, K.-i. Sugiura, M.Yamashita, R.Clérac, *Inorg. Chem.* **2004**, *43*, 5486; b) H. Miyasaka, R. Clérac, K. Mizushima, K.-i. Sugiura, M. Yamashita, W. Wernsdorfer, C. Coulon, *Inorg. Chem.* **2003**, 42, 8203, c) R. Clérac, H. Miyasaka, M. Yamashita, and C. Coulon, *J. Am. Chem. Soc.* **2002**, *124*, 12837; d) H. Miyasaka, T. Nezu, K. Sugimoto, K.-i. Sugiura, M. Yamashita, R. Clérac *Chem. E-J.* **2005**, 1592.

45. a) S. P. Watton, P. Fuhrmann, L. E. Pence, A. Caneschi, A. Cornea, G. L. Abbati, S. J. Lippard, *Angew. Chem. Int. Ed.* **1997**, *36*, 2774; b) R. A. Reynolds III, D. Cocouvanis, *J. Am. Chem, Soc.* **1998**, *120*, 209; c) M. Murrie, S. Parsons, R. E. P. Winpenny, *J. Chem. Soc. Dalton Trans.* **1998**, 1423; d) H. O. Stumpf, L. Ouahab, Y. Pei, P. Bergerat, O. Kahn, *J. Am. Chem. Soc.* **1994**, *116*, 3866; e) C. Benelli, S. Parsons, G. A. Solan, R. E. P. Winpenny, *Angew. Chem., Int. Ed.* **1996**, *35*, 1825.

46. a) Y. Zhang, P. J. Zapf, L. M. Meyer, R. C. Haushalter, J. Zubieta, *Inorg. Chem,* **1997**, *36*, 2159; b) L. Suber, M. Bonamico, V. Fares, *Inorg. Chem.* **1997**, *36*, 2030; c) A.

Müller, E. Krickemeyer, H. Bögge, M. Schmidtmann, C. Beugholt, P. Kögerler, C. Lu, *Angew. Chem., Int. Ed.* **1998**, *37*, 1220; d) A. K. Powell, S. L. Heath, D. Gatteschi, L. Pardi, R. Sessoli, G. Pina, F. Del Giallo, F. Pieralli, *J. Am. Chem. Soc.* **1995**, *117*, 2491; e) A. Müller, F. Peters, M. J. Pope, D. Gatteschi, *Chem. Rev*. **1998,** *98*, 239.

47. D. M. J. Doble, C. H. Benison, A. J. Blake, D. Fenske, M. S. Jackson, R. D. Kay, Wan-Sheung Li and M. Schröder, *Angew. Chem., Int. Ed.* **1999**, *38*, 1915.

48. a) A. Simon, *Angew. Chem., Int. Ed.* **1988**, *27*, 156; b) M. D. Vargas, J. N. Nicholls, *Adv. Inorg. Chem. Radiochem.* **1986**, *30*, 123; c) S. M. Owen, *Polyhedron* **1988**, *7*, 253; d) K. Wade, *Adv. Inorg. Chem. Radiochem.* **1976**, *18*, 1; e) D. M. P. Mingos, M. J. Watson, *Adv. Inorg. Chem.* **1992**, *39*, 327.

Chapter 2

Alkali Metal-Containing Transition Metal Clusters: $Na_2Ni^{II}_{16}$, NaV^{IV}_6

2.1 Introduction

The current interest in the synthesis of high-nuclearity 3d-metal complexes has been sparked due to their relevance to various fields, ranging from metallobiochemistry[1] to molecular magnetic materials.[2,3] However, there is no obvious synthetic route to high nuclearity clusters.[4] Thus far routes to well-controlled structures rely upon judicious design of ligands and the selective use of other effects such as hydrogen-bonding and/or template effects.

In several recent reports, examples of self-assembly and templates have been found to control the outcome of the assembly. For example, halide and oxygen anions have been reported to template several poly-lanthanide clusters[5] and lanthanide ions such as La^{3+} and Tb^{3+} template aggregation of Cu_6 moieties.[6] Na^+ can template Fe_6, Cu_6 and Mn_6 wheels, while alternating the template to Cs^+ affords Fe_8 wheels.[7] These examples demonstrate and confirm that metal directed self-assembly can be a versatile tool in the construction of the 3-D polymetallic architectures.

On the other hand, the aggregation of soft metal centers to form covalently bonded clusters is well known,[8] and there are well established theories regarding the structure and bonding in these polynuclear complexes, for example Ru- and Os-carbonyl[8b] and Au clusters.[8c] In contrast, hard metal cations do not readily form metal-metal bonds, and usually require bridging ligands such as carboxylate, oxide, or hydroxide ligands to induce aggregation.[9-12]

The search for ligands containing good bridging groups, thus fostering formation of polynuclear products, has become an active research area. In this field we have been exploring the feasibility of hydroxyl-group containing ligands[12] to influence the nuclearity and topology of metal complexes. Recently we have chosen *N*-methyldiethanolamine as an OH-group containing ligand. *N*-methyldiethanolamine has

been previously reported in the literature to influence the nuclearity and topology of metal complexes. [14c,15] In the present work we report some other interesting developments regarding the magneto-structural chemistry of complexes incorporating this ligand.

2.2 $[Na^{I}_{2}\{Ni^{II}_{4}(HL)_{3}(OOCCH_{3})_{5}(HCOO)_{0.5}\}_{4}]\cdot 3CH_{3}CN\cdot 21H_{2}O$

Since nickel(II), in octahedral geometry, is known to have a large single-ion zero-field splitting and often gives rise to ferromagnetic coupling, we have focused our attention on polynuclear nickel(II) complexes with the aim of obtaining "high-spin" molecules.[12] Although polynuclear nickel(II) complexes containing up to four metal ions are not rare,[12a,13] assemblies with more nickel(II) ions still remain a matter of curiosity. Herein we report an interesting example of metal–ligand frameworks can be successfully self-assembled about an alkali metal cation as a template.[16] The synthesis and preliminary magnetic properties of an octadecanuclear supracage $Ni^{II}_{16}Na^{I}_{2}$ in which four star-shaped Ni^{II}_{4} triangular units are linked through two octahedral sodium cations and two bridging formate ligands are discussed. There are very few magnetically characterized nickel complexes with more than sixteen metal centers reported in the literature.[14] Noteworthy is the presence of the smallest carboxylate, formate, as a bridging ligand.[16] Such molecular nickel–sodium metal aggregates are potential candidates for single molecule magnet (SMMs).

2.2.1 Synthesis

Reaction of $Ni(CH_3COO)_2\cdot 4H_2O$ with *N*-methyldiethanolamine (H_2L) and $NaOCH_3$ (ratio 4 : 3 : 6) in methanol yielded a green solution, which was heated to reflux for two hours in presence of air. Methanol was removed in *vacuo* to obtain a green solid, which was recrystallized from acetonitrile, X-ray quality crystals in 70% yield grew over two days. X-Ray diffraction studies show formation of $[(LH)_{12}Ni_{16}(OOCCH_3)_{20}(\mu\text{-}Na)_2(\mu_2\text{-}OOCH)_2]\cdot 3CH_3CN\cdot 21H_2O$ **1**. To investigate whether the isolated crystals consist of a single compound, we have compared the powder-diffraction pattern of the bulk material with the diffraction pattern of the single crystal. In this way we have confirmed that compound **1** is of single composition.

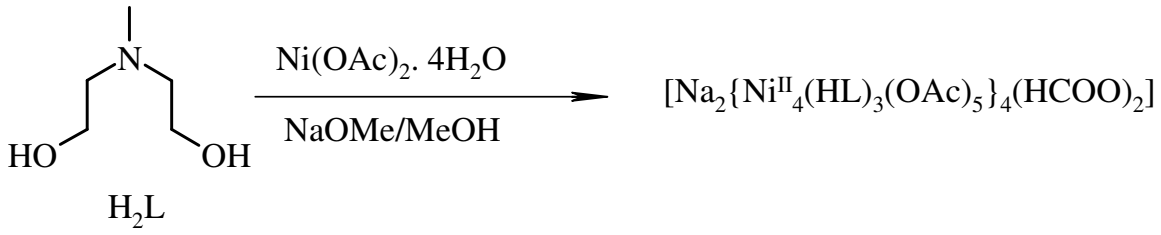

Figure 2.2.1 Synthesis of $[Na^{I}_{2}Ni^{II}_{16}(HL)_{12}(OAc)_{20}(HCOO)_{2}]$.

Use of other bases such as Et_3N, CH_3COO^-, NaOH did not yield **1**. Presumably the OCH_3^- ion gets oxidized to $HCOO^-$ during the aerial aggregation process and the bridging formate does not originate from carbon dioxide in the air. The yield of **1** did not increase by introduction of additional formate ions.

2.2.2 Infrared Spectroscopy and Mass Spectrometry

The band in the IR spectrum of complex **1** at 3422 cm^{-1} corresponds to the O-H stretching of the protonated alcoholic groups of LH_2. A strong intense peak at 1618 cm^{-1} is assigned to the C=O stretch of carboxylate ions. The absorption peaks below 600 cm^{-1} are assigned to the Ni-O and Na-O symmetric and asymmetric stretches. A moderately strong peak at 1451 cm^{-1} is due to the stretching of the C-N bond.

Electronspray-ionization mass spectrometry (ESI-MS) in the positive ion mode and negative ion modes does not show the characteristic molecular ion peak, however peaks assigned to the fragments of complex **1** are observed. ESI-MS in the positive ion mode shows a strong peak at 867.0 which is assigned to $[Ni_4(LH)_2(AcO)_5]^+$ fragments.

2.2.3 Electronic Spectroscopy

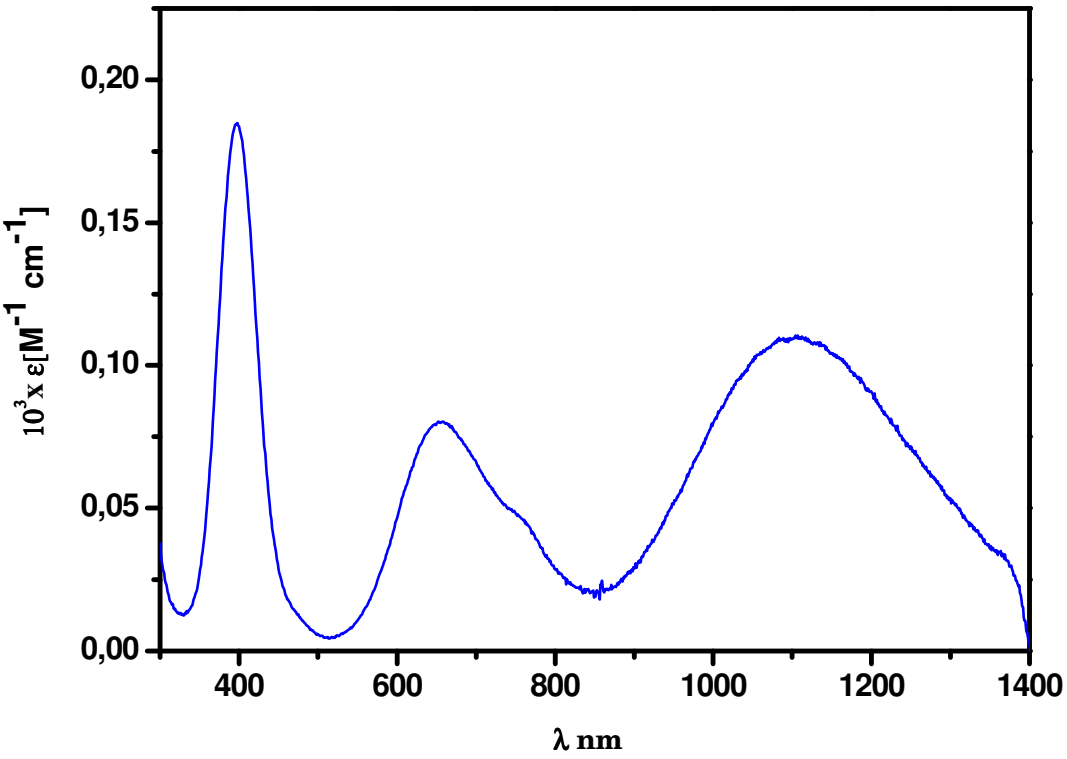

Figure 2.2.3 Electronic spectrum for complex **1** at room temperature in MeOH.

The electronic absorption measurement has been performed on a $1x10^{-3}$(M) methanolic solution of **1**, shown in Figure 2.2.3. The electronic absorption spectrum of **1** in dry methanol exhibits d–d bands at λ_{max} = 1105 nm with an extinction coefficient of 110 $M^{-1}cm^{-1}$. As the mass spectrometry in different solvents, *viz.* CH_3OH, CH_3CN, CH_2Cl_2 indicates the presence of a tetranuclear unit in solution, the d–d bands are assigned to this tetranuclear core.

2.2.4 X-ray Structure of $[Na^{I}_2\{Ni^{II}_4(HL)_3(OOCCH_3)_5(HCOO)_{0.5}\}_4]$

The structure of the complex **1** is depicted in Figure 2.2.4a. Selected bond lengths and angles for **1** are given in Table 2.2.1.

The structure of **1**, $[Na^{I}_2\{Ni^{II}_4(HL)_3(OOCCH_3)_5(HCOO)_{0.5}\}_4]$, $Ni^{II}_{16}Na^{I}_2$, consists of four trigonal-pyramidal building blocks, $[Ni^{II}_4(LH)_3(OOCCH_3)_5]$, which are connected

to each other by two sodium cations and two formate anions. Each of the three tridentate ligands (HL^-) connects two nickel centers from the base of the pyramid with the apical nickel center through a μ_3-O ethanolate donor. In addition, one nitrogen atom and one μ-OH donor from the alcohol ligand are bound to a nickel cation in the base. Moreover, the three nickel centers in the base are coordinated to non-bridging monodentate acetate ions and one formate anion, which bridges the two halves of the structure **1**. Three additional acetate ions each bridge the nickel centers at the base with the fourth nickel center at the apex of the trigonal pyramid, thus satisfying the hexa-coordination of all four nickel centers of the building block $[Ni^{II}_4(LH)_3(OOCCH_3)_5(HCOO)_{0.5}]$. A sodium ion connects two such building blocks and is thus coordinated to six oxygen atoms of the acetate ions originating from the building blocks. The nickel pyramids are apex-linked and rotated by approximately 180° relative to each other, resulting in a dimer $[Na^I\{Ni^{II}_4(HL)_3(OOCCH_3)_5(HCOO)_{0.5}\}_2]$. Two such dimers are bridged by two formate anions resulting in the neutral molecule **1** $[Na^I_2\{Ni^{II}_4(HL)_3(OOCCH_3)_5(HCOO)_{0.5}\}_4]$ whose ORTEP view is shown in Figure 2.2.4a The building block containing the tetranickel(II) center is shown in Figure 2.2.4b while Ni(1) occupying the apex of the trigonal pyramid Ni^{II}_4 is in a $Ni(1)O_6$ coordination environment, Ni(2), Ni(3) and Ni(4) are in an NO_5 environment and form a nearly equilateral triangle of the pyramidal base. The Ni(2) and Ni(4) are coordinated to one amine nitrogen, two μ_3-O alkoxo oxygens, two acetate oxygens and one protonated oxygen atom of the alcohol ligand. On the other hand, Ni(3) differs from Ni(2) and Ni(4) in the carboxylate coordination; instead of two acetate, Ni(3) is coordinated to one acetate oxygen and one oxygen of the bridging formate. Ni(1) is bonded to three μ_3-O of the alkoxo groups and three acetate oxygen atoms. Table 2.2.1 summarizes selected bond lengths and angles of complex **1**. Strong hydrogen bonds between the μ_3-alkoxo oxygen atoms, protonated alcohol oxygen and the oxygen atom of the acetate groups with the O···H···O separation in the range 2.547–2.979 Å are presumably responsible for building up of the supramolecular structure for complex **1**.

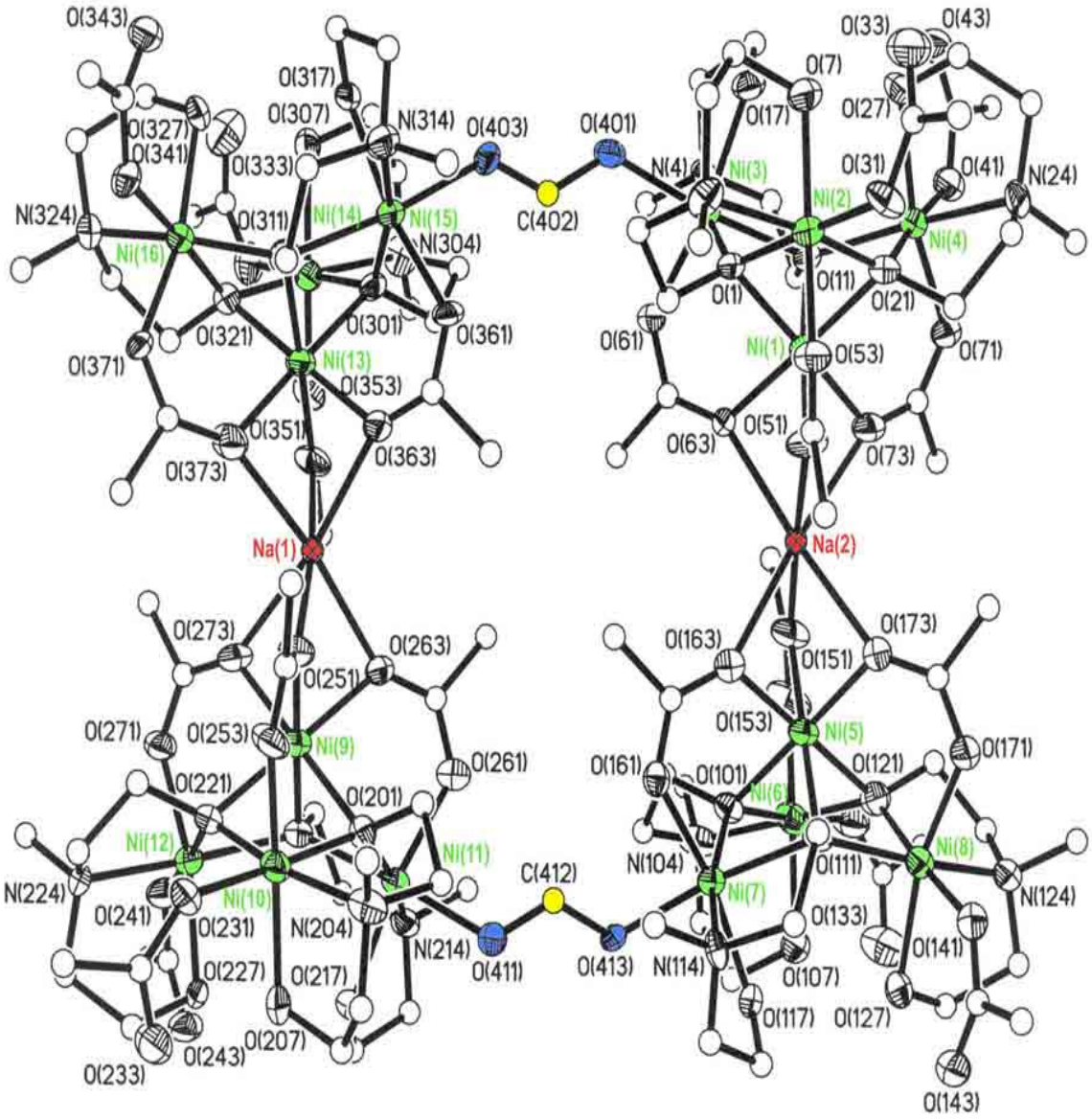

Figure 2.2.4a An ORTEP plot of $[Na^{I}_{2}\{Ni^{II}_{4}(HL)_{3}(OOCCH_{3})_{5}(HCOO)_{0.5}\}_{4}]$ (40% ellipsoids).

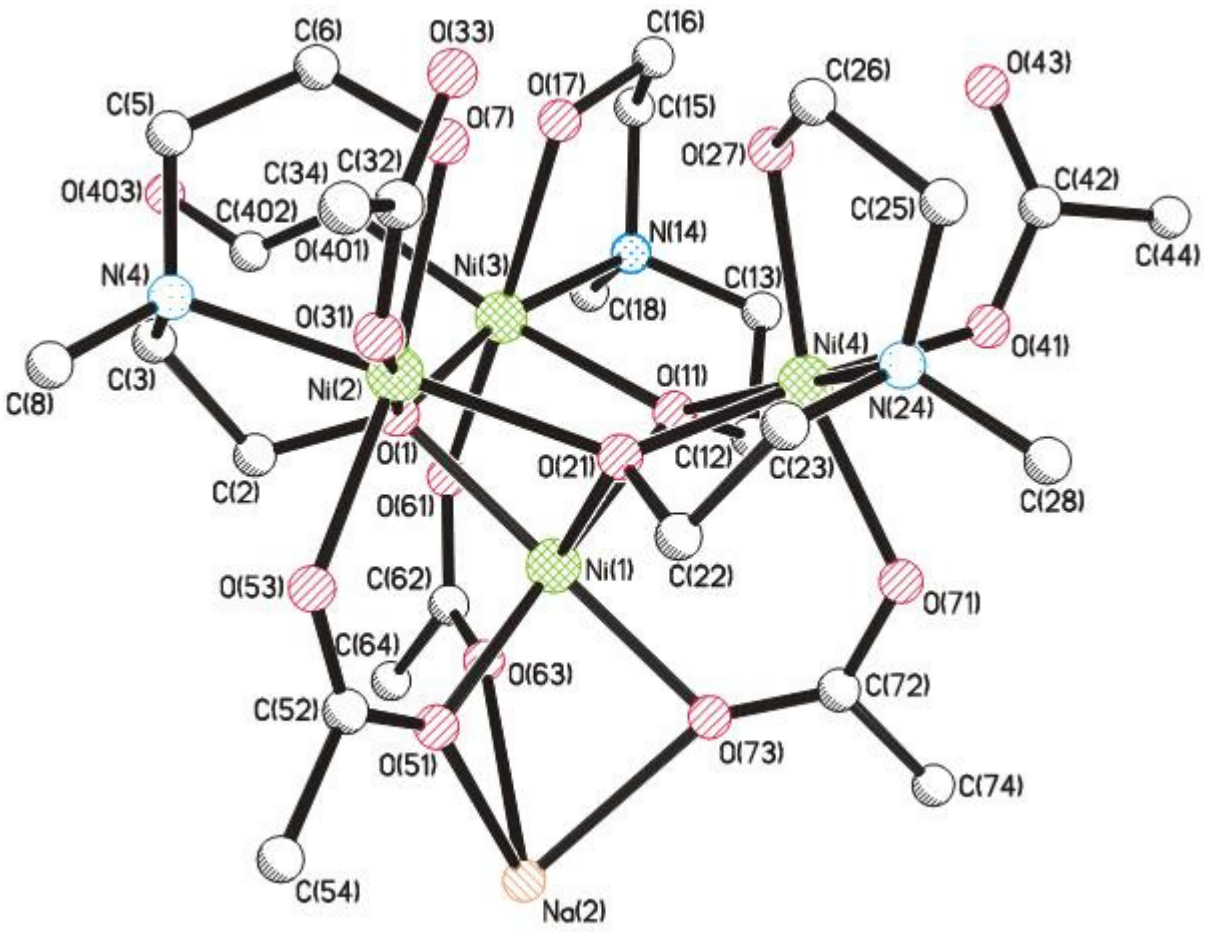

Figure 2.2.4b An ORTEP plot of $[Na^{I}_{0.5}Ni^{II}_{4}(HL)_3(OOCCH_3)_5(HCOO)_{0.5}]$ (50% ellipsoids).

Table 2.2.1 Selected Bond Lengths (Å) and Angles (deg) of Complex **1**.

Ni(1)···Ni(2)	2.964(2)	Ni(2)···Ni(4)	3.866(3)
Ni(1)···Ni(3)	2.977(2)	Ni(2)···Ni(3)	3.826(6)
Ni(1)···Ni(4)	2.971(3)	Ni(4)···Ni(3)	3.841(6)
Ni(1)-O(1)	2.044(7)	Ni(2)-O(31)	2.058(8)
Ni(1)-O(73)	2.027(8)	Ni(2)-O(1)	2.070(8)
Ni(1)-O(51)	2.051(8)	Ni(2)-O(53)	2.060(7)
Ni(1)-O(63)	2.036(8)	Ni(2)-O(7)	2.091(8)
Ni(1)-O(11)	2.088(8)	Ni(2)-O(21)	2.093(8)
Ni(1)-O(21)	2.079(7)	Ni(2)-Ni(4)	2.131(9)

Ni(3)-O(11)	2.084(8)	Ni(4)-O(21)	2.079(8)
Ni(3)-O(401)	2.043(8)	Ni(4)-O(71)	2.036(8)
Ni(3)-O(61)	2.044(7)	Ni(4)-O(41)	2.119(9)
Ni(3)-N(14)	2.108(9)	Ni(4)-N(24)	2.134(9)
Ni(3)-O(1)	2.098(8)	Ni(4)-O(11)	2.096(8)
Ni(3)-O(17)	2.128(8)	Ni(4)-O(27)	2.133(8)
Bond Angles (deg)		Bond Angles (deg)	
Ni(1)-O(1)-Ni(2)	92.2(3)	Ni(2)-O(1)-Ni(3)	133.0(3)
Ni(1)-O(21)-Ni(2)	90.50(3)	Ni(3)-O(11)-Ni(4)	133.3(4)
Ni(1)-O(1)-Ni(3)	91.90(3)	Ni(2)-O(21)-Ni(4)	135.5(4)
Ni(1)-O(11)-Ni(3)	91.0(3)		
Ni(1)-O(11)-Ni(4)	90.5(3)		
Ni(1)-O(21)-Ni(4)	91.2(3)		

2.2.5 Magnetic Properties of Complex 1

The magnetic susceptibility data for a dry polycrystalline sample of **1** were collected in the temperature range 2–290 K in an applied magnetic field of 1 T, and a plot of μ_{eff} (magnetic moment) *vs*. T (temperature) is shown in Figure 2.2.5a. The effective magnetic moment μ_{eff} = 11.81 μ_B ($\chi_M T$ = 17.430 cm^3 mol^{-1} K) at 290 K decreases monotonically with decreasing temperature to reach a value of μ_{eff} = 7.50 μ_B ($\chi_M T$ = 7.023 cm^3 mol^{-1} K) at 10 K; below 10 K there is a sharp drop reaching a value of μ_{eff} = 6.22 μ_B ($\chi_M T$ = 4.834 cm^3 mol^{-1} K) at 2 K. This magnetic behavior clearly indicates the presence of an overall antiferromagnetic exchange coupling between the Ni(II) centers in **1**. The μ_{eff} value at 2 K indicates a non-diamagnetic low-lying state. The sharp drop at the lower temperatures might be to due to the zero-field splitting (D) of the ground state and/or very weak antiferromagnetic interactions.

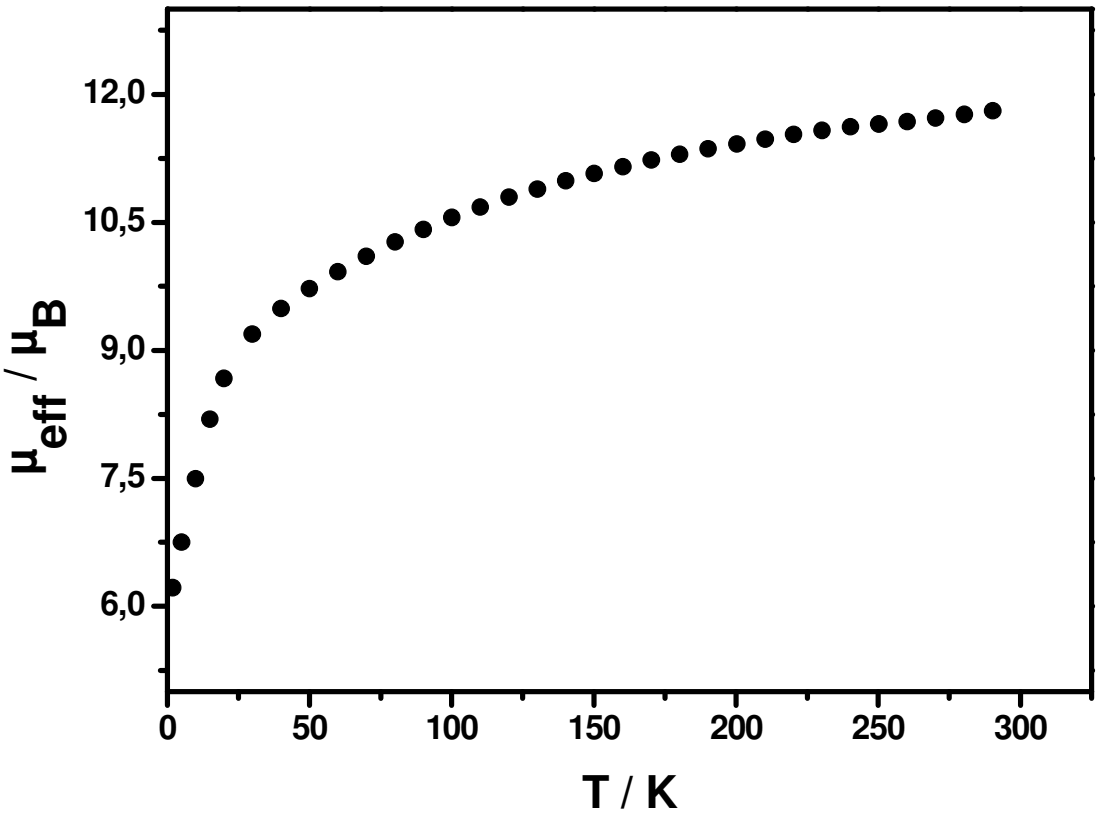

Figure 2.2.5a Temperature-dependence of the magnetic moment μ_{eff}/molecule for complex **1**, $Ni^{II}_{16}Na_2$, at an applied magnetic field of 1 T.

The total spin degeneracy of the hexadecanuclear Ni(II) complex is 3^{16} leading to a matrix of $3^{16}\times 3^{16}$ to be diagonalized for simulation of the experimental data. It is apparent that reduction of the dimension of the matrix is required for simulation. A close examination of the structure indicates that application of the symmetry of the cluster can lead to the desired reduction of the matrix. Thus, the tetranuclear Ni(II) units, which does not interact strongly with each other can be considered as separate units, as the Ni···Ni separations of 5.93 and 6.03 Å between the tetranuclear units are too long. These separations correspond to the formate ($HCOO^-$) and Na-bridges, respectively. Thus, we have analyzed the magnetic data by considering the smallest core of **1**, *i.e.* $[Ni^{II}_4(LH)_3(OOCCH_3)_5(HCOO)_{0.5}]Na_{0.5}$.

As is evident from the structure of the Ni(II)centers in the tetranuclear unit, at least two types of exchange interactions, J_1 and J_2 have to be considered for simulating

the susceptibility data. J_1 represents the exchange interaction between the Ni(II)-center (Ni(1) in Figure 2.2.5b) at the apex of the pyramid and the Ni(II) centers (Ni(2), Ni(3) and Ni(4) of Figure 2.2.5b), which constitute the triangular base of the pyramid; whereas J_2 the exchange parameter between the three centers Ni(2), Ni(3) and Ni(4) of Figure 2.2.5b). Thus, the spin Hamiltonian used is:

$$H = -2J_1(S_1.S_2 + S_1S_3 + S_1S_4) - 2J_2(S_2.S_3 + S_3S_4 + S_4S_2)$$

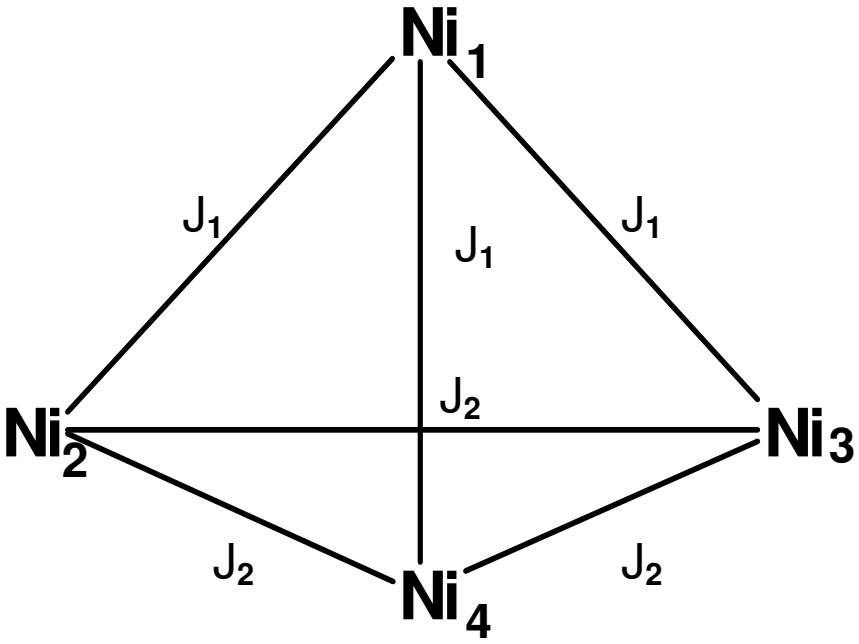

Figure 2.2.5b Schematic representation of probable exchange pathways of tetramer of **1**.

A satisfactory simulation, shown as a solid line in Figure 2.2.5c, using a least-squares fitting computer program with a full-matrix diagonalization, is obtained with the parameters $J_1 = +4.3$ cm^{-1}, $J_2 = -15.1$ cm^{-1}, $g_1 = g_2 = g_3 = g_4 = 2.18$. The nature of the evaluated *J*-values are in accord with the Ni–O(alkoxo)–Ni angles prevailing in the cluster: Ni(1)–O_{alk}–Ni(X) lying between 90 and 93°, whereas Ni–O_{alk}–Ni angles between the Ni(2), Ni(3) and Ni(4) centers are 132–134°. The strength of ferromagnetic coupling J_1 related to the angle 90–93° is relatively weak, presumably due to the additional presence of an acetate ligand in *syn–syn* mode. In general acetates bridging contribute antiferromagnetic coupling to the overall exchange and thus reduce the magnitude of the

ferromagnetic coupling. It is known that the average bridging angle of 133° leads to antiferromagnetic interactions, and J_2 is also accordingly antiferromagnetic in nature.[13,14,17] The nature of the exchange coupling constants J_1 and J_2 are thus in full agreement with the Ni–O–Ni/*J* correlation, supporting the use of the simple "two-*J*"-model. Moreover, that the contributions to the exchange coupling of the bridging formate and sodium ions are negligible are also supported by the good quality of the fit obtained by using a tetranuclear core with a "two-*J*" model. Noteworthy, by setting $J_1 = 0$, the quality of the simulation could not be reproduced, indicating the importance of J_1 for the fitting procedure.

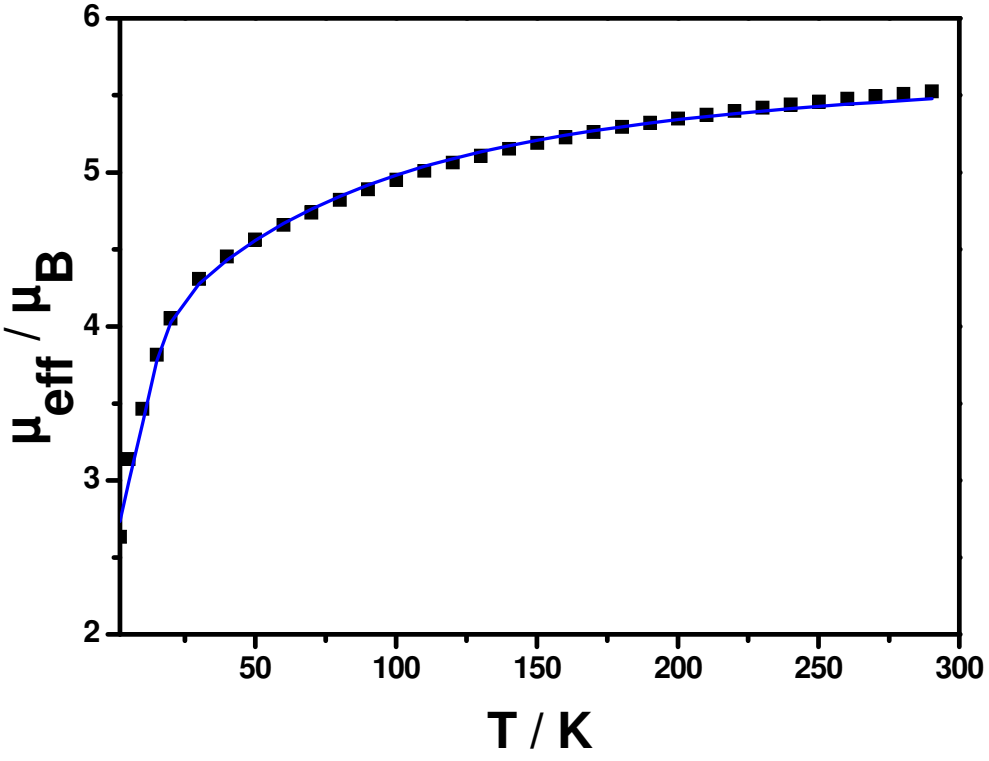

Figure 2.2.5c Temperature-dependence of the magnetic moment μ_{eff} for the tetranickel(II) core at an applied magnetic field of 1 T. The bold points represent the experimental data while the solid line represents the simulation.

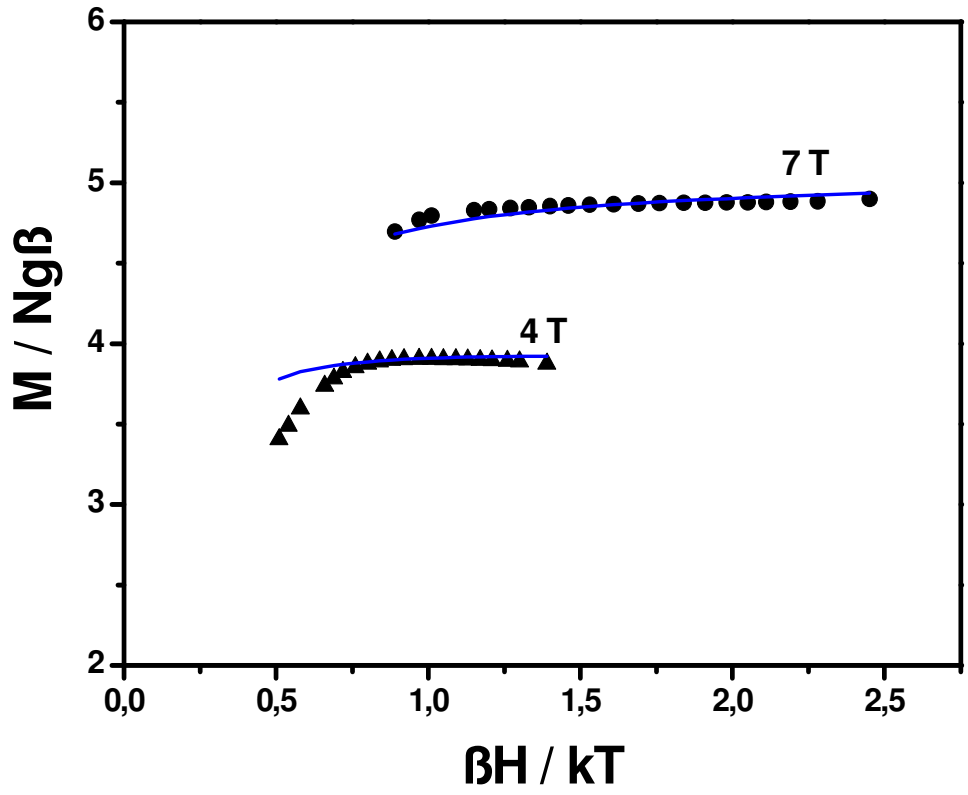

Figure 2.2.5d Variable temperature variable field (VTVH) magnetic data for **1**, plot of M/Ngß vs. ßH/kT. The bold points represent the experimental data while the solid line represents the simulation.

The presence of paramagnetic low-lying states has been verified by the variable-temperature (1.9–5 K), variable-field (4 and 7 T) magnetization (VTVH) measurements, shown in Figure 2.2.5d. The magnetization increases with the field up to $M/Ng\beta = 4.94$ at 7 T and 1.9 K where it is nearly saturated. Furthermore, the magnetization data for different fields do not superimpose, which reveals the presence of excited states at energies in the order of the Zeeman splitting. The saturated magnetization value of 4.94 measured at 1.9 K and 7 T clearly indicates the participation of $M_S = -4$ or -5 Zeeman components. We conclude that the expected lowest energy state $S_t = 4$, 3, 2, 1 or zero (as the ground state for the tetranuclear core with the evaluated positive and negative J values is $S_{core} = 1$) is not well isolated and the excited states with S values 4 or higher are within a few wavenumbers from the lowest lying state.

2.3 $[NaL_6(V{=}O)_6]ClO_4{\cdot}2CH_3OH$

Vanadium oxides and their complexes are of current interest due to their relevance to catalysis and biochemical systems, their variable geometries and their redox properties.[19-25] Polynuclear clusters have become a subject of considerable interest not only because of their relevance to molecular magnetism but also to understand the function of metalloproteines as well as their potential applications as magnetic materials. Magnetic metal oxides clusters are considered a promising class of chemical systems that offers the opportunity of designing well defined molecular magnetic systems.[2,3,18,20,26]

The functionalization of a metal oxide cluster with an organic ligand would further expand their overall application as building blocks for materials design and development. Progress in this direction can pave the way for connecting oxometallic clusters with organic and biological systems (enzymes, cells, proteins, etc). Functionalized clusters are employed for designing hybrid materials, including optically active ones, and have possible applications in chemical and biological sensing.

Here we report a hexanuclear wheel-shaped vanadium(IV)-oxo containing a Na^+ ion at the center of the wheel. Though wheel-shaped vanadium(IV)-oxo complexes are not uncommon, there are only a very few magnetically characterized complexes reported in the literature.[27-32] Most of those reported compounds have been synthesized at high temperatures and high pressures. In contrast, the synthesis described here we have used just simple schlenck line techniques.

2.3.1 Synthesis

Reaction of VCl_3 with N-methyldiethanolamine (LH_2) and $NaOCH_3$ (ratio: 1:1:2), shown in Figure 2.3.1 in dry methanol yielded a green solution which was heated to reflux for three hours. The solution was kept as it was for two days under inert atmosphere but no change observed. $NaClO_4$ was added to the solution, and the color turned blue very slowly. X-ray quality deep blue crystal was obtained by slow evaporation of methanol solution for two days. X-ray diffraction studies show formation of $[NaL_6(V{=}O)_6]ClO_4{\cdot}2CH_3OH$ **2**.

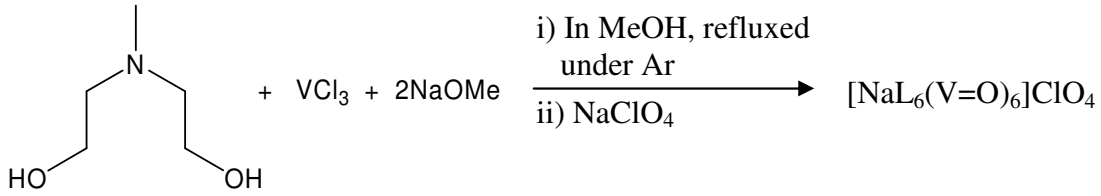

Figure 2.3.1 Synthesis of $[NaL_6(V=O)_6]ClO_4$.

Use of other counter anions such as PF_6^-, maintaining the same reaction condition did not yield **2**. Presumably V(III) gets oxidized to V(IV) to form V=O abstracting an oxygen atom from the ClO_4^- ions. This means that the ClO_4^- ion itself is acting as an oxygen transfer agent.

2.3.2 Infrared Spectroscopy and Mass Spectrometry

The band in the IR spectrum of complex **2** at 2850-2950 cm^{-1} corresponds to the C-H stretching of the $-CH_3$ and $-CH_2-$ groups of the ligand. Strong and moderately intense bands at 1075 and 1037 cm^{-1} respectively are assigned to the V=O stretch. The absorption peaks around 600 cm^{-1} are assigned to the V-O-V and Na-O symmetric and asymmetric stretches. A moderately strong peak at 1459 cm^{-1} is due to the stretching of the C-N bond.

ESI-MS in the positive ion mode has proven to be very successful in characterizing complex **2**. The monopositively charged species $[M\text{-}ClO_4]^+$ is observed as the base peak at 1127.1. On the other hand, ESI-MS in the negative ion mode is successful in characterizing the ClO_4^-, which shows a strong peak at 99.1.

2.3.3 X-ray Structure of $[NaL_6(V=O)_6]ClO_4 \cdot 2CH_3OH$

The lattice consists of discrete hexanuclear monocations, perchlorate anions and methanol molecules of crystallization. The X-ray structure confirms that a wheel shaped hexanuclear vanadium complex has indeed been formed with six octahedral vanadium centers and one central Na^+ cation.

Table 2.3.1a Selected Bond Lengths (**Å**) and Angles (deg) of Complex **2**.

	Bond Lengths (**Å**)		Bond Lengths (**Å**)
V(1)···V(2)	3.276	V(2)···V(3)	3.269
V(3)···V(4)	3.275	V(4)···V(5)	3.265
V(5)···V(6)	3.295	V(6)···V(1)	3.296
Na(1)-O(14)	2.301(7)	Na(1)-O(24)	2.294(7)
Na(1)-O(34)	2.305(7)	Na(1)-O(44)	2.295(7)
Na(1)-O(54)	2.334(7)	Na(1)-O(64)	2.262(7)
V(1)-O(1)	1.620(7)	V(1)-O(17)	1.944(7)
V(1)-O(64)	1.987(7)	V(1)-O(27)	2.050(6)
V(1)-O(14)	2.197(6)	V(1)-N(11)	2.198(9)
V(2)-O(2)	1.613(7)	V(2)-O(27)	1.953(6)
V(2)-O(14)	1.992(6)	V(2)-O(37)	2.025(6)
V(2)-O(24)	2.193(6)	V(2)-N(21)	2.209(8)
V(3)-O(3)	1.616(6)	V(3)-O(37)	1.970(6)
V(3)-O(24)	2.015(6)	V(3)-O(47)	2.044(6)
V(3)-O(34)	2.204(6)	V(3)-N(31)	2.192(8)
V(4)-O(4)	1.621(6)	V(4)-O(47)	1.959(6)
V(4)-O(34)	1.992(6)	V(4)-O(57)	2.049(6)
V(4)-O(44)	2.195(6)	V(4)-N(41)	2.192(8)
V(5)-O(5)	1.626(6)	V(5)-O(57)	1.942(6)
V(5)-O(44)	1.984(5)	V(5)-O(67)	2.029(6)
V(5)-O(54)	2.219(6)	V(5)-N(51)	2.194(8)
V(6)-O(6)	1.608(7)	V(6)-O(67)	1.966(6)
V(6)-O(54)	1.997(6)	V(6)-O(17)	2.065(6)
V(6)-O(64)	2.204(6)	V(6)-N(61)	2.174(8)
Bond Angles (deg)		Bond Angles (deg)	
O(17)-V(1)-O(27)	159.4(3)	O(27)-V(2)-O(37)	160.4(3)
O(1)-V(1)-O(14)	160.2(3)	O(2)-V(2)-O(24)	161.2(3)
O(64)-V(1)-N(11)	151.7(3)	O(14)-V(2)-N(21)	153.2(3)

O(37)-V(3)-O(47)	160.1(3)	O(47)-V(4)-O(57)	160.0(3)
O(3)-V(3)-O(34)	160.7(3)	O(4)-V(4)-O(44)	160.9(3)
O(24)-V(3)-N(31)	151.3(3)	O(34)-V(4)-N(41)	151.4(3)
O(57)-V(5)-O(67)	159.8(3)	O(67)-V(6)-O(17)	159.0(3)
O(5)-V(5)-O(54)	160.2(3)	O(6)-V(6)-O(64)	159.8(3)
O(44)-V(5)-N(51)	152.7(3)	O(54)-V(6)-N(61)	152.3(3)

The crystal structure of **2** consists of a V_6 loop with crystallographic C_i symmetry. There are two crystallographically independent molecules in a unit cell. Selected bond lengths and angles for **2** are given in full detail in Table 2.3.1a. Oxidation states for the vanadium ions in these hexanuclear complexes are readily assigned by examining the bond distances in each vanadium ion. Many compounds containing vanadium(IV) ions exhibit the classic Jahn-Teller distorted geometry expected for d^1 system, making the identification of this oxidation state for vanadium straightforward.

All the vanadium centers are six coordinate and possess distorted octahedral geometry. The octahedral environment of each V(IV) ion is comprised of four alkoxo O atoms, a N- atom from the *N*-methyldiethanolamine ligand, and a terminal O atom. The lengths of the V-O bonds range from 1.944(7) to 2.197(6) Å, V-N bonds are from 2.174(8) to 2.219(6) Å, and V=O bonds are from 1.613(7) to 1.626(6) Å. All the V(IV) ions are crystallographically equivalent as can be seen in Figure 2.3.3a. The cyclic core shown in Figure 2.3.3b, is comprised of edge-sharing VO_5N octahedrons to each other and to the central NaO_6 unit. Two types of μ-oxo (μ_2 and μ_3) groups are associated with cyclic core and the charge balance and bond distance analysis indicate that both are deprotonated. There is a significant amount of H-bonding between the terminal oxygen of vanadium and the proton of the MeOH solvent molecule with the H···O···H separation in the range 2.746-2.760 Å. An oxygen from the counter anion also participates in H-bonding with the proton of the solvent molecule.

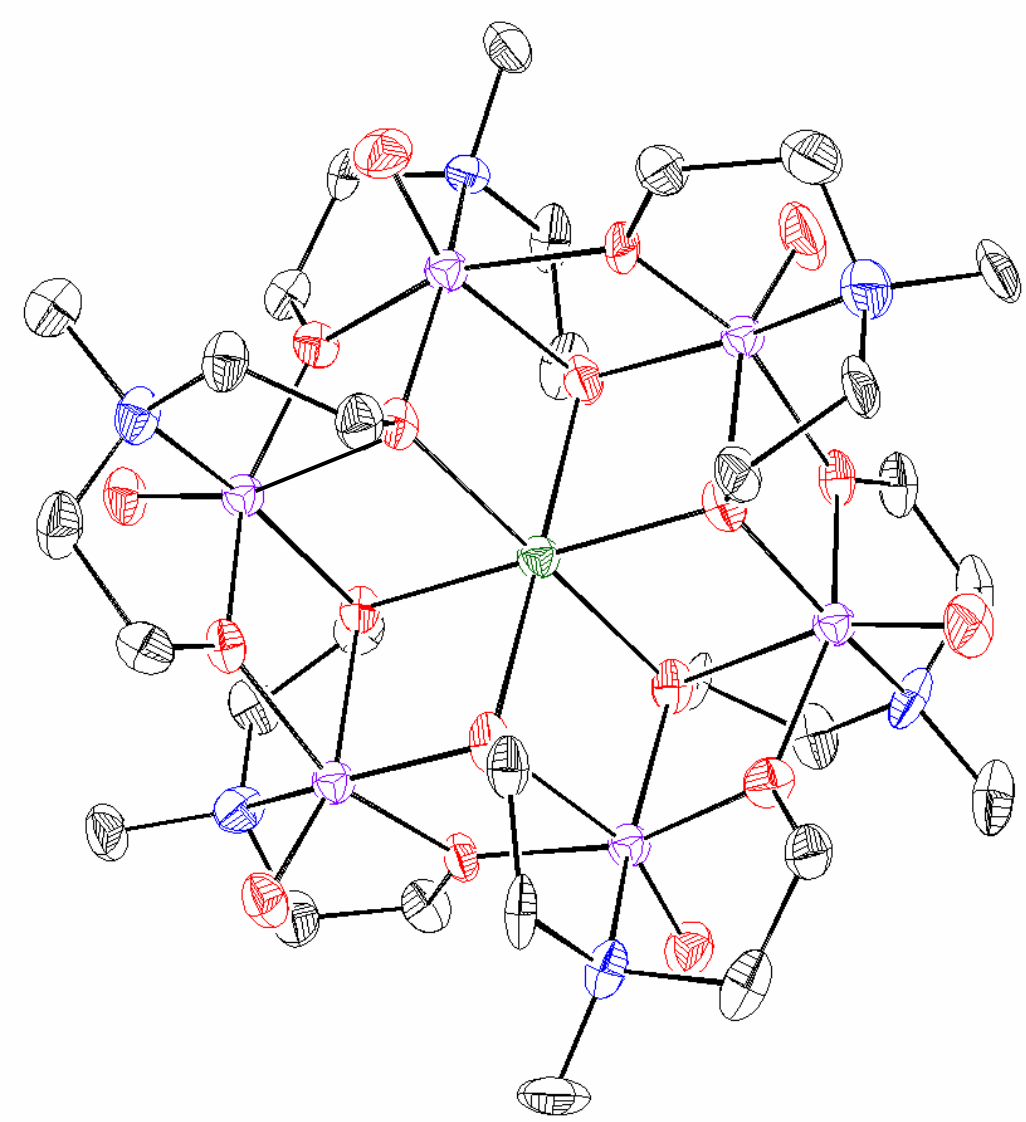

Figure 2.3.3a An ORTEP representation of $[NaL_6(V{=}O)_6]ClO_4$ (40% ellipsoids). Color code: V, purple; Na, green; O, red; N, blue; C, grey.

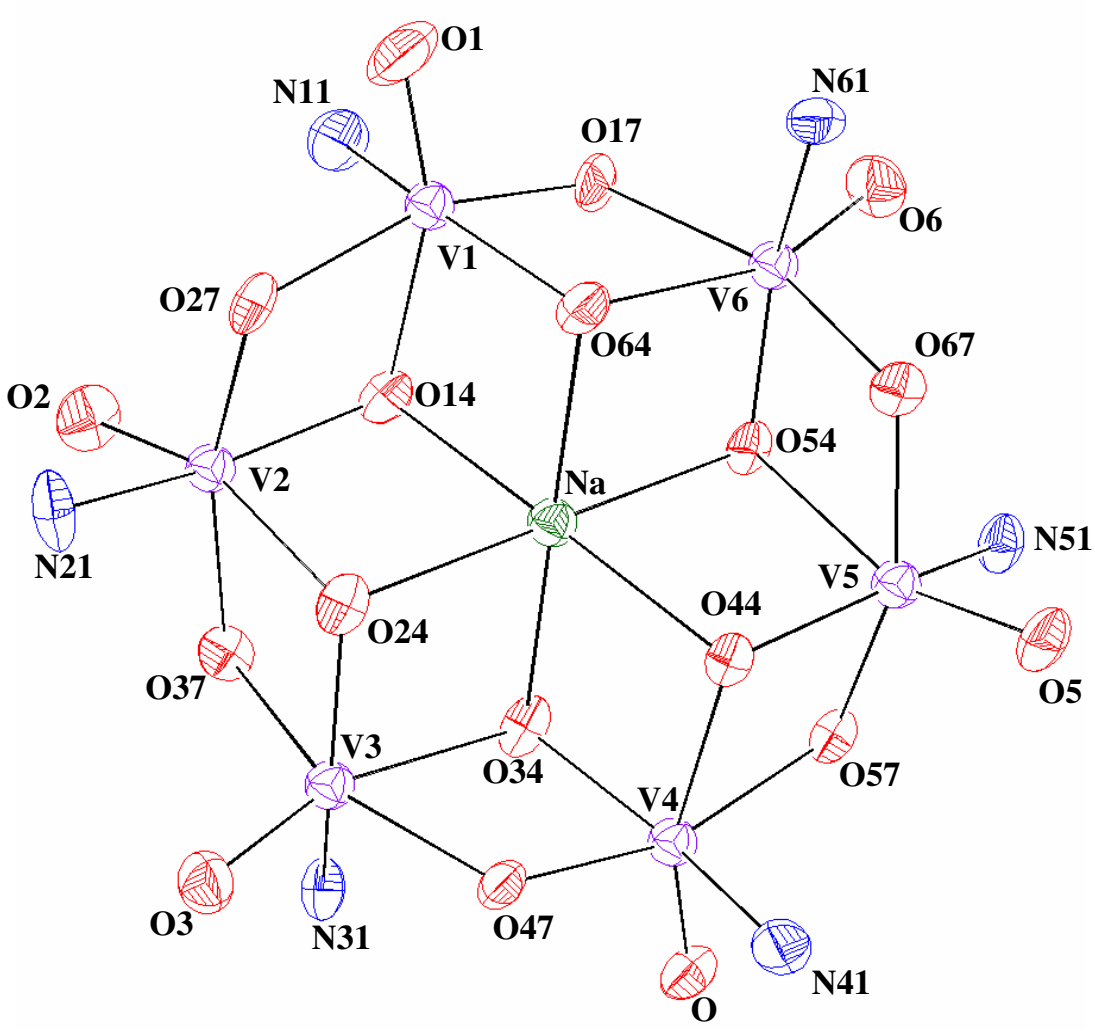

Figure 2.3.3b An ORTEP representation of the core structure of the metal and their coordination geometry (40% ellipsoids) (top view).

Table 2.3.2a Selected Dihedral Angles (deg) of Complex **2**.

O(1)V(1)V(2)/ V(1)V(2)O(2)	70.3	O(2)V(2)V(3)/ V(2)V(3)O(3)	70.2
O(3)V(3)V(4)/ V(3)V(4)O(4)	69.1	O(4)V(4)V(5)/ V(4)V(5)O(5)	71.2
O(5)V(5)V(6)/ V(5)V(6)O(6)	72.6	O(6)V(6)V(1)/ V(6)V(1)O(1)	71.1

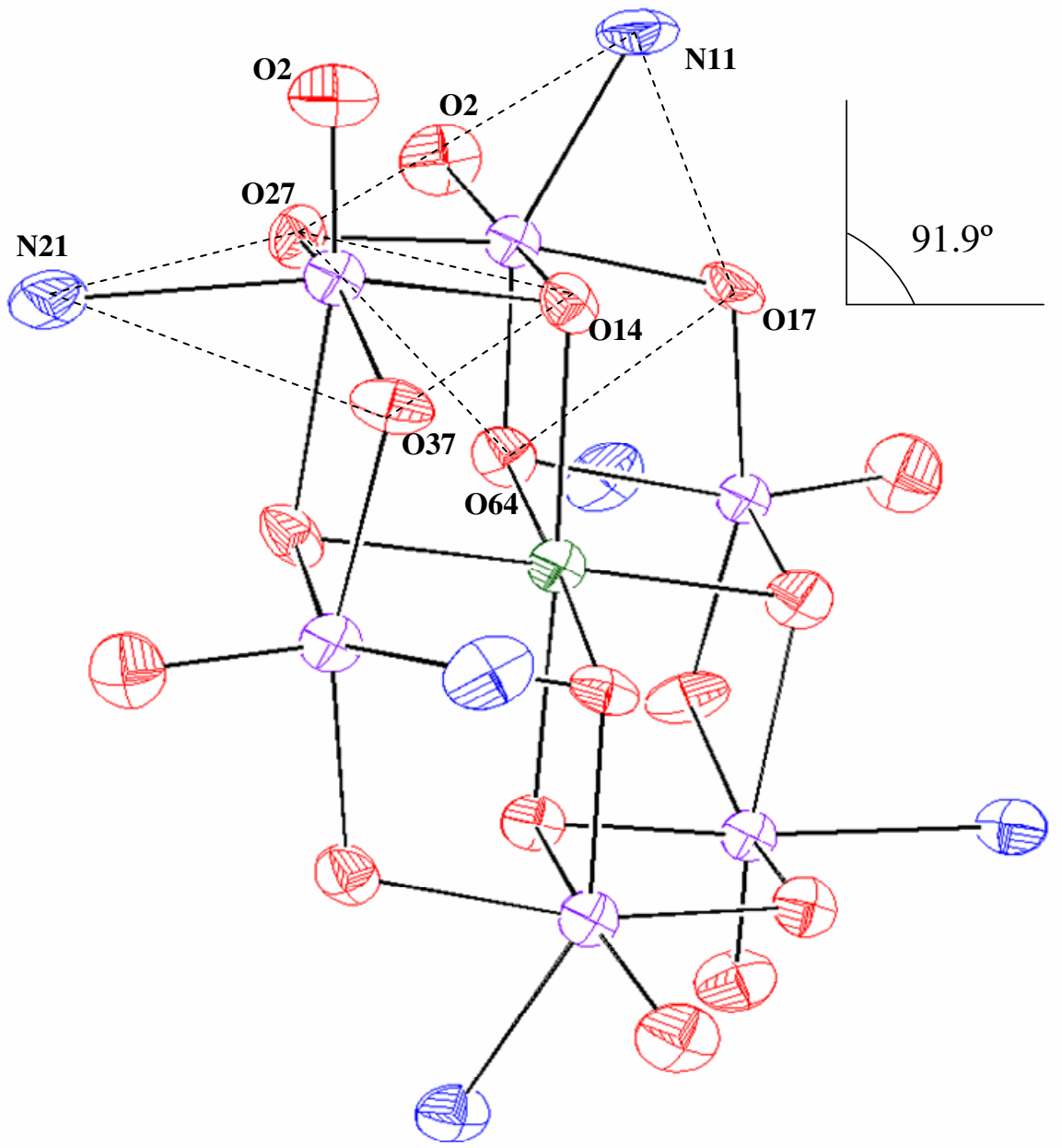

Figure 2.3.4c An ORTEP representation of the core structure of the metal and their coordination geometry (40% ellipsoids) (side view). Angle indicates the angle between the xy-planes of V(1) and V(2) centered.

Table 2.3.2b Angles (deg) Between the xy-Planes of Two Consecutive Vanadium Ions of Complex **2**.

Plane 1	Plane 2	Angle between plane 1 & 2 (deg)
O(64)O(17)V(1)N(11)O(27)	O(14)O(27)V(2)N(21)O(37)	91.9
O(14)O(27)V(2)N(21)O(37)	O(24)O(37)V(3)N(31)O(47)	88.1
O(24)O(37)V(3)N(31)O(47)	O(34)O(47)V(4)N(41)O(57)	86.2
O(34)O(47)V(4)N(41)O(57)	O(44)O(57)V(5)N(51)O(67)	91.7
O(44)O(57)V(5)N(51)O(67)	O(54)O(67)V(6)N(61)O(17)	89.0
O(54)O(67)V(6)N(61)O(17)	O(64)O(17)V(1)N(11)O(27)	88.2

The selected dihedral angles and the angles between the xy-plane of two consecutive vanadium ions have been given in Table 2.3.2a and Table 2.3.2b, respectively. The dihedral angles between two consecutive V=O (Table 2.3.3a) are approximately 70º. The bridging oxygen atoms are coordinated through the p_x orbital with one vanadium atom and through the p_y orbital with the next vanadium atom. The angles between two consecutive xy-planes of vanadium containing VNO_3 are in the range of 86.2 – 91.9º, shown in figure 2.3.3c. Analysis of the dihedral angles between the plane enables us to say that the xy-planes of two consecutive vanadium ions are mainly orthogonal to each other.

2.3.4 Magnetic Properties of Complex 2

Magnetic susceptibility data measured on a polycrystalline sample of **2** at B = 1 T are displayed in Figure 2.3.4a as μ_{eff} per molecule *vs* temperature. At 290 K, μ_{eff} is equal to 4.36 μ_B ($\chi_M \cdot T$ = 2.377 cm^3 K mol^{-1}) which is slightly higher than the high-temperature limit expected for six magnetically uncoupled S = ½ centers presuming g = 2.0. Upon cooling μ_{eff} continuously increases and reaches a maximum of 6.44 μ_B at about 10 K ($\chi_M \cdot T$ = 5.189 cm^3 K mol^{-1}). This magnetic behavior is characteristic of ferromagnetic coupling between the adjacent vanadium(IV) centers within the wheel. Below 5 K, μ_{eff} drops to 5.99 μ_B ($\chi_M \cdot T$ = 4.491 cm^3 K mol^{-1}) and may be due to the combined effects of field saturation and intermolecular interactions. The magnetic susceptibility data of the

same polycrystalline sample of **2** at B = 0.1 and 0.01 T were also measured and are displayed in Figure 2.3.4b and Figure 2.3.4c respectively as μ_{eff} per molecule *vs* temperature. For these two measurements μ_{eff} changes in a similar fashion as that for B = 1 T measurement, from room temperature to low temperature, except for the 2 K measurement. At 2 K μ_{eff} value is also increasing at B = 0.1 and 0.01 T unlike B = 1 T.

The experimental results have been described using the Heisenberg six-atom ring model (S = ½) [33] . According to model the Hamiltonian is

$$H = -2J\sum_{i=1}^{6}\mathbf{S_i}\mathbf{S_{i+1}} - g\mu_B H.\sum\mathbf{S_i} \qquad \textbf{equation 1}$$

where S_7 is defined as S_1. The energy of the levels for this system was obtained accord as Orbach *et.al*.[33] Using those values in van Vleck's equation gives

$$\chi_M = \frac{N_A\sum_n\left[-2E(n)^{(2)} + \{E(n)^{(1)}\}2 / KT\right]\exp(-E(n)^{(0)}/KT}{\sum_n \exp(-E(n)^{(0)}/KT} \qquad \textbf{equation 2}$$

To consider the intermolecular interaction, we use equation 3,

$$\chi_M = \frac{\chi_0}{1-(2\theta/N_A g^2 \mu_B{}^2)\chi_M} \qquad \textbf{equation 3}$$

where θ is the intermolecular exchange interaction. The best fit parameters are given in the table 2.3.4.

Table 2.3.4 Best Fit Parameters of **2**.

B (T)	J (cm^{-1})	g	TIP (cm^3/mol)	Θ_{weiss}
1	16.7	1.97	360.0x10-6	0.205
0.1	17.0	1.97	644.5x10-6	0.074
0.01	16.4	1.97	661.1x10-6	0.070

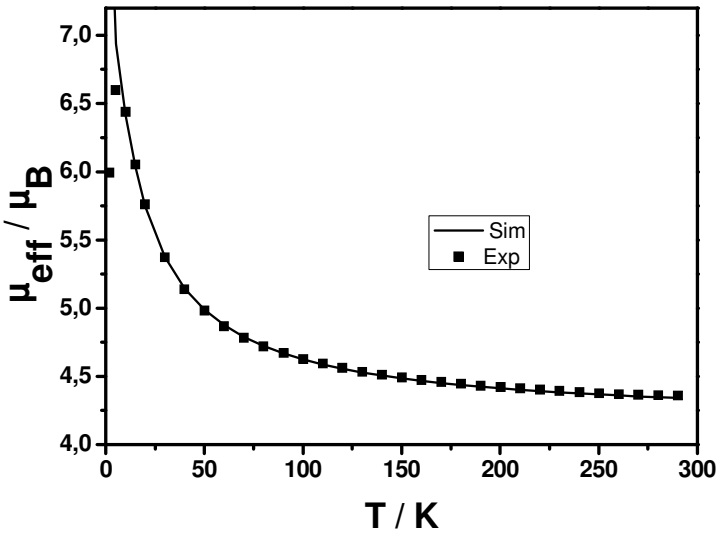

Figure 2.3.4a Temperature-dependence of the magnetic moment μ_{eff}/molecule for complex **2**, V_6 loop, at an applied magnetic field 1 T.

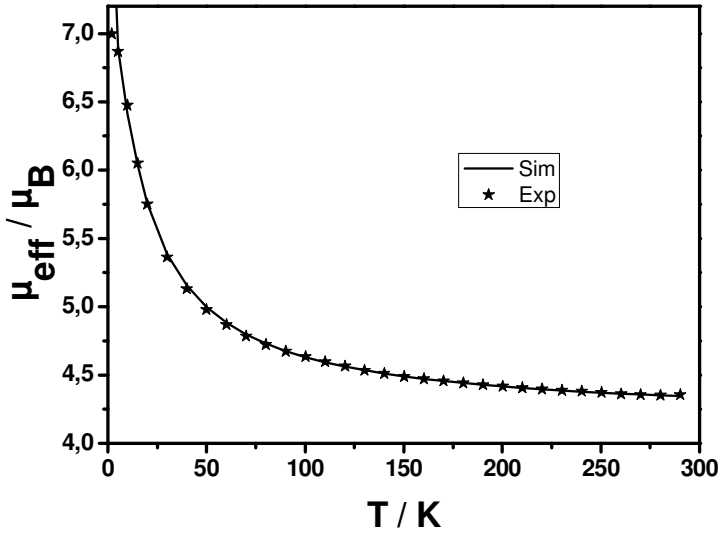

Figure 2.3.4b Temperature-dependence of the magnetic moment μ_{eff}/molecule for complex **2**, V_6 loop, at an applied magnetic field 0.1 T.

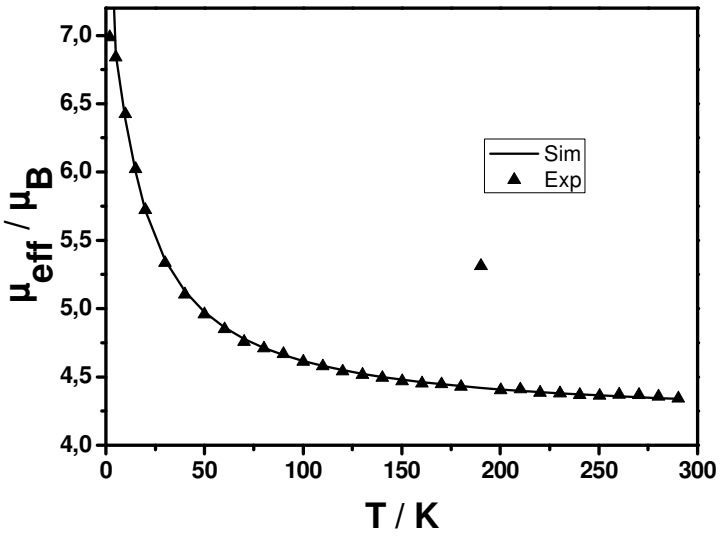

Figure 2.3.4c Temperature-dependence of the magnetic moment μ_{eff}/molecule for complex **2**, V_6 loop, at an applied magnetic field 0.01 T.

Electronic configuration of vanadium(IV) is d^1. Thus the coupling between the oxovanadium(IV) centers is determined by the interaction between the xy magnetic orbitals because this is where the d-electron is housed. The angles between two consecutive xy-planes of vanadium containing VNO_3 are near to 90º. Thus the interacting magnetic orbitals are getting accidental orthogonality to show the ferromagnetic exchange interactions. A possible scheme of the interaction in such a wheel shaped oxovanadium(IV) compound is suggested in Figure 2.3.4d. Weak coupling constants may be attributed to the lack of efficient interaction of the magnetic orbitals, which are considered as d_{xy}, because of the cyclic nonplanar structure of the V_6 subunit. It is believed that the magnetic coupling pathways can also be afforded by double μ-O bridging groups. Magneto-structural correlations have been established for oxo-bridged [V-μ_2O-V] fragments wherein ferromagnetic coupling was observed due to the orthogonality of the d_{xy} magnetic orbitals (where a local reference system with the x and y axis pointing towards the oxo-bridging ligands is considered). Regarding the *inter*molecular exchange interaction, without Θ_{weiss} it does not fit well at lower temperature (2-15 K). If we look at the intermolecular distances, 6.296 Å is the shortest. Again there are two crystallographically identical molecules in a unit cell. So we can not avoid the intermolecular interaction. Finally, we have carried out the magnetic moment

measurements at different magnetic field to know the change of magnetic moment values at low temperature (2 – 10 K) with magnetic field. In that sense these values do not change significantly and the fitting parameters show that only the SQUID is not enough to say the exact value of the coupling constants. SQUID analysis allows us to get the idea of the coupling constants at a certain range.

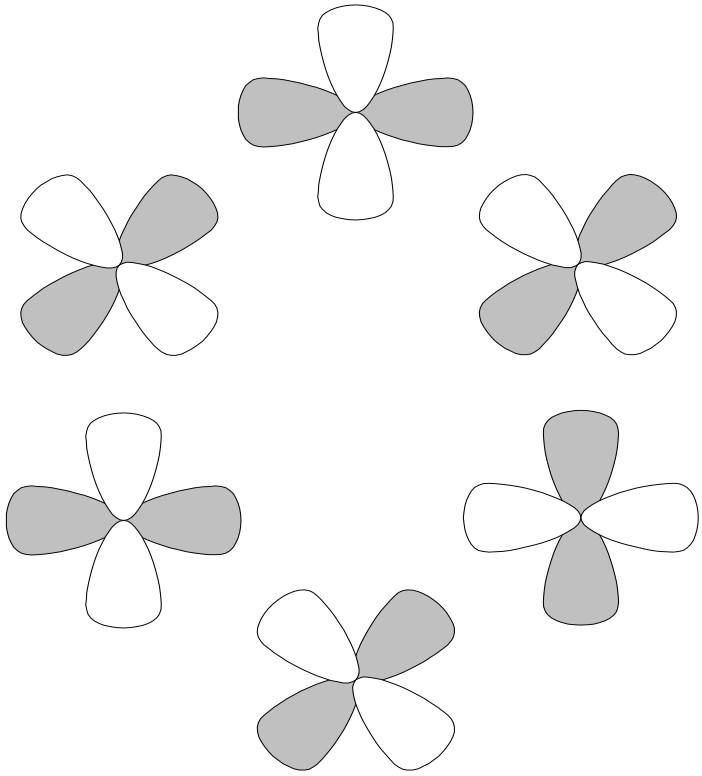

Figure 2.3.4d The orthogonal arrangement of d_{xy} orbitals of six V^{IV} sites of syn-vanadyl groups may give rise to the ferromagnetic exchange interactions.

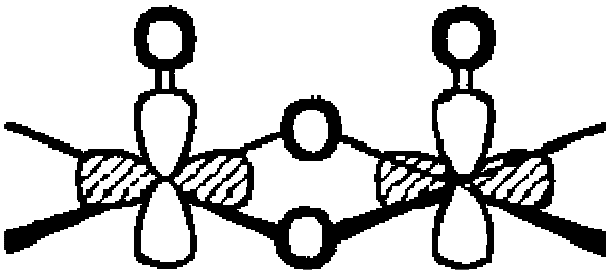

Figure 2.3.4e Magnetic orbitals for di-μ-oxo bridged oxovanadium pairs.

2.4 Experimental Section

$[Na^{I}_{2}\{Ni^{II}_{4}(HL)_3(OOCCH_3)_5(HCOO)_{0.5}\}_4]\cdot 3CH_3CN\cdot 21H_2O$ (1)

A solution of $Ni(CH_3COO)_2\cdot 4H_2O$ (1.0 g, 4 mmol) in dry MeOH (40 mL) was treated with *N*-methyldiethanolamine (H_2L) (0.36 g, 3 mmol) and $NaOCH_3$ (0.32 g, 6 mmol). The resulting green solution was heated to reflux for two hours in presence of air. Methanol was removed in *vacuo* to obtain a green solid, which was recrystallized from acetonitrile, X-ray quality crystals in 70% yield grew over two days. MS-ESI (pos.) in MeOH: m/z, 820.0, 704.0, 644.9, MS-ESI (neg.) in MeOH: m/z, 2819.5, 2219.7, 1619.8, 767.0. UV-vis in MeOH: λ_{max} (ε, M^{-1} cm^{-1}): 1105 (110), IR (KBr, cm^{-1}): 3412, 2873, 1622, 1590, 1449, 1058, 1022, 905, 884, 667, 566.

Elemental analysis:

	%C	%H	%N	%Ni
Calculated	31.2	6.2	4.7	22.6
Found	32.2	6.1	4.95	23.5

$[NaL_6(V{=}O)_6]ClO_4\cdot 2CH_3OH$ (2)

Reaction of VCl_3 (0.32 g, 2 mmol) with *N*-methyldiethanolamine (LH_2) (0.24 g, 2 mmol) and $NaOCH_3$ (0.22 g, 4 mmol) in dry methanol yielded a green solution which was heated to reflux for three hours. The solution was kept as it was for two days under inert atmosphere but no change observed. $NaClO_4$ was added to the solution, and the color turned blue very slowly. X-ray quality deep blue crystal was obtained by slow evaporation of methanol solution for two days. MS-ESI (pos.) in MeOH: m/z, 1127.1 (100%) $[M\text{-}ClO_4]^+$, MS-ESI (neg.) in MeOH: m/z, 99.1 (100%)ClO_4^-. IR (KBr, cm^{-1}): 2865, 1645, 1567, 1459, 1075, 1037, 978, 897, 660, 585, 514.

Elemental analysis:

	%C	%H	%N	%V
Calculated	29.8	5.8	6.5	23.7
Found	29.5	5.9	6.4	23.2

References

1. R. H. Holm and E. I. Soloman (Guest editors), *Chem. Rev.* **2004**, *104*(2).

2. O. Kahn, *Molecular Magnetism*, VCH, New York **1993**.

3. *a*) D. Gatteschi, R. Sessoli, *Angew. Chem., Int. Ed.* **2003**, *42*, 268; *b*) G. Christou, D. Gatteschi, D. N. Hendrickson, R. Sessoli, *MRS Bull.* **2000**, 66.

4. R. E. P. Winpenny, *Adv. Inorg. Chem.* **2001**, 52, 1.

5. a) R. Wang, D. H. Selby, H. Liu, D. M. Carducci, T. Jin, Z. Zheng, W. J. Anthis, J. R. Staples, *Inorg. Chem.* **2002**, *41*, 278; b)R. Wang, Z. Zheng, T. Jin, J. R. Staples, *Angew. Chem., Int. Ed.* **1999**, *38*, 1813.

6. Q.-D. Liu, S. Gao, J.-R. Li, Q.-Z. Zhou, K.-B. Yu, B.-Q.Ma, S.-W. Zhang, X.-X. Zhang, T.-Z. Jin, *Inorg. Chem.* **2000**, *39*, 2488.

7. a) W. R. Saalfrank, I. Bernt, E. Uller, F. Hampel, *Angew. Chem., Int. Ed.* **1997**, *36*, 2482; b) O. Waldmann, J. Schuelein, R. Koch, P. Mueller, I. Bernt, W. R. Saalfrank, P. H. Andres, U. H. Guedel, P. Allenspach, *Inorg. Chem.* **1999**, *38*, 5879; c) W. R. Saalfrank, I. Bernt, F. Hampel, *Angew. Chem., Int. Ed.* **2001**, *40*, 1700.

8. a) A. Simon, *Angew. Chem., Int. Ed.* **1988**, *27*, 156; b) M. D. Vargas, J. N. Nicholls, *Adv. Inorg. Chem. Radiochem.* **1986**, *30*, 123; c) S. M. Owen, *Polyhedron* **1988**, *7*, 253; d) K. Wade, *Adv. Inorg. Chem. Radiochem.* **1976**, *18*, 1; e) D. M. P. Mingos, M. J. Watson, *Adv. Inorg. Chem.* **1992**, *39*, 327.

9. a) S. P. Watton, P. Fuhrmann, L. E. Pence, A. Caneschi, A. Cornea, G. L. Abbati, S. J. Lippard, *Angew. Chem., Int. Ed.* **1997**, *36*, 2774; b) R. A. Reynolds III, D. Cocouvanis, *J. Am. Chem, Soc.* **1998**, *120*, 209; c) M. Murrie, S. Parsons, R. E. P. Winpenny, *J. Chem. Soc. Dalton Trans.* **1998**, 1423; d) H. O. Stumpf, L. Ouahab, Y. Pei, P. Bergerat, O. Kahn, *J. Am. Chem. Soc.* **1994**, *116*, 3866; e) C. Benelli, S. Parsons, G. A. Solan, R. E. P. Winpenny, *Angew. Chem., Int. Ed*. **1996**, *35*, 1825.

10. a) Y. Zhang, P. J. Zapf, L. M. Meyer, R. C. Haushalter, J. Zubieta, *Inorg. Chem,* **1997**, *36*, 2159; b) L. Suber, M. Bonamico, V. Fares, *Inorg. Chem.* **1997**, *36*, 2030; c) A. Müller, E. Krickemeyer, H. Bögge, M. Schmidtmann, C. Beugholt, P. Kögerler, C. Lu, *Angew. Chem., Int. Ed.* **1998**, *37*, 1220; d) A. K. Powell, S. L. Heath, D. Gatteschi, L. Pardi, R. Sessoli, G. Pina, F. Del Giallo, F. Pieralli, *J. Am. Chem. Soc.* **1995**, *117*, 2491; e) A. Müller, F. Peters, M. J. Pope, D. Gatteschi, *Chem. Rev*. **1998,** *98*, 239.

11. For example: *a*) X. Lin, D. M. J. Doble, A. J. Blake, A. Harrison, C. Wilson, M. Schröder, *J. Am. Chem. Soc.* **2003**, *125*, 9476; *b*) D. M. J. Doble, C. H. Benison, A. J. Blake, D. Fenske, M. S. Jackson, R. D. Kay, Wan-Sheung Li, M. Schröder, *Angew. Chem., Int. Ed.* **1999**, *38*, 1915; *c*) G. Aromi, A. R. Bell, M. Helliwell, J. Raftery, J. Teat Simon, G. A. Timco, O. Roubeau, R. E. P. Winpenny, *Chem.–Eur. J.* **2003**, *9*, 3024; *d*) E. K. Brechin, R. O. Gould, S. G. Harris, S. Parsons, R. E. P. Winpenny, *J. Am. Chem. Soc.* **1996**, *118*, 11293; *e*) A. Bell, G. Aromi, S. J. Teat, W. Wernsdorfer, R. E. P. Winpenny, *Chem. Commun.* **2005**, 2808; *f*) R. W. Saalfrank, T. Nakajima, N. Mooren, A. Scheurer, H. Maid, F. Hampel, C. Trieflinger, J. Daub, *Eur. J. Inorg. Chem.* **2005**, 1149; *g*) E. M. Rumberger, L. N. Zakharov, A. L. Rheingold, D. N. Hendrickson, *Inorg. Chem.***2004**, *43*, 6531.

12. *a*) T. K. Paine, E. Rentschler, T. Weyhermüller, P. Chaudhuri, *Eur. J. Inorg. Chem.* **2003**, 3167; b) S. Khanra, T. Weyhermüller, E. Rentschler, P. Chaudhuri, *Inorg. Chem.* **2005**, *44*, 8176; and references therein.

13. Selected recent examples: *a*) J. M. Clemente-Juan, B. Chansou, B. Bonnadieu, J.-P. Tuchages, *Inorg. Chem.* **2000**, *39*, 5515; *b*) M.-L. Tong, S.-L. Zheng, J.-X. Shin, Y.-X. Tong, H. K. Lee, X.-M. Chen, *J. Chem. Soc., Dalton Trans.* **2002**, 1727; *c*) E.-C. Yang, W. Wernsdorfer, S. Hill, R. S. Edwards, M. Nakano, S. Maccagnano, L. N. Zakharov, A. L. Rheingold, G. Christou, D. N. Hendrickson, *Polyhedron* **2003**, *22*, 1727; *d*) M. Moragues-Cánovas, M. Helliwell, L. Ricard, E. Riviére, W. Wernsdorfer, E. Brechin, T. Mallah, *Eur. J. Inorg. Chem.* **2004**, 2219; *e*) S. Mukherjee, T. Weyhermüller, E. Bothe, K. Wieghardt, P. Chaudhuri, *Eur. J. Inorg. Chem.* **2003**, 863; *f*) C. G. Efthymiou, C. P. Raptopoulou, A. Terzis, R. Boca, M. Korabic, J. Mrozinski, S. P. Perlepes, E. G. Bakalbassis, *Eur. J. Inorg. Chem.* **2006**, 2236 and references therein.

14. *a*) M. Murrie, H. Stoeckli-Evans, H. U. Güdel, *Angew. Chem., Int. Ed.* **2001**, *40*, 1957; *b*) A. L. Dearden, S. Parsons, R. E. P. Winpenny, *Angew. Chem., Int. Ed.* **2001**, *40*, 152; *c*) D. Foguet-Albiol, K. A. Abboud and G. Christou, *Chem. Commun.* **2005**, 4282; *d*) G. Aromi, A. Bell, S. J. Teat, R. E. P. Winpenny, *Chem. Commun.* **2005**, 2927.

15. *a*) R. W. Saalfrank, I. Bernt, M. M. Chaudhuri, F. Hauptel, G. B. M. Vaughan, *Chem.–Eur. J.* **2001**, *7*, 2765; *b*) R. W. Saalfrank, I. Bernt, E. Uller, F. Haupel, *Angew. Chem., Int. Ed.* **1997**, *36*, 1482; *c*) E. M. Rumberger, S. J. Shah, C. C. Beedle, L. N.

Zakharov, A. L. Rheingold, D. N. Hendrickson, *Inorg. Chem.* **2005**, *44*, 2742; *d*) D. Foguet-Albiol, T. A. O'Brien, W. Wernsdorfer, B. Moulton, M. J. Zaworotko, K. A. Abboud, G. Christou, *Angew. Chem., Int. Ed.* **2005**, *44*, 897; *e*) R. W. Saalfrank, T. Nakajima, N. Mooren, A. Scheurer, H. Maid, F. Hampel, C. Trieflinger, J. Daub, *Eur. J. Inorg. Chem.* **2005**, 1149.

16. B. Biswas, S. Khanra, T. Weyhermüller, P. Chaudhuri, *Chem. Commun.* **2007**, 1059.

17. *a*) S. Mukherjee, T. Weyhermüller, E. Bothe, K. Wieghardt, P. Chaudhuri, *Eur. J. Inorg. Chem.* **2003**, 863; *b*) C. Krebs, M. Winter, T. Weyhermüller, E. Bill, K. Wieghardt, P. Chaudhuri, *J. Chem. Soc., Chem. Commun.* **1995**, 1913; *c*) P. Chaudhuri, H.-J. Küppers, K. Wieghardt, S. Gehring, W. Haase, B. Nuber, J. Weiss, *J. Chem. Soc., Dalton Trans.* **1988**, 1367.

18. A. Müller, F. Peters, M. T. Pope, D. Gatteschi, *Chem. Rev.* **1998**, *98*, 239.

19. L. C. Hill (Guest Ed.) *Chem. Rev.* **1998**, *98*, 1.

20. T. M. Pope, A. Müller, *Angew. Chem., Int. Ed*. **1991**, *30*. 34.

21. M. G. Kanatzidis, C.-G. Wu, H. O. Marcy, C. R. Kannewurf, *J. Am. Chem. Soc.* **1989**, *111*, 4139.

22. A. R. Raju, C. N. Ramachandra Rao, *J. Chem. Soc., Chem. Commun.* **1991**, 1260.

23. D. Rehder, *Angew. Chem., Int. Ed.* **1991**, *30*, 148.

24. J. E. Baran, *J. Inorg. Biochem.* **2000**, *80*, 1.

25. C. D. Crans, *J. Inorg. Biochem.* **2000**, *80*, 123.

26. D. Hou, S. G. Kim, S. K. Hagen, L. C. Hill, *Inorg. Chim. Acta* **1993**, *211*, 127.

27. M. I. Khan, S. Tabussum, R. J. Doedens, V. O. Golub, C. J. O'Connor, *Inorg. Chem. Commun.* **2004**, *7*, 54.

28. M. I. Khan, S. Tabussum, R. J. Doedens, V. O. Golub, C. J. O'Connor, *Inorg. Chem.* **2004**, *43*, 5850.

29. T. Kurata, Y. Hayashi, A. Uehara, K. Isobe, *Chem. Lett.* **2003**, *32*, 1040.

30. Y. Chen, H. Zhu, Q. Liu, C. Chen, *Chem. Lett.* **1999**, 585.

31. Y. Chen, Q. Liu, Y. Deng, H. Zhu, C. Chen, H. Fan, D. Liao, E. Gao, *Inorg. Chem.* **2001**, *40*, 3725.

32. M. I. Khan, S. Tabussum, R. J. Doedens, *Chem. Commun.* **2003**, 532.

33. R. Orbach, *Physical Review* **1959**, 1181.

Chapter 3

An Unprecedented Single Oximate-Bridged One-Dimensional Chain: Ferromagnetically Coupled S_T=4 Ground State via Mn^{III}-N-O-Mn^{III} Bridge

3.1 Introduction

Complexes containing two or more metal ions are of increasing interest because of their relevance to biological systems[1] (as evidenced by the many multinuclear complexes in biology) and to molecular magnetism.[2] Polynuclear systems are also ideal candidates for the synthesis of single-molecule magnets[3] (SMMs). The prerequisites for molecules to show SMM behavior are the presence of a high-spin ground state and a significant negative zero-field-splitting parameter *D*.[4] So, the interest in polynuclear complexes of 3d transition metals has been augmented by the search for new magnetic clusters. Furthermore the fundamental understanding regarding the factors that determine the spin state of polynuclear transition metal complexes owes much to the study of compounds where magnetostructural correlations[5] can be established in a systematic way.

One of the most fertile areas in transition metal polynuclear complexes is based on oxime[6-11] ligand, because of the propensity of the oxime function (C=N-O) for varying bridging modes to yield magnetically interesting compounds. That the oximate as bridging ligands can efficiently transmit exchange coupling has also been well documented. Moreover, manganese (III) is known to have a large single-ion zero-field splitting and often gives rise to ferromagnetic coupling; thus, polynuclear manganese (III) complexes are potential candidates for SMMs. As far as Mn^{III} complexes bridged by only oximate group are quite rare, although complexes in presence of other co-bridging ligands like oxo, hydroxo or carboxylate are not unprecedented. Polynuclear Mn^{III} complexes with oximate (-N-O-) bridges have been reported recently,[7b, 8j, 9] however the coexistence of the multibridging pathways precludes clear studies on the magnetic coupling via oximate bridge only. To clarify the nature of exchange interaction via oximate pathway, the synthesis of such compound is expected. Working towards this goal, we did successfully furnish such an interesting 1D Mn^{III} complex,

$[Mn^{III}_2(^{H}ImOx)_4(CH_3COO)_2]_n$ (**3**) which is composed of dimeric Mn^{III} unit connected by single oximato bridge.

3.2 Synthesis

Reaction of imidazolealdoxime (^{H}ImOxH) with the well known Mn(III) carboxylate triangles $[Mn_3O(CH_3COO)_6(H_2O)_3](CH_3COO)$ in MeOH-MeCN mixture afforded $[Mn^{III}_2(^{H}ImOx)_4\ (CH_3COO)_2]_n$ The formulation of **3** can be summarized in equation 1.

$$12\ ^{H}ImOxH + 2\ Mn_3O(CH_3COO)_6(H_2O)_3](CH_3COO) \xrightarrow{\text{MeOH:MeCN (1:1)}} 2\ [Mn^{III}_2(^{H}ImOx)_4(CH_3COO)_2]_n + 8\ H_2O + 8\ CH_3CO_2H \qquad \text{equation 1}$$

3.3 Infrared Spectroscopy

Since the relevant bands in the IR spectra of comparable oxime-containing homo- and heterometal complexes have been described earlier[7] and the spectrum of complex **3** is also very similar, we refrain from discussing that.

3.4 X-ray Structure

Complex **3** crystallizes in the triclinic space group P-1 and the lattice consists of 1D chain containing the $\{Mn^{III}_2\}$ unit, Figure 3.1 displays the structure of the neutral molecule in **3**. The selected bond distances and angles are listed in Table 3.1. The X-ray structure confirms that a linear 1D complex has indeed been formed in such a way that each alternate manganese center is in MnN_2O_4 and MnN_4O_2 coordination environment, respectively.

All of the oxime groups are deprotonated and the manganese atoms are linked together via single oximato bridge. Mn(1) center is coordinated by two imidazole nitrogen atoms N(1) and symmetry equivalents (Mn(1)-N(1) bond distance 1.997Å), two oximato oxygen atoms O(1) and symmetry equivalents (Mn(1)-O(1) bond distance 1.90Å) and two carboxylato oxygen atoms O(21) and symmetry equivalents (Mn(1)-O(21) distance 2.216Å) thus giving a distorted N_2O_4 octahedral environment; whereas Mn(2) is coordinated by two imidazole nitrogen atoms N(2) and symmetry equivalents

(Mn(1)-N(11) bond distance 2.001Å), two oximato nitrogen atoms N(7) and symmetry equivalents (Mn(1)-N(7) bond distance 2.313Å) and two oximato oxygen atoms O(18) and symmetry equivalents (Mn(1)-O(18) distance 1.897Å) and is in distorted N_4O_2 coordination environment.

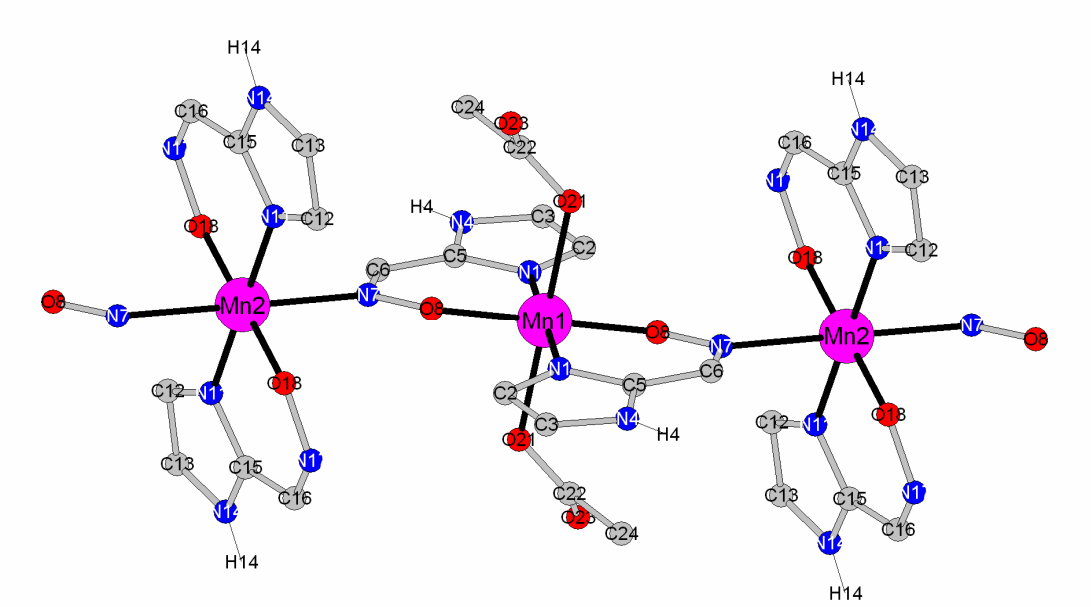

Figure 3.1 An ORTEP plot of $[Mn^{III}_2(^{H}ImOx)_4(CH_3COO)_2]_n$ **3** (40% ellipsoids). H atoms are omitted for clarity.

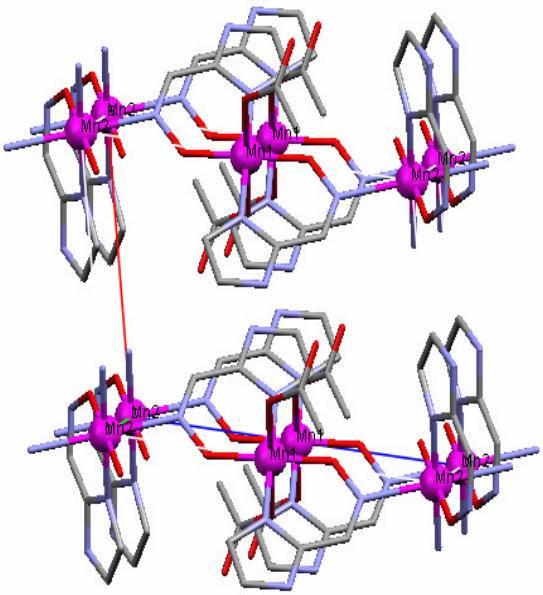

Figure 3.2 A 3-D network of **3**. H atoms are omitted for clarity.

Table 3.1 Selected Bond Lengths (**Å**) and Angles (deg) of Complex **3**.

Mn(1)···Mn(2)	5.002		
Mn(1)-O(8)	1.900(3)	Mn(2)-O(18)	1.896(3)
Mn(1)-O(8)#1	1.900(3)	Mn(2)-O(18)#2	1.896(3)
Mn(1)-N(1)	1.997(3)	Mn(2)-N(11)	2.001(4)
Mn(1)-N(1)#1	1.997(3)	Mn(2)-N(11)#2	2.001(4)
Mn(1)-O(21)	2.216(3)	Mn(2)-N(7)	2.314(3)
Mn(1)-O(21)#1	2.216(3)	Mn(2)-N(7)#1	2.314(3)
C(6)-N(7)	1.294(5)	N(7)-O(8)	1.345(4)
C(16)-N(17)	1.296(6)	N(17)-O(18)	1.354(4)
Bond Angles (deg)		Bond Angles (deg)	
O(8)#1-Mn(1)-O(8)	180.0	O(18)#2-Mn(2)-O(18)	180.0
N(1)#1-Mn(1)-N(1)	180.0	N(11)#1-Mn(2)-N(11)	180.0
O(21)-Mn(1)-O(21)#1	180.0	N(7)-Mn(2)-N(7)#2	180.0
O(8)-Mn(1)-N(1)	90.67(12)	O(18)-Mn(1)-N(11)	89.95(13)
O(8)#1-Mn(1)-N(1)#1	90.68(12)	O(18)#2-Mn(1)-N(11)#2	89.95(13)
N(7)-O(8)- Mn(1)	131.5(2)	N(17)-O(18)- Mn(2)	131.5(2)

The Mn-O-N angles fall in the range of 131.5° and are similar to that of Mn-O-N angle observed in $Mn^{III}Ni^{II}Mn^{III}$ single chain magnet;[11] whereas the Mn-O_{ox} bond distance is about 1.9 Å. The apical Mn-$O_{carboxylate}$ bond lengths in Mn(1) and Mn-N_{ox} bond lengths in Mn(2) are significantly larger than the equatorial ones as expected for Jahn-Teller distorted Mn^{III} ions with d^4 electronic configuration. The torsion angle of Mn(1)–O(8)–N(7)–Mn(2) in $[Mn_2]_n$ are 171.4°. The interatomic Mn–Mn distance is 5.002 Å(5).

3.5 Magnetic Properties

The dc magnetic susceptibility data for a polycrystalline sample of **3** were collected in the temperature range 2–290 K in an applied magnetic field of 1 T. The magnetic moment μ_{eff} vs. T plot with an applied field of 1 T for **3** in the range 2-290 K is

shown in Figure 3.3. The magnetic moment (μ_{eff}) at 290 K is 7.1 μ_B ($\chi_M \cdot T$ = 6.225 cm^3 mol^{-1} K), which is significantly greater than the spin-only value of 6.93 μ_B for two high-spin Mn(III) ions. On lowering the temperature, μ_{eff} increases monotonically reaching at 20 K a maximum value of 7.66 μ_B ($\chi_M \cdot T$ = 7.329 cm^3 mol^{-1} K), which is close to the value of 8.94 μ_B for a hypothetically isolated S = 4.0 with g = 2.0. An S_t = 4.0 value is expected as the ground state resulting from ferromagnetic interactions between two spins of $S = {}^4/_2$. Below 20 K there is a decrease in μ_{eff} for **3**, which reaches a value of 4.00 μ_B ($\chi_M \cdot T$ = 2.00 cm^3 mol^{-1} K) at 2 K. The sharp drop at the lower temperatures might be to due to the zero-field splitting (D) of the ground state and/or very weak intermolecular antiferromagnetic interactions.

The susceptibility of $[Mn^{III}{}_2]_n$ **3**, was calculated by using a full-matrix diagonalization approach of the spin Hamiltonian:

$H = -2J\ S_1S_2 + D_{Mn} \sum Sj^2 + g\mu BH \sum S_j$; where D is the axial single ion zero-field splitting parameter (ZFS). The consideration of all these parameters includes a simple calculation of the dimer's spin levels by Kambe method.[14] The correspondingly calculated (Figure 3, solid line) μ_{eff} vs. T curve, with J = + 1.4 cm^{-1}, D_{Mn} = - 3.6 cm^{-1} and g_{Mn} = 2.02, shows very good agreement with the experimental data. No other terms were used for the simulation shown in Figure 3.3. The ferromagnetic nature of exchange coupling interaction in **3** can be explained by assuming prevalent e_g-e_g contributions. Given the elongated natute of the distortion from octahedral symmetry, the dx^2-y^2 orbitals are empty. Due to the arrangement of local elongated axes in the structure $d_z{}^2$ magnetic orbitals have a non-zero overlap with the empty dx^2-y^2 orbitals. This dx^2-y^2 || $d_z{}^2$ pathway via oximate (C=N-O) bridge is expected to provide a ferromagnetic exchange interaction.[12]

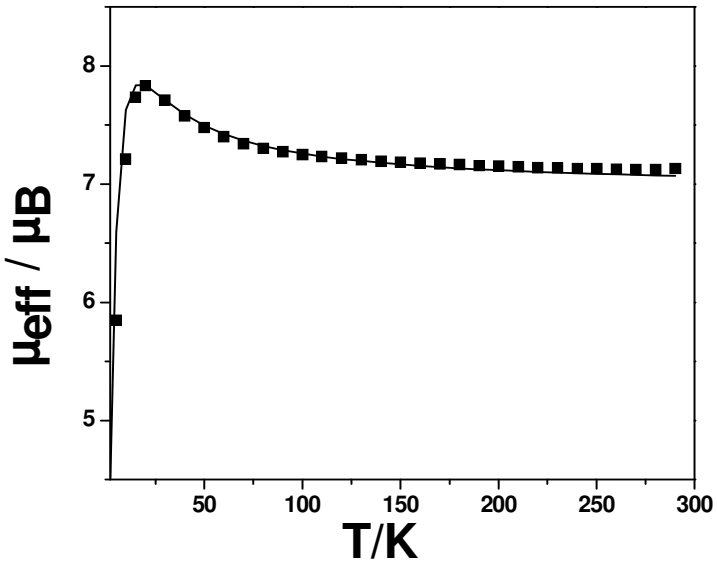

Figure 3.3 Temperature-dependence of the magnetic moment μ_{eff} of **3** at an applied magnetic field of 1 T. The bold points represent the experimental data while the solid line represents the simulation.

To determine the spin ground state, magnetization data were collected at 1, 4 and 7 T in the temperature range 2-290 K and plotted as reduced magnetization (M/Ngβ) vs. (βH/kT) (vide infra), where N is the Avogadro's number, β is the Bohr magneton and k is the Boltzmann's constant (Figure 3.4). For a system occupying only the ground state and experiencing no zero-field splitting (*D*), the various isofield lines would be superimposed and M/Ngβ would saturate at a value *S*. The non-superposition of the variable temperature variable field (VTVH) plots at low temperature clearly indicates the presence of zero-field splitting (ZFS or *D*).

The experimental magnetic data were analyzed on the basis of the Spin Hamiltonian: $H = - 2J \sum SiSj + D_{Mn} \sum Sj^2 + g\mu BH \sum S_i$; where *D* is the axial single ion zero-field splitting parameter (ZFS).Attempts to simulate the data by using the method of full-matrix diagonalization of the spin Hamiltonian matrix including axial ZFS, with the pairwise exchange interactions, produced best fits with, $J = + 1.0$ cm^{-1}, $D_{Mn} = |3.5 \pm 0.2|$ cm^{-1} and $g_{Mn} = 1.98$.

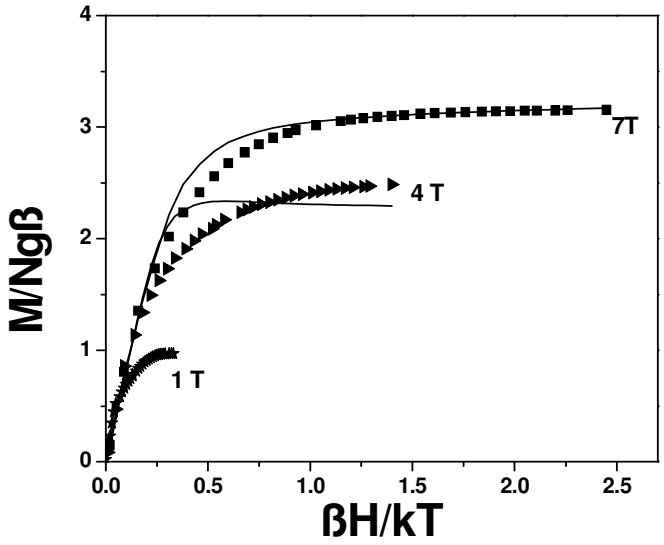

Figure 3.4 Variable temperature variable field (VTVH) magnetic data for **3**, plot of M/Ngß vs. ßH/kT. The bold points represent the experimental data while the solid line represents the simulation.

It is also well known that Mn(III) complexes exhibit a large anisotropy (typically $D \sim -4$ cm^{-1} for an elongation). The D values are in accord with the literature data.[4,13] It should be pointed that the main source of the molecular anisotropy is due to the presence of two Jahn-Teller distorted Mn^{III} ions. The projections of these single-ion anisotropies onto the molecular anisotropy axis will determine the molecular parameter D. As it is difficult, if not impossible, to determine the sign of ZFS parameter from powder magnetic susceptibility measurements, one should not put too much weight on the absolute value of D as a parameter that was included in the simulation of magnetic measurement. To confirm that simulated parameters are the true global rather than a local minimum, and to assess the uncertainty in the simulated J and D values, a two-dimensional contour projection of the relative error surface for fitting the magnetic data as a function of both J and D was generated using a computer program (Figure 3.5).[15] It can be concluded that the above parameters lie well in a global minimum in the parameter space for this system and allow us to estimate the approximate error bars on the J and D values: $J = +0.1 \pm 0.1$ cm^{-1} and $D = -4.2 \pm 1.2$ cm^{-1}.

Noteworthy is that the simulation is much superior with negative D value although it is difficult to accurately estimate the sign of D from bulk magnetic data.

These parameters are in well accord with the literature value. The ferromagnetic nature of the oximate mediated coupling in the chain compound is quite clear from the above analysis. Weak ferromagnetic exchange interaction between high spin d^4 Mn^{III} ions through oximate bridged is known in some of the complexes and in the range of 0.4 to 6.5 cm^{-1}. Intermolecular antiferromagnetic interactions and π-π stackings involving the imidazole rings interactions are negligible due to the larger separations (> 8 A).

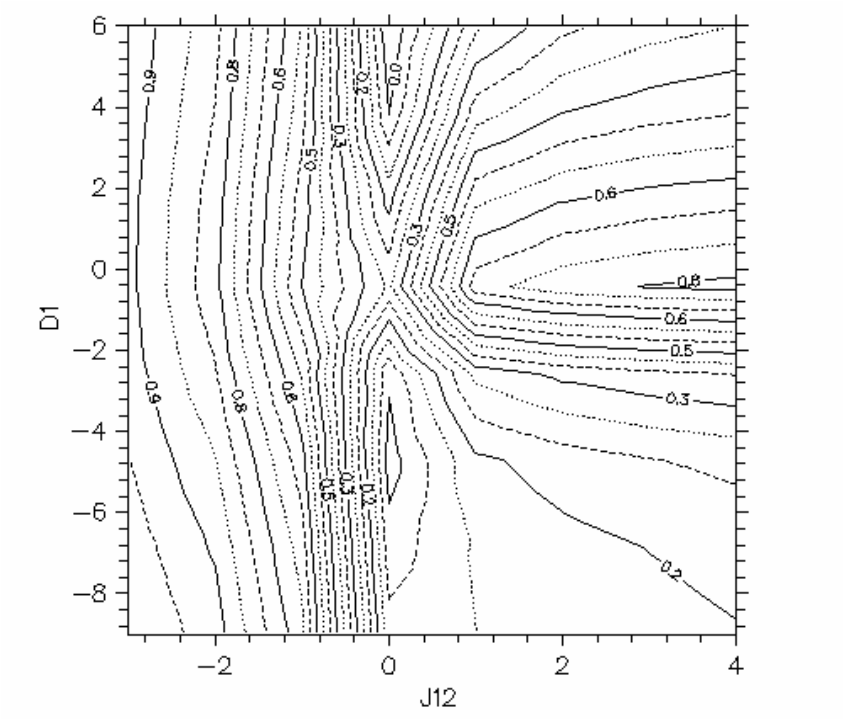

Figure 3.5 Error contour plot (in relative units) obtained for D and J value varied in the range -8 to 6 cm^{-1} and -3.0 to 4.0 cm^{-1}, respectively.

In summary, we have successfully prepared a single oximato-bridged $[Mn^{III}_2]_n$ in a facile way. As far as we are aware, the title complex is the first reported single oximato-bridged 1-D chain Mn^{III} complex. Ferromagnetic Mn^{III}-Mn^{III} coupling stabilizes an $S_T = 4$ ground state and a negative axial zero-field-splitting parameter (D_{Mn}) has been observed. This work shows that the oximato-bridged Mn^{III} complexes should form an interesting system of high-spin molecule. Future work involves the synthesis of more oximato-bridged

Mn^{III} complexes to gain a clear magnetostructural relationship and to improve the magnetic properties.

3.6 Experimental Section

1-H-2-imidazolecarboxaldehyde oxime (^{H}ImOxH)

2-Imidazole carboxaldehyde (2.0 g, 21 mmol) was dissolved in MeOH (25 cm^3), a solution of hydroxylamine hydrochloride (1.6 g, 23 mmol) and NaOH (0.95 g, 23 mmol) in $MeOH{\cdot}H_2O$ (15 cm^3, 2:1 by volume) was prepared and added to the 2-imidazole carboxaldehyde solution. The resulting solution was heated to reflux with stirring for 1 h. After removing methanol a white precipitate began to form. The mixture was cooled and the white precipitate was collected by suction filtration and recrystallized from MeOH. ^{1}H NMR (CD_3OD, 400 MHz): δ 7.08-7.38 (3H), 7.96 (1H); MS: m/z 111 (M^+, 100%); IR (KBr) υ = 3195 (NH), 1625 (CN), 1094, 984 (NO), 1532, 1497, 1440 (imidazole) cm^{-1}.

Elemental Analysis:

	%C	%H	%N
Calculated	43.2	4.5	37.8
Found	43.1	4.6	38.0

$[Mn^{III}_2(^{H}ImOx)_4(CH_3COO)_2]_n$ (3)

To a brown solution of $Mn_3O(CH_3COO)_6(H_2O)_3](CH_3COO)$ (0.66 g, 1 mmol) in MeOH-MeCN (30 mL, 1:1 by volume) solid ^{H}ImOxH (0.33 g, 3 mmol) was added with stirring. The resulting solution was heated to reflux for 1 h yielding a brown solution. On cooling a deep brown microcrystalline solid separated out. X-ray quality crystals in 75% yield grew over two days from a MeOH-MeCN (1:1) solution. IR (KBr): υ = 1636 (CN), 1093 (ClO_4^-), 1003 (NO), 1565, 1512, 1464 (imidazole) cm^{-1}.

Elemental analysis:

	%C	%H	%N	%Mn
Calculated	35.9	3.3	25.2	16.4
Found	35.5	3.4	25.6	16.2

References

1. A. Messerschmidt, R. Huber, T. Poulos, K.Wieghardt, K. Eds. *Handbook of Metalloproteins*; John Wiley and Sons: Chichester, U.K., **2001**.

2. a) O. Kahn, *Molecular Magnetism*; VCH: New York, **1993**; b) O. Kahn, *Adv. Inorg. Chem*. **1995,** *43*, 179.

3. a) G. Christou, D. Gatteschi, D. N. Hendrickson, R. Sessoli, *MRS Bull*. **2000**, 66; b) D. Gatteschi, R. Sessoli, R. *Angew. Chem.,* Int. Ed. **2003**, *42*, 268.

4. J. Krzystek, A. Ozarowski and J. Telser, *Coord. Chem. Rev*. **2006**, *250*, 2308.

5. "*Magneto-Structural Correlations in Exchange Coupled Systems*", Eds. R. D. Willet, D. Gatteschi, O. Kahn, NATO ASI Series C, Vol. 140, Reidel, Dordrecht **1985**.

6. a) P. Chaudhuri, *Coord. Chem. Rev*. **2003**, *343*, 143; b) P. Chaudhuri, *Proc. Indian Acad. Sci*. **1999**, *111*, 397.

7. a) S. Khanra, T. Weyhermüller, E. Rentschler, P. Chaudhuri, *Inorg. Chem.* **2005**, *44*, 8176; b) S. Khanra, T. Weyhermüller, E. Bill, P. Chaudhuri, *Inorg. Chem.* **2006**, *45*, 5911; c) P. Chaudhuri, T. Weyhermüller, R. Wagner, S. Khanra, B. Biswas, E. Bothe, and E. Bill, *Inorg. Chem.* **2007**, *46*, 9003: d) S. Khanra, T. Weyhermüller, P. Chaudhuri, *Dalton Trans*. 2**007**, 4675; e) S. Khanra, B. Biswas, C. Golze, B. Büchner, V. Kataev, T. Weyhermüller, P. Chaudhuri, *Dalton Trans.* 2**006**, 481; f) T. Weyhermüller, R. Wagner, S. Khanra, P. Chaudhuri, *Dalton Trans*. **2005**, 2539

8. a) F. Birkelbach, M. Winter, U. Florke, H.-J. Haupt, C. Butzlaff, M. Lengen, E. Bill, A. X. Trautwein, K. Wieghardt, P. Chaudhuri, *Inorg. Chem.* **1994**, *33*, 3990; b) D. Burdinski, F. Birkelbach, T. Weyhermüller, U. Flörke, H.-J. Haupt, M. Lengen, A. X. Trautwein, E. Bill, K. Wieghardt, P. Chaudhuri, *Inorg. Chem.* **1998**, *37*, 1009; c) F. Birkelbach, T. Weyhermüller, M. Lengen, M. Gerdan, A. X. Trautwein, K. Wieghardt, P. Chaudhuri, *J. Chem. Soc., Dalton Trans*. **1997**, 4529; d) C. N. Verani, E. Rentschler, T. Weyhermuller, E. Bill, P. Chaudhuri, *J. Chem. Soc., Dalton Trans.* **2000**, 4263; e) F. Birkelbach, U. Florke, H.-J. Haupt, C. Butzlaff, A. X. Trautwein, K. Wieghardt, P. Chaudhuri, *Inorg. Chem.* **1998**, *37*, 2000; f) V. V. Pavlishchuk, F. Birkelbach, T. Weyhermüller, K. Wieghardt, P. Chaudhuri. *Inorg. Chem.* **2002**, *41*, 4405; g) P. Chaudhuri, E. Rentschler, F. Birkelbach, C. Krebs, E. Bill, T. Weyhermüller, U. Flörke, *Eur. J. Inorg. Chem.* **2003**, 541; h) S. Ross, T. Weyhermüller, E. Bill, K. Wieghardt, P.

Chaudhuri, *Inorg. Chem.* **2001**, *40*, 6656; i) S. Ross, T. Weyhermüller, E. Bill, E. Bothe, U. Flörke, K. Wieghardt and P. Chaudhuri, *Eur. J. Inorg. Chem.* **2004**, 984; j) C. N. Verani, E. Bothe, D. Burdinski, T. Weyhermüller, U. Flörke, P. Chaudhuri, *Eur. J. Inorg. Chem.* **2001**, 2161.

9. a) T. Afrati, C. Dendrinou-Samara, C. P. Raptopoulou, A. Terzis, V. Tangoulis, D. P. Kessissoglou, *Angew. Chem., Int. Ed***. 2002**, *41*, 2148, b) S. G. Sreerama, S. Pal, *Inorg. Chem*. **2002**, *41*, 4843, c) C. J. Milios, A. Vinslava, W. Wernsdorfer, S. Moggach, S. Parsons, S. P. Perlepes, G. Christou, E. K. Brechin. *J. Am. Chem. Soc.* **2007**, *129*, 2754; d) C. J. Milios, A. Vinslava, W. Wernsdorfer, A. Prescimone, P. A. Wood, S. Parsons, S. P. Perlepes, G. Christou, E. K. Brechin. *J. Am. Chem. Soc.* **2007**, *129*, 6547; e) C. J. Milios, A. Vinslava, P. A. Wood, S. Parsons, W. Wernsdorfer, G. Christou, S. P. Perlepes, E. K. Brechin. *J. Am. Chem. Soc*. **2007**, *129*, 8; f) T. C. Stamatatos, D. Foguet-Albiol, C. C. Stoumpos, C. P. Raptopoulou, A. Terzis, W. Wernsdorfer, S. P. Perlepes, G. Christou, *J. Am. Chem. Soc.* **2005**, *127*, 15380; g) Y-B. Jiang, H-Z. Kou, R-J. Wang, A-L. Cui, J. Ribas. *Inorg. Chem*. **2005**, *44*, 709; h) C. J. Milios, A. Prescimone, A. Mishra, S. Parsons, W. Wernsdorfer, G. Christou, S. P. Perlepes, E. K. Brechin, *Chem. Commun***. 2007**, 153.

10. S. Khanra, Ph. D. Thesis, University of Paderborn, **2005**.

11. a) H. Miyasaka, T. Nezu, K. Sugimoto, K.-i. Sugiura, M. Yamashita, and R. Clérac, *Inorg. Chem.* **2004**, *43*, 5486, b) H. Miyasaka, R. Clérac, K. Mizushima, K.-i. Sugiura, M. Yamashita, W. Wernsdorfer, and C. Coulon, *Inorg. Chem.* **2003**, *42*, 8203; c) R. Clérac, H. Miyasaka, M. Yamashita, and C. Coulon, *J. Am. Chem. Soc.* **2002**, *124*, 12837; d) H. Miyasaka, T. Nezu, K. Sugimoto, K.-I. Sugiura, M. Yamashita, R. Clérac, *Chem. E-J.* **2005**, 1592.

12. A. P. Ginsberg, *Inorg. Chim. Acta. Rev.* **1971**, *5*, 45.

13. a) J.-P. Costes, F. Dahan, B. Donnadieu, M.-J. Rodriguez Douton, M.-I. Fernandez Garcia, A. Bousseksou, J.-P. Tuchagues, *Inorg. Chem*. **2004**, *43*, 2736 ; b) S. Mossin, H. Weihe, H. O. Sorenson, N. Lima and R. Sessoli, *Dalton. Trans.* **2004**, 632; c) C. Mantel, H. Chen, R. H. Crabtree, G. W. Brudvig, J. Pecaut, M.-N. Collomb and C. Duboc, *Chem. Phys. Chem,* **2005**, *6*, 541

14. K. Kambe, *J. Phys. Soc. Jpn.* **1950**, *5*, 48.

15. E. Bill, *Max-Planck-Institute for Bioinorganic Chemistry*, Muelheim an der Ruhr, Germany **2005**.

Chapter 4

A Ferromagnetically Coupled Diiron(III) Complex with a m-Phenylenediamine Based Ligand: Spin Polarisation

4.1 Introduction

The last two decades have witnessed an upsurge in studies related to magnetism with the aim of understanding the phenomenon of exchange coupling.[1] Particularly, designed synthesis of multinuclear complexes exhibiting ferromagnetic exchange coupling has attracted the unbeaten interest of inorganic chemists, and deals with two-fold challenges: i) synthesis and ii) control of the mechanism of exchange coupling.[2]

When the interacting centers are sufficiently close so that the exchange interaction is mediated *via* small bridging group like oxo, hydroxo, etc, then the sign of the interaction depends on the relative symmetries of the two magnetic orbitals involved, in accord with the Goodenough-Kanamori rules,[3] and this principle has been exploited in controlling the magnetic properties of polynuclear coordination complexes.[1,4] When the interacting orbitals are not close together, the interaction is more dependent on the orbitals of the bridging ligand in two mechanistic ways: i) superexchange and ii) spin polarization mechanisms. The superexchange mechanism arises from the mixing of the pure metal orbitals with the orbitals of the bridging ligand which suggests magnetic orbitals may not be pure but also have a significant ligand-based component, and in such cases overlap of the magnetic orbitals can still occur.

Another well known strategy to explain the magnetic properties between the interacting paramagnetic centers when they are not close to each other, is the spin polarization mechanism. This mechanism arises from the molecular orbital model proposed by Longuet-Higgins for conjugated alternate hydrocarbons,[5] which results in ferromagnetic coupling between two radicals separated by a m-phenylene bridge. This is due to the two unpaired electrons residing in a pair of mutually orthogonal but degenerate SOMOs.[5a] A consequence of this molecular orbital behavior is the well-known alteration

of α and β spin density induced on the investigated atoms, which has actually been detected and measured in some cases.[5b,c] This simple principle has been the driving force behind the preparation of numerous organic polyradicals exhibiting a very high spin ground state, Figure 4.1a,[5] however this mechanism has received relatively limited attention. The use of m-phenylene based linkages to achieve parallel spin coupling in transition metal complexes has indeed been successful in some cases[2] and anti ferromagnetic interactions have also been reported.[6]

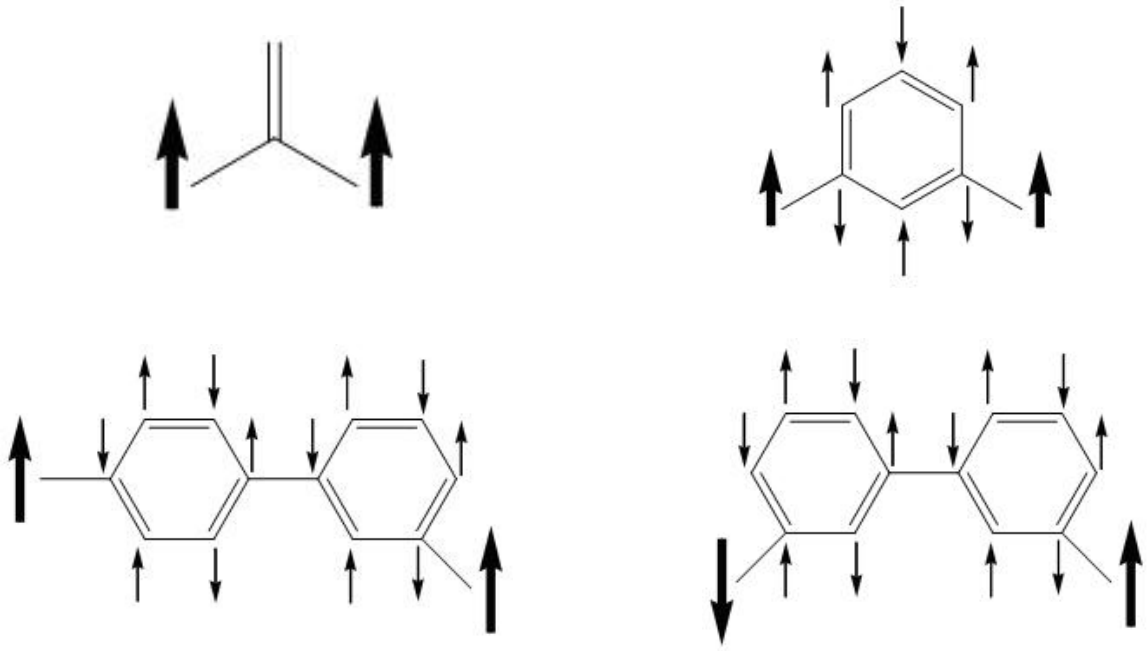

Figure 4.1a A possible scheme for interaction of diradical systems using spin polarization mechanism.

In our research into ligand design as a means to control the electronic and magnetic properties of polynuclear complexes, we prepared the new ligand, *N*'*N*-di(3,5-di-*tert*-butyl-salicylidene)-1,3-diaminobenzene (L"H_2), (Figure 4.1b) using meta phenylenediamine as a linker.[7] This ligand can not act in a tetradentate manner towards a metal ion to give a monomeric unit. Instead, it can self-assemble with metal ions in a 2:2 or 2:3 ratios to give a dimeric metal complex. Here we report a diferric(III)

$[L"_2Fe_2(NO_3)_2]$ **4**, which exhibits ferromagnetic coupling through spin polarization mechanism.

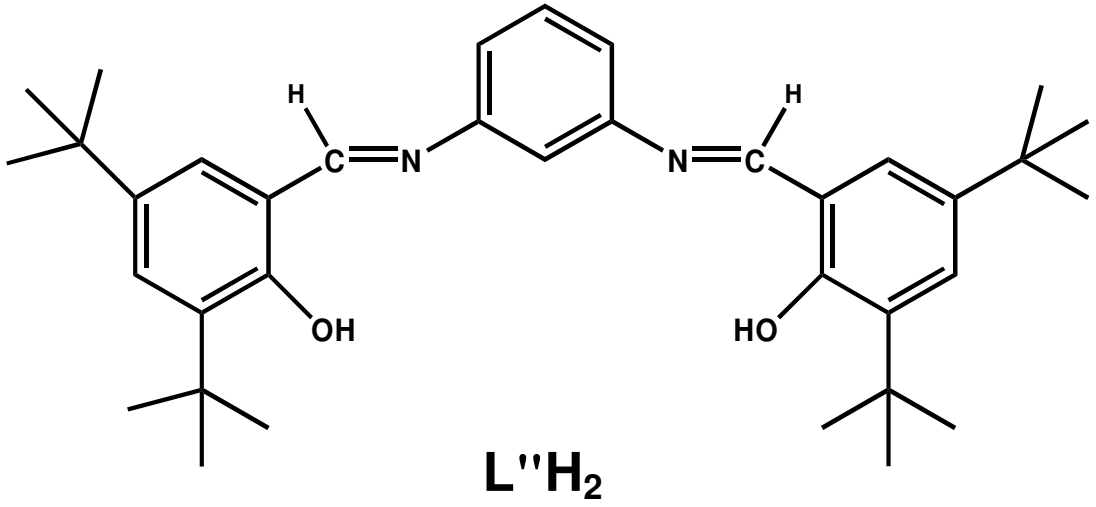

L"H$_2$

Figure 4.1b The structure of *N*'*N*-di(3,5-di-*tert*-butyl-salicylidene)-1,3-diaminobenzene ($L"H_2$).

4.2 Synthesis

The reaction of $Fe^{III}(NO_3)_3.9H_2O$ with $L"H_2$, in a 1:1 ratio in methanol yield dark green solid which is the dinuclear complex $L"_2Fe^{III}_2(NO_3)_2$, **4** (Figure 4.2). X-ray quality crystals of **4** were obtained by diffusion of hexane into a methylene chloride solution of **4**.

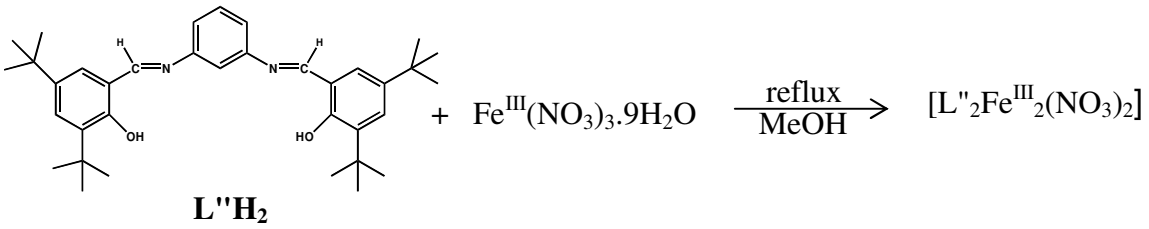

L"H$_2$

Figure 4.2 Synthesis of $L"_2Fe^{III}_2(NO_3)_2$, **4**.

4.3 Infrared Spectroscopy and Mass Spectrometry

The band in the IR spectrum of complex **4** at around 2900 cm^{-1} corresponds to the C-H stretching of the *tert*-butyl groups of the ligand. A strong intense peak at 1384 cm^{-1} is assigned to the N-O stretch of nitrate ions. The absorption peaks at 1577 cm^{-1} and 1534 cm^{-1} are assigned to the C=N and C=C stretches, respectively.

ESI-MS in the positive ion mode has been very successful in characterizing complex **4**. The monopositively charged species $[M\text{-}NO_3]^+$ is observed as the base peak at m/z = 1250.7; an additional peak at m/z = 594.5 is due to the $[M\text{-}2(NO_3)]^{2+}$ ion. Further more, ESI-MS in the negative ion mode was successful in characterizing the $[M+NO_3]^-$ ion, which shows a strong peak at m/z = 1374.8.

4.4 Electronic Spectroscopy

The electronic absorption measurement was performed on a $1x10^{-4}$(M) methylene chloride solution of **4**, shown in Figure 4.3. The electronic absorption spectrum of **4** in dry methylene chloride exhibits a ligand to metal charge transfer (LMCT) band at 635 nm with an extinction coefficient of 11.4 x 10^3 $M^{-1}cm^{-1}$ and a π-π^* transition of the coordinated ligand at 367 nm with an extinction coefficient of 32.0 x 10^3 $M^{-1}cm^{-1}$. No pure d-d transitions are observed due to the d^5 h.s. electronic configuration of the metal.

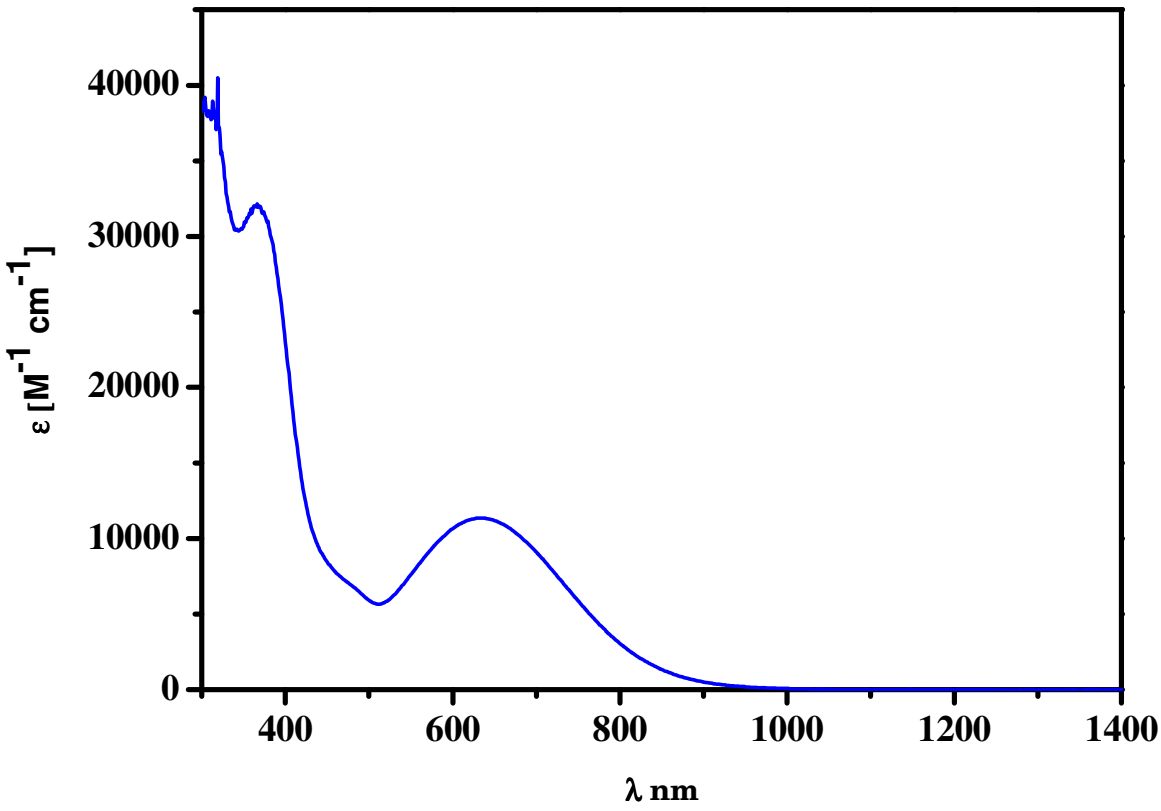

Figure 4.3 Electronic spectrum for complex **4** at room temperature in dry CH_2Cl_2.

4.5 X-ray Structure of $[L''_2Fe_2(NO_3)_2]$

The molecular geometry and atom labeling scheme of **4** are shown in Figure 4.4. Crystallographic analysis of the complex revealed that the structure of **4** can be formulated as $[Fe^{III}{}_2L''_2(NO_3)_2]$. One hexane and one dichloromethane molecule are present as solvent of crystallization. The selected bond distances and angles are listed in Table 4.1.

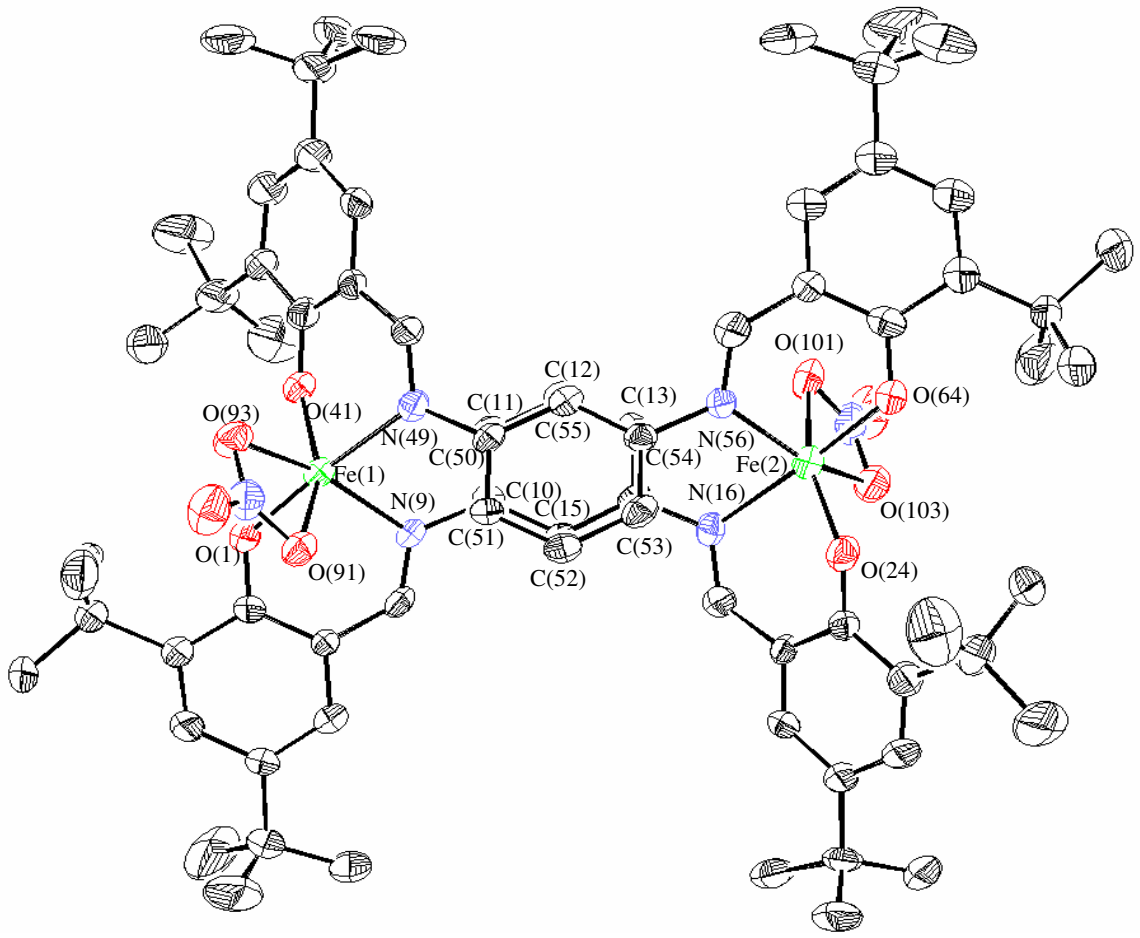

Figure 4.4 An ORTEP plot of $[L''_2Fe_2(NO_3)_2]\cdot CH_2Cl_2\cdot$hexane **4** (40% ellipsoids). H atoms are omitted for clarity.

The neutral molecule **4** contains two FeN_2O_4 hexacoordinated cores separated by a m-phenylene spacer. The coordination geometry of each iron ion is pseudo-octahedral, resulting, from coordination of two oxygen atoms of a chelating nitrate ion, two phenolate oxygen atoms and nitrogen atoms from the m-phenylene linkers. The average values of the Fe-N and Fe-O distances agree well with those reported for high-spin ferric

ions,[8] thus, the average bond lengths are Fe-N at 2.13 ± 0.06 Å, Fe-O (phenoxide) at 1.88 ± 0.01 Å and Fe-O (nitrate) at 2.19 ± 0.06 Å. The Fe-O (nitrate) bond lengths are significantly longer than the Fe-O (phenoxide) bonds which could be because of some ionic character in the Fe-O (nitrate) bonds.

Scheme 4.1 Dimensions of the Metallamacrocyclic Moiety of Complex **4**.

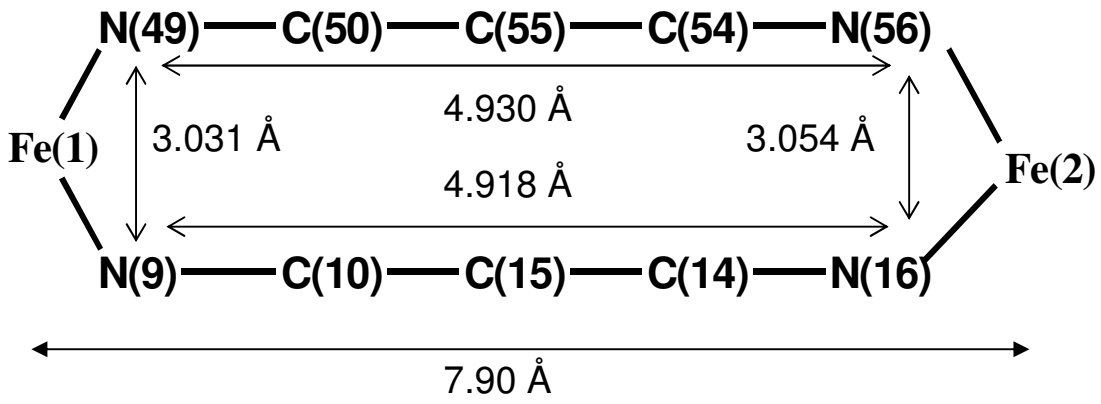

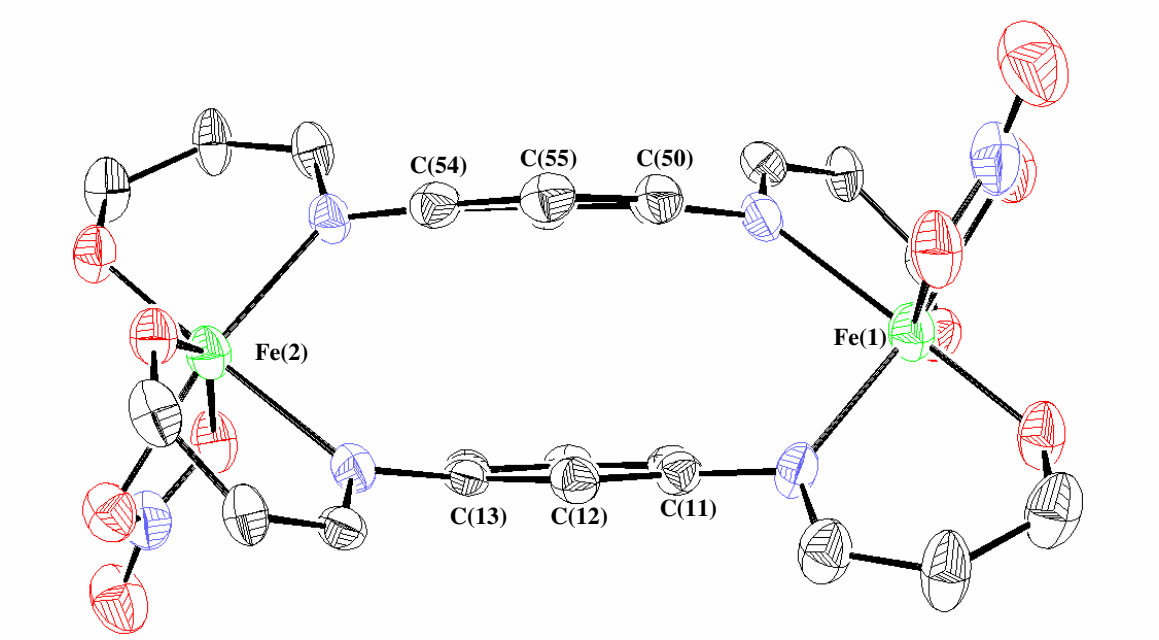

Figure 4.5 Side view of the $[Fe_2(\eta^2{:}\eta^2\text{-L''})_2(NO_3)_2]$ unit of **4** with the relevant dimensions for the metallamacrocyclic moiety.

The deprotonated ligand $[L"]^{2-}$ acts in a bis-bidentate fashion to generate a 12-membered metallmacrocycle, $[Fe_2(\eta^2{:}\eta^2\text{-}L")_2]^{2+}$-unit, which is depicted in Scheme 4.1, and Figures 4.5 and 4.6, the positive charge of which is neutralized by two chelating nitrate monoanions yielding the neutral complex **4** $[L"_2Fe_2(NO_3)_2]$. The intramolecular iron-iron separation, Fe(1)···Fe(2), is 7.90 Å, while the shortest *inter*molecular separation between metals is 7.78 Å. The m-phenylene linkers are almost parallel with a dihedral angle of only 1.1° between the two benzene ring planes with an average interplanar separation of 3.46 Å. In fact, a rather unusual near to perfect face-to-face π-π stacking interaction exists between two aromatic rings; a ring carbon atom e.g. C(55) lies just over another carbon atom *viz*. C(12) of the other ring do not superimpose on that of the other ring. Interestingly, the 1,3-positions of one benzene ring do not superimpose on that of the other ring.

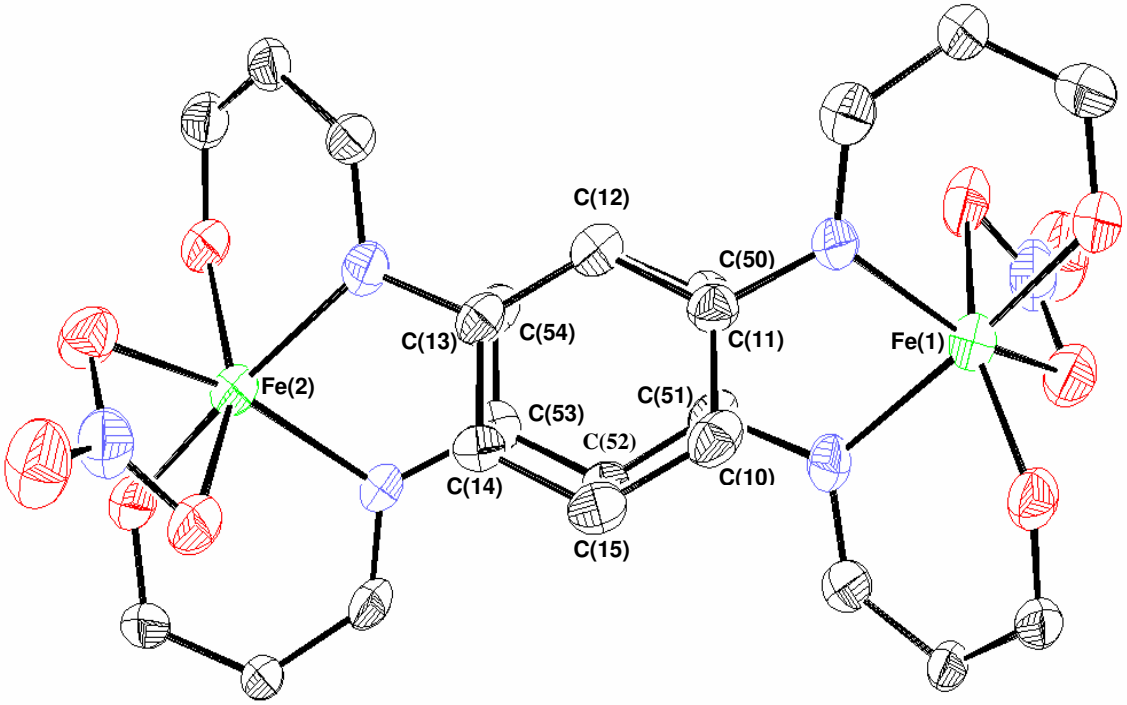

Figure 4.6 Side views of the $[Fe_2(\eta^2{:}\eta^2\text{-}L")_2(NO_3)_2]$ unit of **4** with the relevant dimensions for the metallamacrocyclic moiety.

Table 4.1 Selected Bond Lengths (**Å**) and Angles (deg) of Complex **4**.

Fe(1)-O(41)	1.859(4)	Fe(2)-O(24)	1.863(4)
Fe(1)-O(1)	1.890(4)	Fe(2)-O(64)	1.893(4)
Fe(1)-N(9)	2.088(5)	Fe(2)-N(56)	2.076(5)
Fe(1)-O(93)	2.140(4)	Fe(2)-O(103)	2.129(4)
Fe(1)-N(49)	2.176(5)	Fe(2)-N(16)	2.190(5)
Fe(1)-O(91)	2.229(4)	Fe(2)-O(101)	2.258(5)
Bond Angles (deg)		Bond Angles (deg)	
N(9)-Fe(1)-O(93)	158.5(2)	N(56)-Fe(2)-O(103)	154.2(2)
O(1)-Fe(1)-N(49)	175.3(2)	O(64)-Fe(2)-N(16)	176.4(2)
O(41)-Fe(1)-O(91)	152.4(2)	O(24)-Fe(2)-O(101)	152.8(2)

Inspection of the bond angles at the iron centers indicates that the ideal trans-positioned angles are O(1)-Fe(1)-N(49) at 175.3(2)º and O(64)-Fe(2)-N(16) at 176.4(2)º, showing that the best equatorial planes for the iron centers are O(91)O(93)O(41)N(9)Fe(1) and O(101)O(103)O(24)N(56)Fe(2); the iron centers are displaced only 0.0413 Å from these planes. The two equatorial planes are parallel to each other with an angle of only 0.7º. The iron basal planes are not perpendicular to the benzene plane and there is an angle of 125.4º between them. The nitrate ions are trans to each other (Figure 4.6) and occupy cis-positions, as expected, to the equatorial planes of the iron centers in an asymmetric bidentate (η^2) mode, as shown by one long (viz. Fe(1)-O(91) 2.229(4) Å) and one comparatively short (viz. Fe(1)-O(93) 2.140(4) Å) bond distances.

4.6 Zero-Field Mössbauer Study

The zero-field Mössbauer spectrum of solid **4** at 80 K is shown in Figure 4.7. The Mössbauer spectrum yields an isomer shift $\delta = 0.55$ mm s^{-1} and quadrupole splitting $\Delta E_Q = 1.16$ mm s^{-1}. These values are in complete accord with the d^5 h.s. nature of the ferric centers.[9] The value for the quadrupole splitting is remarkably large in view of the fact that the d^5 configuration has no valence contribution of the electric field gradient;

presumably this reflects the ionic nature bonds to the iron-nitrate bonds in contrast to the covalence of the other ligands.

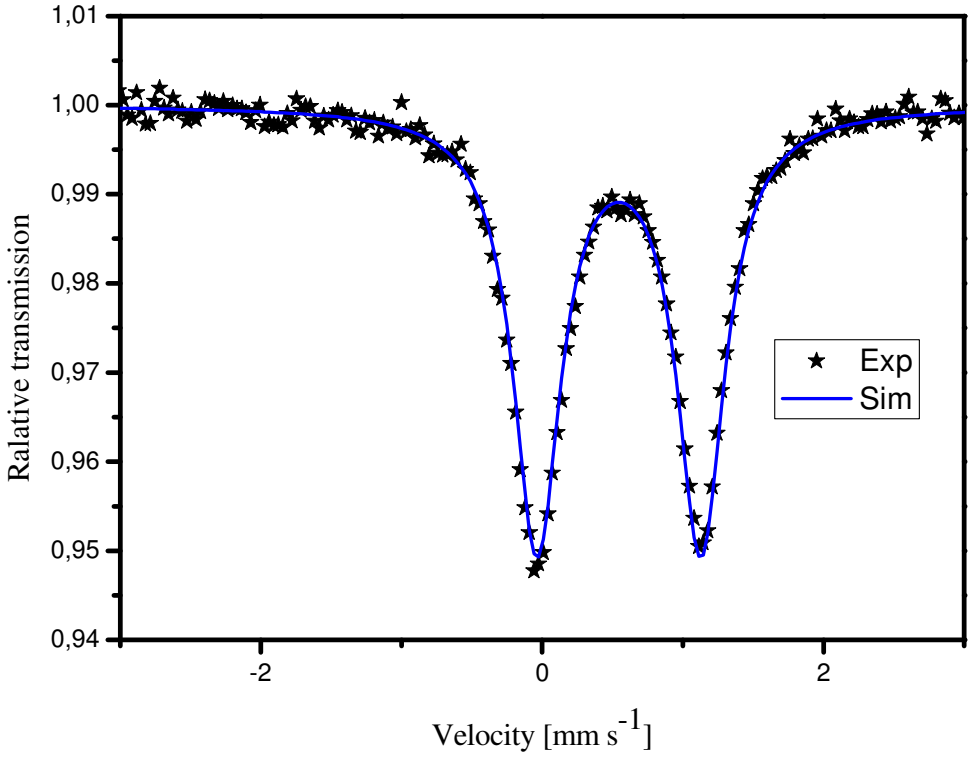

Figure 4.7 Mössbauer spectrum of **4** at 80 K.

4.7 Magnetic Properties

The magnetic susceptibility data for a polycrystalline dried sample of **4** were collected in the temperature range 2–290 K in an applied magnetic field of 1 T, and a plot of μ_{eff} (magnetic moment) *vs*. *T* (temperature) is displayed in Figure 4.8. At 290 K, the effective magnetic moment, μ_{eff}, is equal to 8.39 μ_B ($\chi_M T$ = 8.789 cm^3 mol^{-1} K) which is identical to the high temperature limit expected for two magnetically weakly interacting iron(III) ions. Upon cooling μ_{eff} continuously increases and reaches a maximum of 9.09 μ_B at about 5 K ($\chi_M T$ = 8.789 cm^3 mol^{-1} K). This magnetic behavior is characteristic of ferromagnetic coupling between the adjacent iron(III) centers within the metallacycle in **4**. Bellow 5 K, μ_{eff} drops to 8.02 μ_B (2 K) due to the combined effects of field saturation, exchange and single ion zero-field splitting.

To further verify the weak ferromagnetic interaction, variable temperature variable field (VTVH) measurements have been performed at 2 – 290 K at 1, 4 and 7 T. The molar magnetization per Fe^{III}_2 cluster at 1, 4 and 7 T are shown in Figure 4.9. Theoretically, when ferromagnetic coupling exists between the paramagnetic centers, the magnetization would saturate more rapidly than that in the uncoupled system. On the other hand, if the coupling is antiferromagnetic, the magnetization would increase less rapidly than that in the uncoupled system. In the case of **4**, the magnetization increases more rapidly than that of the uncoupled system and saturates at 10 Ngβ, confirms the ferromagnetic interaction between the adjacent iron(III) centers.

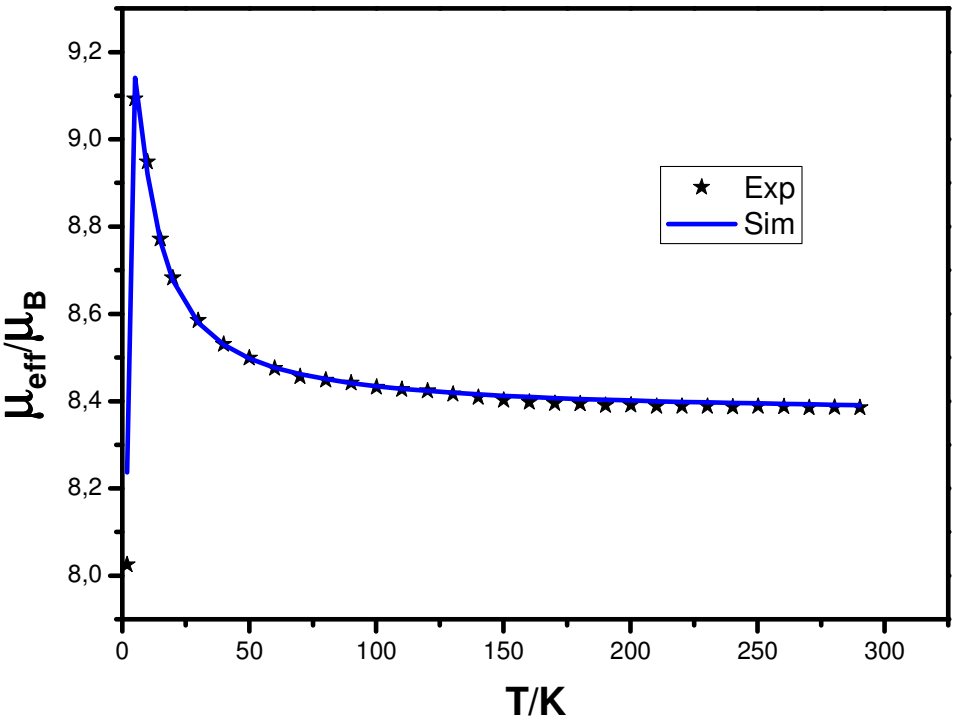

Figure 4.8 Temperature-dependence of the magnetic moment μ_{eff} of **4** at an applied magnetic field of 1 T. The bold points represent the experimental data while the solid line represents the simulation.

The susceptibility and magnetization data were simulated using an in-house package, julX, for exchange coupled systems written by Dr. Eckhard Bill. The simulations are based on the usual spin-Hamilton operator for dinuclear ferric complexes with spin $S_1 = S_2 = 5/2$ (equation 1):

$$\hat{H} = -2J[\hat{\vec{S}}_1 \cdot \hat{\vec{S}}_2] + g\beta(\vec{S}_1 + \vec{S}_2) \cdot \vec{B}$$
$$+ \sum_{i=1,2} D_{Fe}\,[\hat{S}_{i,z}^2 - 1/3\ S(S+1) + E/D_{Fe}\,(\hat{S}_{i,x}^2 - \hat{S}_{i,y}^2)]$$

equation 1

where g_{Fe} is the average electronic g value of the ferric ions, and D_{Fe} and E/D_{Fe} are the axial zero-field splitting and rhombicity parameters. The magnetic moments were obtained from the first order derivative of the eigen values of equation 1. Intermolecular interaction was considered by using a Weiss temperature, Θ_w, as perturbation of the temperature scale, $kT' = k(T - \Theta_w)$ for the calculation. Powder simulations were carried out using a 16-point Lebedev grid.

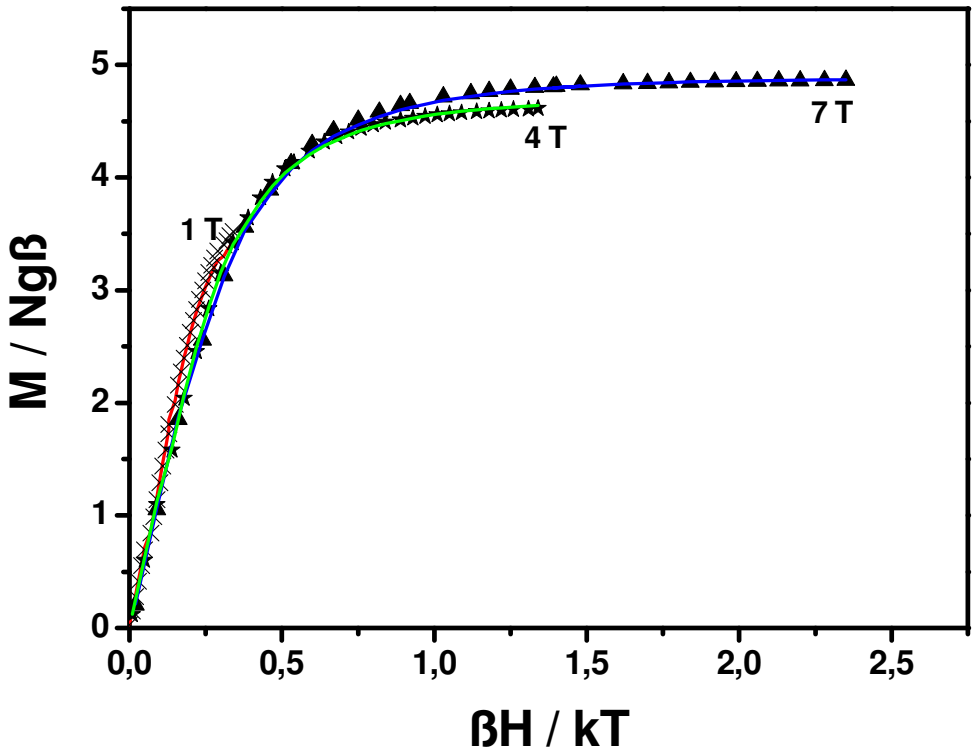

Figure 4.9 Variable temperature variable field (VTVH) magnetic data for **4**, plot of M/Ngß vs. ßH/kT. The bold points represent the experimental data while the solid line represents the simulation.

Simulation of the experimental data, shown as a solid line in Figure 4.8, yields J = 0.195 cm^{-1}, $D_1 = D_2 = 0.9$ cm^{-1}, $g_{Fe} = g_1 = g_2 = 2.00$ (fix.). The VTVH measurements were

also simulated, shown as solid lines in Figure 4.9 with the parameters $J = 0.2$ cm^{-1}, $D_1 = D_2 = 0.9$ cm^{-1}, $g_{Fe} = g_1 = g_2 = 2.00$ (fixed) for the single-ion g values, axial zero-field splitting parameter and the exchange coupling constant. No other parameters were invoked to obtain the excellent fits, particularly no TIP (temperature-independent paramagnetism) was necessary, or Θweiss to account for inter-molecular interactions. However, since we were uncertain about the possible co-variances of D_{Fe} and J, we calculated a two-dimensional error surface as a function of the two parameters to ensure that there was only one solution. From the two-dimensional error surface calculation we could get an idea of how many possible solutions are there. The result, shown in Figure 4.10, nicely demonstrates the true global solution. For further verification we also calculated the-three dimensional error surface as a function of two parameters, D_{Fe} and J, shown in Figure 4.11. Both solutions demonstrate the true global solution and rule out the presence of the other local minima. The range of confidence for the exchange coupling constant is confidently estimated to be J = + 0.2 (±0.05) cm^{-1}.

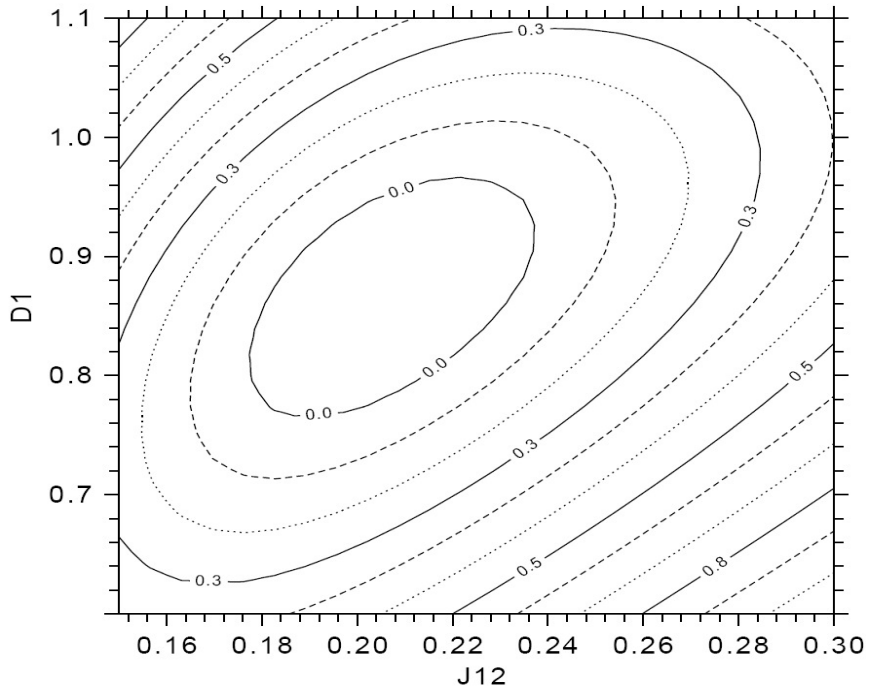

Figure 4.10 Error contour plot (in relative units) obtained for D_{Fe} and J value varied in the range 0.6 - 1.1 cm^{-1}, and 0.14 - 0.30 cm^{-1}.

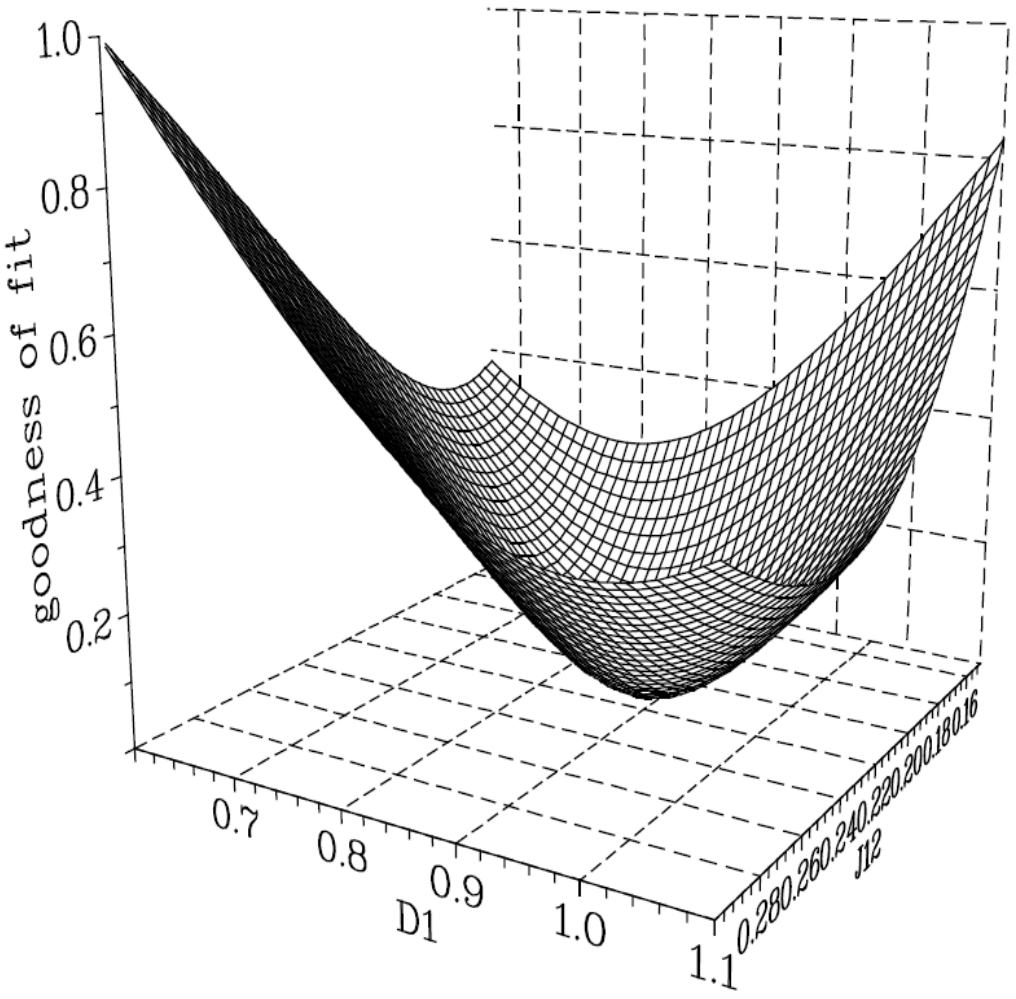

Figure 4.11 Error surface for D_{Fe} and J from spin Hamiltonian simulation for the VTVH measurement of solid **4**. The goodness-of-fit is given in arbitary units.

For further verification of a positive value of J, we carried out an iso-thermal magnetization measurement at 2K in different field, from 0.5 T to 7.0 T. The isothermal measurement is shown in Figure 4.12. The best values for the spin-Hamiltonian parameters obtained from the corresponding simulations of the iso-thermal magnetization are D_{Fe} = 0.9 cm^{-1}, J = 0.2 cm^{-1}, $g_{Fe} = g_1 = g_2$ = 2.00 (fixed), which are in accord with the μ_{eff}(T) and VTVH data.

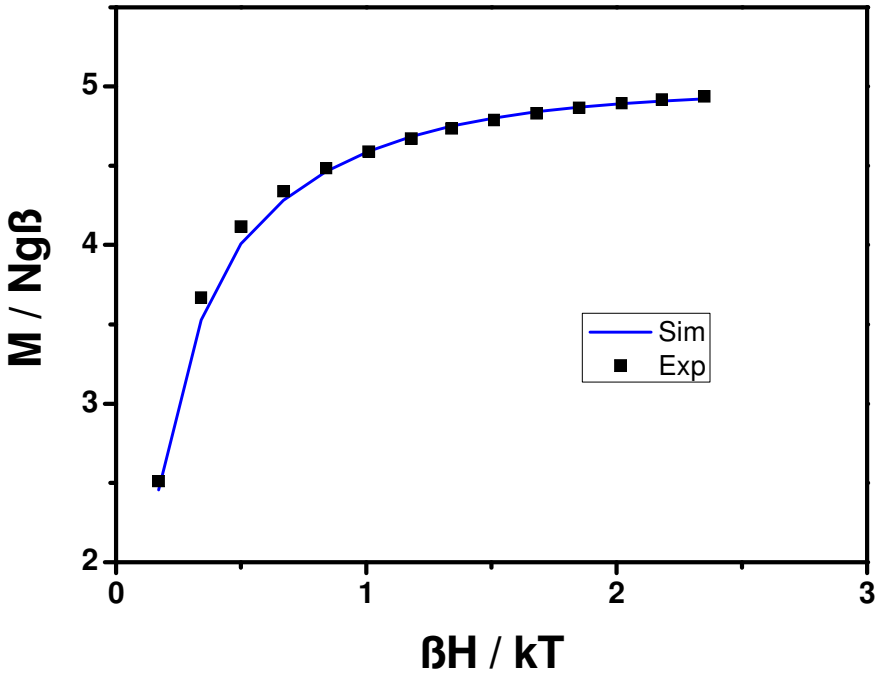

Figure 4.12 An isothermal magnetization measurement performed at 2K. The bold points represent the experimental data while the solid line represents the simulation.

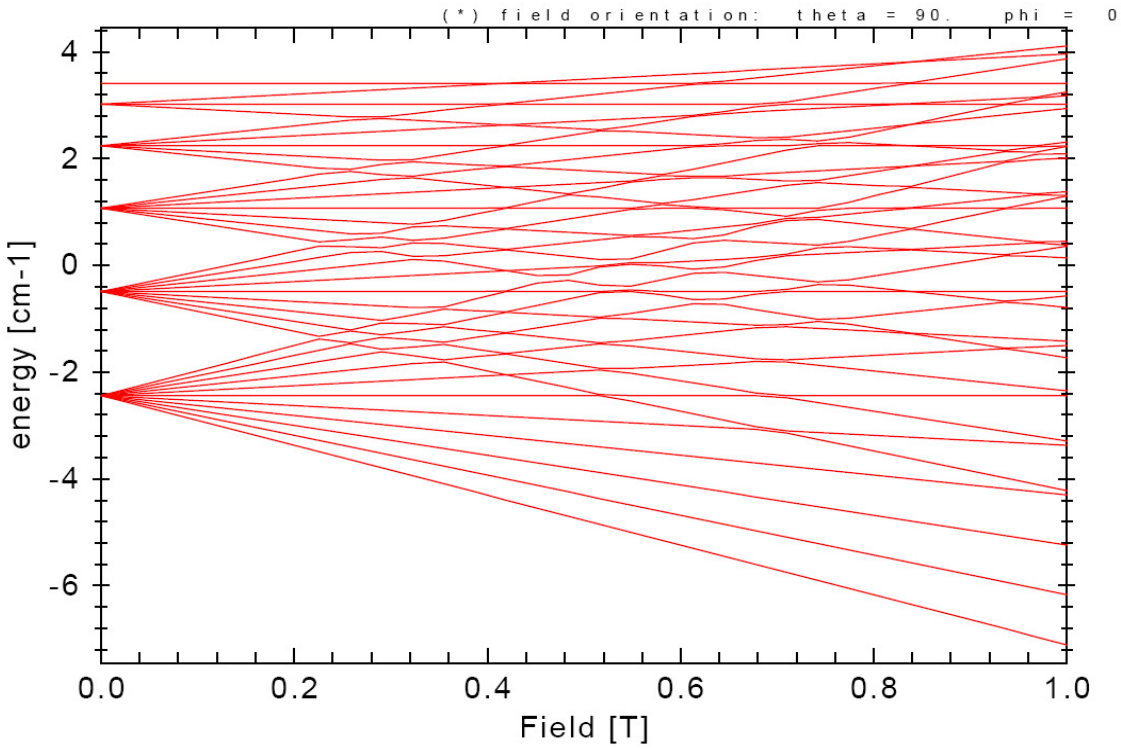

Figure 4.13 Energy level plots for complex **4**, as calculated with the spin-Hamiltonian for a symmetric dimmer with $J = 0.2$ cm^{-1}, $D_{Fe} = 0$ cm^{-1} (fix.), $g_{Fe} = 2$.

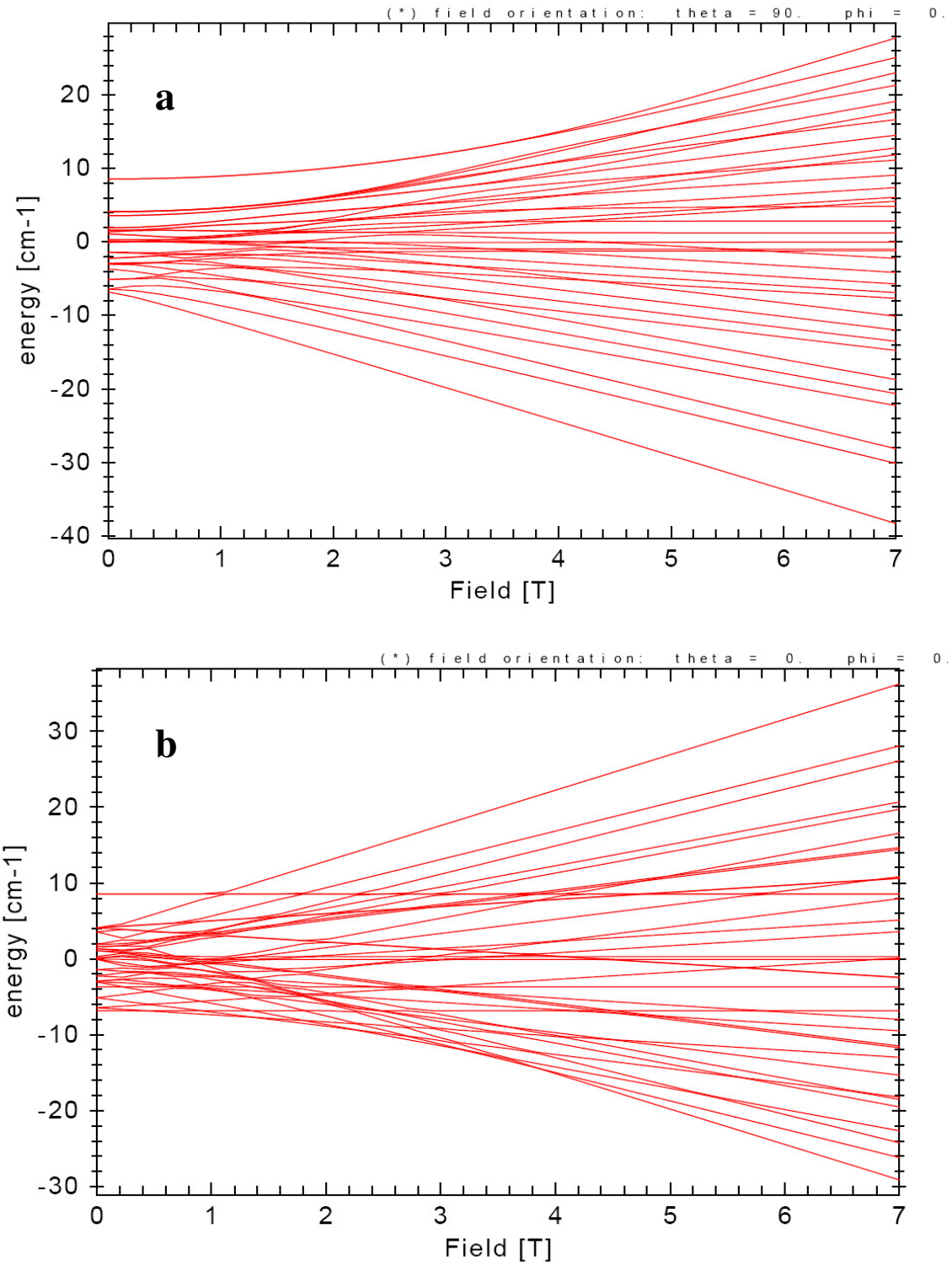

Figure 4.14 Energy level plots for complex **4**, as calculated with the spin Hamiltonian for a symmetric dimmer with $J = 0.2$ cm^{-1}, $D_{Fe} = 0.9$ cm^{-1}, $g_{Fe} = 2$, and for applied fields parallel to the x-axis (**a**) and y-axis (**b**) of the zero-field interaction.

In this case the zero-field splitting parameter, D_{Fe}, for iron(III) in **4** is larger than the ferromagnetic exchange coupling constant J of the dimer. This means the competing zero-field and exchange interactions mix the total spin manifolds (shown in Figure 4.13 and Figure 4.14), and thus, S_{total} and $M_{s,\ total}$ are no longer good quantum numbers. Therefore we refrain from describing our system as having an $S_{total} = 5$ ground state. The mixing of the levels with crossings and avoided crossings for fields applied to our dimer in different directions is shown in level plots given in Figure 4.14. We note also that a field dependent magnetization performed at 2 K shows saturation at the level expected for an isolated ground state with $S_{total} = 5$ (Figure 4.12), but that should not be misinterpreted; since two weakly uncoupled or coupled spins of $S_{Fe} = 5/2$ would exhibit the same behavior.

As the shortest *inter*molecular separation between the iron centers is 7.78 Å for complex **4**, spin coupling devoid of any intervening atoms can be neglected. The iron(III) atoms are in a high-spin state, so the iron centers have both d_σ- and d_π spins. There are two contributions to magnetic interactions. The two iron atoms are isolated by two nitrogen and three carbon atoms. This makes a direct overlap of the magnetic orbitals (the d_σ spins on the iron atoms) negligible, which leads to the absence of an antiferromagnetic exchange interaction through a σ pathway. As the iron basal planes are not perpendicular to the spacer m-phenylene rings, and the intramolecular separation is as long as 7.90 Å, the ferromagnetic coupling observed in **4** can not be attributed to the mechanism based on orbital symmetry. The second contribution is the propagation of the ferromagnetic interaction due to the spin polarization by the d_π spins of the p_π electrons on the organic ligands, which has been analyzed by the DFT calculation.

4.8 Magnetic Mössbauer Spectroscopy

The nature of the magnetic ground state of the dimer, **4**, was also investigated 'microscopically' by Mössbauer spectroscopy at liquid helium temperature with applied fields of 1 – 7 T, (Figure 4.15). The hyperfine patterns show large magnetic splitting due to the presence of strong internal fields of about 51.6 T, as expected for monomeric ferric complexes, or ferromagnetically coupled dimers.[9] The large splitting particularly rules out again anti-ferromagnetic spin coupling, because this would generate non-magnetic

ground state levels, so that components with small splitting only from the applied field would superimpose the inner part of the spectrum at v = ± 2 mms^{-1}. The persistent large splitting for all applied fields and the sharp lines with a clear quadrupole shift (difference between peaks 1, 2 and 5, 6 Figure 4.15) indicate an 'easy axis' of magnetization. This can be induced only by a sizable zero-field interaction. These spectra were simulated by using the electronic spin-Hamiltonian of eq. 1, together with the usual nuclear Hamiltonian for the hyperfine interactions of the ^{57}Fe nuclei: (equation 2):

$$\hat{H}_{nuc} = \hat{\vec{I}} . \overline{\overline{A}} . \hat{\vec{S}} - g_N \beta_N \hat{\vec{I}} . \vec{B} + \hat{\vec{H}}_Q \qquad \textbf{equation 2}$$

where **I.A.S** is the magnetic hyperfine coupling which connects **S** an the nuclear spin **I**, and **A** is the hyperfine coupling tensor. The nuclear quadrupole interaction is given by equation 3:

$$H_Q = eQV_{zz}/4I(2I - 1)\left[3\hat{\vec{I}}_z^2 - I^2 + \eta(\hat{\vec{I}}_x^2 - \hat{\vec{I}}_y^2)\right] \qquad \textbf{equation 3}$$

where Q is the quadrupole moment and V_{zz} and η are the main component and the asymmetry parameter of the electric field gradient tensor. In zero-field condition the quadrupole splitting is given by equation 4:

$$\Delta E_Q = eQV_{ZZ}/2\sqrt{1 + \eta^2/3} \qquad \textbf{equation 4}$$

The best values for the spin-Hamiltonian parameters obtained from the simulations of the magnetic Mössbauer spectra are D_{Fe} = 0.8 (± 0.15) $cm^{-1}$and J = 0.25 (± 0.1) cm^{-1}, which are in nice accord with the SQUID result. The introduction of rhombic contribution to the zero field-field interaction, E/D = 0.3, was necessary to account for the magnetic anisotropy, (as is often observed, this term could not be resolved from the 'macroscopic' SQUID magnetization data of powder samples.) Moreover, the magnetic hyperfine coupling constants obtained with the usual nuclear spin Hamiltonian (eq. 2) for ^{57}Fe are $\mathbf{A}/g_N\mu_N$ = (-21.6, -19.4, -20.9) T. We find the anisotropy of A relatively large for ferric ions, but that is in apparent agreement with the large (positive) quadrupole splitting, and also results from the anisotropy in the covalent bonds of the iron. From the

magnetic spectra also the sign of the quadrupole interaction and asymmetry parameter (η = 0.2) of the electric field gradient could be determined and were shown to be positive.

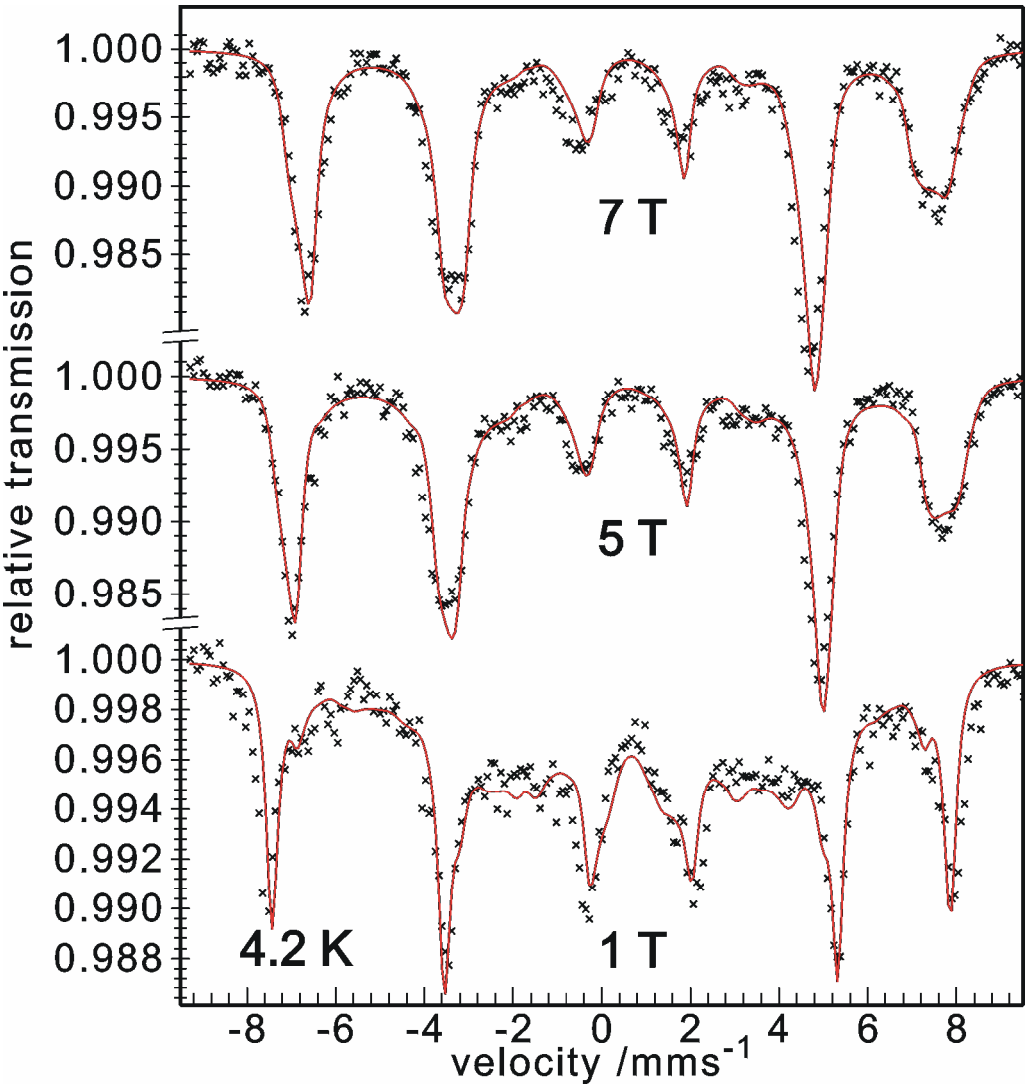

Figure 4.15 Mössbauer spectra of solid **4** recorded at 4.2 K with applied fields of 1, 5 and 7 T. The bold points represent the experimental data while the solid line represents the simulation.

4.9 DFT Calculations

The spin-polarization mechanism predicts a sign alternation of spin densities on adjacent bridging atoms of the ligand. Experimental geometry of complex **4** was used to perform the density functional theory (DFT) calculations for S = 5 high spin state. We applied the Gaussian03 suit of programs[10] and the unrestricted B3LYP[11] DFT scheme as activated by the Gaussian method keyword UB3LYP. The Fe and the directly bonded O and N atoms were described by the (TZVP) basis set.[10,12] Thus, for all atoms directly involved in coordination, a rather flexible set has been used. The remaining C and H atoms have been treated by means of the split valence polarization (SVP)[10,12] and split valence (SV)[10,12] basis sets, respectively. Mulliken spin densities on all the atoms are shown in Table 4.2. To simplify, only two iron atoms and one connecting group are shown below (Figure 4.16). The largest spin density is computed for the iron atoms. The spin densities at the imine nitrogens have the same sign as the iron atom, indicating spin delocalization toward the donor atoms. The spin densities at both iron atoms have the same sign, resulting in a net ferromagnetic exchange. The very weak nature of the coupling results from various competing exchange coupling paths arising from the highest number of unpaired electrons (five) possible for a transition metal center and the path length of the intervening atoms involved.

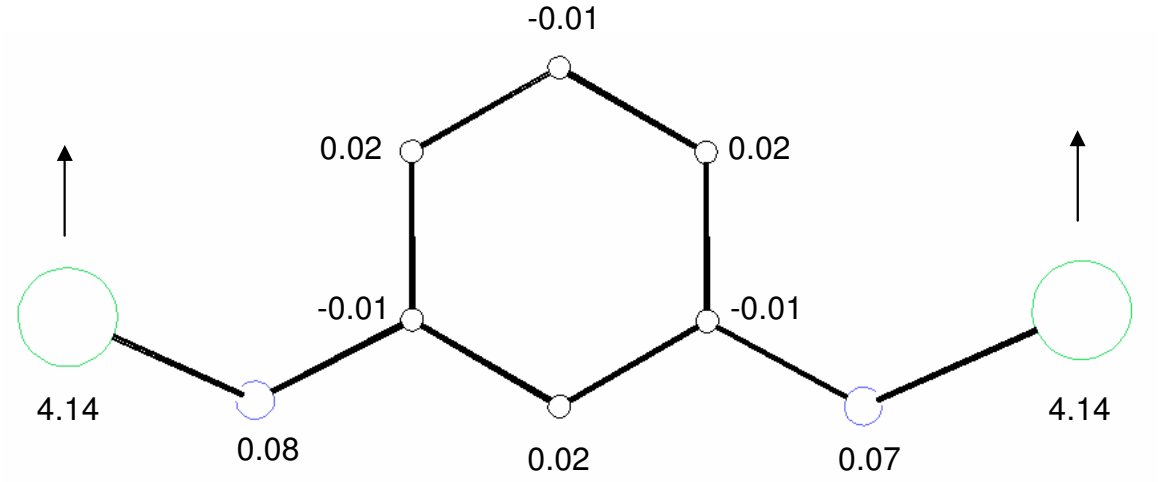

Figure 4.16 Spin-density distribution in the bridging atoms of **4** for the S = 5 state.

Table 4.2 Mulliken Spin Densities of Selected Atoms of Complex **4**.

Atom	Mulliken spin density	Atom	Mulliken spin density
Fe(1)	4.14	Fe(2)	4.14
O(1)	0.20	O(41)	0.21
C(2)	-0.02	C(42)	-0.03
C(3)	0.04	C(43)	0.05
C(4)	-0.02	C(44)	-0.03
C(5)	0.04	C(45)	0.05
C(6)	-0.02	C(46)	-0.02
C(7)	0.04	C(47)	0.05
C(8)	-0.02	C(48)	-0.02
N(9)	0.08	N(49)	0.07
C(10)	-0.01	C(50)	-0.01
C(11)	0.02	C(51)	0.02
C(12)	-0.01	C(52)	-0.01
C(13)	0.02	C(53)	0.02
C(14)	-0.01	C(54)	-0.01
C(15)	0.02	C(55)	0.02
N(16)	0.07	N(56)	0.08
C(17)	-0.02	C(57)	-0.02
C(18)	0.05	C(58)	0.04
C(19)	-0.02	C(59)	-0.02
C(20)	0.05	C(60)	0.03
C(21)	-0.03	C(61)	-0.02
C(22)	0.05	C(62)	0.04
C(23)	-0.03	C(63)	-0.02
O(24)	0.21	O(64)	0.20

4.10 Experimental

***N'N*-di(3,5-di-*tert*-butyl-salicylidene)-1,3-diaminobenzene (L''H_2)**

To a solution of 1,3-diaminobenzene (1.08 g; 10 mmol) in methanol (50 mL), 3,5-di-tert-butylsalicylaldehyde (4.65 g; 20 mmol) was added with stirring. The resulting mixture was refluxed for 2 h yielding a yellow precipitate, which was collected by filtration and recrystallized from acetone-water. Yield: 5.0 g (90%). m.p. 181-183 °C. EI-MS: m/z, 540 (100%) $[M]^+$, 525 (62.5%) $[M\text{-}CH_3]^+$, 497 (13.6%) $[M\text{-}C(CH_3)_2]^+$. ^1H NMR (CD_2Cl_2, 400 MHz): δ, ppm = 1.34 (18 H, s, ^{t}Bu), 1.47 (18 H, s, ^{t}Bu), 7.26-7.49 (8H, m, Ar), 8.75 (2H, s, HC=N). IR (KBr, cm^{-1}): 3450, 2956, 2906, 2869, 1621, 1572, 1467, 1439, 1390, 1361, 1273, 1251, 1148, 965, 879, 770, 684, 643.

Elemental analysis:

	%C	%H	%N
Calculated	80.0	8.9	5.2
Found	79.7	8.8	5.3

[Fe_2L''$_2(NO_3)_2$] (4)

A methanolic (40 mL) solution of $Fe(NO_3)_3{\cdot}9H_2O$ (0.40 g; 1 mmol) and H_2L'' (0.54 g; 1 mmol) was refluxed for 1 h yielding a green solution. On cooling a green microcrystalline solid separated out. X-ray quality crystals in 75 % yield grew over two days from a dichloromethane-hexane (2:1) solution. MS-ESI (pos.) in CH_2Cl_2: m/z, 1250.7 (100%) $[M\text{-}NO_3]^+$, 594.5 (~90%) $[M\text{-}2(NO_3)]^{2+}$, MS-ESI (neg.) in CH_2Cl_2: m/z, 1374.8 (100%) $[M+NO_3]^-$. UV-vis in CH_2Cl_2: λ_{max} (ε, M^{-1} cm^{-1}): 635 (11.4 x 10^3), 367 (32.0 x 10^3). IR (KBr, cm^{-1}): 2959, 2902, 2868, 1069, 1577, 1534, 1483, 1462, 1424, 1384, 1272, 1254, 1175, 964, 870, 834, 781, 748, 693, 539.

Elemental analysis:

	%C	%H	%N	%Fe
Calculated	63.9	7.3	5.7	7.5
Found	64.6	7.0	5.7	7.7

References

1. O. Kahn, *Molecular magnetism,* Wiely-VCH, Weinheim, Germany, **1993**.

2. Selected examples: a) V. A. Ung, A. M. W. Cargill Thompson, D. A. Bardwell, D. Gatteschi, J. C. Jeffery, J. A. McCleverty, F. Totti, M. D. Ward, *Inorg. Chem.* **1997**, *36*, 3447; b) T. Ishida, S. Mitsubori, T. Nogami, N. Takeda, M. Ishikawa, H. Iwamura, *Inorg. Chem.* **2001**, *40*, 7059; c) X. Ottenwaelder, J. Cano, Y. Journax, E. Riviére, C. Brennan, M. Nielrich, R. Ruiz-García, *Angew. Chem., Int. Ed.* **2004**, *43*, 850; d) M. Pascu, F. Lloret, N. Avarvari, M. Julve, M. Andruh, *Inorg. Chem.* **2004**, *43*, 5189; e) T. Glaser, M. Heidemeier, S. Grimme, E. Bill, *Inorg. Chem.* **2004**, *43*, 5192; f) F. Lloret, G. De Munno, J. Cano, R. Ruiz, A. Caneshi, *Angew. Chem., Int. Ed.* **1998**, *37*, 135; g) E. Pardo, K. Bernot, M. Julve, F. Lloret, J. Cano, R. Ruiz-García, F. S. Delgado, C. Ruiz-Perez, X. Ottenwaelder, Y. Journaux, *Angew. Chem., Int. Ed.* **2004**, *43*, 2768; h) E. Pardo, J. Faus, M. Julve, F. Lloret, M. C. Munoz, J. Cano, X. Ottenwaelder, Y. Journaux, R. Carrasco, G. Blay, I. Fernandez, R. Ruiz-Garcia, *J. Am. Chem. Soc.* **2003**, *125*, 10770; i) A. R. Paital, T. Mitra, D. Ray, W. T. Wong, J. Ribas-Arino, J. J. Nova, J. Ribas, G. Aromi, *Chem. Commun.* **2005**, 5172; j) I. Fernandez, R. Ruiz, J. Faus, M. Julve, F. Lloret, J. Cano, X. Ottenwaelder, Y. Journaux, M. Carmen Munoz, *Angew. Chem., Int. Ed.* **2001**, *40*, 3039.

3. a) O. Kahn, *Struct. Bonding* **1987**, *68*, 89; b) B. J. Goodenough, *Phys. Rev.* **1955**, *100*, 564; c) J. B. Goodenouh, *J. Phys. Chem. Solids* **1958**, *6*, 287; d) J. Kanamori, *J. Phys. Chem. Solids* **1959**, *10*, 87; e) P. A. Ginsberg *Inorg. Chim. Acta Rev.* **1971**, *5*, 45.

4. See for example: a) P. Chaudhuri, *Coord. Chem. Rev.* **2003**, *243*, 143; b) H. Okawa, H. Furutachi, D. E. Fenton, *Coord. Chem. Rev.* **1998**, *174*, 51; c) P. A. Figato, S. Tamburini, *Coord. Chem. Rev.* **2004**, *248*, 1717.

5. a) J. C. Longuet-Higgins, *J. Chem. Phys.* **1950**, *18*, 265 ; b) H. Iwamura, *Adv. Phys. Org. Chem.* **1990**, *26*, 179; c) A. Rajca, *Chem. Rev.* **1994**, *94*, 871; d) S. Rajca, A. Rajca, *J. Am. Chem. Soc.* **1995**, *117*, 9172; e)A. Rajca, S. Rajca, *J. Am. Chem. Soc.* **1996**, *118*, 8121.

6. a) E. F. Hasty, L. J. Wilson, D. N. Hendrickson, *Inorg. Chem.* **1978**, *17*, 1834; b) T. Ishida, T. Kawakami, S. Mitsubori, T. Nogami, K. Yamaguchi, H. Iwamura, *J. Chem. Soc., Dalton Trans.* **2002**, 3177; c) M. Matsushita, T. Yasuda, R. Kawano, T. Kawai, T.

Iyoda, *Chem. Lett.* **2000**, 812; d) H. Torayama, T. Nishida, H. Asada, M. Fujiwara, T. Matushita, *Polyhedron*, **1997**, *16*, 3787; e) A. Dei, D. Gatteschi, C. Sangregorio, L. Sorace, M. G. F. Vaz, *Inorg. Chem.* **2003**, *42*, 1701; f) A. Mederos, S. Dominguez, R. Hernádez-Molina, J. Sanchiz, F. Brito, *Coord. Chem. Rev.* **1999**, *193-195*, 857 and references therein.

7. a) S. Mukherjee, E. Rentschler, T. Weyhermüller, K. Wieghardt, P. Chaudhuri, *Chem. Commun.* **2003**, 1828; b) S. Mukherjee, T. Weyhermüller, E. Bothe, K. Wieghardt, P. Chaudhuri, *Dalton Trans.* **2004**, 3842.

8. a) F. A. Cotton, G. Wilkinson, C. A. Murillo, M. Bochmann, "*Advanced Inorganic Chemistry*", sixth ed., Wiley-öInterscience, New York, NY, **1999**; b) "*Comprehensive Coordination Chemistry*", ed. G. Wilkinson, R. D. Gillard, J. A. McCleverty, Pergamon Press, Oxford, 1**987**.

9. A. X. Trautwein, E. Bill, E. L. Bominaar, H. Winkler, *Structure and Bonding* **1991**, *78*, 1.

10. Gaussian 03, Revision C.01, M. J. Frisch, G. W. Trucks, H. B. Schlegel, G. E. Scuseria, M. A. Robb, J. R. Cheeseman, J. A, Montgomery, Jr., T. Verven, K. N. Kudin, J. C. Burant, J. M. Millam, S. S. Iyengar, J. Tomasi, V. Barone, B. Mennucci, M. Cossi, G. Scalmani, N. Rega, G. A. Peterson, H. Nakatsuji, M. Hada, M. Ehara, K. Toyota, R. Fukuda, J. Hasegawa, M. Ishida, T. Nakajima, Y. Honda, O. Kitao, H. Nakai, M. Klene, X. Li, J. E. Knox, H. P. Hratchian, J. B. Cross, C. Adamo, J. Jaramillo, R. Gomperts, R. E. Stratmann, O. Yazyev, A. J. Austin, R. Cammi, C. Pomelli, J. W. Ochterski, P. Y. Ayala, K. Morokuma, G. A. Voth, P. Salvador, J. J. Dannenberg, V. G. Zakarzewski, S. Dapprich, A. D. Daniels, M. C. Strain, O. Farkas, D. K. Malick, A. D. Rabuck, K. Raghavachari, J. B. Foresman, J. V. Ortiz, Q. Cui, A. G. Baboul, S. Clifford, J. Cioslowski, B. B. Stefanov, G. Liu, A. Liashenko, P. Piskorz, I. Komaromi, R. L. Martin, D. J. Fox, T. Keith, M. A. Al-Laham, C. Y. Peng, A. Nanayakkara, M. Challacombe, P. M. W. Gill, B. Johnson, W. Chen, M. W. Wong, C. Gonzalez, J. A. Pople, Gaussian, Inc., Wallingford CT, **2004**.

11. a) A. D. Becke, *J. Chem. Phys.* **1993**, *98*, 5648; b) C. Lee, W. Yang, R. G. Parr, *Phys. Rev. B* **1988**, *37*, 785; c) B. Mielchlich, A. Savin, H. Stoll, H. Preuss, *Chem. Phys. Lett.* **1989**, *157*, 200.

12. a) A. Schaefer, H. Horn, A. Ahlrichs, *J. Chem.* **1992**, *97*, 2571; b) A. Schaefer, C. Huber, R. Ahlrichs, *J. Chem. Phys.* **1994**, *100*, 5829.

13. a) ShelXTL, version 5; Siemens Analytical X-ray Instruments, Inc, **1994**; b) G. M. Sheldric; Universtät Göttingen, Germany **1997**.

Chapter 5

A Mixed-Valance Tetranuclear $[V(III)V(IV)]_2$-Complex

5.1 Introduction

Vanadium-cluster chemistry has extraordinary flexibility due to the range of metal oxidation states and coordination geometries. However, the literature is dominated by high-valent, V^{IV}/V^{V} chemistry[1] and there are very few low valent V^{III} or V^{III}/V^{IV} clusters reported[2,3] due to the reducing nature of the V^{III} and the inherent stability of the $[V^{IV}O]^{2+}/[V^{V}O]^{3+}$ ions. The electronic configuration of V^{III} ion is d^2; this d^2, S = 1 ion typically exhibits a large zero-field splitting (ZFS)[4] and, hence, is attractive as a building block toward magnetic materials such as single-molecule magnets. Some V^{III} or V^{III}/V^{IV} clusters are known either with carboxylate or with phosphate containing ligands.[2,3,5] Apart from these with carboxylate or phosphate ligands polynuclear V^{III} complexes are rare.[6-10] There are very few magnetic studies on V^{III} or $V^{III}V^{IV}$ clusters, and detailed magnetic and EPR studies on polynuclear V^{III} or $V^{III}V^{IV}$ clusters still remain a matter of curiosity.

Here we report an interesting example of a valance-trapped tetranuclear $[V^{III}_2V^{IV}_2]$ cluster with the non-carboxylate, non-phosphate *N'N*-di(3,5-di-*tert*-butyl-salicylidene)-1,3-diaminobenzene (L"H_2) ligand. This complex has been characterized by elemental analysis, X-ray crystallography, detailed magnetic studies and a low temperature EPR study. The complex contains two $V^{III}(\mu\text{-}Cl_3)V^{IV}$ units. Complexes with such a $V(\mu\text{-}X_3)V$ are not unknown,[11-23] but there are very few magnetically characterized complexes containing this unit.[17-23]

5.2 Synthesis

The reaction of VCl_3 with $L''H_2$, in a 1:1 ratio in dry THF yielded a dark brown solid (Scheme 5.1). It was established by X-ray and other spectroscopic methods (viz. SQUID, EPR and UV-vis) that the solid was a mixed valance tetranuclear vanadium complex, $[C_6H_4(NH_2)_2][L_2V^{III}{}_2V^{IV}{}_2(\mu\text{-}Cl)_6(Cl)_4]$ (**5**). The reaction and spectroscopic sample preparations were performed under strictly anaerobic condition.

Scheme 5.1 Noteworthy is the Presence of m-Phenylenediamine in the Crystals of **5**.

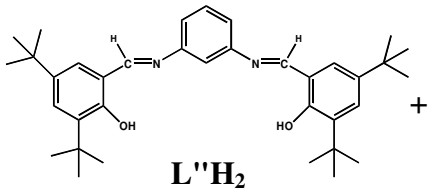

L''H$_2$

$$+ VCl_3 \xrightarrow[THF]{RT} [C_6H_4(NH_2)_2][L''_2V^{III}{}_2V^{IV}{}_2(\mu\text{-}Cl)_6(Cl)_4]$$

Initially, it was supposed that this $C_6H_4(NH_2)_2$ came from the impure ligand, ($L''H_2$), as it had been prepared by the condensation of 1,3-diaminobenzene and 3,5-di-*tert*-butyl-salicylaldehyde. But different spectroscopic methods (viz. IR, NMR, MS) and chromatography showed that no starting material, $C_6H_4(NH_2)_2$, was present there in the bulk ligand system. Additionally during the reaction (Scheme 5.1), 50% of the vanadium ions got oxidized to +IV. Though the actual mechanism of the reaction is unknown, it can be suggested that the hydrolysis of the $L''H_2$ takes place during the reaction with the resultant oxidation of V(III) to V(IV).

5.3 Mass Spectrometry

Electronspray-ionization mass spectrometry (ESI-MS) in the positive ion mode or negative ion modes do not show the characteristic molecular ion peak; however peaks assigned to the fragments of complex **5** are observed. ESI-MS spectra indicate that the complex **5** is stable in solution.

5.4 Electronic Spectroscopy

Electronic absorption measurements were performed on a 8.85×10^{-5}(M) THF solution of **5**, shown in Figure 5.1. The electronic absorption spectrum of **5** consists of three distinct absorption bands at 370 ($\varepsilon/M^{-1}cm^{-1} = 36.0 \times 10^3$), 555 ($\varepsilon/M^{-1}cm^{-1} = 6800$) and 670 nm ($\varepsilon/M^{-1}cm^{-1} = 5000$). It has been shown in Chapter 4 that in the case of the iron complex with the same coordinated ligand, L", one π-π* transition at 367 nm ($\varepsilon/M^{-1}cm^{-1} = 32.0 \times 10^3$) is observed. Additionally the same iron complex exhibits one LMCT at 655 nm ($\varepsilon/M^{-1}cm^{-1} = 11.4 \times 10^3$). For the present vanadium(III) complex, **5**, the band at 370 nm can be assigned unequivocally to a π-π* transition of the coordinated ligand, while the intensity of the band at 555 and 670 nm is rather high for normal d–d transitions.

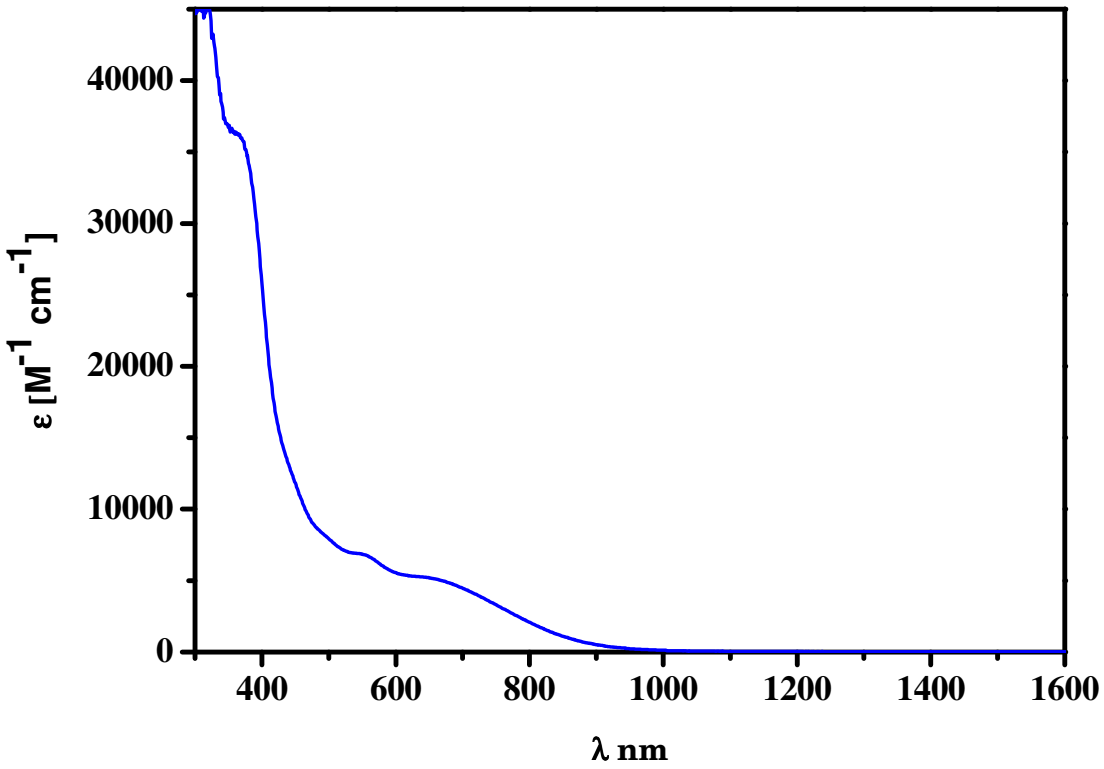

Figure 5.1 Electronic absorption spectrum for complex **5** at room temperature in dry THF.

5.5 X-ray Structure of $[C_6H_4(NH_2)_2][L''_2V_4(\mu\text{-}Cl)_6(Cl)_4]$

The molecular geometry and atom labeling scheme of **5** are shown in Figures 5.2 and 5.3. Crystallographic analysis of the complex revealed that the structure of **5** can be formulated as $[C_6H_4(NH_2)_2][L''_2V_4(\mu\text{-}Cl)_6(Cl)_4]$. 5.5 diethylether molecules are also present as solvent of crystallization. Selected bond distances and angles are listed in Table 5.1.

The X-ray structure confirms that a tetranuclear vanadium complex has indeed been formed. In the structure two dimeric unit, V_2Cl_5, are connected by two deprotonated *N'N*-di(3,5-di-*tert*-butyl-salicylidene)-1,3-diaminobenzene, L", ligands (Figure 5.3). The C-O bond lengths (average 1.332(6) Å) are nearly identical to those for complexes containing a coordinated phenolate anion. The C=N bond lengths (average 1.293(7) Å) are very similar to the C=N bond distances in the free imine ligand.

Complex **5** crystallizes in the space group P-1. The coordination geometry of each vanadium ion is pseudo-octahedral, resulting, from the coordination of three μ_2- bridged chloride ions, one terminal chloride ion, one phenolate oxygen atom and nitrogen atom from the ligand, L". The structure contains two face sharing bioctahedron of V(1)···V(2) and V(3)···V(4) with an average distance of 3.097Å, which is too long for direct metal-metal bonding. The $V_2(\mu\text{-}Cl)_3$ unit is not unusual and it is interesting to see that in different complexes the V-Cl bond lengths are different depending upon their environments.[11-18] Thus it is very difficult to predict the oxidation states of the vanadium ions only based on V-Cl bond distances. However, the shortest V-Cl bond distances in $V(1)(\mu\text{-}Cl)_3$ and $V(3)(\mu\text{-}Cl)_3$ are 2.409(1) Å and 2.415(1) Å, respectively. On the other hand, the shortest V-Cl bond distances in $V(2)(\mu\text{-}Cl)_3$ and $V(4)(\mu\text{-}Cl)_3$ are 2.444(2) Å and 2.438(2) Å, respectively. The oxidation states of the V ions are tentatively assigned +IV for V(1) and V(3) and +III for V(2) and V(4).

One deprotonated ligand coordinates in a bis-bidentate fashion to connect two vanadium ions, V(1) and V(3). Another deprotonated ligand acts in a similar fashion to connect the V(2) and V(4) ions. The m-phenylene linkers are not in a parallel orientation as in complex **4**, (Chapter 4). The dihedral angle between the benzene ring planes is 51.0º. So face-to-face π-π stacking interaction are not possible between the benzene rings of the m-phenylene linkers. Inspection of the bond angles at the vanadium centers

indicates that the ideal trans-positioned angles are N(9)-V(1)-Cl(3) at 179.2(1)º, N(49)-V(2)-Cl(3) at 179.1(1)º, N(16)-V(3)-Cl(13) at 178.8(1)º and N(56)-V(4)-Cl(13) at 178.6(1)º, showing that the best equatorial planes for the vanadium centers are Cl(1)Cl(2)V(1)O(1)Cl(4), Cl(1)Cl(2)V(2)O(41)Cl(5), Cl(11)Cl(12)V(3)O(24)Cl(14), and Cl(11)Cl(12)V(4)O(64)Cl(15); the vanadium centers are displaced only 0.039-0.050 Å from these planes.

Table 5.1 Selected Bond Lengths (Å) and Angles (deg) for Complex **5**.

V(1)-V(2)	3.112(1)	V(3)-V(4)	3.081(1)
V(1)-O(1)	1.842(3)	V(3)-O(24)	1.842(4)
V(1)-N(9)	2.084(4)	V(3)-N(16)	2.075(4)
V(1)-Cl(4)	2.360(2)	V(3)-Cl(14)	2.348(2)
V(1)-Cl(1)	2.409(1)	V(3)-Cl(11)	2.415(2)
V(1)-Cl(2)	2.457(2)	V(3)-Cl(13)	2.447(2)
V(1)-Cl(3)	2.458(1)	V(3)-Cl(12)	2.451(2)
V(2)-O(41)	1.842(4)	V(4)-O(64)	1.845(4)
V(2)-N(49)	2.061(5)	V(4)-N(56)	2.069(5)
V(2)-Cl(5)	2.369(2)	V(4)-Cl(15)	2.370(2)
V(2)-Cl(3)	2.443(2)	V(4)-Cl(11)	2.438(2)
V(2)-Cl(1)	2.446(2)	V(4)-Cl(13)	2.438(2)
V(2)-Cl(2)	2.455(1)	V(4)-Cl(12)	2.445(2)
O(1)-C(2)	1.335(6)	O(41)-C(42)	1.332(6)
C(2)-C(7)	1.389(7)	C(42)-C(47)	1.410(7)
C(2)-C(3)	1.425(7)	C(42)-C(43)	1.414(8)
C(3)-C(4)	1.385(7)	C(43)-C(44)	1.396(8)
C(4)-C(5)	1.396(8)	C(44)-C(45)	1.397(8)
C(5)-C(6)	1.375(8)	C(45)-C(46)	1.373(8)
C(6)-C(7)	1.414(7)	C(46)-C(47)	1.403(7)
C(7)-C(8)	1.431(7)	C(47)-C(48)	1.427(8)
C(8)-N(9)	1.286(6)	C(48)-N(49)	1.298(7)
N(9)-C(10)	1.458(7)	N(49)-C(50)	1.443(7)

C(10)-C(15)	1.365(8)	C(50)-C(55)	1.379(7)
C(10)-C(11)	1.368(8)	C(50)-C(51)	1.383(7)
C(11)-C(12)	1.370(8)	C(51)-C(52)	1.376(8)
C(12)-C(13)	1.377(8)	C(52)-C(53)	1.377(8)
C(13)-C(14)	1.385(8)	C(53)-C(54)	1.375(7)
C(14)-C(15)	1.380(7)	C(54)-C(55)	1.383(7)
N(16)-C(17)	1.292(7)	N(56)-C(57)	1.295(7)
C(17)-C(18)	1.431(8)	C(57)-C(58)	1.437(8)
C(18)-C(23)	1.404(7)	C(58)-C(63)	1.406(8)
C(18)-C(19)	1.413(7)	C(58)-C(59)	1.397(7)
C(19)-C(20)	1.379(8)	C(59)-C(60)	1.366(8)
C(20)-C(21)	1.393(8)	C(60)-C(61)	1.397(9)
C(21)-C(22)	1.385(8)	C(61)-C(62)	1.382(8)
C(22)-C(23)	1.410(8)	C(62)-C(63)	1.410(7)
C(23)-O(24)	1.331(6)	C(63)-O(64)	1.335(6)
Bond Angles (deg)		Bond Angles (deg)	
O(1)-V(1)-N(9)	87.1(2)	O(24)-V(3)-N(16)	87.42(16)
O(41)-V(2)-N(49)	87.2(2)	O(64)-V(4)-N(56)	87.33(17)
V(1)-Cl(1)-V(2)	79.76(5)	V(3)-Cl(11)-V(4)	78.80(5)
V(1)-Cl(2)-V(2)	78.63(5)	V(3)-Cl(12)-V(4)	77.98(5)
V(1)-Cl(3)-V(2)	78.84(5)	V(3)-Cl(13)-V(4)	78.19(5)
N(9)-V(1)-Cl(3)	179.16(14)	N(16)-V(3)-Cl(13)	178.81(14)
Cl(4)-V(1)-Cl(2)	170.60(5)	Cl(14)-V(3)-Cl(12)	171.33(6)
O(1)-V(1)-Cl(1)	174.98(1)	O(24)-V(3)-Cl(11)	173.99(13)
N(49)-V(2)-Cl(3)	179.12(14)	N(56)-V(4)-Cl(13)	178.55(13)
Cl(5)-V(2)-Cl(2)	168.08(6)	Cl(15)-V(4)-Cl(12)	169.06(6)
O(41)-V(2)-Cl(1)	178.35(12)	O(64)-V(4)-Cl(11)	176.25(12)

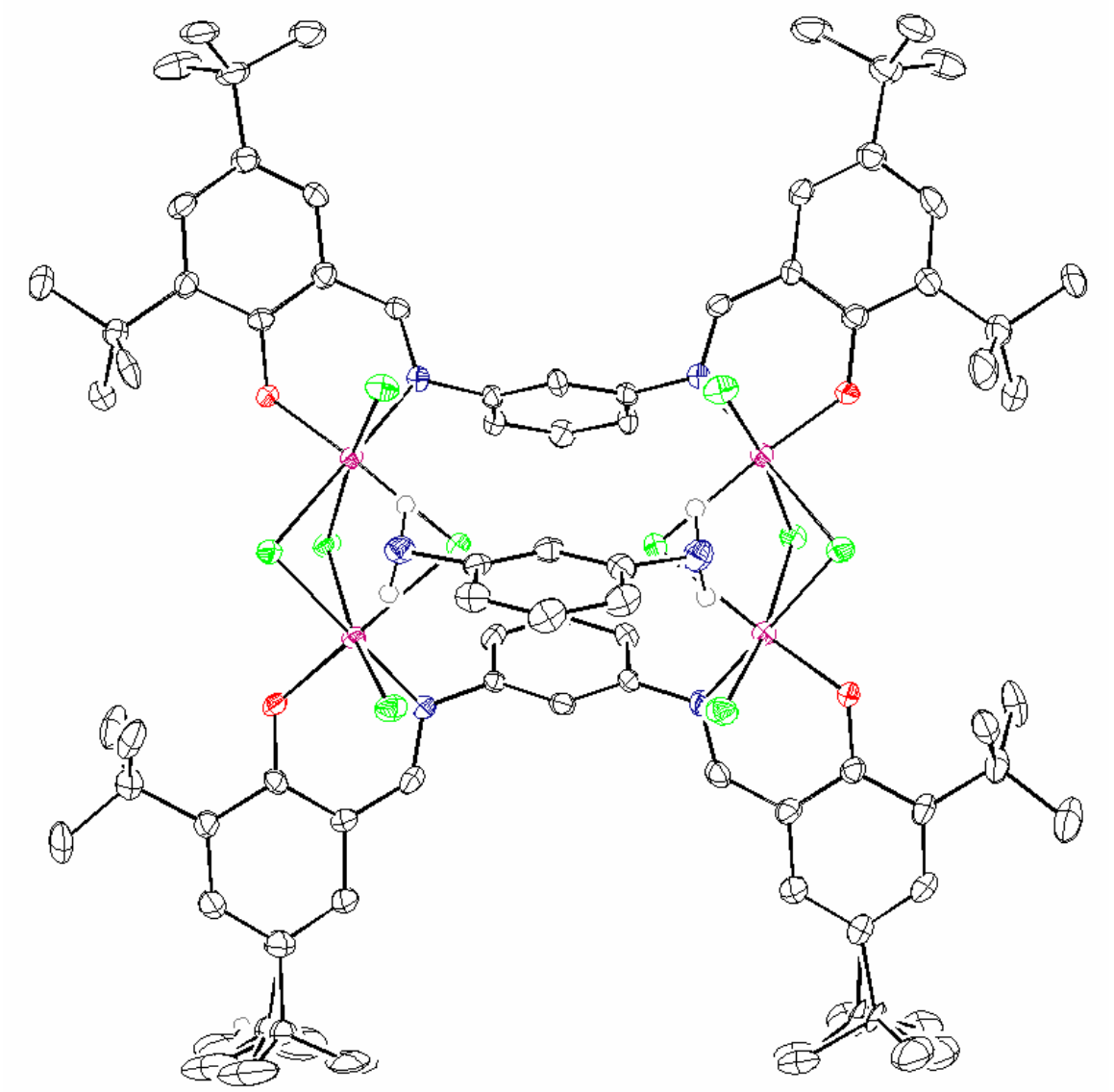

Figure 5.2 An ORTEP plot of $[C_6H_4(NH_2)_2][L"_2V^{III}_2V^{IV}_2(\mu\text{-}Cl)_6(Cl)_4]$ **5** (40% ellipsoids). H atoms are omitted for clarity.

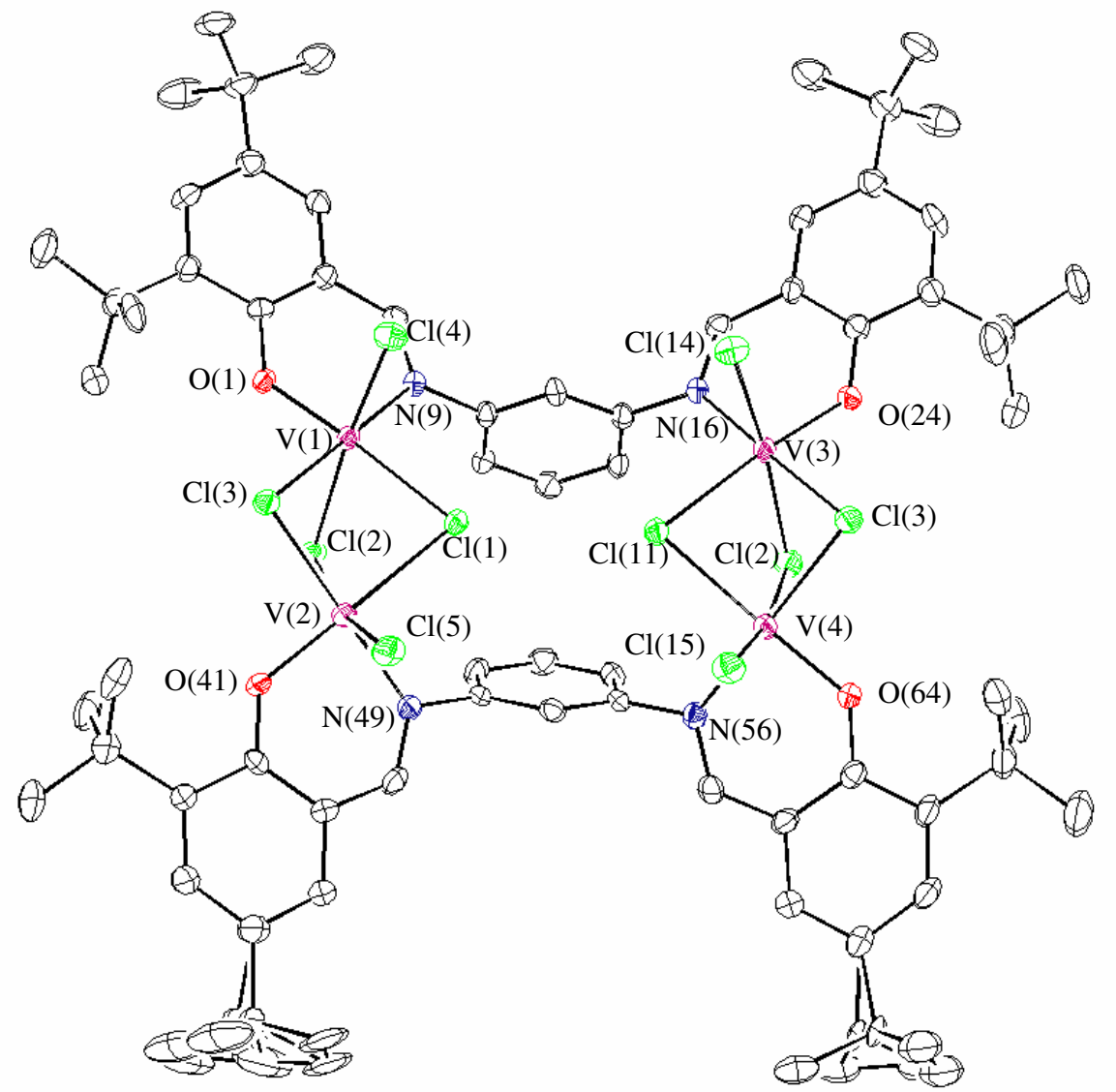

Figure 5.3 An ORTEP plot of $[L"_2V^{III}_2V^{IV}_2(\mu\text{-}Cl)_6(Cl)_4]$ **5** (40% ellipsoids). H atoms are omitted for clarity.

5.6 Magnetic Properties of Complex 5

The magnetic susceptibility data for a dried polycrystalline sample of **5** were collected in the temperature range 2–290 K in an applied magnetic field of 1 T to investigate the nature and magnitude of the exchange interaction propagated by the bridging chloride ligands and also to see the effect of the m-phenylene linker. A plot of μ_{eff} (magnetic moment) *vs*. *T* (temperature) is displayed in Figure 5.4. At 290 K, the effective magnetic moment, μ_{eff}, is equal to 4.14 μ_B ($\chi_M T$ = 2.14 cm^3 mol^{-1} K) which is lower than the high temperature limit expected, 4.69 μ_B, for two magnetically uncoupled vanadium(III) ions and two vanadium(IV) ions. Upon cooling μ_{eff} continuously decreases and reaches a value of 2.16 μ_B at about 5 K ($\chi_M T$ = 0.59 cm^3 mol^{-1} K). This magnetic behavior clearly indicates the presence of an overall antiferromagnetic exchange coupling between the paramagnetic centers in **5**. Below 5 K, μ_{eff} drops to 1.61 μ_B (2 K) due to the combined effects of field saturation, exchange and single ion zero-field splitting.

As is evident from the structure of the V(III)/V(IV) centers in the tetranuclear unit, at least two types of exchange interactions, J_1 and J_2 have to be considered in order to simulate the susceptibility data. J_1 represents the exchange interaction between the two vanadium centers, [V(III)-V(IV)], in a dimeric unit and J_2 represents the exchange interaction between vanadium ions mediated through the m-phenylene linkers. The susceptibility data were simulated using an in-house package, julX, for exchange coupled systems written by Dr. Eckhard Bill. The simulations are based on the Heisenberg spin-Hamilton operator for tetranuclear mixed valance $V(III)_2V(IV)_2$ complex with spin S_1 = S_4 = 1 and S_2 = S_3 = 0.5 (equation 1):

$$H = -2J_1(S_1S_2 + S_3S_4) - 2J_2(S_2S_4 + S_1S_3) \qquad \text{equation 1}$$

A satisfactory simulation, shown as a solid line in Figure 5.4, using a least-squares fitting computer program with a full-matrix diagonalization, is obtained with the parameters $J_1 = J_{12} = J_{34}$ = - 47.6 cm^{-1}, $J_2 = J_{13} = J_{24}$ = +1.5 cm^{-1}, $g_{V(III)} = g_1 = g_4$ = 1.95 and $g_{V(IV)} = g_2 = g_3$ = 1.85. Another simulation was also obtained with the parameters J_1 = - 52.6 cm^{-1}, J_2 = +1.6 cm^{-1}, $g_{V(III)} = g_{V(IV)} = g_1 = g_2 = g_3 = g_4$ = 1.97. There are two types of vanadium ions in **5**, which suggest that there should be different g values for the different oxidation states. Again, applying the spin projection formula ($g_t = 4/3g_{V(III)} - 1/3g_{V(IV)}$),

from the first set of parameters, g_t = 1.982, which is in complete agreement to the g value from the EPR simulation.

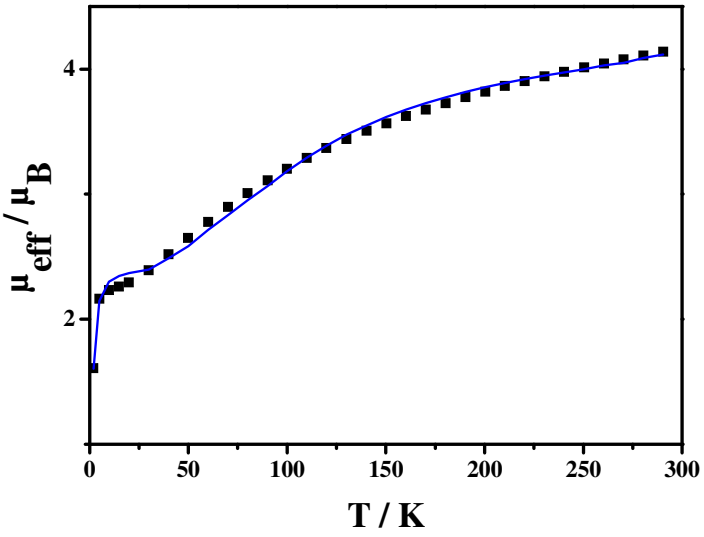

Figure 5.4 Temperature-dependence of the magnetic moment μ_{eff} of **5** at an applied magnetic field of 1 T. The bold points represent the experimental data while the solid line represents the simulation.

Exchange interactions within the $[V_2(\mu_2\text{-}X)_3]^{n+}$ (X = Cl^- or Br^-) ions have been investigated by several groups.[17-23] On the whole a good fit for the experimental data using the Heisenberg spin Hamiltonian (equation 1) could not be obtained. Only spin angular momentum is involved in Heisenberg spin Hamiltonian. However, in O_h symmetry $^3T_{1g}$ is the ground state of the V(III) ion, which suggests the existence of unquenched orbital angular momentum. Thus, the calculated data do not fit well with the experimental data in the entire temperature range. Previously reported values for the $[V_2(\mu\text{-}Cl)_3]^{n+}$ unit are in the range -13.4 to - 75.0 $cm^{-1}$and in our case this value is -47.6 cm^{-1}. J_2 values are very small compared to J_1 values (which can be explained by structural parameters). Interestingly, all attempts to fit the data gave positive values of J_2.

The energy diagram (Figure 5.5) shows that at low magnetic fields the singlet state is the lowest energy state, where as the triplet state is the lowest energy state at high magnetic fields.

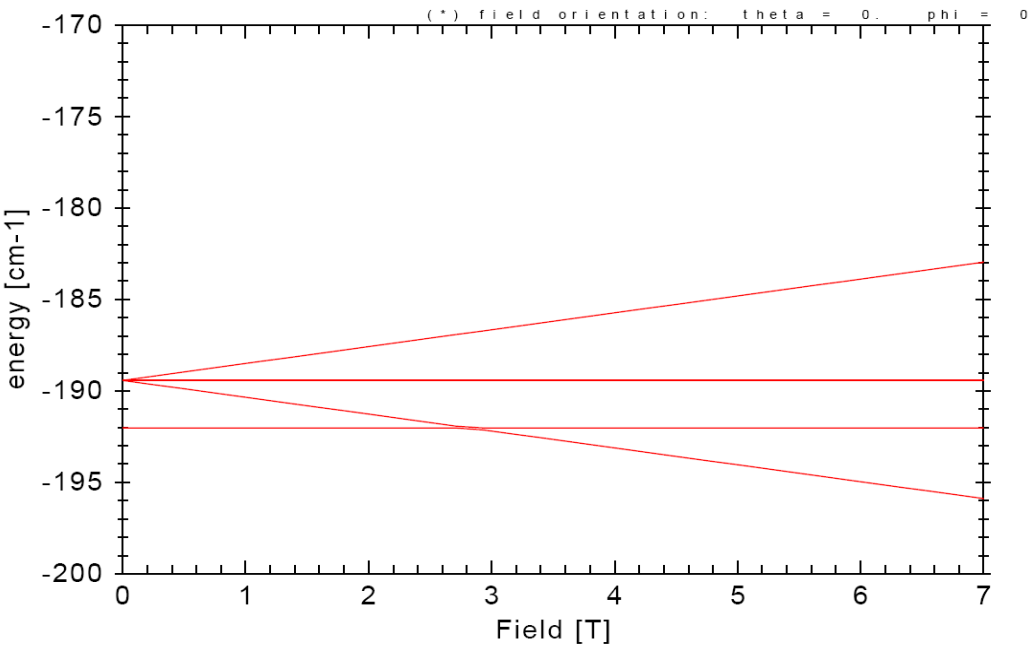

Figure 5.5 Energy level plots for complex **5**, as calculated with the spin Hamiltonian (equation 1) with J_1 = - 47.5 cm^{-1}, J_2 = 1.6 cm^{-1}, $g_{V(III)} = g_1 = g_4 = 1.95$ and $g_{V(IV)} = g_2 = g_3 = 1.85$.

Variable temperature variable field (VTVH) measurements have been performed at 2 – 290 K and at 1, 4 and 7 T. The molar magnetization per $V^{III}_2V^{IV}_2$ cluster at 1, 4 and 7 T is shown in Figure 5.6. From the susceptibility measurement it has been already shown that the energy gap between the singlet and triplet states is only about Δ_{S-T} = 2.5 cm^{-1} (≈ 3.5 K) at zero external field.

Magnetization measurements also give similar information; at 7 T magnetization saturates at around 1 Ngβ to confirm the triplet state. But at lower field (1 and 4 T) the magnetization values are well below 1 Ngβ, which suggests that the triplet and singlet states are very close in energy to each other. The 4 and 7 T measurements at different temperature were simulated with the parameters $S_1 = S_4 = 1.0$, $S_2 = S_3 = 0.5$, $D_1 = D_3 = 44 \pm 2$ cm^{-1}, $J_{12} = J_{34} = -48.0$ cm^{-1}, $J_{14} = J_{23} = 4.5$ cm^{-1}, $g_1 = g_4 = 1.95$ and $g_2 = g_3 = 1.85$ (Figure 5.7). The susceptibility and magnetization measurements suggest that the singlet and triplet states are very close to each other and thus, S_{total} and $M_{s, total}$ are no longer good quantum numbers.

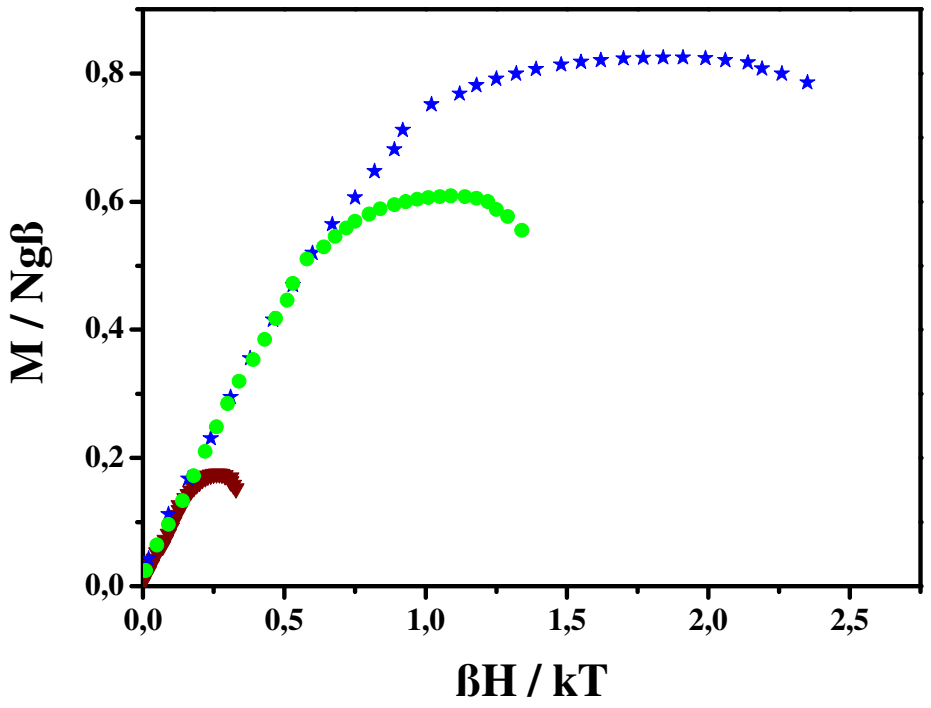

Figure 5.6 Variable temperature variable field (VTVH) magnetic data for **5**, plot of M/Ngß vs. ßH/kT.

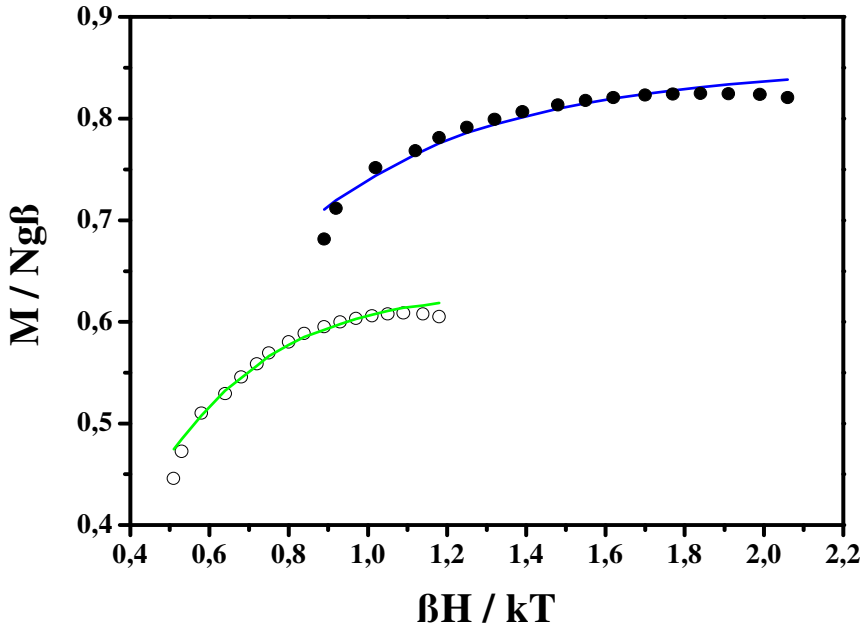

Figure 5.7 Variable-temperature (2.3 – 5.3 K), variable-field (4 and 7 T) magnetization (VTVH) measurements.

5.7 EPR Study of Complex 5

The X-band EPR spectrum of **5**, recorded in CH_3CN solution at 10.9 K, is displayed in Figure 5.8. The derivative spectrum consists of multiple lines around g = 2. The multiple lines are divided into two sets. One set of lines belongs to the above of the zero crossing line, while the second set belongs to the below of the zero crossing line (Figure 5.8).

During preliminary simulations it was supposed that the clusters are not intact in solution and the free V^{IV} ions (S = ½) are responsible for the spectrum. However, these assumptions did not give a good simulation. For further simulations it was supposed that the spectrum might be due to the presence of an antiferromagnetically coupled $V^{III}V^{IV}$ dimeric unit (S = ½). But, again this attempt did not yield a good solution. Finally, the production of a similar theoretical spectrum to the experimental spectrum was achieved by considering that the vanadium core was intact. Taking the entire molecule, the experimental spectrum could be simulated reasonably well by using the parameters shown in Table 5.2 for S = 1 state (Figure 5.8).

Table 5.2 The Principal Values of the g and V^{III} and V^{IV} Hyperfine Tensors (A^{III} and A^{IV} respectively) for complex **5**.

g	A^{III} [x 10^{-4} cm^{-1}]	A^{IV} [x 10^{-4} cm^{-1}]	g_{iso}	A^{III}_{iso} [x 10^{-4} cm^{-1}]	A^{IV}_{iso} [x 10^{-4} cm^{-1}]
g_x = 1.995	45.0	-10.0			
g_y = 1.995	45.0	-10.0	1.987	48.9	-11.1
g_z = 1.970	56.7	-13.3			

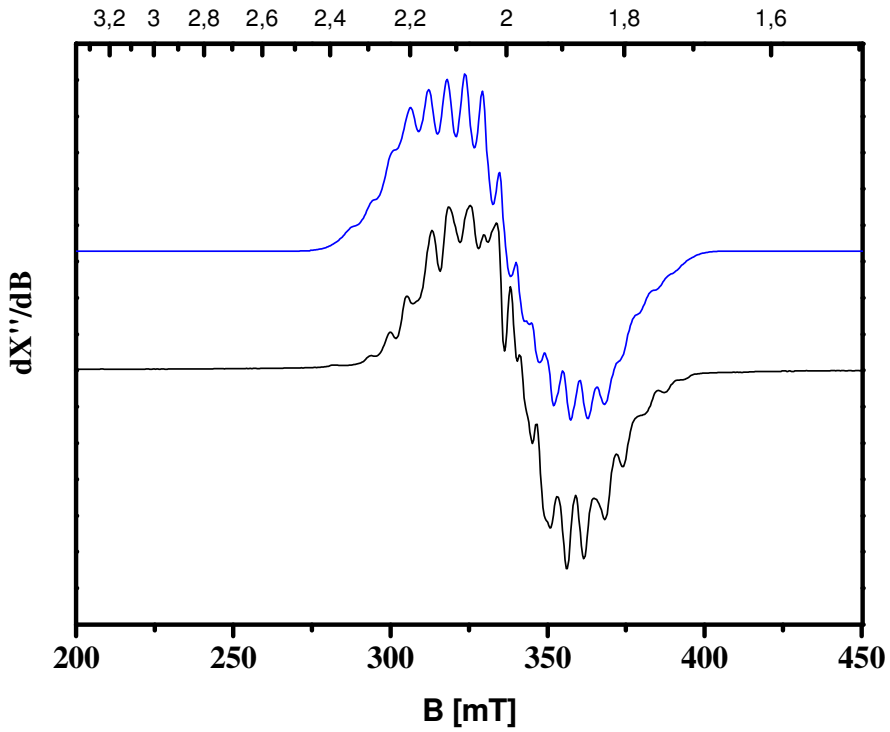

Figure 5.8 X-band EPR spectrum of **5**, $V^{III}_2V^{IV}_2$, in DCM at 10.9 K (experimental conditions: microwave frequency 9.43 GHz, power 0.25 mW, modulation amplitude 10.0 G) together with the simulated spectrum (blue line).

The entire molecule needs to be considered to analyze the EPR spectrum and the triplet states are responsible for giving such an unusual EPR spectrum. Theoretically, the hyperfine tensor ratio for free V^{III} and V^{IV} is 4:(-1). From the simulated hyperfine tensors A^{III}_{iso} and A^{IV}_{iso} are $48.9x10^{-4}$ and $-11.1x10^{-4}$ cm^{-1}, respectively and the ratio between them is 4:(-0.91), which is very similar to the theoretical ratio expected for V^{III}-V^{IV} system. Hence from the EPR analysis it can be said that the mixed valence V^{III}-V^{IV} has indeed been formed and the mixed-valence tetranuclear core remains intact in solution.

5.8 Experimental Section

N'N-di(3,5-di-*tert*-butyl-salicylidene)-1,3-diaminobenzene (L''H_2)

Synthesis of L''H_2 has been discussed in Chapter 4.

$[C_6H_4(NH_2)_2][L''_2V^{III}_2V^{IV}_2(\mu\text{-}Cl)_6(Cl)_4]$, 5

A solution of VCl_3 (0.16 g, 1 mmol) in dry THF was treated with N'N-di(3,5-di-*tert*-butyl-salicylidene)-1,3-diaminobenzene ($L''H_2$) (0.54 g, 1 mmol). The resulting dark-brown solution was stirred for 1 day at an ambient temperature inside the glove-box. Resulting precipitate was filtered using celite and the filtrate was collected. From the filtrate THF was removed *in vacuo* to obtain a dark-brown solid, which was recrystallized from diethylether, X-ray quality crystals in 20% yield grew over two days. Complex **5** is very sensitive to air, so entire procedures were carried out strictly under anaerobic condition inside the glove-box. MS-ESI (pos.) in THF: m/z, 1853.5, 1886.9, 1146.7, 840.5, MS-ESI (neg.) in THF: m/z, 1319, 1281.4, 676.3. UV-vis in THF: λ_{max} (ε, M^{-1} cm^{-1}): 370 (36000), 555 (6800), 670 (5000).

Elemental analysis:

	%C	%H	%N	%V
Calculated	56.0	7.3	3.9	9.5
Found	54.9	7.3	4.1	9.3

References

1. a) T. M. Pope, A. Müller, *Angew. Chem., Int. Ed.* **1991***, 30,* 34; b) Q. Chen, J. Zubieta, *Coord. Chem. Rev.* **1992**, *114*, 107; c) J. Zubieta, *Mol. Eng.* **1993**, *3*, 93; d) M. I. Khan, J. Zubieta, *Prog. Inorg. Chem.* **1995***, 43,* 1.

2. a) I. S. Lee, J. R. Long, *Chem. Commun*. **2004**, 3234; b) F. H. Fry, B. A. Dougan, N. McCann, C. Ziegler, N.E. Brasch, *Inorg. Chem*. **2005**, *44*, 5197; c) H. Kumagai, S. Kitagawa, *Chem. Lett*. **1996**, 471; d) J. Salta, J. Zubieta, *J. Cluster Sci.* **1996**, *7*, 531.

3. M. Mikuriya, T. Kotera, F. Adachi, S. Bandow, *Chem. Lett*. **1993**, 945.

4. (a) P. L. W. Tregenna-Piggott, H. Weihe, J. Bendix, A.–L. Barra, H. U. Güdel, *Inorg. Chem.* **1999**, *38*, 5928; b) J. Krzystek, A. T. Fiedler, J. Sokol, A. Ozarowski, S. A. Zvyagin, T. C. Brunold, J. R. Long, L-C. Brunel, J. Telser, *Inorg. Chem.* **2004**, *43*, 4654.

5. S. Khanra, M. Kloth, H. Mansary, C. A. Muryn, F. Tuna, E. C. Sañudo, M. Helliwell, E. L. McInnes, R. E. P. Winpenny, *Angew. Chem., Int. Ed.* **2007**, *46*, 5568.

6. I. S. Tidmarsh, E. Scales, P. R. Brearley, J. Wolowska, L. Sorace, A. Caneschi, R. H. Laye, E. J. L. McInnes, *Inorg. Chem.* **2007**, *46*, 9743.

7. I. S. Tidmarsh, R. H. Laye, P. R. Brearley, M. Shanmugam, E. C. Sañudo, L. Sorace, A. Caneschi, E. J. L. McInnes, *Chem. Eur. J.* **2007**, *13*, 6329.

8. R. H. Laye, Q. Wei, P. V. Mason, M. Shanmugam, S. J. Teat, E. K. Brechin, D. Collison, E. J. L. McInnes, *J. Am. Chem. Soc.* **2006**, *128*, 9020.

9. a) J. K. Johnson, D. C. Johnston, H. E. King, Jr., T. R. Halbert, J. F. Brody, D. P. Goshorn, *Inorg. Chem.* **1988**, *27*, 1646; b) J. A. Cissell, N. Kaur, S. Nellutla, N. S. Dalal, T. P. Vaid, *Inorg. Chem.* **2007**, *46*, 9672; c) D. W. Aldous, N. F. Stephens, P. Lightfoot, *Inorg. Chem.* **2007**, *46*, 3396.

10. V. Soghomonian, R. C. Haushalter, J. Zubieta, *Chem. Mater.* **1995**, 1648.

11. F. A. Cotton, S. A. Duraj, M. W. Extine, G. E. Lewis, W. J. Roth, C. D. Schmulbach, W. Schwotzer, *Chem. Commun.* **1983**, 1377.

12. R. J. Bouma, J. H. Teuben, W. R. Beukema, R. L. Bansemer, J. C. Huffman, K. G. Caulton, *Inorg. Chem.* **1984**, *23*, 2715.

13. F. A. Cotton, S. A. Duraj, W. J. Roth, *Inorg. Chem.* **1985**, *24*, 913.

14. J. A. M. Canch, F. A. Cotton, S. A. Duraj, W. J. Roth, *Polyhedron*, **1987**, *6*, 1433.

15. F. A. Cotton, S. A. Duraj, L. E. Manzer, W. J. Roth, *J. Am. Chem. Soc.* **1985**, *107*, 3850.

16. F. CAlderzzo, G. E. De Benedetto, G. Pampaloni, C. M. Mossmer, J. Strahle, K. Wurst, *J. Oraganomet. Chem.* **1993**, *451*, 73.

17. J. R. Rambo, S. L. Bartley, W. E. Streib, G. Christou, *J. Chem. Soc., Dalton Trans.* **1994**, 1813.

18. G. B. Karet. S. L. Castro, K. Folting, J. C. Bollinger, R. A. Heintz, G. Christou, *J. Chem. Soc., Dalton Trans.* **1998**, 67.

19. T. Casey, R. J. H. Clark, *Inorg. Chem.* 1968, **7**, 1598.

20. R. Saillant, R. A. D. Wentworth, *Inorg. Chem.* **1968**, *7*, 1606.

21. B. Leuenberger, H. U. Gudel, *Mol. Phys.* **1984**, *51*, 1.

22. B. Leuenberger, H. U. Gudel, *Inorg. Chem.* **1986**, *25*, 181.

23. B. Leuenberger, B. Briat, J. C. Canit, A. Furrer, P. Fischer, H. U. Gudel, *Inorg. Chem.* **1986**, *25*, 2930.

Chapter 6

Tris(N-methylimidazoleoximato)metal(II) Complexes as Ligands for the Synthesis of Asymmetric Heterodinuclear $Fe^{III}M^{II}/Cr^{III}M^{II}/Ga^{III}Ni^{II}$ Species: A Magneto-Structural Study

6.1 Introduction

The study of exchange interactions between paramagnetic metal centers through various bridging ligands is one of the most active research field in coordination chemistry; this is largely due to its relevance to many different research areas, from chemistry to solid-state physics and biology, and because of the potential impact on material science, catalysis, and metallobiochemistry. Such exchange interactions in metalloproteins that involve more than one metal center have elicited the interests of bioinorganic chemists.[1-6]

In terms of magnetochemistry, there are very few studies of heterometallic complexes, despite the fact that such studies might be more informative than those of homometal complexes. New exchange pathways can be expected for heteronuclear complexes where unusual sets of magnetic orbitals can be brought into close proximity.[7-19] There are several interesting features associated with heteronuclear clusters. Firstly, these complexes can have unusual electronic structures and may serve as sources of fundamental information about exchange coupling in multinuclear assemblies. A second general reason to study heterodinuclear metal complexes is that they may be building blocks for molecular based magnetic materials.

We emphasize the fact that the investigations of a series of isostructural polynuclear complexes with varying d^n-electron configurations are more informative in comparison to those comprising singly isolated, exchange coupled clusters only. In several cases we have used suitably designed metal-oximates as ligands as part of our program to investigate different exchange pathways. In this way we have synthesized a series of

dioximato-bridged (-N-O-) linear heterotrinuclear complexes of general formula $[L'M_t\{\mu\text{-}(dioxime)_3M_c\}M_tL]^{2+/4+}$, where M_t = Fe(III), Mn(III), Mn(IV) and Cr(III) and M_C = Zn(II), Cu(II), Ni(II), Fe(II), and Mn(II) and dioxime(2-) is the dianion of a variety of oximes; and a dioximato-bridged (-N-O-) linear tetranuclear complexes of general formula $[L'M'_2Mn^{II}_2(dfmp)_3]^{2+}$, where M' = Fe(III), Mn(III), Mn(IV), and L' represents the tridentate cyclic amine 1,4,7-trimethyl-1,4,7-triazacyclononane and dfmp(2-) is the dianion 2,6-diformyl-4-methyl phenol dioxime .[8, 24-26]

Applying a very similar strategy, we have also succeeded in preparing the asymmetric dinuclear motif $M^{III}\mu\text{-}(O\text{-}N)_3M^{II}$ by using [tris(pyridinealdoximato)M^{II}]$^-$ anions, $[M(PyA)_3]^-$, as a ligand for the $L'M^{III}$ unit, where M^{III} = Fe^{III}, Mn^{III}, Cr^{III} and Co^{III}.[27-28] In our current work we have used 1-methylimidazole-2-aldoxime, ^{Me}ImOxH, as a bridging ligand to synthesize asymmetric dinuclear complexes and to explore the ability of $[M^{II}(^{Me}ImOx)_3]^-$ monoanions in generating such homo- and heterometallic complexes (Figure 6.1), which will allow us to compare the exchange coupled interactions in dimers. We report the synthesis, magnetic, electrochemical, spectroscopic and other physical properties including the structures of the following complexes.

$[L'Fe^{III}(^{Me}ImOx)_3Ni^{II}](ClO_4)_2$	**6**
$[L'Fe^{III}(^{Me}ImOx)_3Zn^{II}](ClO_4)_2$	**7**
$[L'Ga^{III}(^{Me}ImOx)_3Ni^{II}](ClO_4)_2$	**8**
$[L'Fe^{III}(^{Me}ImOx)_3Mn^{II}](ClO_4)_2$	**9**
$[L'Fe^{III}(^{Me}ImOx)_3Fe^{II}](ClO_4)_2$	**10**
$[L'Fe^{III}(^{Me}ImOx)_3Cu^{II}](ClO_4)_2$	**11**
$[L'Co^{III}(^{Me}ImOx)_3Fe^{II}](ClO_4)_2$	**12**
$[L'Cr^{III}(^{Me}ImOx)_3Ni^{II}](ClO_4)_2$	**13**
$[L'Cr^{III}(^{Me}ImOx)_3Zn^{II}](ClO_4)_2$	**14**

Additionally, we chose to study first the Fe^{III}-Ni^{II}-system (**6**) in our MCD project to investigate the nature of the d-d and CT transitions. A moderate antiferromagnetic exchange interaction is present in complex **6**. Consequently the d-d and CT transitions would not only arise from pure iron or nickel ions, but also from their combination. Moreover, we have prepared isostructural Fe^{III}-Zn^{II}, **7** and Ga^{III}-Ni^{II}, **8** species to identify

the independent spectroscopic mark of Fe and Ni, respectively, as Zn(II) and Ga(III) are devoid of any unpaired d-electrons.

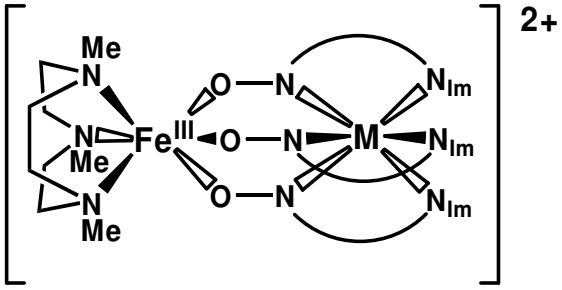

Figure 6.1 Schematic representation of this series of dinuclear complexes (where M = Mn(II), Fe(II), Ni(II), Cu(II) and Zn(II)).

6.2 Synthesis

An interesting synthetic strategy for heterometallic complex is the use of metal complexes as ligands which can act as a building block for polynuclear complexes. Therefore, metal complexes containing potential donor atoms can act as a bridging ligand for another metal ion or metal complex with empty or available coordination sites. The following strategy is used to obtain heterometal complexes, in which tris(N-methylimidazolealdoximato)metalates act as ligands (scheme 6.1).

Scheme 6.1

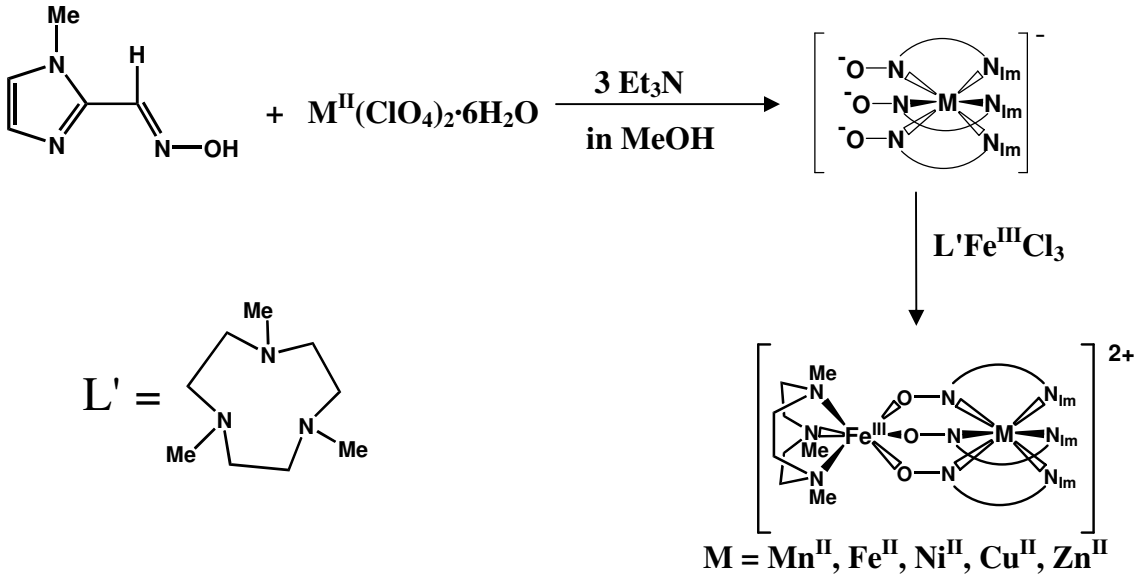

1-methylimidazole-2-aldoxime (^{Me}ImOxH) reacts with metal-perchlorate salts, $[M^{II}(ClO_4)_2]\cdot 6H_2O$, in the presence of Et_3N in methanol to form tris(N-methylimidazolealdoximato)metalates, $[M^{II}(^{Me}ImOx)_3]^-$. These tris(N-methylimidazolealdoximato)metalates produced in situ react with either $[L'Fe^{III}]^{3+}$ or $[L'Cr^{III}]^{3+}$ unit in a 1:1 molar ratio to lead to the formation of asymmetrical heterodinuclear complexes.

6.3 Infrared Spectroscopy and Mass Spectrometry

IR spectra of complexes **6-14** show C=N stretching bands for the ligand at 1635 cm^{-1}. Peaks at 2920-3000 cm^{-1} correspond to the C-H stretching mode of the L' and ^{Me}ImOx groups present as the terminal and bridging ligands, respectively. The NO stretching bands for all the dinuclear complexes are observed at 1099, 1052 and 1005 cm^{-1}. Strong bands at 1079 and 623 cm^{-1} correspond to the ClO_4 unit which is the counteranion in all six dinuclear complexes. Though it is not possible to distinguish the stretching frequencies for NO and ClO_4 around 1080 cm^{-1} but the peak at 623 cm^{-1} confirms the presence of ClO_4 group.

Electronspray-ioniziation mass spectrometry (ESI-MS) in the positive ion mode has been proved to be very successful in characterizing complexes **6-14**. All the spectra show the monopositively charged species $[M\text{-}ClO_4]^+$ as the base peak for every complex. Peak for the fragment $[M\text{-}2ClO_4]^{2+}$ were also observed. Electrospray-ioniziation mass spectrometry (ESI-MS) in the positive ion mode is successful in characterizing complexes **8**, **9** and **10** as the spectra show mononegatively charged species $[M+ClO_4]^-$ as characteristic peaks. Thus, as with earlier reported complexes with the pyridinealdoxime ligand, in this case electronspray-ionization mass spectrometry is an important tool to characterize the complexes.

6.4 Electronic Spectroscopy

The electronic spectra for complexes **6-14** have been measured in MeCN in the range 250-1500 nm. All peak positions are listed in Table 6.1 and all of the spectra are shown in Figure 6.2. The electronic spectral results indicate that complexes **6-14** are stable and retain their dinuclear entities in acetonitrile solution. On the basis of high

extinction coefficients all the bands below 350 nm are assigned to π-π* transitions of the oxime ligand. Second spin allowed transitions $^4A_2(F) \rightarrow {}^4T_1(F)$ are observed at 433 nm for **13** and 420 nm for **14** with the extinction coefficients 390 and 270 M^{-1} cm^{-1}, respectively. Both of these complexes, **13** and **14**, also exhibit an additional weak shoulder at 540 (with ε_M 230 M^{-1} cm^{-1}) and 529 nm (with ε_M 120 M^{-1} cm^{-1}), respectively. The extinction coefficient of this band is rather large in comparison to those reported for mononuclear $L'CrX_3$ complexes.[31] This is probably due to enhancement of intensity via exchange coupling and of the strong trigonal distortion of the Cr(III) geometry, resulting in a lowering of the symmetry to C_3.[36]

Judge on the basis of extinction coefficients, the bands at 823 and 890 nm for **6**, 820 and 894 nm for **8** and 867 nm for **13** are tentatively ascribed to the d-d transitions at the Ni(II) center. Apart from these all the bands are assigned to the MLCT and LMCT transitions which indicate the strong interactions of the metal d orbitals with the conjugated π system of the oxime.[30]

Table 6.1 Optical Spectral Data for Complexes **6-8** and **10-14**.

Complex	λmax, nm [ε, M^{-1} cm^{-1}]
6 $Fe^{III}Ni^{II}$	290 (33200), 402 (4280), 505(2370), 823 (40), 890 (34)
7 $Fe^{III}Zn^{II}$	303 (22800), 380 (6500)
8 $Ga^{III}Ni^{II}$	820 (26), 894 (25)
9 $Fe^{III}Mn^{II}$	300 (21200)
10 $Fe^{III}Fe^{II}$	312 (17450), 460 (12700), 960 (310)
11 $Fe^{III}Cu^{II}$	286 (30800), 406 (4900), 770 (85), 1102 (63)
12 $Co^{III}Fe^{II}$	298 (26000), 484 (4400), 590 (900)
13 $Cr^{III}Ni^{II}$	300 (>15000), 433 (390), 540 (230), 867 (12)
14 $Cr^{III}Zn^{II}$	293 (21100), 420 (270), 529 (120)

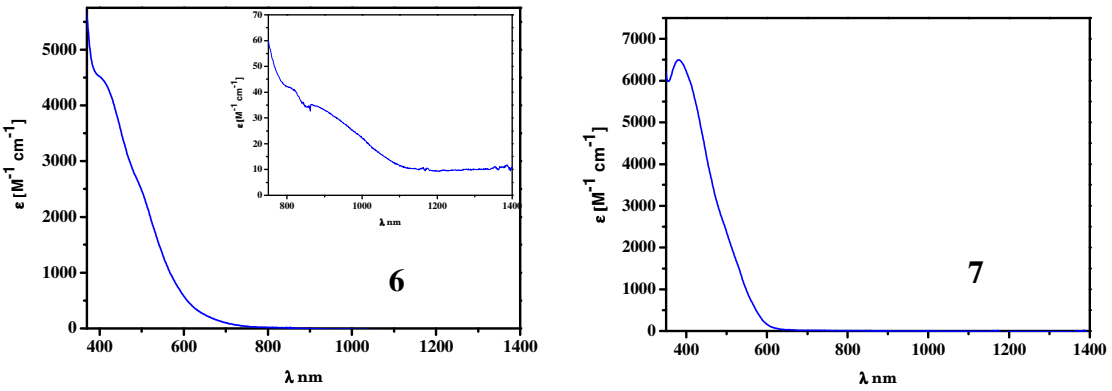

Figure 6.2a Electronic spectra for complexes **6** (left) and **7** (right) at room temperature in dry MeCN

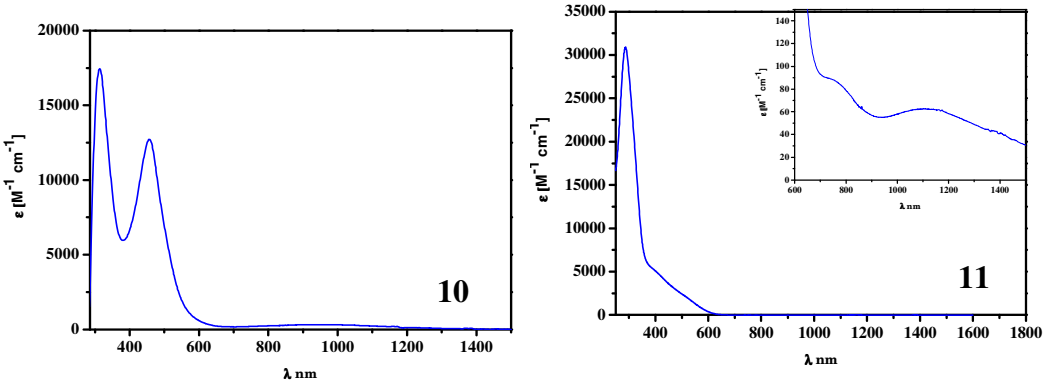

Figure 6.2b Electronic spectra for complexes **10** (left) and **11** (right) at room temperature in dry MeCN.

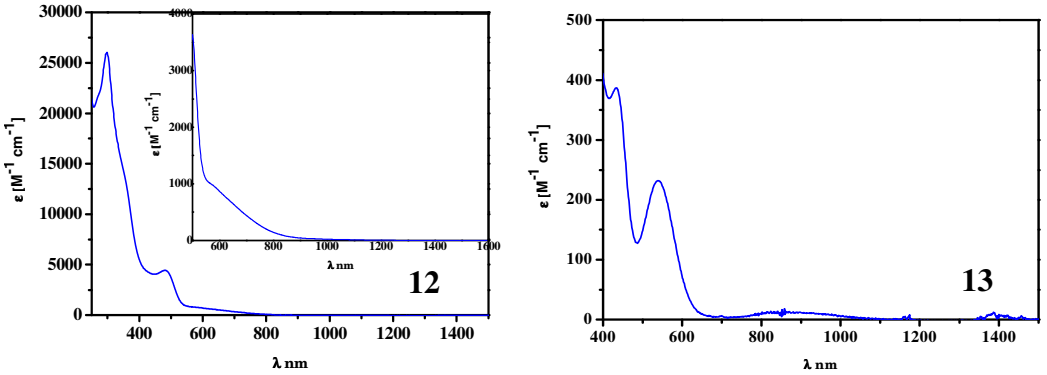

Figure 6.2c Electronic spectra for complexes **12** (left) and **13** (right) at room temperature in dry MeCN.

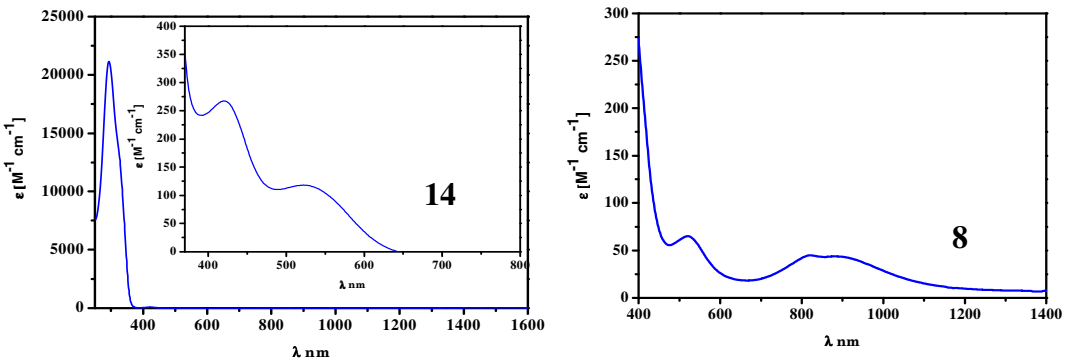

Figure 6.2d Electronic spectra for complexes **14** (left) and **8** (right) at room temperature in dry MeCN.

6.5 Mössbauer Spectroscopy

The zero-field Mössbauer spectra of solid samples of complexes **6**, **7** and **9-12** were recorded at 80 K in zero-field, shown in Figure 6.3. These measurements were carried out to find out the spin and oxidation states of the iron centers and also to compare with those earlier reported analogous complexes with the pyridinealdoxime ligand.[28] In complexes **6**, **7** and **9-11**, the Fe(1) centers are in an FeN_3O_3 environment, whereas the coordination environment for Fe(2) of **10** and Fe(1) of **12** are FeN_6. Isomer shifts (δ_{Fe}) and quadrupole splitting (ΔE_Q) values of the current complexes and the earlier reported analogous complexes are shown in Table 6.2a and Table 6.2b, respectively. All the spectra, except for that of **10**, fit well with a single quadrupole split doublet. Isomer shifts (δ_{Fe}) and quadrupole splitting (ΔE_Q) values for **6**, **7**, **9** and **11** are in accord with those observed for high-spin Fe(III) ions in octahedral environments.[29] The spectrum of **10** fits well with two equal area are doublets, which imply two iron sites having different coordination spheres, in agreement with the analogous complex with the pyridinealdoxime ligand. Thus, as in the analogous complex, they are assigned to the Fe^{III} and Fe^{II} ions, which is also supported by the X-structure analysis. For **12** the isomer shift (δ_{Fe}) is lower than that of **6**, **7**, **9** and **11** and similar with that of **10**. Summarily, the Mössbauer parameters of complexes **6**, **7** and **9-11** containing the FeN_3O_3 core are in agreement with those observed for high-spin Fe(III) ions in octahedral and distorted octahedral environments. Mössbauer data for **10** and **12** indicates the low-spin d^6 electronic configuration of Fe(II) ions contained in the FeN_6 core; these above Mössbauer

parameters are in agreement with those of previously reported analogous complexes with the pyridinealdoxime ligand.[28]

Table 6.2a Mössbauer Parameters of Current Complexes at 80 K in Zero-Field.

Complex	δ_{Fe} [mm·s^{-1}]	ΔE_Q [mm·s^{-1}]
6 $Fe^{III}Ni^{II}$	0.45	0.02
7 $Fe^{III}Zn^{II}$	0.41	0.01
9 $Fe^{III}Mn^{II}$	0.44	0.33
10 $Fe^{III}Fe^{II}$	0.32, 0.40	0.33, 0.35
11 $Fe^{III}Cu^{II}$	0.45	-0.19
12 $Co^{III}Fe^{II}$	0.30	0.22

Table 6.2b Mössbauer Parameters of Previously[28] Reported Complexes with the Pyridinealdoxime Ligand at 80 K in Zero-Field for Comparison.

Complex	δ_{Fe} [mm·s^{-1}]	ΔE_Q [mm·s^{-1}]
$Fe^{III}Ni^{II}$	0.47	0.12
$Fe^{III}Zn^{II}$	0.45	0.01
$Fe^{III}Mn^{II}$	0.46	0.43
$Fe^{III}Fe^{II}$	0.41, 0.26	0.39, 0.33
$Fe^{III}Cu^{II}$	0.45	0.01
$Co^{III}Fe^{II}$	0.30	0.40

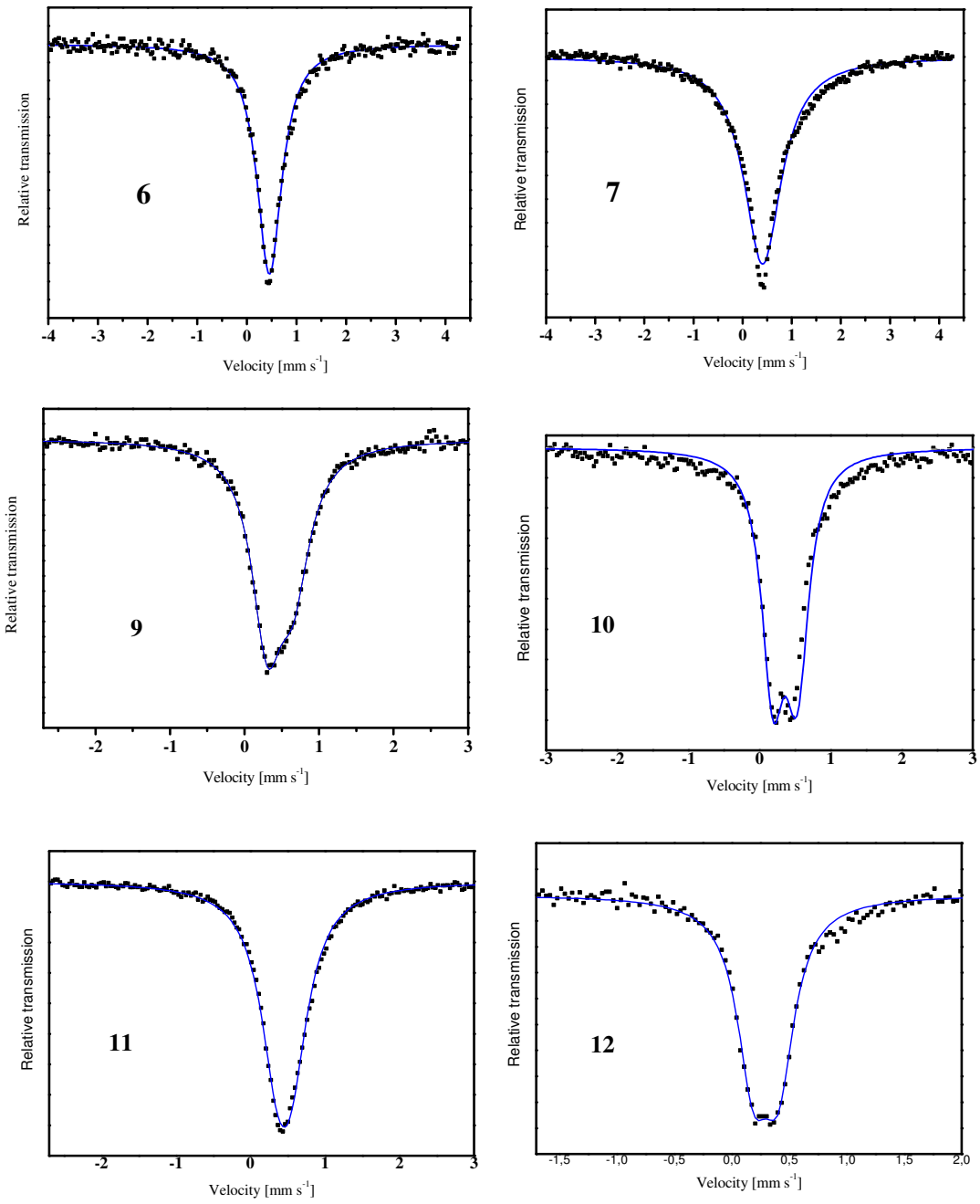

Figure 6.3 Mössbauer spectra of complexes **6**, **7** and **9-12** at 80 K.

6.6 Electrochemistry

Cyclic voltammograms (CV) of complexes **6-11** and **13** were recorded in MeCN solutions containing 0.10 M $[(n\text{-}Bu)_4N]PF_6$ as the supporting electrolyte. A conventional three electrode arrangement was used, consisting of a glassy carbon working electrode, a $Ag/AgNO_3$ reference electrode and a Pt wire counter electrode. The redox potentials were referenced versus the ferrocenium/ferrocene (Fc^+/Fc) couple. The cyclic voltammograms of the complexes are shown in Figure 6.4 and the redox potentials obtained from the voltammograms are presented in Table 6.3.

Complex **7**, $Fe^{III}Zn^{II}$, contain one redox active Fe^{III} metal ion and one redox inactive Zn^{II} metal ion. Its cyclic voltammogram exhibits one reversible oxidation at 0.73 V. Since Zn^{II} is redox inactive and the oxidation of Fe^{III} to Fe^{IV} is highly unlikely at this potential, then this oxidation must occur at the ligand. Since the triazacylononane ligand L' is not oxidizable in this potential range,[31] the oxidation must be due to the oxidation of the 1-methyl-2-imidazolealdoxime moiety. The cyclic voltammogram of **7** also features a reversible one-electron reduction at -0.93 V, which likely corresponds to the reduction of iron from Fe^{III} to Fe^{II}.

Complexes **6**, **8** and **13** also show one ligand centered reversible oxidation at 0.82, 0.79 and 1.00 V, respectively. Like complex **7**, complex **6** also shows one Fe^{III} centered reversible reduction at -0.84 V. But there is no reduction for complex **8** as Ga^{III} is redox inactive in nature. Complex **13** also does not show any peak for reduction. Cyclic voltammograms of **6** exhibits one quasi reversible oxidation at 1.25 V which is assigned as the oxidation of nickel ion from Ni^{II} to Ni^{III} whereas complexes **8** and **13** show one reversible oxidation of Ni^{II} at 1.26 and 1.27 V, respectively

Cyclic voltammograms of **9-11** exhibit two reversible waves: one for an oxidation (in the range from +0.31 to +0.79 V) and one for a reduction (in the range from –0.75 to -0.85 V). Complex **7** shows that the oxidation must occurs at the ligand centered and the reduction is most likely because of the reduction of iron center form Fe^{III} to Fe^{II}. The CV of **9** shows one additional oxidation like previously reported $Fe^{III}Mn^{II}$ complex with pyridinealdoxime ligand. The reason for this behavior is still unknown. The CV of **11** also shows one additional reduction at –1.20 V which is assigned as the reduction of the cupper ion from Cu^{II} to Cu^{I}.

It has been discussed that for both cases, complexes with ^{Me}ImOx and PyA ligands, 1st oxidations are ligand centered. From the Table 6.3 and Table 6.4 it is very clear the 1st oxidation for $Fe^{III}M$ complexes with ^{Me}ImOx ligand occurs at lower potential compare to the $Fe^{III}M$ complexes with PyA ligand. Though the reason for this behavior is still unknown, but it can be suggested that it can be because of higher electron density at five membered imidazole ring compare to six membered pyridine ring. 1st reduction for the current complexes occurs at more negative potential compare to the earlier reported complexes with PyA. Apart from these, cyclic voltammograms are very similar for both the cases.

Table 6.3 Formal Electrode Potentials for Oxidation and Reduction (in V vs Fc^+/Fc) of Complexes **6-11** and **13** (Measured at Ambient Temperatures in MeCN Solutions Containing 0.1 M $[(n\text{-}Bu)_4N]PF_6$).

Complex	$E_{1/2}^{ox}(2)$, V	$E_{1/2}^{ox}(1)$, V	$E_{1/2}^{red}(1)$, V	$E_{1/2}^{red}(2)$, V
7 $Fe^{III}Zn^{II}$	-	0.73	-0.93	-
11 $Fe^{III}Cu^{II}$	-	0.79	-0.75	-1.20
6 $Fe^{III}Ni^{II}$	1.25	0.82	-0.84	-
10 $Fe^{III}Fe^{II}$	-	0.31	-0.82	-
9 $Fe^{III}Mn^{II}$	-	0.67	-0.76	-0.94
13 $Cr^{III}Ni^{II}$	1.27	1.00	-	-
8 $Ga^{III}Ni^{II}$	1.26	0.79	-	-

Table 6.4 Formal Electrode Potentials for Oxidation and Reduction (in V vs Fc^+/Fc) of reported Complexes[27,28] (Measured at Ambient Temperatures in MeCN Solutions Containing 0.1 M $[(n\text{-}Bu)_4N]PF_6$).

Complex	$E_{1/2}^{ox}(2)$	$E_{1/2}^{ox}(1)$	$E_{1/2}^{red}(1)$	$E_{1/2}^{red}(2)$
$Fe^{III}Zn^{II}$	-	0.83	-0.80	-
$Fe^{III}Cu^{II}$	-	0.89	-0.62	-1.14
$Fe^{III}Ni^{II}$	1.25	0.89	-0.72	-
$Fe^{III}Fe^{II}$	-	0.76	-0.62	-

$Fe^{III}Mn^{II}$	-	0.45, 0.73	-0.85	-1.07
$Cr^{III}Ni^{II}$	1.29	0.90	-	-

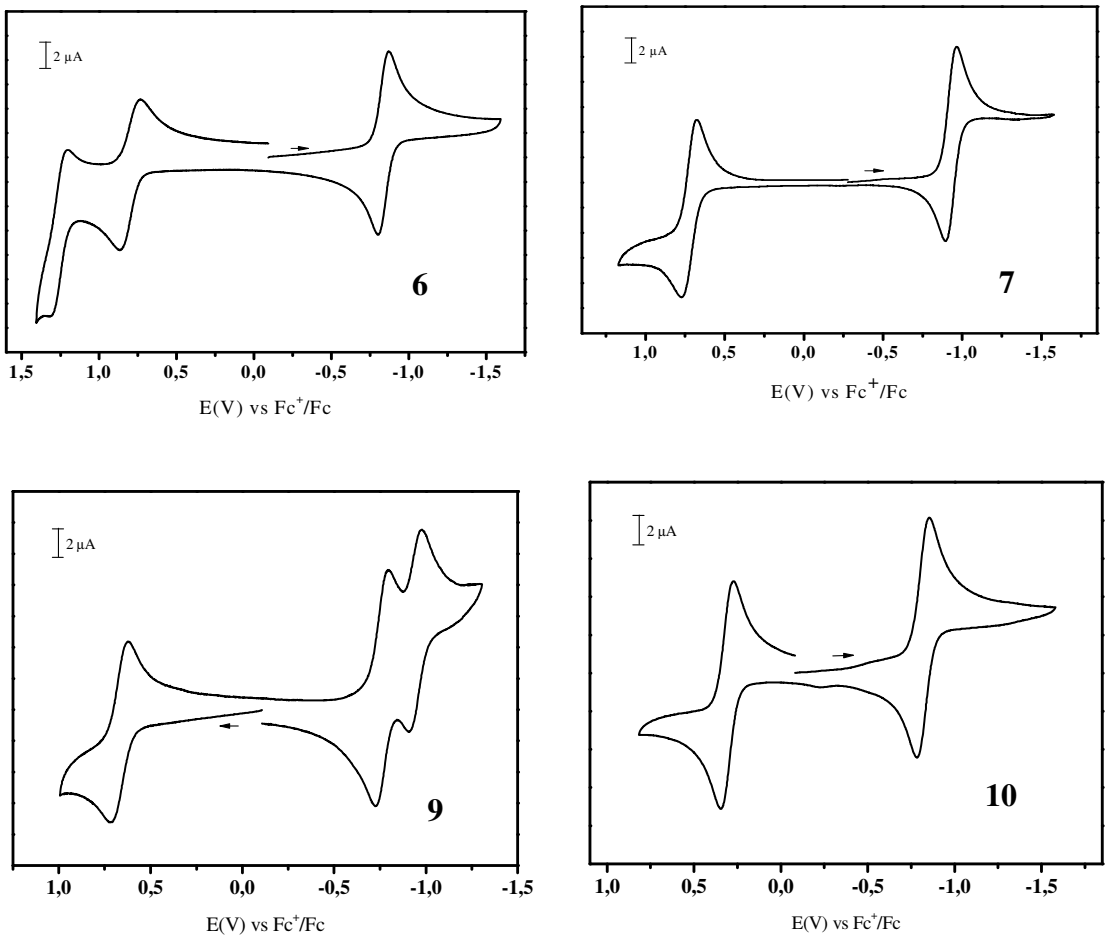

Figure 6.4a Cyclic voltammograms of complexes **6**, **7**, **9** and **10** recorded in MeCN solutions containing 0.1 M $[(n\text{-}Bu)_4N]PF_6$ as the supporting electrolyte at ambient temperatures. A glassy carbon electrode (0.03 cm^2) was used, and potentials are referenced versus the Fc^+/Fc couple.

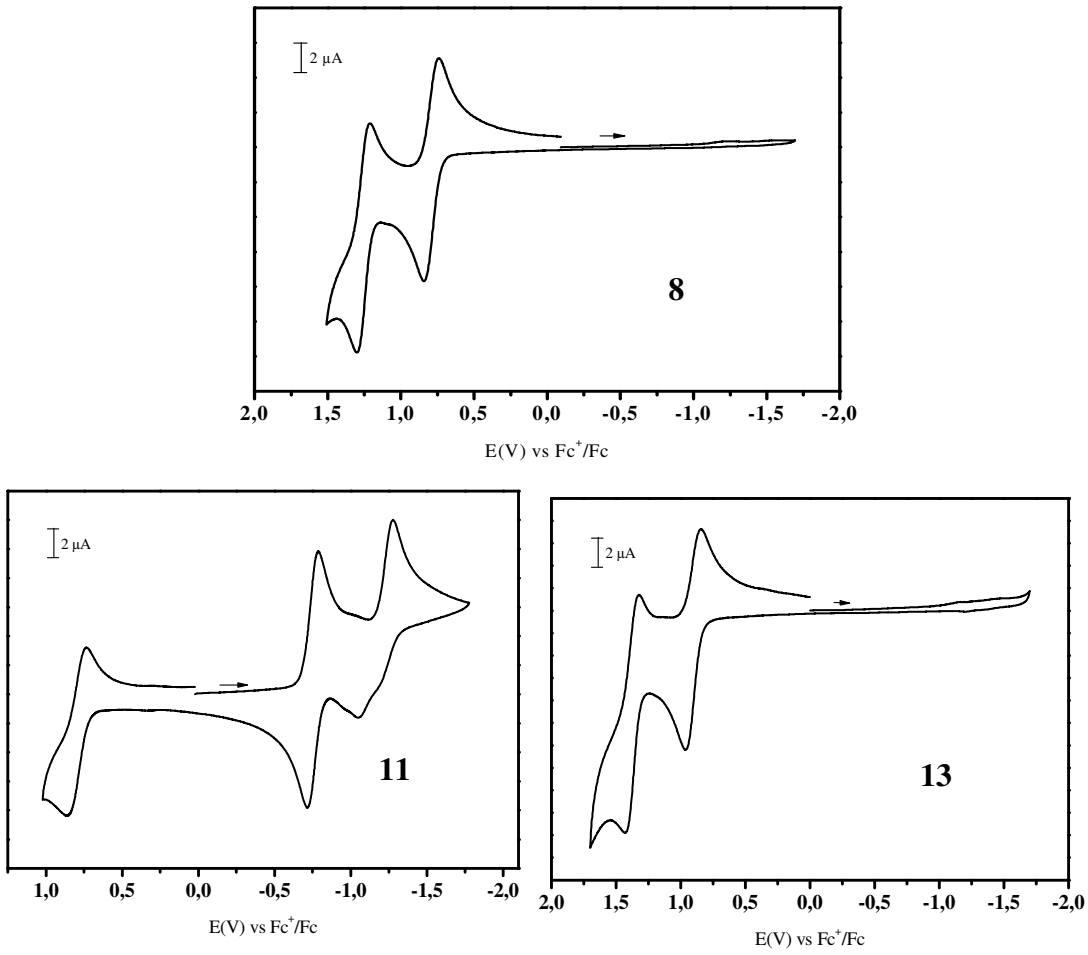

Figure 6.4b Cyclic voltammograms of complexes **8**, **11** and **13** recorded in MeCN solutions containing 0.1 M $[(n\text{-}Bu)_4N]PF_6$ as the supporting electrolyte at ambient temperatures. A glassy carbon electrode (0.03 cm^2) was used, and potentials are referenced versus the Fc^+/Fc couple.

6.7 X-ray Structures

The crystal structures of complexes **6 – 13** have been determined by single crystal X-ray crystallography. The X-ray structures confirm that mixed metal $Fe^{III}M^{II}$ (where M = Mn, Fe, Ni, Cu and Zn), $Ga^{III}Ni^{II}$, $Co^{III}Fe^{II}$ and $Cr^{III}Ni^{II}$ complexes have indeed been formed with 1-methyl-2-imidazolealdoxime, ^{Me}ImOxH, ligand in a similar fashion like pyridine-2-aldoxime, PyOxH.[27-28] In all the complexes two pseudooctahedral polyhedra are joined face-to-face by three oximato N-O groups. The $C=N_{Ox}$ bond lengths of average 1.291 ± 0.006 Å (**6**), 1.284 ± 0.009Å (**7**), 1.294 ± 0.006 Å (**8**), 1.290 ± 0.012 Å (**9**), 1.308 ± 0.015 Å (**10**), 1.275 ± 0.009 Å (**11**), 1.307 ± 0.015 Å (**12**) and 1.294 ± 0.006 Å (**13**) and the N_{ox}-O bond lengths of average 1.353 ± 0.006 Å (**6**), 1.357 ± 0.009 Å (**7**), 1.349 ± 0.006 Å (**8**), 1.349 ± 0.009 Å (**9**), 1.339 ± 0.012 Å (**10**), 1.342 ± 0.012 Å (**11**), 1.353 ± 0.021 Å (**12**) and 1.349 ± 0.006 Å (**13**) are nearly identical to those for other $Fe^{III}M^{II}$, $Mn^{III}M^{II}$, $Ni^{II}Ni^{II}$, $Zn^{II}Ni^{II}$ and $Cr^{III}Mn^{II}$-complexes containing pyridine-2-aldoximato reported by us.[27-28] The N_{ox}-O bond lengths are significantly shorter than ~ 1.40 Å in general for free oxime ligands. The C-N-O bond angles of average 115.2º (**9**), 117.9 ± 0.3º (**10**), 118.0 ± 0.4º (**11**), 118.0 ± 0.4º (**12**) and 118.4 ± 0.3º (**13**) are also identical to those for previously reported comparable structure containing pyridine-2-aldoximato ligand.[27-28]

X-ray Structure of $[L'Fe^{III}(^{Me}ImOx)_3M^{II}](ClO_4)_2$ (M = Mn (9), Fe (10), Ni (6), Cu (11), Zn (7))

The lattices consist of dinuclear dications and perchlorate anions. Complexes **6**, **7**, **10** and **11** crystallize in the space group R-3c. Perspective views of the cations are shown in Figure 6.6. The donor atoms for the metal ions of the cations are identical (FeN_3O_3 and $M^{II}(N_{ox})_3(N_{Im})_3$) in all the complexes, but the coordination geometry of the divalent metal centers is not.

Coordination geometry of the iron center is distorted octahedral with three nitrogen atoms from the facially coordinated tridentate macrocyclic amine L' and three oxygen atoms from the bridging oximato group (Figure 6.5). The largest deviation from the idealized 90º interbound angle is 11.7º, which occurs within the six-membered O-Fe-O chelate rings, the O-Fe-O angles ranging between 101.7(1) and 96.8(1)º, whereas the

N-Fe-N angles fall between 79.67(8) and 80.1(1)°. The Fe(1)-N(1) (in the range 2.191 ± 0.009 – 2.209 ± 0.006 Å) and Fe(1)-O(11) (in the range 1.955 ± 0.009 – 1.974 ± 0.006 Å) distances correspond to those of known values for Fe^{III} complexes with this macrocyclic amine[24,31] and are in accord with the similar complexes with pyridine-2-aldoximato ligand (Table 6.6).[28] Additionally these bond distances are in agreement with a d^5 high-spin electronic configuration of the Fe^{III} centers, which is in complete agreement with the Mössbauer results.

The second metal center, Fe(II), Mn(II), Ni(II), Cu(II) or Zn(II), is also hexa coordinated yielding an MN_6 core (Figure 6.5). Coordination occurs facially through three pyridine nitrogen atoms, $N_{Im}(18)$, and three azomethine nitrogen atoms, $N_{ox}(12)$, from the imidazolealdoxime (^{Me}ImOx) ligand like pyridinealdoxime (PyA) ligand.[28] It is noteworthy that the Fe(2)-N_{ox} bond lengths in **10** are significantly shorter than M-N_{ox} bond lengths in **6**, **7** and **11**, which is due to low-spin d^6 electronic configuration of the Fe^{II} center. From the M-N bond distances and twist angles (Table 6.6) analysis it is clear that the coordination sphere around the manganese center in **9** is strongly distorted, which is also supported by the dihedral angles (Fe-O-N and M-N-O) analysis. The geometry of the Mn center may be assigned as pseudo-trigonal-pyramidal with a nonbanded imidazole N.

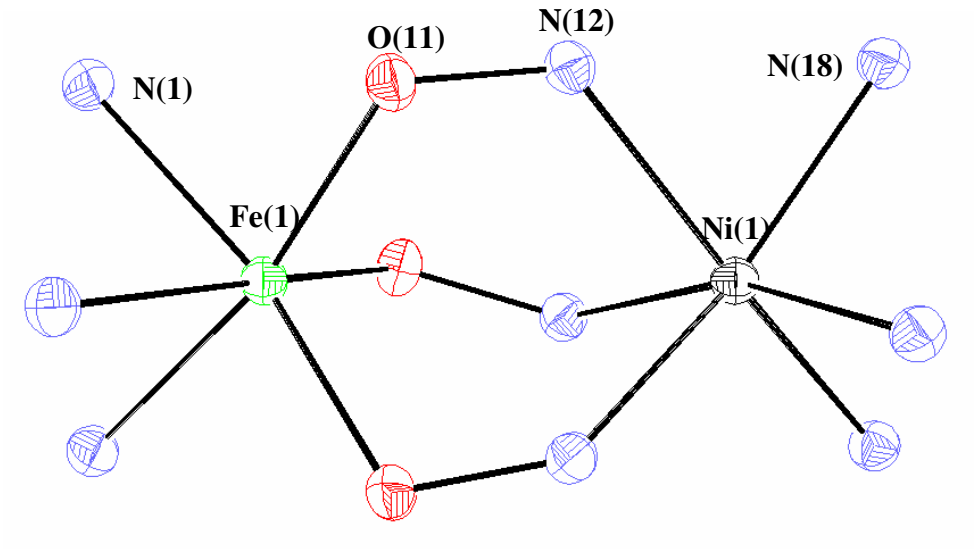

Figure 6.5 First coordination sphere of complex **6**. The atom connectivities are identical for **7**, **9**, **10** and **11**.

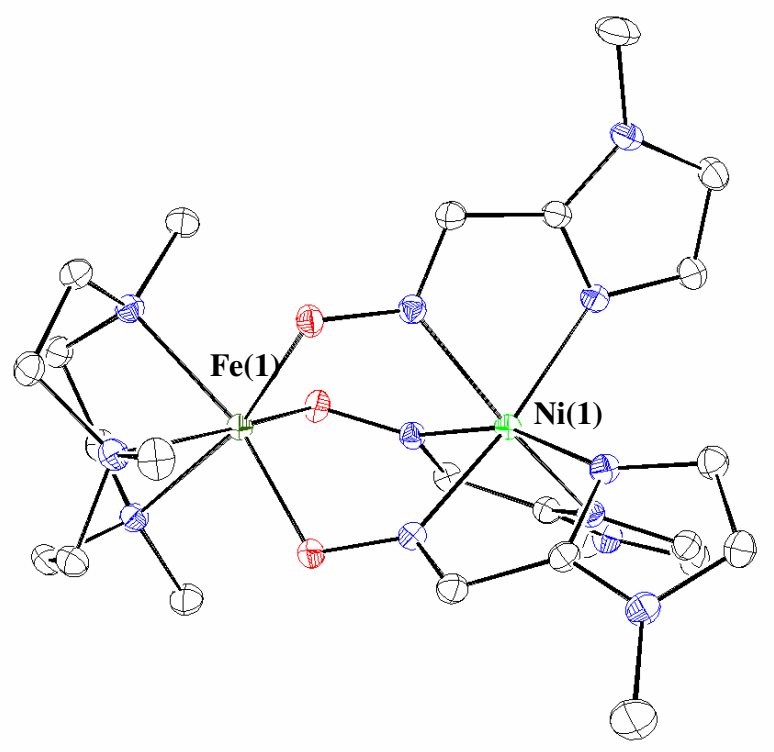

Figure 6.6a Molecular structure of the cation in complex **6**, $Fe^{III}Ni^{II}$.

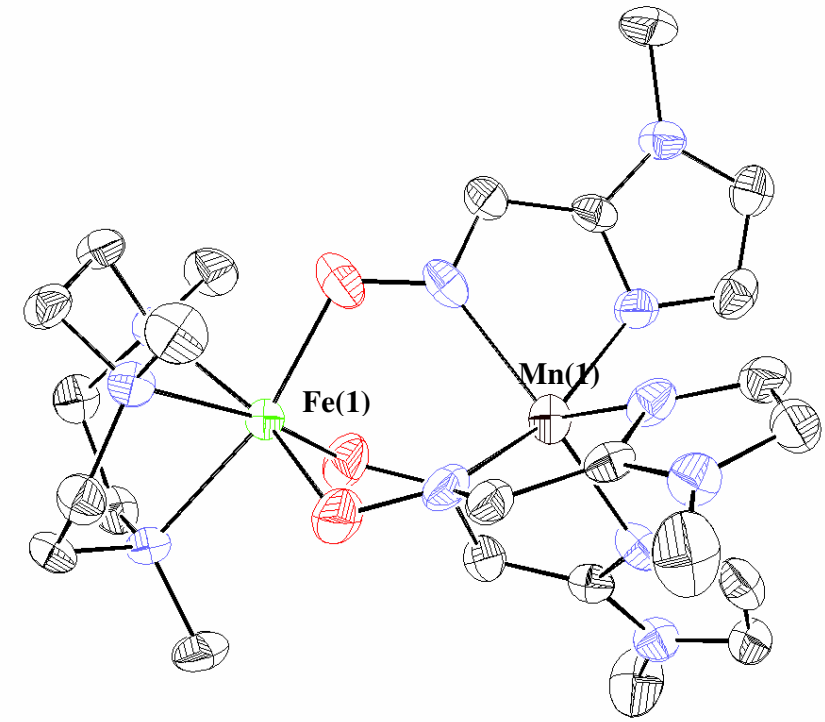

Figure 6.6b Molecular structure of the cation in complex **9**, $Fe^{III}Mn^{II}$.

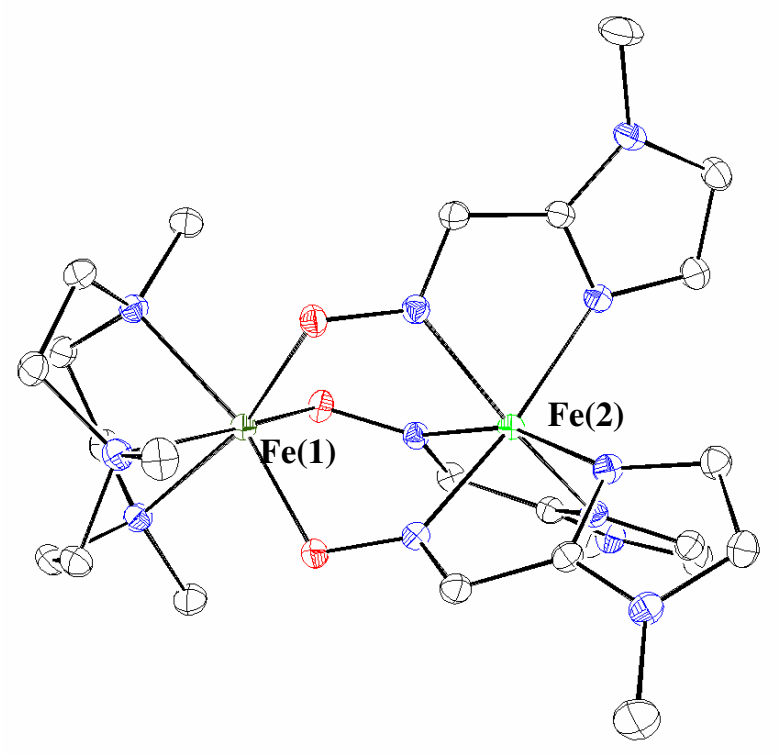

Figure 6.6c Molecular structure of the cation in complex **10**, $Fe^{III}Fe^{II}$.

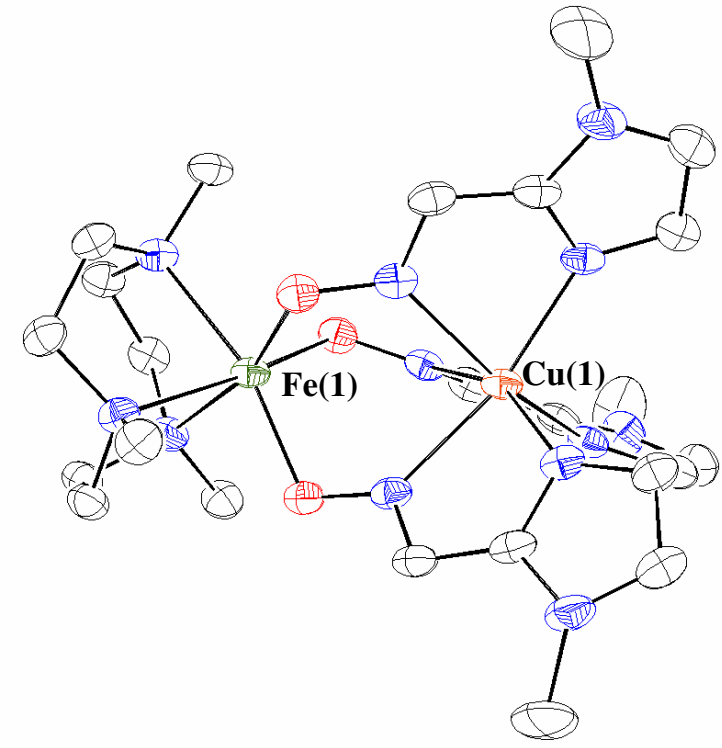

Figure 6.6d Molecular structure of the cation in complex **11**, $Fe^{III}Cu^{II}$.

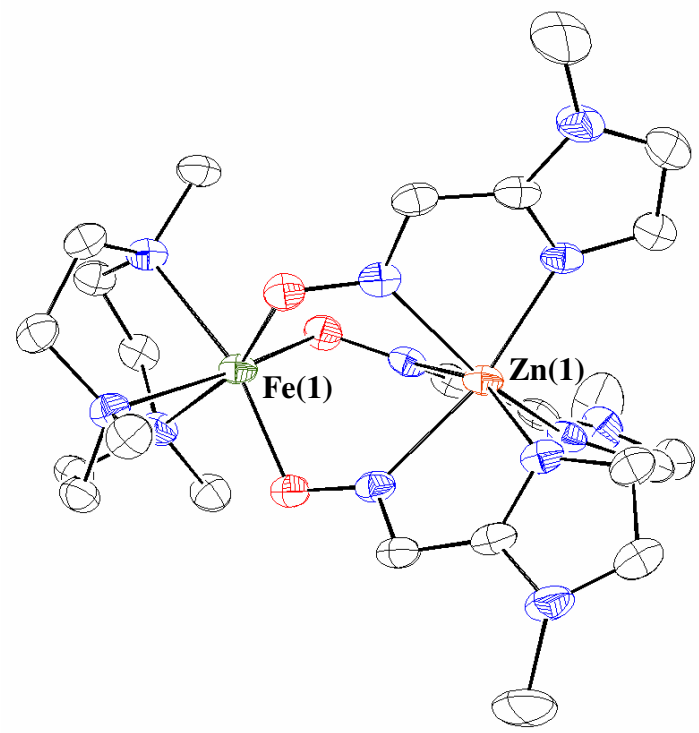

Figure 6.6e Molecular structure of the cation in complex **7**, $Fe^{III}Zn^{II}$.

Table 6.5a Selected Bond Lengths (Å) and Angles (deg) for Complex **6**, $[L'Fe^{III}(^{Me}ImOx)_3Ni^{II}](ClO_4)_2$.

Fe(1)···Ni(1)	3.477		
Fe(1)-N(1)	2.203(1)	Fe(1)-O(11)	1.974(1)
Fe(1)-N(1)#1	2.203(1)	Fe(1)-O(11)#1	1.974(1)
Fe(1)-N(1)#2	2.203(1)	Fe(1)-O(11)#2	1.974(1)
Ni(1)-N(18)	2.077(1)	Ni(1)-N(12)	2.077(1)
Ni(1)-N(18)#1	2.077(1)	Ni(1)-N(12)#1	2.077(1)
Ni(1)-N(18)#2	2.077(1)	Ni(1)-N(12)#2	2.077(1)
N(12)-C(13)	1.291(2)	O(11)-N(12)	1.353(2)
Bond Angles (deg)		Bond Angles (deg)	
N(12)-Ni(1)-N(18)	78.88(5)	N(1)#1-Fe(1)-N(1)#2	80.06(5)
N(12)#1-Ni(1)-N(18)#1	78.88(5)	N(1)#1-Fe(1)-N(1)	80.05(5)
N(12)#2-Ni(1)-N(18)#2	78.88(5)	N(1)#2-Fe(1)-N(1)	80.05(5)
N(12)#1-Ni(1)-N(12)#2	88.16(5)	O(11)#1-Fe(1)-O(11)#2	98.88(4)

N(12)#1-Ni(1)-N(12)	88.15(5)	O(11)#1-Fe(1)-O(11)	98.89 (4)
N(12)#2-Ni(1)-N(12)	88.15(5)	O(11)#2-Fe(1)-O(11)	98.89 (4)
N(18)#1-Ni(1)-N(18)#2	92.20(5)		
N(18)#1-Ni(1)-N(18)	92.20(5)		
N(18)#2-Ni(1)-N(18)	92.20(5)		

Table 6.5b Selected Bond Lengths (Å) and Angles (deg) for Complex **7**, $[L'Fe^{III}(^{Me}ImOx)_3Zn^{II}](ClO_4)_2$.

Fe(1)···Zn(1)	3.608		
Fe(1)-N(1)	2.209(2)	Fe(1)-O(11)	1.974(2)
Fe(1)-N(1)#1	2.209(2)	Fe(1)-O(11)#1	1.974(2)
Fe(1)-N(1)#2	2.209(2)	Fe(1)-O(11)#2	1.974(2)
Zn(1)-N(18)	2.096(2)	Zn(1)-N(12)	2.198(2)
Zn(1)-N(18)#1	2.096(2)	Zn(1)-N(12)#1	2.198(2)
Zn(1)-N(18)#2	2.096(2)	Zn(1)-N(12)#2	2.198(2)
N(12)-C(13)	1.284(3)	O(11)-N(12)	1.357(3)
Bond Angles (deg)		Bond Angles (deg)	
N(12)-Zn(1)-N(18)	76.52(8)	N(1)#1-Fe(1)-N(1)#2	79.67(8)
N(12)#1-Zn(1)-N(18)#1	76.51(8)	N(1)#1-Fe(1)-N(1)	79.67(8)
N(12)#2-Zn(1)-N(18)#2	76.51(8)	N(1)#2-Fe(1)-N(1)	79.67(8)
N(12)#1-Zn(1)-N(12)#2	84.46(8)	O(11)#1-Fe(1)-O(11)#2	99.96(8)
N(12)#1-Zn(1)-N(12)	84.46(8)	O(11)#1-Fe(1)-O(11)	99.96(8)
N(12)#2-Zn(1)-N(12)	84.46(8)	O(11)#2-Fe(1)-O(11)	99.96(8)
N(18)#1-Zn(1)-N(18)#2	96.02(7)		
N(18)#1-Zn(1)-N(18)	96.01(7)		
N(18)#2-Zn(1)-N(18)	96.01(7)		

Table 6.5c Selected Bond Lengths (Å) and Angles (deg) for Complex **10**, $[L'Fe^{III}(^{Me}ImOx)_3Fe^{II}](ClO_4)_2$.

Fe(1)···Fe(2)	3.364		
Fe(1)-N(1)	2.195(4)	Fe(1)-O(11)	1.972(3)
Fe(1)-N(1)#1	2.194(4)	Fe(1)-O(11)#1	1.972(3)
Fe(1)-N(1)#2	2.194(4)	Fe(1)-O(11)#2	1.972(3)
Fe(2)-N(18)	1.966(3)	Fe(2)-N(12)	1.944(3)
Fe(2)-N(18)#1	1.966(3)	Fe(2)-N(12)#1	1.944(3)
Fe(2)-N(18)#2	1.966(3)	Fe(2)-N(12)#2	1.944(3)
N(12)-C(13)	1.308(5)	O(11)-N(12)	1.339(4)
Bond Angles (deg)		Bond Angles (deg)	
N(12)-Fe(2)-N(18)	80.1(1)	N(1)#1-Fe(1)-N(1)#2	80.8(1)
N(12)#1- Fe(2)-N(18)#1	80.1(1)	N(1)#1-Fe(1)-N(1)	80.8(1)
N(12)#2- Fe(2)-N(18)#2	80.1(1)	N(1)#2-Fe(1)-N(1)	80.8(1)
N(12)#1- Fe(2)-N(12)#2	91.0(1)	O(11)#1-Fe(1)-O(11)#2	96.8(1)
N(12)#1- Fe(2)-N(12)	91.0(1)	O(11)#1-Fe(1)-O(11)	96.8(1)
N(12)#2- Fe(2)-N(12)	91.0(1)	O(11)#2-Fe(1)-O(11)	96.8(1)
N(18)#1- Fe(2)-N(18)#2	90.5(1)		
N(18)#1- Fe(2)-N(18)	90.5(1)		
N(18)#2- Fe(2)-N(18)	90.5(1)		

Table 6.6d Selected Bond Lengths (Å) and Angles (deg) for Complex **11**, $[L'Fe^{III}(^{Me}ImOx)_3Cu^{II}](ClO_4)_2$.

Fe(1)···Cu(1)	3.493		
Fe(1)-N(1)	2.191(3)	Fe(1)-O(11)	1.955(3)
Fe(1)-N(1)#1	2.191(3)	Fe(1)-O(11)#1	1.955(3)
Fe(1)-N(1)#2	2.191(3)	Fe(1)-O(11)#2	1.955(3)
Cu(1)-N(18)	2.067(3)	Cu(1)-N(12)	2.096(4)
Cu(1)-N(18)#1	2.067(3)	Cu(1)-N(12)#1	2.096(4)
Cu(1)-N(18)#2	2.067(4)	Cu(1)-N(12)#2	2.096(4)

N(12)-C(13)	1.275(5)	O(11)-N(12)	1.342(7)
Bond Angles (deg)		Bond Angles (deg)	
N(12)-Cu(1)-N(18)	77.8(1)	N(1)#1-Fe(1)-N(1)#2	79.8(1)
N(12)#1-Cu(1)-N(18)#1	77.8(1)	N(1)#1-Fe(1)-N(1)	79.8(1)
N(12)#2-Cu(1)-N(18)#2	77.8(1)	N(1)#2-Fe(1)-N(1)	79.8(1)
N(12)#1-Cu(1)-N(12)#2	86.9(1)	O(11)#1-Fe(1)-O(11)#2	99.1(1)
N(12)#1-Cu(1)-N(12)	86.9(1)	O(11)#1-Fe(1)-O(11)	99.1(1)
N(12)#2-Cu(1)-N(12)	86.9(1)	O(11)#2-Fe(1)-O(11)	99.1(1)
N(18)#1-Cu(1)-N(18)#2	93.1(1)		
N(18)#1-Cu(1)-N(18)	93.1(1)		
N(18)#2-Cu(1)-N(18)	93.1(1)		

X-ray Structure of $[L'Co^{III}(^{Me}ImOx)_3Fe^{II}](ClO_4)_2$ (12)

The molecular geometry and atom labeling scheme of **12** are shown in the Figure 6.6f. The crystallographic analysis of the complex revealed that the structure of **12** consists of a dinuclear dication, $[L'Co^{III}(^{Me}ImOx)_3M^{II}]^{2+}$, and two perchlorate anions. The selected bond distances and angles are listed in Table 6.5e. The cobalt center has distorted octahedral coordination with three nitrogen atoms from the facially coordinated tridentate macrocyclic amine L' and three oxygen atoms from the bridging oximato groups. The Co(1)-N(1) (average 2.032 ± 0.012 Å) and Co(1)-O(11) (average 1.955 ± 0.012 Å) distances correspond well with literature values for low-spin Co^{III} with d^6 electronic configuration[31] and also in agreement with the similar complex with pyridine-2-aldoximato ligand.[28]

The second metal center, iron, is also sixfold coordinated yielding a FeN_6 core. Coordination occurs through three imidazole nitrogen atoms and three azomethine nitrogen atoms (Figure 6.6f). The Fe(11)-N(12) (average 1.917 ± 0.012 Å) and Fe(1)-N(18) (average 1.954 ± 0.009 Å) bond lengths are consistent with a d^6 low-spin electron configuration for the Fe^{II} center, which was confirmed also by Mössbauer analysis.

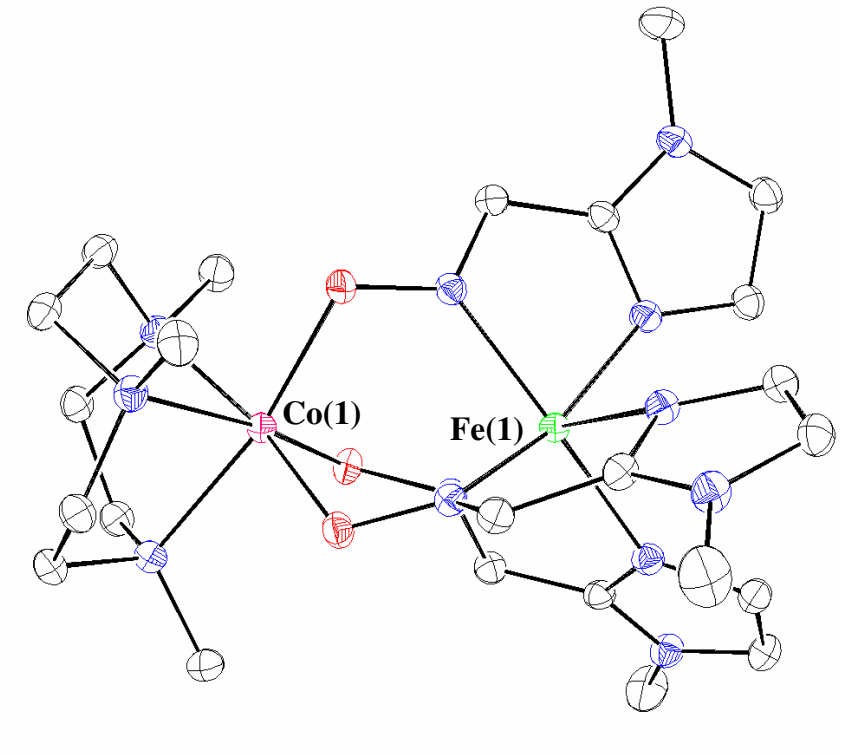

Figure 6.6f Molecular structure of the cation in complex **12**, $Co^{III}Fe^{II}$.

Table 6.5e Selected Bond Lengths (Å) and Angles (deg) for Complex **12**, $[L'Co^{III}(^{Me}ImOx)_3Fe^{II}](ClO_4)_2$.

Co(1)···Fe(1)	3.477		
Co(1)-N(1)	1.955(4)	Co(1)-O(11)	2.032(4)
Co(1)-N(1)#1	1.955(5)	Co(1)-O(11)#1	2.032(4)
Fe(1)-N(1)#2	1.955(4)	Co(1)-O(11)#2	2.032(4)
Fe(1)-N(18)	1.954(3)	Fe(1)-N(12)	1.917(4)
Fe(1)-N(18)#1	1.954(3)	Fe(1)-N(12)#1	1.917(4)
Fe(1)-N(18)#2	1.954(3)	Fe(1)-N(12)#2	1.917(4)
N(12)-C(13)	1.307(5)	O(11)-N(12)	1.353(7)
Bond Angles (deg)		Bond Angles (deg)	
N(12)-Fe(1)-N(18)	81.7(2)	N(1)#1-Co(1)-N(1)#2	85.1(2)
N(12)#1-Fe(1)-N(18)#1	81.7(2)	N(1)#1-Co(1)-N(1)	85.1(2)
N(12)#2-Fe(1)-N(18)#2	81.7(2)	N(1)#2-Co(1)-N(1)	85.1(2)

N(12)#1-Fe(1)-N(12)#2	90.1(2)	O(11)#1-Co(1)-O(11)#2	94.3(2)
N(12)#1-Fe(1)-N(12)	90.1(2)	O(11)#1-Co(1)-O(11)	94.3(2)
N(12)#2-Fe(1)-N(12)	90.1(2)	O(11)#2-Co(1)-O(11)	94.3(2)
N(18)#1-Fe(1)-N(18)#2	90.4(2)		
N(18)#1-Fe(1)-N(18)	90.4(2)		
N(18)#2-Fe(1)-N(18)	90.4(2)		

X-ray Structure of $[L'Cr^{III}(^{Me}ImOx)_3Ni^{II}](ClO_4)_2$ (13)

The molecular geometry and atom labeling scheme of the dication are shown in Figure 6.6g. The X-ray structure confirms that the mixed-metal $Cr^{III}Ni^{II}$ complex has indeed been formed. The selected bond distances and angles are listed in Table 6.5f.

The chromium ion in the dinuclear dication is in a distorted octahedral ligand environment, having CrN_3O_3 coordination sphere. The Cr(1)-N(1) (average 2.116 ± 0.012 Å) and Cr(1)-O(11) (average 1.968 ± 0.012 Å) distances correspond well with literature values for high-spin Cr^{III} complexes with this macrocyclic amine and again in good agreement with a similar complex with pyridine-2-aldoximato ligand.[27] Deviations from the idealized octahedral geometry are found for the ligand L', the average N-Cr-N angle is 83.02(5)º, whereas the average O-Cr-O angle is 97.08(4)º. The second metal ion, Ni^{II}, is also in six-fold coordination geometry yielding a NiN_6 core as in the above complexes. The Ni(1)-N(18) (average 2.084 ± 0.003 Å) and Ni(1)-N(12) (average 2.069 ± 0.003 Å) bond lengths are very similar to the analogous complex $[L'Cr^{III}(PyA)_3Ni^{II}]$ with the pyridinealdoxime ligand and also to the complex $[L'Fe^{III}(^{Me}ImOx)_3Ni^{II}]^{2+}$, **6**.[27] These bond distances are also in good agreement with a d^8 high-spin electronic configuration for the Ni^{II} centers, which is in complete agreement with the EPR and SQUID results.

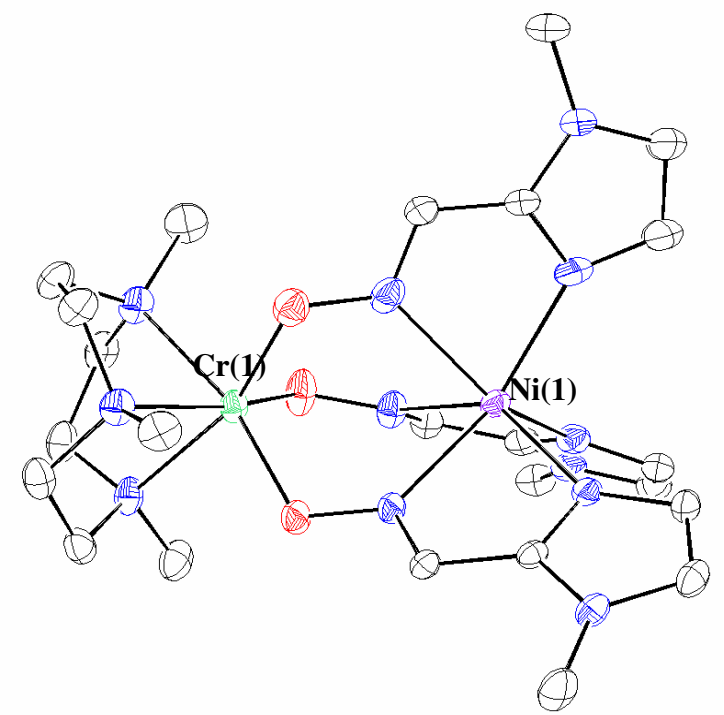

Figure 6.6g Molecular structure of the cation in complex **13**, $Cr^{III}Ni^{II}$

X-ray Structure of $[L'Ga^{III}(^{Me}ImOx)_3Ni^{II}](ClO_4)_2$ (8)

The molecular geometry and atom labeling scheme of **8** are shown in the Figure 6.6h. The crystallographic analysis of the complex revealed that the structure of **8** consists of a dinuclear dication, $[L'Ga^{III}(^{Me}ImOx)_3M^{II}]^{2+}$, and two perchlorate anions. The selected bond distances and angles are listed in Table 6.5f. The gallium center has distorted octahedral coordination with three nitrogen atoms from the facially coordinated tridentate macrocyclic amine L' and three oxygen atoms from the bridging oximato groups. The Ga(1)-N(1) and Ga(1)-O(11) bond lengths are 2.0132 ± 0.003 and 1.964 ± 0.003 Å, respectively. Deviations from the idealized octahedral geometry are found for the ligand L', the average N-Ga-N angle is 82.80(5)º, whereas the average O-Ga-O angle is 97.86(4)º.

The second metal ion, Ni^{II}, is also in six-fold coordination geometry yielding a NiN_6 core as in the above complexes. The Ni(1)-N(18) (average 2.083 ± 0.003 Å) and Ni(1)-N(12) (average 2.067 ± 0.003 Å) bond lengths are very similar to the analogous complex $[L'Fe^{III}(^{Me}ImOx)_3Ni^{II}]^{2+}$, **6** and $[L'Cr^{III}(^{Me}ImOx)_3Ni^{II}]^{2+}$, **13**. These bond

distances are also in good agreement with a d^8 high-spin electronic configuration for the Ni^{II} centers, which is in complete agreement with the SQUID result.

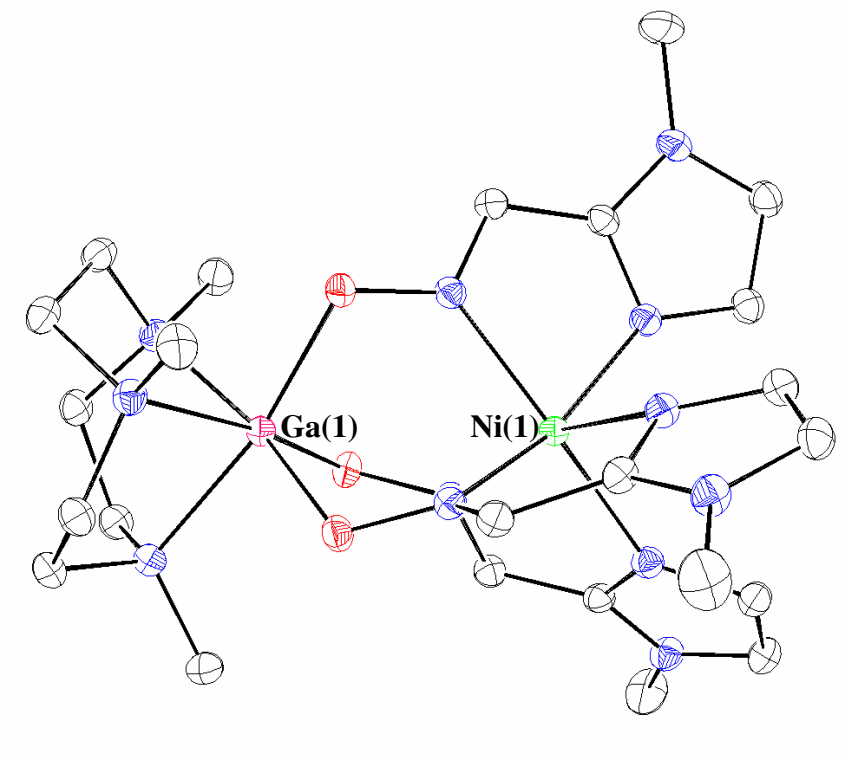

Figure 6.6h Molecular structure of the cation in complex **8**, $Ga^{III}Ni^{II}$

Table 6.5f Selected Bond Lengths (Å) and Angles (deg) for Complex **13**, $[L'Cr^{III}(^{Me}ImOx)_3Ni^{II}](ClO_4)_2$.

Cr(1)···Ni(1)	3.518		
Cr(1)-N(1)	2.111(6)	Cr(1)-O(11)	1.968(1)
Cr(1)-N(1)#1	2.111(6)	Cr(1)-O(11)#1	1.968(1)
Cr(1)-N(1)#2	2.111(6)	Cr(1)-O(11)#2	1.968(1)
Ni(1)-N(18)	2.084(1)	Ni(1)-N(12)	2.069(1)
Ni(1)-N(18)#1	2.084(1)	Ni(1)-N(12)#1	2.069(1)
Ni(1)-N(18)#2	2.084(1)	Ni(1)-N(12)#2	2.069(1)
N(12)-C(13)	1.294(2)	O(11)-N(12)	1.349(2)
Bond Angles (deg)		Bond Angles (deg)	
N(12)-Ni(1)-N(18)	79.0(5)	N(1)#1-Cr(1)-N(1)#2	83.0(5)

N(12)#1-Ni(1)-N(18)#1	79.0(5)	N(1)#1-Cr(1)-N(1)	83.0(5)
N(12)#2-Ni(1)-N(18)#2	79.0(5)	N(1)#2-Cr(1)-N(1)	83.0(5)
N(12)#1-Ni(1)-N(12)#2	87.8(5)	O(11)#1-Cr(1)-O(11)#2	97.1(4)
N(12)#1-Ni(1)-N(12)	87.8(5)	O(11)#1-Cr(1)-O(11)	97.1(4)
N(12)#2-Ni(1)-N(12)	87.8(5)	O(11)#2-Cr(1)-O(11)	97.1(4)
N(18)#1-Ni(1)-N(18)#2	91.9(5)		
N(18)#1-Ni(1)-N(18)	91.9(5)		
N(18)#2-Ni(1)-N(18)	91.9(5)		

Table 6.5g Selected Bond Lengths (Å) and Angles (deg) for Complex **8**, $[L'Ga^{III}(^{Me}ImOx)_3Ni^{II}](ClO_4)_2$.

Ga(1)···Ni(1)	3.499		
Ga(1)-N(1)	2.132(1)	Ga(1)-O(11)	1.964(1)
Ga(1)-N(1)#1	2.132(1)	Ga(1)-O(11)#1	1.964(1)
Ga(1)-N(1)#2	2.133(1)	Ga(1)-O(11)#2	1.964(1)
Ni(1)-N(18)	2.083(1)	Ni(1)-N(12)	2.067(1)
Ni(1)-N(18)#1	2.083(1)	Ni(1)-N(12)#1	2.067(1)
Ni(1)-N(18)#2	2.083(1)	Ni(1)-N(12)#2	2.067(1)
N(12)-C(13)	1.294(2)	O(11)-N(12)	1.349(2)
Bond Angles (deg)		Bond Angles (deg)	
N(12)-Ni(1)-N(18)	78.96(5)	N(1)#1-Ga(1)-N(1)#2	82.80(5)
N(12)#1-Ni(1)-N(18)#1	78.97(5)	N(1)#1-Ga(1)-N(1)	82.80(5)
N(12)#2-Ni(1)-N(18)#2	78.97(5)	N(1)#2-Ga(1)-N(1)	82.79(5)
N(12)#1-Ni(1)-N(12)#2	87.7(5)	O(11)#1-Ga(1)-O(11)#2	97.86(4)
N(12)#1-Ni(1)-N(12)	87.7(5)	O(11)#1-Ga(1)-O(11)	97.86(4)
N(12)#2-Ni(1)-N(12)	87.7(5)	O(11)#2-Ga(1)-O(11)	97.86(4)
N(18)#1-Ni(1)-N(18)#2	91.99(5)		
N(18)#1-Ni(1)-N(18)	91.98(5)		
N(18)#2-Ni(1)-N(18)	91.98(5)		

Table 6.6 Important Structural Parameters for Complex **6**, **7** and **9**-**13**.

Complex	M'···M (Å)	av. twist angle ϕ (deg)*	dihedral angle θ (deg)**
6 $Fe^{III}Ni^{II}$	3.477	38.5	33.9/33.9/33.9
7 $Fe^{III}Zn^{II}$	3.608	33.3	33.4/33.4/33.4
9 $Fe^{III}Mn^{II}$	3.657	16.7	23.7/27.5/25.3
10 $Fe^{III}Fe^{II}$	3.364	44.2	36.6/36.6/36.6
11 $Fe^{III}Cu^{II}$	3.493	35.4	33.3/33.3/33.3
12 $Co^{III}Fe^{II}$	3.429	44.9	37.4/37.4/37.4
13 $Cr^{III}Ni^{II}$	3.518	37.6	33.9/33.9/33.9

* The Trigonal twist angle is the angle between the triangular faces comprising N(12)N(12)#1N(12)#2 and N(18)N(18)#1N(12)#2 and has been calculated as the mean of the Newman projection angles viewed along the centroids of focus. For an ideal trigonal prismatic arrangement, ϕ is 0º and for an octahedron or trigonal-antiprismatic arrangement ϕ is 60º.

**Dihedral angles θ between the planes comprising M'(O-N) and M(N-O) atoms show that the cores M'(O-N)M are not linear.

Table 6.7 Selected Bond Lengths [Å] for $[L'Fe^{III}M^{II}(PyA)_3]^{2+}$ &$[L'Fe^{III}M^{II}(ImOx)_3]^{2+}$.[28]

With PyA	$Fe^{III}Zn^{II}$	$Fe^{III}Cu^{II}$	$Fe^{III}Ni^{II}$	$Fe^{III}Fe^{II}$
Fe-N(1)	2.201(4)	2.187(3)	2.192(6)	2.202(6)
Fe-N(2)	2.206(4)	2.201(3)	2.186(6)	2.174(8)
Fe-N(3)	2.196(4)	2.186(3)	2.190(6)	2.195(8)
Fe-O(1)	1.973(3)	1.950(2)	1.971(4)	1.963(5)
Fe-O(2)	1.967(3)	1.993(2)	1.967(5)	1.970(7)
Fe-O(3)	1.949(4)	1.967(2)	1.989(5)	1.976(7)
M-N(5)py	2.149(4)	2.293(3)	2.108(6)	1.977(7)
M-N(7)py	2.159(4)	2.114(3)	2.116(6)	1.990(8)
M-N(9)py	2.160(4)	2.023(3)	2.093(6)	2.001(8)
M-N(6)ox	2.155(4)	2.002(3)	2.052(6)	1.926(8)
M-N(8)ox	2.155(4)	2.129(3)	2.071(6)	1.907(8)
M-N(4)ox	2.205(4)	2.150(3)	2.063(6)	1.922(8)

With ^{Me}ImOx	$Fe^{III}Zn^{II}$	$Fe^{III}Cu^{II}$	$Fe^{III}Ni^{II}$	$Fe^{III}Fe^{II}$
Fe-N(1)	2.209(2)	2.191(3)	2.203(1)	2.195(4)
Fe-N(1)#1	2.209(2)	2.191(3)	2.203(1)	2.194(4)
Fe-N(1)#2	2.209(2)	2.191(3)	2.203(1)	2.194(4)
Fe-O(11)	1.974(2)	1.955(3)	1.974(1)	1.972(3)
Fe-O(11)#1	1.974(2)	1.955(3)	1.974(1)	1.972(3)
Fe-O(11)#2	1.974(2)	1.955(3)	1.974(1)	1.972(3)
M-N(12)	2.198(2)	2.096(4)	2.077(1)	1.944(3)
M-N(12)#1	2.198(2)	2.096(4)	2.077(1)	1.944(3)
M-N(12)#2	2.198(2)	2.096(4)	2.077(1)	1.944(3)
M-N(18)	2.096(2)	2.067(3)	2.077(1)	1.966(3)
M-N(18)#1	2.096(2)	2.067(4)	2.077(1)	1.966(3)
M-N(18)#2	2.096(2)	2.067(3)	2.077(1)	1.966(3)

6.8 Magnetic Properties

The magnetic susceptibility data for a polycrystalline dried sample of **6-14** were collected in the temperature range 2–290 K in an applied magnetic field of 1 T to investigate the nature and magnitude of the exchange interaction propagated by the bridging oxime ligands. A plot of μ_{eff} (effective magnetic moment) *vs*. *T* (temperature) is displayed in Figure 6.7 The experimental magnetic data were simulated using the least-squares fitting computer program JulX with a full-matrix diagonalization exchange coupling. The solid lines in Figure 6.7 represent the simulations.

Complexes **7** and **8** each contain only one paramagnetic center, Fe(III) and Ni(II), respectively and thus, are magnetically mononuclear complexes. Above 20 K, complex **7** exhibits temperature independent μ_{eff} values of 5.87 ± 0.07 μ_B, which is simply the spin-only value for an S = 5/2 system. Simulations of the experimental magnetic moment data yield a g_{Fe}-value of 2.00 with S_{Fe} = 5/2 and S_{Zn} = 0, for **7**. The magnetic moment μ_{eff}/molecule for **8** decreases slowly from 3.07 μ_B ($\chi_M T$ = 1.18 cm^3 mol^{-1} K) at 290 K and to 2.98 μ_B ($\chi_M T$ = 1.11 cm^3 mol^{-1} K) at 10 K. Below 10 K, the μ_{eff} decreases rapidly and reaches a value of 2.51 μ_B ($\chi_M T$ = 0.79 cm^3 mol^{-1} K) at 2 K. This μ_{eff}/molecule value is higher than the spin only vale for S = 1 system at 5 – 290 K, which is in agreement with a certain amount of spin-orbit coupling at h.s. Ni(II) center. Simulations of the experimental magnetic moment data yield a g_{Ni}-value of 2.13 with S_{Ni} = 1 and S_{Ga} = 0, for **8**. The observed g_{Ni} value agrees well with the comparable g_{Ni} values reported earlier. [22,27,28]

Complexes **10** and **14** also contain only one paramagnetic center viz. Fe(III) (h.s.)/Cr(III), thus those complexes are again magnetically mononuclear. In the range 10-290 K complexes **10** and **14** exhibit temperature independent μ_{eff} values of 5.80 ± 0.1 μ_B and 3.74 ± 0.01 μ_B, respectively. Below 10 K those values drop rapidly to 4.77 μ_B and 3.53 μ_B. Below 10 K, the decrease in μ_{eff} values due to the combined effects of field saturation, exchange and single ion zero-field splitting. There are five unpaired electrons localized on the Fe(III) center in **10** and three unpaired electrons localized on the Cr(III) center in **14**, and the 'spin-only' (g = 2.00) magnetic moments are 5.91 μ_B and 3.87 μ_B, respectively. The experimental μ_{eff} values clearly indicate that those complexes are genuine Fe(III)Fe(II) (h.s.-l.s.) and Cr(III)Zn(II) with a low spin Fe(II) ion or a

diamagnetic d^{10} Zn(II) ion. Simulations of the magnetic moment data yield a $g_{Fe(III)}$-value of 2.00 with $S_{Fe(III)} = 5/2$ and $S_{Fe(II)} = 0$ for **10** and a g_{Cr} value of 1.94 with $S_{Cr(III)} = 5/2$ and $S_{Zn(II)} = 0$ for **14** (Figure 6.7b).

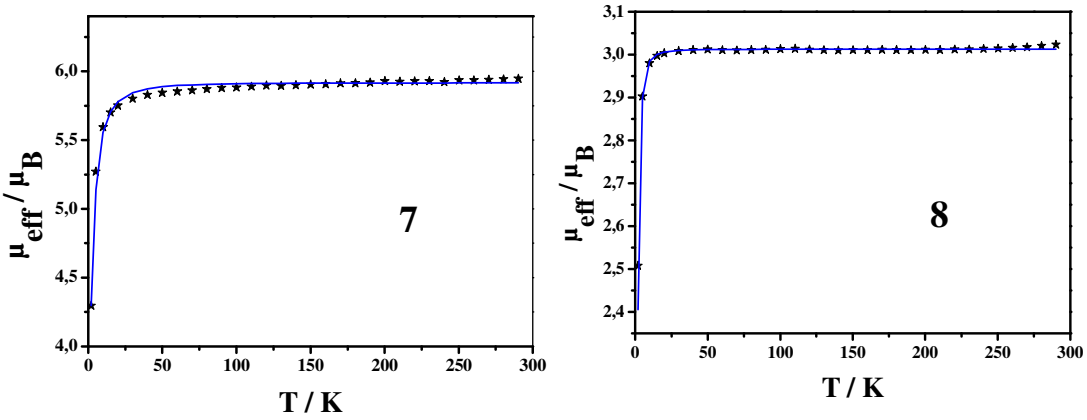

Figure 6.7a Temperature-dependence of the magnetic moment μ_{eff} of **7** (left) and **8** (right) at an applied magnetic field of 1 T. The bold points represent the experimental data while the solid line represents the simulation.

At 290 K, complex **6** exhibits an effective magnetic moment, μ_{eff}, of 5.55 μ_B ($\chi_M T$ = 3.85 cm^3 mol^{-1} K) which is lower than the high temperature limit expected for magnetically uncoupled one h.s. iron(III) ion and one nickel(II) ion. This magnetic moment decreases monotonically with decreasing temperature to reach a value of μ_{eff} = 3.26 μ_B ($\chi_M T$ = 1.33 cm^3 mol^{-1} K) at 10 K; below 5 K there is a sharp drop reaching a value of μ_{eff} = 2.54 μ_B ($\chi_M T$ = 0.81 cm^3 mol^{-1} K) at 2 K. This magnetic behavior clearly indicates the presence of an antiferromagnetic exchange coupling between the h.s. Fe(III) center and h.s. Ni(II) center in **6**. The μ_{eff} value at 2 K indicates a non-diamagnetic low-lying state. The sharp drop of μ_{eff} at 2 K is due to the combined effects of field saturation, exchange and single-ion zero-field. The temperature dependence of μ_{eff} was well simulated, shown as a solid line in Figure 6.7c, with the parameters J = -28.7 cm^{-1}, g_{Fe} = 2.00, g_{Ni} = 2.15 cm^{-1}, D_{Fe} = - 3.8 cm^{-1}, D_{Ni} = - 7.5 cm^{-1} (fixed), E/D = 0.1. It should be mentioned that it is difficult to evaluate the D and E/D value accurately from SQUID measurements, but in this case without such kind of D and E/D values experimental values at low temperature (2-20 K) do not fit well with the experimental values.

Moreover, these *D* and E/D values are in well accord with the EPR simulation. The observed antiferromagnetic coupling constant agrees well with the comparable exchange coupling constants reported earlier.[27]

At 290 K, complex **11** exhibits the effective magnetic moment, μ_{eff}, of 5.61 μ_B ($\chi_M T$ = 3.93 $cm^3\ mol^{-1}\ K$) which is lower than the high temperature limit expected, 6.16 μ_B, for magnetically uncoupled one h.s. iron(III) ion and one Cu(II) ion. This magnetic moment decreases monotonically with decrease in temperature to reach a value of μ_{eff} = 4.71 μ_B ($\chi_M T$ = 2.77 $cm^3\ mol^{-1}\ K$) at 15 K; below 15 K there is a sharp drop reaching a value of μ_{eff} = 3.74 μ_B ($\chi_M T$ = 1.75 $cm^3\ mol^{-1}\ K$) at 2 K. This magnetic behavior clearly indicates the presence of an antiferromagnetic exchange coupling between the h.s. Fe(III) center and Cu(II) center in **11**. The μ_{eff} value at 2 K indicates a non-diamagnetic low-lying state. The sharp drop at 2 K due to the combined effects of field saturation, exchange and single-ion zero-field. The temperature dependence of μ_{eff} was well simulated, shown as a solid line in Figure 6.7c, with the parameters J = -38.0 cm^{-1}, g_{Fe} = 2.00, g_{Cu} = 2.15 and $|D_{Fe}|$ = 3.8 cm^{-1}.

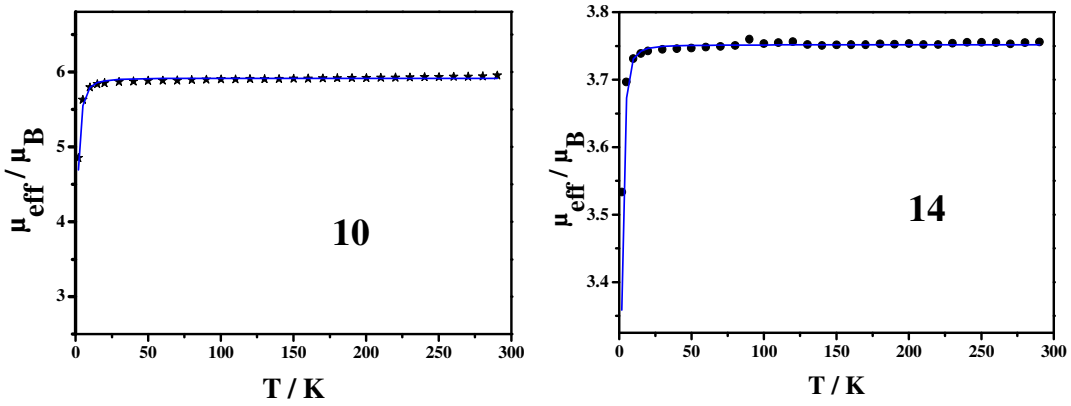

Figure 6.7b Temperature-dependence of the magnetic moment μ_{eff} of **10** (left) and **14** (right) at an applied magnetic field of 1 T. The bold points represent the experimental data while the solid line represents the simulation.

The magnetic moment μ_{eff}/molecule for **9**, Fe(III)Mn(II), of 6.72 μ_B ($\chi_M \cdot T$ = 5.64 $cm^3 \cdot K \cdot mol^{-1}$) at 290 K, is smaller than the spin only value of μ_{eff}/molecule (g = 2) for a unit composed of noninteracting [Fe(III)Mn(II)] ions is 8.37 μ_B ($\chi_M \cdot T$ = 7.02 $cm^3 \cdot K \cdot mol^{-1}$) and decreases continuously with decreasing temperature until it reaches a value of 0.37

μ_B (χ_M·T = 0.02 cm^3·K·mol^{-1}) at 2 K. Hence the molecule appears to have an antiferromagnetic exchange coupling between the paramagnetic Fe(III) (S = 5/2) and Mn(II) (S = 5/2) ions. This temperature dependence behavior is in agreement with a diamagnetic ground state, evident from the μ_{eff} value at 2 K. The temperature dependence of μ_{eff} was well simulated, shown as a solid line in Figure 6.7d, with the parameters J = -7.3 cm^{-1}, g_{Fe} = 2.00 and g_{Mn} = 2.00.

The magnetic moment μ_{eff}/molecule for **13**, Cr(III)Ni(II), of 4.40 μ_B (χ_M·T = 2.42 cm^3·K·mol^{-1}) at 290 K, is smaller than the spin only value of μ_{eff}/molecule (g = 2) for a unit composed of noninteracting [Cr(III)Ni(II)] ions is 4.80 μ_B (χ_M·T = 7.02 cm^3·K·mol^{-1}). This magnetic moment decrease monotonically until it reaches a value of 3.38 μ_B ((χ_M·T = 1.43 cm^3·K·mol^{-1}) at 30 K. Because of normal field saturation the magnetic moment decreases further and reaches a value of 1.28 μ_B ((χ_M·T = 0.21 cm^3·K·mol^{-1}) at 2 K. This temperature dependence is in accord with a moderate antiferromagnetic coupling between the neighbouring Cr(III) and Ni(II) ions in an S_t = ½ ground state. The temperature dependence of μ_{eff} was well simulated, shown as a solid line in Figure 6.7d, with the parameters J = -5.1 cm^{-1}, g_{Cr} = 1.95, g_{Ni} = 2.10, $|D_{Cr}|$ = 3.0 cm^{-1} and $|D_{Ni}|$ = 5.0 cm^{-1}. The observed g_{Cr} and g_{Ni} values agree well with values reported earlier.[27] One point has to be mentioned that it is not possible to evaluate the exact D value from the SQUID measurements, but it is necessary to use such kind of D values during the simulation.

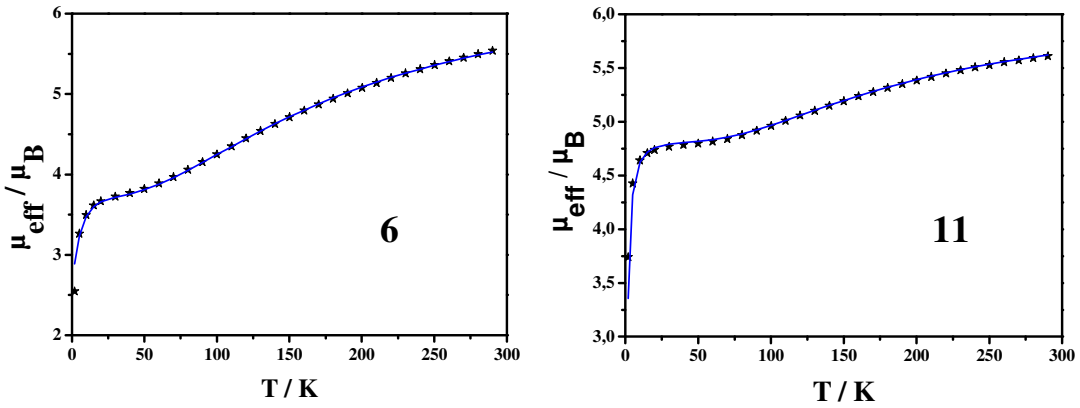

Figure 6.7c Temperature-dependence of the magnetic moment μ_{eff} of **6** (left) and **11** (right) at an applied magnetic field of 1 T. The bold points represent the experimental data while the solid line represents the simulation

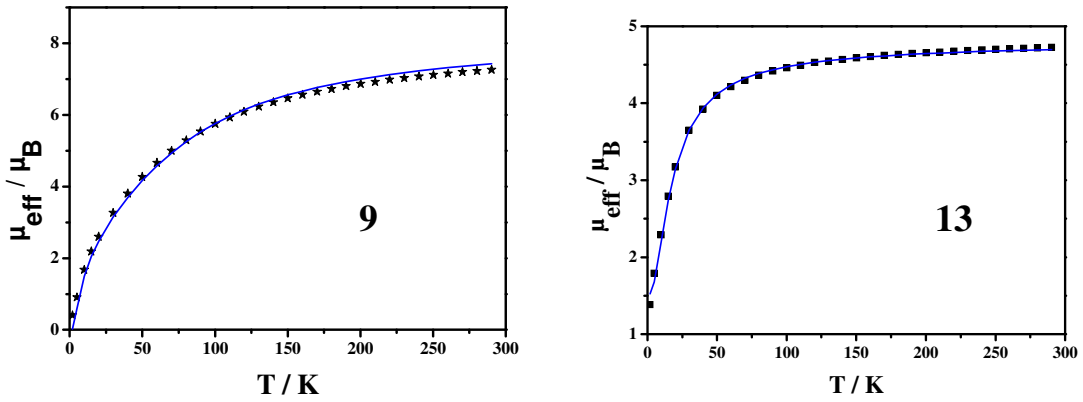

Figure 6.7d Temperature-dependence of the magnetic moment μ_{eff} of **9** (left) and **13** (right) at an applied magnetic field of 1 T. The bold points represent the experimental data while the solid line represents the simulation

Table 6.8a Simulated Magnetic Parameters for Dinuclear Complexes **6**, **7** and **9**-**14**.

Complex	J (cm^{-1})	$g_{M'}$	g_M	Ground state (S_t)
7 $Fe^{III}Zn^{II}$	(μ_{eff} = 5.87 ± 0.07 μ_B)	2.00	-	5/2
11 $Fe^{III}Cu^{II}$	-38.0	2.00	2.15	4/2
6 $Fe^{III}Ni^{II}$	-28.7	2.00	2.15	3/2
10 $Fe^{III}Fe^{II}$	(μ_{eff} = 5.80 ± 0.1 μ_B)	2.00	-	5/2
9 $Fe^{III}Mn^{II}$	-7.3	2.00	2.00	0
13 $Cr^{III}Ni^{II}$	-5.1	1.95	2.10	½
14 $Cr^{III}Zn^{II}$	(μ_{eff} = 3.74 ± 0.01 μ_B)	1.94	-	3/2

Table 6.8b Simulated Magnetic Parameters for Analogous Dinuclear Complexes with Pyridinealdoxime Ligand.[27,28]

Complex	J (cm^{-1})	$g_{M'}$	g_M	Ground state (St)
$Fe^{III}Zn^{II}$	(μ_{eff} = 5.90 ± 0.02 μ_B)	2.00	-	5/2
$Fe^{III}Cu^{II}$	-42.5	2.00	2.05	4/2
$Fe^{III}Ni^{II}$	-34.0	2.00	2.12	3/2
$Fe^{III}Fe^{II}$	(μ_{eff} = 5.80 ± 0.05 μ_B)	1.96	-	5/2
$Fe^{III}Mn^{II}$	-6.1	2.00	2.00	0
$Cr^{III}Ni^{II}$	-9.2	1.98	2.16	½

$Cr^{III}Zn^{II}$	-	1.96	2.10	3/2

Table 6.9 Some Important Magnetic Parameters for Complexes with Imidazoleoxime Ligand and Analogous Dinuclear Complexes with Pyridinealdoxime Ligand.[27,28]

Complexes with ^{Me}**ImOx**	J (cm^{-1}) for Complexes with ^{Me}**ImOx**	J (cm^{-1}) for Complexes with **PyA**	Complexes with **PyA**
7 $Fe^{III}Zn^{II}$	(μ_{eff} = 5.87 ± 0.07 μ_B)	(μ_{eff} = 5.90 ± 0.02 μ_B)	$Fe^{III}Zn^{II}$
11 $Fe^{III}Cu^{II}$	-38.0	-42.5	$Fe^{III}Cu^{II}$
6 $Fe^{III}Ni^{II}$	-28.7	-34.0	$Fe^{III}Ni^{II}$
10 $Fe^{III}Fe^{II}$	(μ_{eff} = 5.80 ± 0.1 μ_B)	(μ_{eff} = 5.80 ± 0.05 μ_B)	$Fe^{III}Fe^{II}$
9 $Fe^{III}Mn^{II}$	-7.3	-6.1	$Fe^{III}Mn^{II}$
13 $Cr^{III}Ni^{II}$	-5.1	-9.2	$Cr^{III}Ni^{II}$
14 $Cr^{III}Zn^{II}$	(μ_{eff} = 3.74 ± 0.01 μ_B)	(μ_{eff} = 3.87 ± 0.01 μ_B)	$Cr^{III}Zn^{II}$

Such kinds of complexes with varying d^n-electron configuration are more informative in comparison to those comprising singly isolated, exchange-coupled clusters only and also to verify the Goodenough-Kanamori rules.[32] Previously Goodenough-Kanamori rules have been analyzed by Ginsberg[33] and later by Kahn.[7] In our earlier work[27,28] we have also seen that the qualitative trend of the antiferromagnetic exchange interactions between the spin carriers in the $Fe^{III}M^{II}$ pairs [M = Cu, Ni and Mn] with PyA ligands are in good accord with the Goodenough-Kanamori rules. From earlier reports it has been established that the exchange interactions between the paramagnetic centers increase upon decreasing the number of unpaired electrons. As part of our current work this trend (Table 6.8a) is very similar to the complexes with PyA (Table 6.8b). From Cu^{II} to Mn^{II} the number of unpaired electrons increases, as a consequence the interacting path ways between the two interacting metal centers also increases. So, a $Fe^{III}Mn^{II}$ system would have a higher number of cross interactions compared to a $Fe^{III}Cu^{II}$ system. Alternatively we can say that the number of ferromagnetic pathways would increase for $Fe^{III}Mn^{II}$ system. As a result the trend for antiferromagnetic exchange interactions would be $Fe^{III}Cu^{II}$ < $Fe^{III}Ni^{II}$ < $Fe^{III}Mn^{II}$, which is in complete agreement with the observed values. Again the strength of the antiferromagnetic interactions is weaker in the present

case compared to complexes with the pyridinealdoxime ligands (Table 6.9). This may be because of the higher sigma donating ability of the pyridine-N than that of imidazole-N. Additionally, the variation in the strength of the exchange couplings within these two set of complexes can be qualitatively correlated to i)M-N_{ox} bond lengths, ii) Non bonding Fe^{III}-M/Cr^{III}-Ni distances and iii) distortion of trigonal prismatic to octahedral geometry of the M(oximato)$_3$-unit, that enhances the antiferromagnetic exchange coupling by making the magnetic orbital-overlap more effective. Only in case of $Fe^{III}Mn^{II}$ the strength of the antiferromagnetic interaction is weaker for complex with imidazoleoxime compared to the complexes with the pyridineoxime, which may be because of the high distortions in the present case.

6.9 EPR Studies

Complex 13, $Cr^{III}Ni^{II}$

The X-band EPR spectrum of **13** was recorded in CH_3CN solution at 10 K to establish the electronic ground state of the complex. The spectrum clearly shows a signal for an S = ½ system. Simulation of the EPR spectrum yields a g value of 1.88 (g_x = 1.882, g_y = 1.884 and g_z = 1.879) with S_t = ½ (Figure 6.8a).

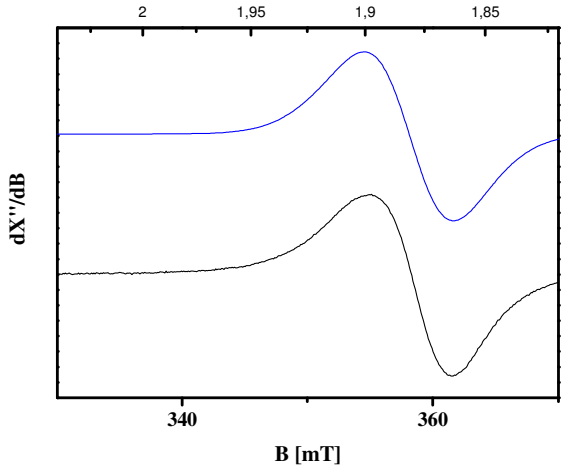

Figure 6.8a X-band EPR spectrum of **13**, in CH_3CN at 10 K (experimental conditions: microwave frequency 9.43 GHz, power 0.01 mW, modulation amplitude 10.0 G) together with the simulated spectrum (blue line).

According to the spin projection properties, the ground state parameters of complex **13** are related to the local single-ion values for chromium and nickel by: $g_t = (5/3)g_{Cr} - (2/3)g_{Ni}$. This spin projection clearly indicates that chromium ion has the dominant influence on the properties of the ground state. With the value $g_{Cr} = 1.95$ derived from the magnetic data (using $g_{Ni} = 2.10$ (fixed)), one obtains for the spin quadruplet $g_t = 1.85$, which is very close to the experimental value obtained from the EPR simulations (1.88). Hence, EPR and SQUID measurements are in good agreement with each other to determine the electronic properties of Cr(III) and Ni(II) ion in **13**.

Complex 6, $Fe^{III}Ni^{II}$

An X-band EPR spectrum of **6** was recorded in CH_3CN solution at 10 K to establish the electronic ground state of the complex. The presence of derivative lines at g ≈ 4 and 2 with strong axial zero-field splitting ($D_t > h\nu$) and low rhombicity ($0 > E/D_t > 0.1$), are a clear indication of $S_t = 3/2$. Additionally, the presence of a distinct sharp peak at g ≈ 6, indicates the $|m_s = \pm 3/2>$ Kramers doublet to be the ground state (Figure 6.9), as a result of the negative zfs parameter D_t. The spectrum could be simulated reasonably well by using equation 1 for total spin $S_t = 3/2$ with parameters $D_t = -7.5$ cm^{-1}, $E/D_t = 0.078$, $g_t = (2.010, 2.010, 1.940)$, and an isotropic g value $g_{t,iso} = 1.987$ (Figure 6.8b).

$$H_e = D[S_{t,z}^2 - S_t(S_t+1)/3 + (E/D)(S_{t,x}^2 - S_{t,y}^2)] + \mu_B B \cdot g \cdot S_t \qquad \text{equation 1}$$

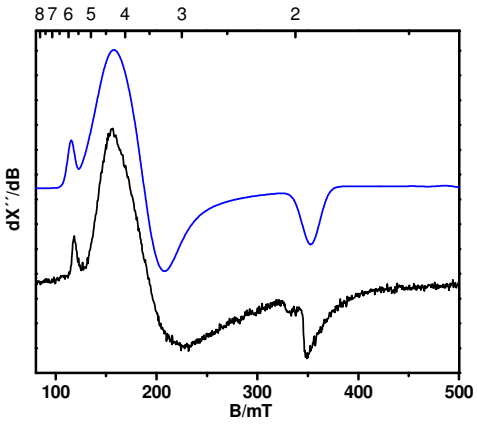

Figure 6.8b X-band EPR spectrum of **6**, $Fe^{III}Ni^{II}$, in CH_3CN at 10 K (experimental conditions: microwave frequency 9.45 GHz, power 0.10 mW, modulation amplitude 14.0 G) together with the simulated spectrum (blue line).

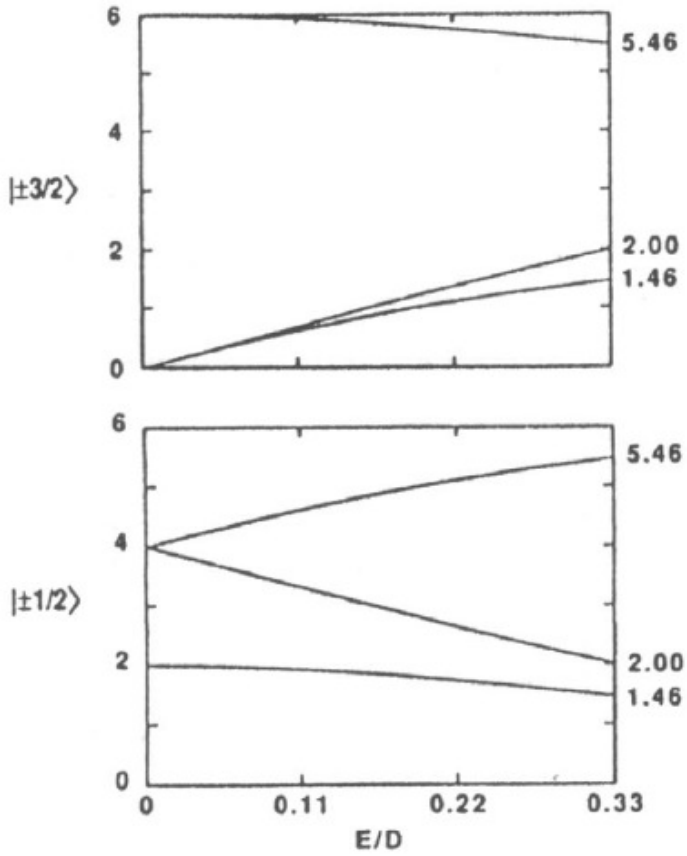

Figure 6.9 A rhombogram for S = 3/2: effective g values of the two intra-doublet transitions as a function of the rhombocity η = E/D.

According to the spin projection properties, the ground state parameters of complex **6** are related to the local single-ion values for iron and nickel by:

$D_t = (28/15)D_{Fe} + (1/15)D_{Ni}$ (neglecting dipolar contributions)

and $g_t = (7/5)g_{Fe} – (2/5)g_{Ni}$.

This spin projection clearly indicates that iron ion has the dominant influence on the properties of the ground state. With the zfs value D_{Fe} = - 3.8 cm^{-1} derived from the magnetic data (using D_{Ni} = 7.5 cm^{-1} (fixed)), one obtains for the spin quadruplet D_t = -7.6 cm^{-1}, which is very close to the experimental value obtained from the EPR simulations (-7.5 cm^{-1}). Hence, EPR and SQUID measurements are in good agreement with each other to determine the electronic properties of Fe(III) and Ni(II) ion in **6**.

6.10 MCD Studies of Complexes 6, 7 and 8

The basic principle of MCD has been discussed in Chapter 1 and herein we show the experimental spectra within the temperature range 1.8-20 K and assignments of the low temperature MCD spectra for **6**-**8**. All other documents have been shown in appendices part.

All the spectra were found to be temperature dependent (Figure 6.10) within the temperature range 1.8-20 K. The temperature dependence of the MCD spectrum of Ga-Ni, **8** shows that the spectrum mainly consists of 'B' or 'C' terms. In Ga-Ni, as the ground state is orbitally nondegenerate, so only 'A' terms are expected due to first order spin-orbit coupling interaction.[37] In this case the 'C' term arises due to the spin degeneracy and second order spin-orbit coupling interaction of the triplet state, and 'B' terms arise from the magnetic field induced mixing of the ground state with the excited state or the excited state with each other.[38,39] The temperature dependence of the MCD spectra of **6** and **7** also show that the spectra mainly consist of 'B' or 'C' terms, which are mainly due to the spin degeneracy of the ground states.

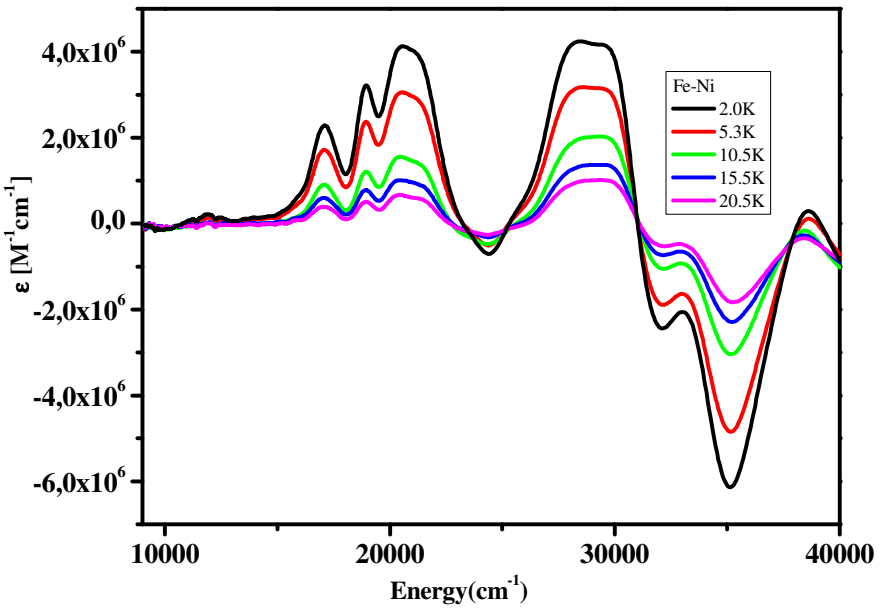

Figure 6.10a MCD spectra at low temperatures for Fe-Ni (**6**). MCD spectra were recorded with a magnetic field of 5 T at 2.0, 5.3, 10.5, 15.5 and 20.5 K.

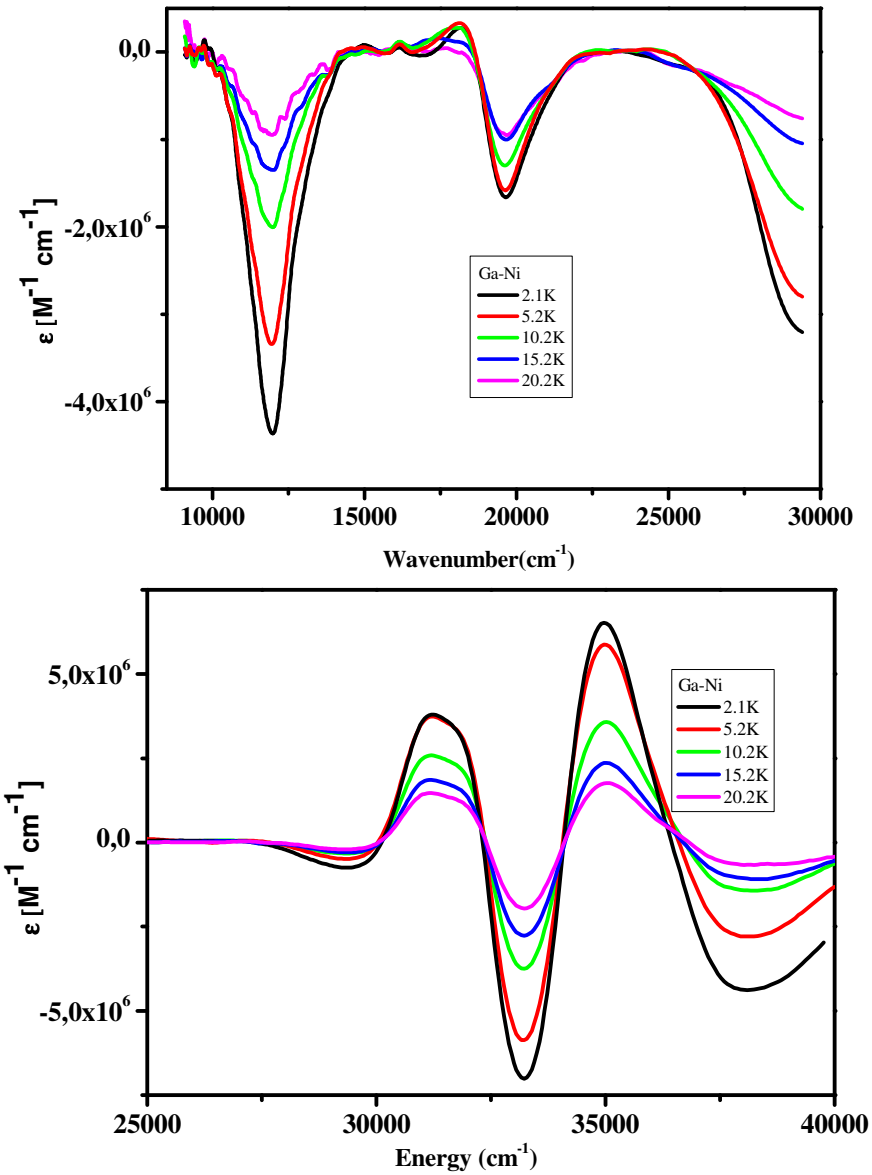

Figure 6.10b MCD spectra at low temperatures for Ga-Ni (**8**). MCD spectra were recorded with a magnetic field of 5 T at 2.1, 5.2, 10.2, 15.2 and 20.2 K.

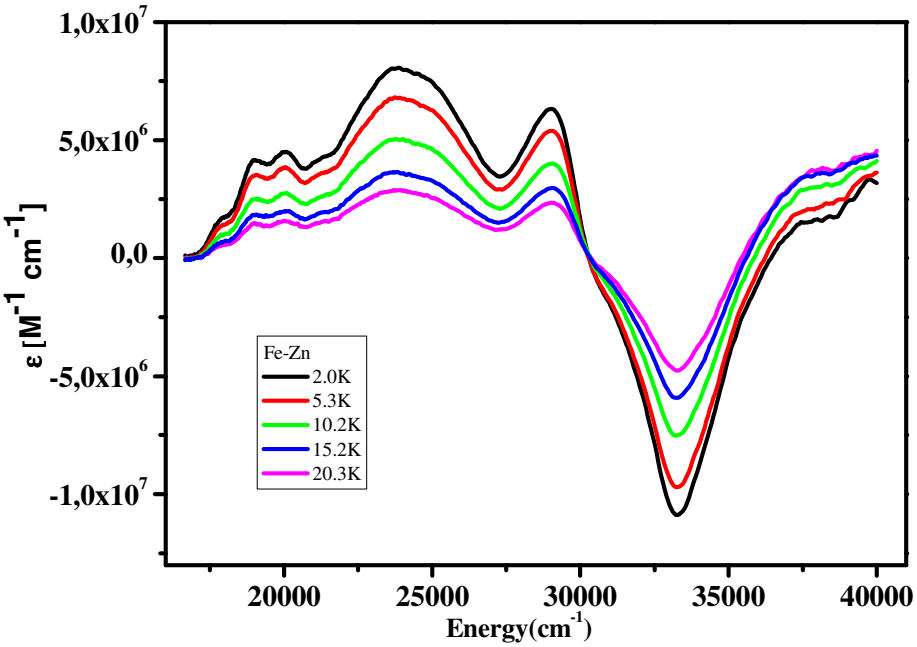

Figure 6.10c MCD spectra at low temperatures for Fe-Zn (**7**). MCD spectra were recorded with a magnetic field of 5 T at 2.0, 5.3, 10.2, 15.2 and 20.3 K.

A moderate exchange interaction is present in complex **6**. Before going to the assignment part, we might ask what are the principal effects of exchange coupling that can be observed in MCD spectra. In exchange coupled systems, the spin allowed d-d bands are basically unaffected by exchange coupling.[49] Spin-forbidden d-d bands also appear at about the same energy in mononuclear and exchange-coupled systems. However, spin-forbidden bands show notable changes as follows: a) The bands increase significantly in intensity in exchange-coupled systems; b) some spin-forbidden bands in exchange-coupled clusters show very noticeable temperature dependences; c) often new absorptions appear at energies near the sum of the energies of two single excitations. As a moderate antiferromagnetic exchange interaction is present in complex **6**, the d-d and CT transitions would not only arise from pure iron or nickel ions, but also from their combination. Hence, we have prepared isostructural Fe^{III}-Zn^{II}, **7** and Ga^{III}-Ni^{II}, **8** species to identify the independent spectroscopic mark of Fe and Ni, respectively, as Zn(II) and Ga(III) are devoid of any unpaired d-electrons.

There is vibronic regression observed in the region ~20,000 cm^{-1} and ~27,000 cm^{-1} due to the overlapping of the bands of the individual transitions of Fe^{3+} and Ni^{2+} for complex **6** (Figure 6.11c). But, alone complex **6** is not enough to assign the spin allowed or spin forbidden d-d transitions of individual iron or nickel ion. Hence, we also investigated the MCD and absorption properties of $Fe^{III}Zn^{II}$, (**7**) and $Ga^{III}Ni^{II}$ (**8**) to make a straight-forward assignments of pure d-d transitions for Fe(III) and Ni(II) ions, respectively. All the spectra were resolved with a minimum number of Gaussian bands required by the simultaneous analysis of both absorption (room temperature) and MCD spectra (2K/ 5T). The band width (full width at half maxima) was fixed at about 1000 cm^{-1} for MCD and at about 2000 cm^{-1} for absorption spectra during the Gaussian analysis.[40] All the optimization data are represented in appendices part.

Complex **8** contains Ni(II) ion with an octahedral NiN_6 environment, which could show several d-d transitions. Theoretically three main d-d transitions are generally observed for the octahedral NiN_6 chromophores, namely $^3A_2 \rightarrow {}^3T_2(^3F)$, $^3A_2 \rightarrow {}^3T_1(^3F)$ and $^3A_2 \rightarrow {}^3T_1(^3P)$ with vibronic regression of the spin forbidden bands. Experimentally three bands are observed at about 12,000 cm^{-1}, 20,000 cm^{-1} and 30,000 cm^{-1} in MCD and absorption spectra (Figure 6.11b). The expected nickel bands were assigned according to the literature assignments of the nickel amine complexes (Table S2)[50] and theory given by Liehr and Ballhausen.[44,45] The shape of the band observed at 20,000 cm^{-1} was found to be 'pseudo A' type formed due to opposite sign 'B' and 'C' terms. The sign of the C terms of the spin-orbit components depend upon the symmetry of the active vibrational modes, namely t_{1u} and t_{2u}, as these are the only vibrations in octahedral symmetry which are mixed with allowed d-d transitions.[46-49]

Theoretically no spin-allowed d-d transition is possible for **7**, as the electronic configuration Fe(III) is d^5-h.s. and Zn(II) is d^{10}. Experimentally a weak transition is observed at around 19,000cm^{-1}, followed by a broad band at around 25,000 cm^{-1} (Figure 6.11a). The transitions were assigned with the help of former reports (Table S3).[41-43] Weak transition at 19,000 cm^{-1} was assigned as $^6A_1 \rightarrow {}^4T_1(^4G)$ and the overlapping transitions of $^6A_1 \rightarrow {}^4T_2(^4G)$ and $^6A_1 \rightarrow {}^4E(^4G)$ are expected in the region of 25,000 cm^{-1}.

The transitions in Fe-Ni (**6**) were assigned by comparing the band positions in the region observed in their magnetically monomeric complexes viz. Fe-Zn (**7**) and Ga-Ni

(**8**). Figure 6.11c and Table S1 show that the bands at ~ 20,000 and ~ 27,000 cm $^{-1}$arise due to the overlapping of the bands of the individual transitions of Fe(III) and Ni(II) ions. Detailed assignments have been shown in appendices part (Table S1).

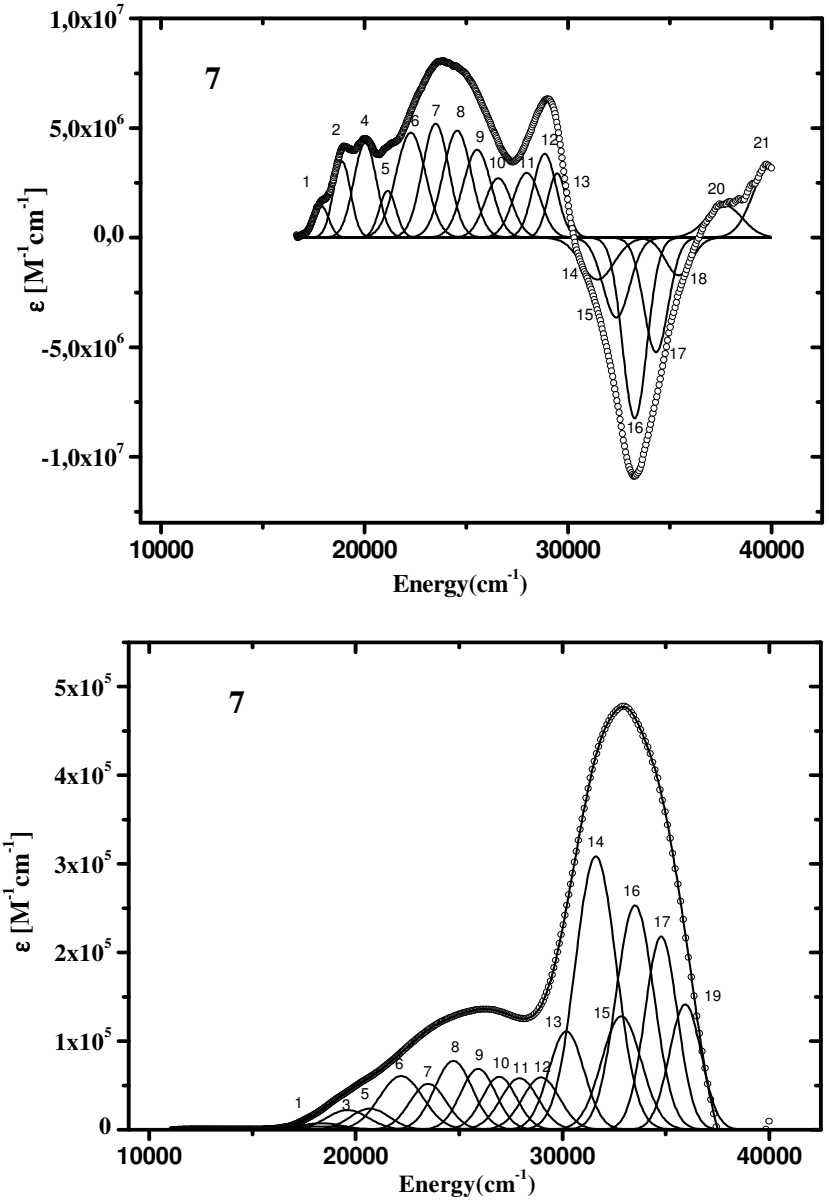

Figgure 6.11a MCD (Top) and Absorption spectra (bottom) of Fe-Zn (**7**). The low temperature MCD spectrum was recorded at 2 K/5 T, and Absorption spectrum was recorded at room temperature.

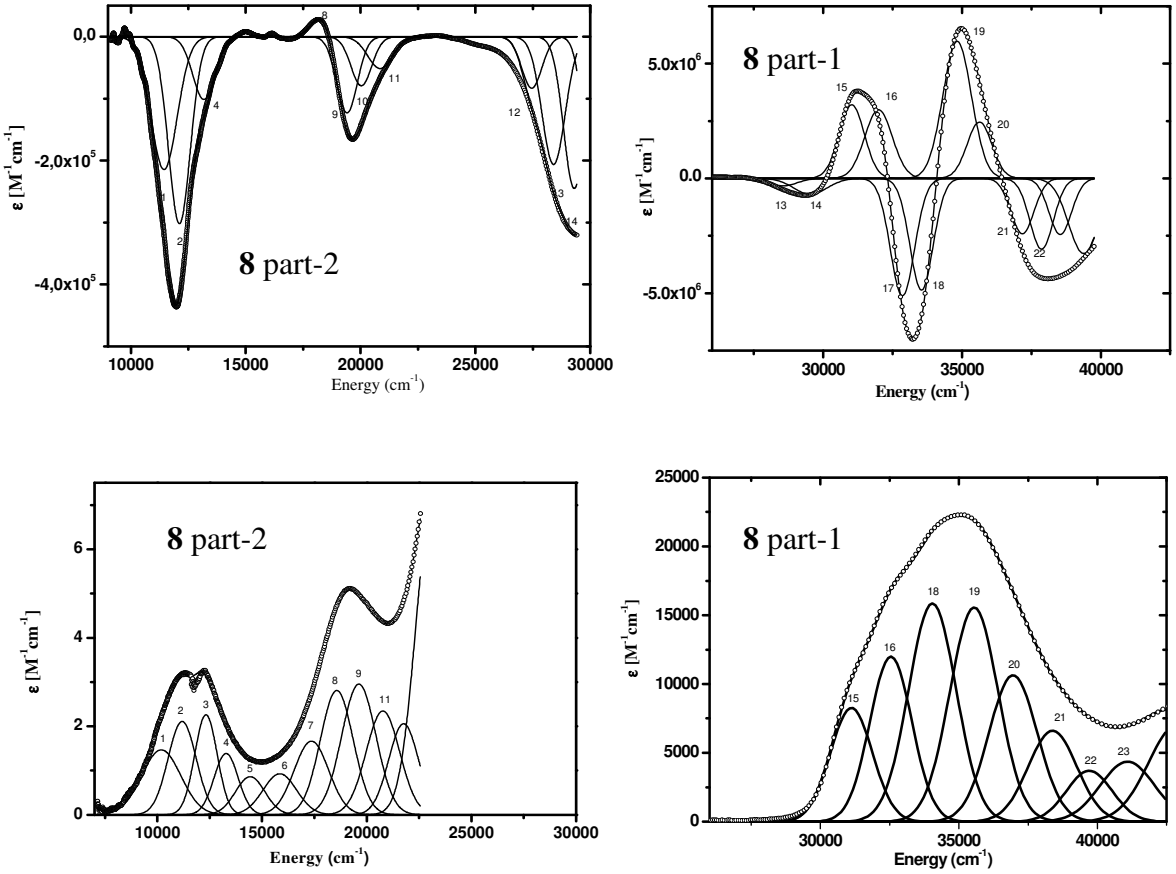

Figure 6.11b MCD (Top) and Absorption spectra (bottom) of Ga-Ni (**8**). The low temperature MCD spectra were recorded at 2 K/5 T, and Absorption spectra were recorded at room temperature.

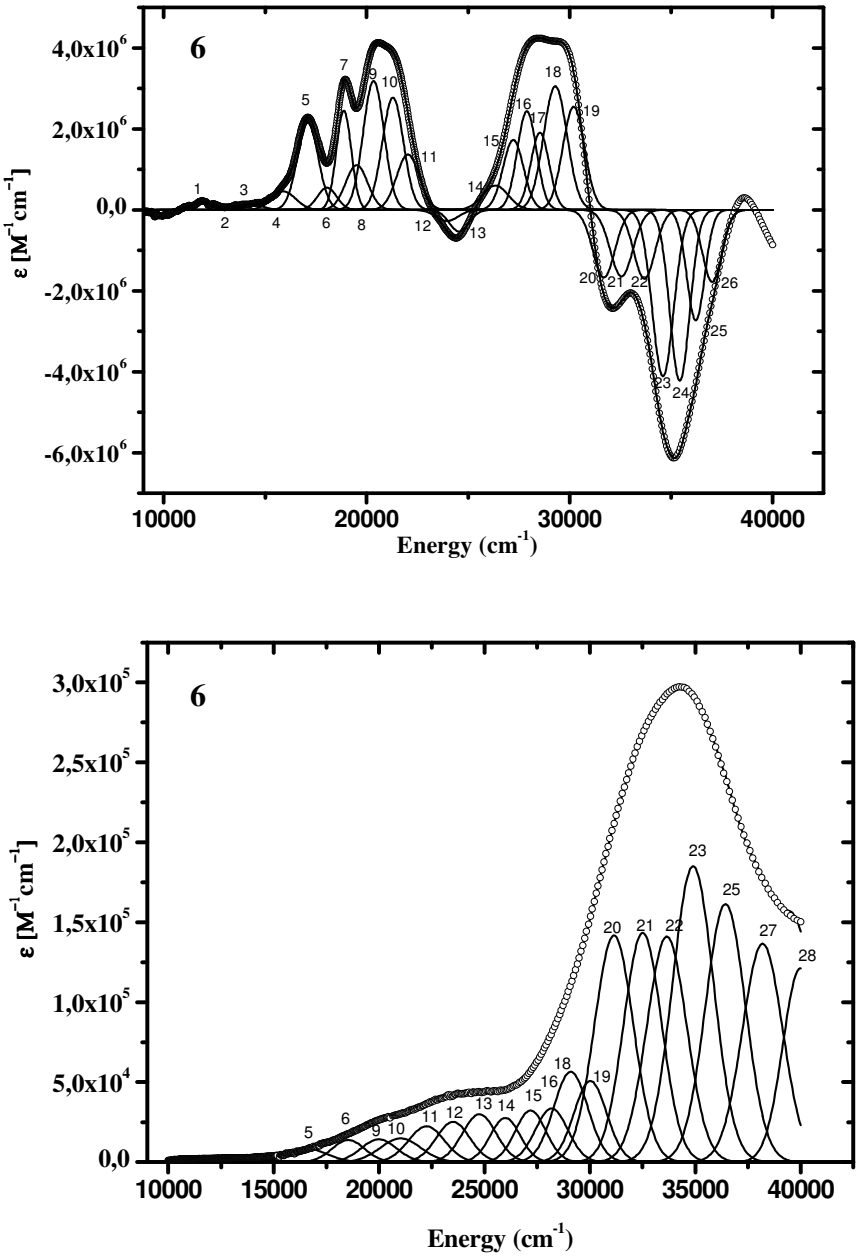

Figure 6.11c MCD (Top) and Absorption spectra (bottom) of Fe-Ni (**6**). The low temperature MCD spectrum was recorded at 2 K/5 T, and Absorption spectrum was recorded at room temperature.

6.11 Experimental Section

L'Fe(III)Cl_3 and L'Cr(III)Br_3

1,4,7-trimethyl-1,4,7-triazacyclononane and its iron(III) and chromium complexes L'Fe(III)Cl_3 and L'Cr(III)Br_3 were prepared as described previously.[34,35]

1-Methyl-2-imidazolecarboxaldehyde oxime (^{Me}ImOxH):

A solution of 1-methyl-2-imidazolecarbaldehyde (2.2 g, 20 mmol) was dissolved in MeOH (30 mL), a solution of hydroxylamine hydrochloride (1. g, 20 mmol) and Na_2CO_3 (1.06 g, 10 mmol) in H_2O (20 mL) cooled to 0°C. The resulting white precipitate was filtered and washed with 30 mL of cold 33% ethanol to give 1.9 g (15.2 mmol) of 1-Methyl-2-imidazolecarboxaldehyde oxime. The mixture was cooled and the white precipitate was collected by suction filtration and recrystallized from MeOH. Yield: 1.9 g (75%). m.p. 167-169 °C. ^{1}H NMR (CD_3OD, 400 MHz): δ 3.8 (3H, s, CH_3), 6.99 (2H, s), 7.1 (1H, s), 8.0 (1H, s); IR (KBr): υ = 1626 (CN), 1091 (ClO_4^-), 1005 (NO), 1569, 1517, 1466 (imidazole) cm^{-1}; MS: m/z 125 (M^+, 100%). Purity checked by GC: ~ 99%.

Elemental analysis:

	%C	%H	%N
Calculated	48.0	5.6	33.6
Found	47.9	5.8	33.4

[L'Fe(III)(^{Me}ImOx)$_3$M(II)](ClO$_4$)$_2$ (M(II) = Ni(6), Zn(7), Mn(9), Fe(10), Cu(11))

As complexes **6**, **7** and **9-11** were prepared in a very similar way, a representative method only is described. An argon-scrubbed solution of 1-methyl-2-imidazolealdoxime (0.37 g, 3 mmol) in methanol (30 mL) was stirred with $M(ClO_4)_2 \cdot 6H_2O$ and triethylamine (0.5 mL) under argon for 0.5 hour. Solid L'FeCl_3 (0.33 g, 1 mmol) was added to the resulting solution and the stirring was continued under argon for a further 1 hour at ambient temperature. The volume of the solution was reduced by passing over the surface of the solution until the micro crystals separated out. The crystals were collected by

filtration and air-dried. X-ray quality crystals in >50% yield grew over two days from acetonitrile solutions.

Complex 6, $Fe^{III}Ni^{II}$

Brown crystals. Yield 0.7 g (82%). IR (KBr): υ = 1636 (CN), 1099 (ClO_4^-), 1005 (NO), 1567, 1479, 1457 (imidazole) cm^{-1}. UV/Vis (CH_3CN): λ_{max} (ε) = 289 (33170), 422 (4270), 505 (2370), 820 (40), 890 (33) nm ($M^{-1}\cdot cm^{-1}$). ESI-MS: m/z = 756, 328.

Elemental analysis:

	%C	%H	%N	%Fe	%Ni
Calculated	33.6	4.6	19.5	6.5	6.8
Found	33.5	4.6	20.4	6.7	6.9

Complex 7, $Fe^{III}Zn^{II}$

Yellowish-brown crystals. Yield 0.60 g (70%). IR (KBr): υ = 1624 (CN), 1100 (ClO_4^-), 1004 (NO), 1567, 1481, 1457 (imidazole) cm^{-1}. UV/Vis (CH_3CN): λ_{max} (ε) = 303 (22800), 481 (6500) nm ($M^{-1}\cdot cm^{-1}$). ESI-MS: m/z = 763, 331.

Elemental analysis:

	%C	%H	%N	%Fe	%Zn
Calculated	33.4	4.6	19.5	6.5	7.6
Found	32.8	4.4	18.9	6.3	7.5

Complex 9, $Fe^{III}Mn^{II}$

Deep-brown crystals. Yield 0.52 g (64%). IR (KBr): υ = 1635 (CN), 1088 (ClO_4^-), 1005 (NO), 1566, 1528 (imidazole) cm^{-1}. UV/Vis (CH_3CN): λ_{max} (ε) = 300 (21200), ESI-MS: m/z = 951, 753, 327.

Elemental analysis:

	%C	%H	%N	%Fe	%Mn
Calculated	34.0	5.0	18.3	5.9	5.8
Found	33.7	4.8	18.5	6.0	5.8

Complex 10, $Fe^{III}Fe^{II}$

Dark-brown crystals. Yield 0.65 g (76%). IR (KBr): υ = 1636 (CN), 1093 (ClO_4^-), 1003 (NO), 1565, 1512, 1464 (imidazole) cm^{-1}. UV/Vis (CH_3CN): λ_{max} (ε) = 312 (17450), 460 (12700), 930 (310) nm ($M^{-1}\cdot cm^{-1}$). ESI-MS: m/z = 754, 630, 327.

Elemental analyis:

	%C	%H	%N	%Fe
Calculated	33.7	4.6	19.7	13.1
Found	33.9	4.6	19.7	13.0

Complex 11, $Fe^{III}Cu^{II}$

Dark-brown crystals. Yield 0.65 g (76%). IR (KBr): υ = 1617 (CN), 1096 (ClO_4^-), 1005 (NO), 1567, 1479, 1468 (imidazole) cm^{-1}. UV/Vis (CH_3CN): λ_{max} (ε) = 286 (30800), 406 (4900), 770 (85), 1102 (63) nm ($M^{-1}\cdot cm^{-1}$). ESI-MS: m/z = 761, 637.
Elemental analysis:

	%C	%H	%N	%Fe	%Cu
Calculated	33.4	4.6	19.5	6.5	7.4
Found	33.3	4.5	19.6	6.3	7.2

$[L'Co^{III}(^{Me}ImOx)_3Fe^{II}](ClO_4)_2$ (12)

Solid $Co(CH_3COO)_2\cdot 4H_2O$ (0.25 g, 1 mmol) was added to a degassed methanolic solution (25 mL) of 1,4,7-trimethyl-1,4,7-triazacyclononane (L') (0.17 g, 1 mmol) under argon; the solution was stirred further for 1 h. A methanolic solution (25 mL) of (0.37 g, 3 mmol) of 1-methyl-2-imidazolealdoxime and $Fe(ClO_4)_2\cdot 6H_2O$ (0.36 g, 1 mmol) was added to the cobalt-containing solution and then stirred at room temperature for 0.5 h. The precipitated dark-brown microcrystalline substance was collected by filtration. X-ray-quality crystals were obtained by recrystallization from CH_3CN. Yield 0.5 g (65%). IR (KBr): υ = 1636 (CN), 1091 (ClO_4^-), 10014 (NO), 1577, 1561, 1517, 1463 (imidazole) cm^{-1}. UV/Vis (CH_3CN): λ_{max} (ε) = 298 (26000), 484 (4400), 590 (900) nm ($M^{-1}\cdot cm^{-1}$). ESI-MS: m/z = 760, 633.

Elemental analysis:

	%C	%H	%N	%Fe	%Co
Calculated	33.6	4.6	19.6	6.5	6.9
Found	33.8	4.5	19.5	6.4	6.7

[L'Cr(III)(^{Me}ImOx)$_3$M(II)](ClO$_4$)$_2$ (M(II) = Ni (13), Zn (14))

As complexes **13** and **14** were prepared in a very similar way, a representative method only is described.

Step 1: To a suspension of L'CrBr$_3$ (0.46 g, 1 mmol) in 30 mL methanol AgClO$_4$·H$_2$O (0.62 g, 2.8 mmol) was added with stirring. The suspension was heated to reflux under argon for 0.5 hour yielding a blue-violet solution of [LCr^{III}(CH$_3$OH)$_3$]$^{3+}$ with concomitant formation of AgBr. The precipitated AgBr was filtered off and a clear blue-violet solution A was stored under an argon atmosphere and used for subsequent synthesis.

Step 2: An argon-scrubbled solution of 1-methylimidazole-2-aldoxime (0.37 g, 3 mmol) in methanol was stirred with Ni(ClO$_4$)$_2$·6H$_2$O/ Zn(ClO$_4$)$_2$·6H$_2$O (1 mmol) in presence of triethylamine (3 mmol) for 0.5 h under argon. The resulting solution was added to the solution A, and the mixture was heated to reflux for 1 h. The volume of the solution was reduced my applying vacuum to get the microcrystalline substance. X-ray quality crystals in 60-70 % yield grew over two days from acetonitrile solutions.

Complex 13, Cr^{III}Ni^{II}

Deep-red crystals. Yield 0.53 g (69%). IR (KBr): υ = 1635 (CN), 1099 (ClO_4^-), 1004 (NO), 1566, 1458 (imidazole) cm^{-1}. UV/Vis (CH$_3$CN): λ_{max} (ε) = 300 (>15000), 433 (390), 540 (230), 867 (12) nm (M^{-1}·cm^{-1}).

Elemental analysis:

	%C	%H	%N	%Cr	%Ni
Calculated	33.8	4.6	19.7	6.1	6.9
Found	33.5	4.5	19.5	6.2	7.8

Complex 14, $Cr^{III}Zn^{II}$

Dark-brown crystals. Yield 0.51 g (58%). IR (KBr): υ = 1635 (CN), 1091 (ClO_4^-), 1004 (NO), 1573, 1464 (imidazole) cm^{-1}. UV/Vis (CH_3CN): λ_{max} (ε) = 293 (21100), 420 (270), 540 (230), 529 (120) nm ($M^{-1}\cdot cm^{-1}$). ESI-MS: m/z = 851, 758, 651.

Elemental analysis:

	%C	%H	%N	%Cr	%Zn
Calculated	33.5	4.6	19.6	6.0	7.6
Found	33.7	4.5	19.7	6.1	7.4

$[L'Ga(III)(^{Me}ImOx)_3Ni(II)](ClO_4)_2$ (8)

Solid $GaCl_3$ (0.18 g, 1 mmol) was added to a degassed methanolic solution solution (30 mL) of 1,4,7-trimethyl-1,4,7-triazacyclononane (0.17 g, 1 mmol) under argon; the solution was stirred further for 1 h. A methanolic solution (30 mL) of ^{Me}ImOxH (0.37 g, 3 mmol) and $Ni(ClO_4)_2\cdot 6H_2O$ (0.36 g, 1 mmol) was added to the gallium-containing solution and then stirred at an ambient temperature for 0.5 h. The precipitated light-brown microcrystalline substance was collected by filtration. X-ray-quality crystals were obtained by recrystallization from MeCN. Yield 0.45 g (52%), IR (KBr): υ = 1624 (CN), 1100 (ClO_4^-), 1004 (NO), 1567, 1481, 1457 (imidazole) cm^{-1}. UV/Vis (CH_3CN): λ_{max} (ε) = 303 (22800), 481 (6500) nm ($M^{-1}\cdot cm^{-1}$). ESI-MS: m/z = 763, 331.

Elemental analysis:

	%C	%H	%N	%Ga	%Ni
Calculated	33.4	4.6	19.5	6.5	7.6
Found	32.8	4.4	18.9	6.3	7.5

References

1. *Handbook of Metalloproteins*, ed. A. Messerschmidt, R. Huber, T. Poulos, K. Wieghardt, John Wiley & Sons, Chichester, U.K., **2001**.

2. a) K. Wieghardt, K. Pohl, I. Jibril, G. Huttner, *Angew. Chem., Int. Ed.* **1984**, *23*, 77; b) C. Delfs, D. Gatteschi, L. Pardi, R. Sessoli, K. Wieghardt, D. Hanke, *Inorg. Chem.* **1993**, *32*, 3099.

3. W. H. Armstrong, M. E. Roth, S. J. Lippard, *J. Am. Chem. Soc*. **1987**, *109*, 6318

4. P. Chaudhuri, M. Winter, P. Fleischhauer, W. Hasse, U. Flörke, H. J. Haupt, *Inorg. Chim. Acta.* **1993**, *212*, 241.

5. M. W. Wempel, D. K. Coggin, J. B. Vincent, J. M. McCusker, W. E. Streib, J. C. Huffman, D. N. Hendrickson, G. Christou, *J. Chem. Soc., Dalton Trans.* **1998**, 719.

6. J. M. McCusker, J. B. Vincent, E. A. Schmitt, M. L. Mino, K. Shin, D. K. Coggin, P. M. Hagen, J. C. Huffman, G. Christou, D. N. Hendrickson, *J. Am. Chem. Soc*. **1991**, *113*, 3012.

7. O. Kahn, *Molecular Magnetism*, VCH Publishers, Weinheim, **1993**.

8. F. Birkelbach, U. Flörke, H-J. Haupt, C. Butzlaff, A. X. Trautwein, K. Wieghardt, P. Chaudhuri, *Inorg. Chem.* **1998**, *37*, 2000.

9. C. Krebs, M. Winter, T. Weyhermüller, E. Bill, K. Wieghardt, P. Chaudhuri, *J. Chem. Soc., Chem. Commun.* **1995**, 1913.

10. C. N. Verani, T. Weyhermüller, E. Rentschler, E. Bill, P. Chaudhuri, *J. Chem. Soc., Chem. Commun.* **1998**, 2475.

11. F. Birkelbach, M. Winter, U. Flörke, H-J. Haupt, C. Butzlaff, M. Lengen, E. Bill, A. X. Trautwein, K. Wieghardt, P. Chaudhuri, *Inorg. Chem.* **1994**, *33*, 3990.

12. P. Chaudhuri, *Coordination Chemistry Reviews*, **2003**, *243*, 143.

13. P. Chaudhuri, M. Winter; P. Fleischhauer; W. Hasse, U. Flörke, H-J. Haupt, *J. Chem. Soc., Chem. Commun.* **1990**, 1728.

14. S. Khanra, B. Biswas, C. Golze, B. Büchner, V. Kataev, T. Weyhermüller, P. Chaudhuri, *J. Chem. Soc., Dalton Trans.* **2007**, 481.

15. C. N. Verani, E. Rentschler, T. Weyhermüller, E. Bill, P. Chaudhuri, *J. Chem. Soc., Dalton Trans.* **2000**, 4263.

16. S. Mohanta, K. K. Nanda, L. K. Thompson, U. Flörke, K. Nag, *Inorg. Chem.* **1998**, *37*, 1465.

17. E. Colacio, J. M. Dominguez-Vera, M. Ghazi, R. Kivekäs, M. Klinga, J. M. Moreno, *Inorg. Chem.* **1998**, *37*, 3040.

18. K. E. Vostrikova, D. Luneau, W. Wernsdorfer, P. Rey, M. Verdauger, *J. Am. Chem. Soc.* **2000**, *122*, 718.

19. a) O. Kahn, *Adv. Inorg. Chem.* 1995, **43**, 179; b) K. S. Murray, *Adv. Inorg. Chem.* **1995***, 43*, 261.

20. F. Birkelbach, T. Weyhermüller, M. Lengen, M. Gerdan, A. X. Trautwein, K. Wieghardt, P. Chaudhuri, *J. Chem. Soc., Dalton Trans.* **1997**, 4529.

21. C. N. Verani, E. Rentschler, T. Weyhermüller, E. Bill, P. Chaudhuri, *J. Chem. Soc., Dalton Trans.* **2000**, 251.

22. P. Chaudhuri, T. Weyhermüller, R. Wagner, S. Khanra, B. Biswas, E. Bothe, E. Bill, *Inorg. Chem.* **2007**, *46*, 9003.

23. S. Khanra, T. Weyhermüller, E. Bill, P. Chaudhuri, *Inorg. Chem.* **2006**, *45*, 5911.

24. P. Chaudhuri, M. Winter, C. P. B. Della Vedova, P. Fleischhauer, W. Hasse, U. Flörke, H. J. Haupt, *Inorg. Chem.* **1991**, *30*, 4777.

25. F. Brikelbach, T. Weyhermüller, M. Lengen, M. Gerdan, A. X. Trautwein, K. Wieghardt, P. Chaudhuri, *J. Chem. Soc., Dalton Trans.* **1997**, 4529.

26. D. Burdinski, E. Bill, F. Birkelbach, K. Wieghardt, P. Chaudhuri, *Inorg. Chem.* **2001**, *40*, 1160.

27. S. Ross, T. Weyhermüller, E. Bill, K. Wieghardt, P. Chaudhuri, *Inorg. Chem.* **2001**, *40*, 6656.

28. S. Ross, T. Weyhermüller, E. Bill, E. Bothe, U. Flörke, K.Wieghardt, P. Chaudhuri, *Eur. J. Inorg. Chem.* **2004**, 984.

29. a) P. Gütlich, R. Link, A.X. Trautwein, *Mössbauer Spectroscopy and Transition Metal Chemistry*, Springer-Verlag, Berlin, **1978**; b) P. Gütlich, in *Mössbauer Spectroscopy* (Ed.: U. Gonser), Springer-Verlag, Berlin, **1975**, chapter 2.

30. P. Krumholz, *Struct. Bonding (Berlin)* **1971**, *9*, 139.

31. P. Chaudhuri, K. Wieghardt, *Prog. Inorg. Chem.* **1987**, *35*, 329.

32. a) J. B. Goodenough, *Magnetism and the Chemical Bond*, Wiley, New York, **1963**; b) J. B. Goodenough , *J. Phys. Chem. Solids* **1958**, *6*, 287; c) J. Kanamori , *J. Phys. Chem. Solids* **1959**, *10*, 87.

33. a) A. P. Ginsberg, *Inorg. Chim. Acta Rev.* **1971**, *5*, 45; b) R. L. Martin, in *New Pathways in Inorganic Chemistry* (Eds.: Ebsworth, Maddock, Sharpe), Cambridge University Press, Cambridge, U. K., **1968**.

34. P. Chaudhuri, M. Winter, K. Wieghardt, S. Gehring, W. Hasse, B. Nuber, J. Weiss, *Inorg. Chem.* **1988**, *27*, 1564.

35. P. Chaudhuri, M. Winter, H. J. Küppers, K. Wieghardt, B. Nuber, J. Weiss, *Inorg. Chem.* **1987**, *26*, 3302.

36. A. B. P. Lever, *Inorganic Electronic Spectroscopy*: Amsterdam, **1984**; b) P. J. McCarthy, H. U. Güdel, *Coord. Chem. Rev.* **1988**, *88*, 69.

37. A. J. McCaffery, P. J. Stephens, P. N. Schatz, *Inorg. Chem.* **1967**, *6*, 1614.

38. A. D. Buckingham, P.J. Stephens, *Ann. Rev. Phys. Chem.* **1966**, *17*, 399.

39. M. J. Harding, S. F. Mason, D. J. Robbins, A. J. Thomson, *J. Chem. Soc. A* **1971**, 3058.

40. P. Kennepohl, F. Neese, D. Schweitzer, H. L. Jackson, J. A. Kovacs, E. I. Solomon, *Inorg. Chem.* **2005**, *44*, 1826.

41. M. Vala, J. C. Rivoal, R. E. Moss, *Mol. Phys.* **1975**, *30*, 1325.

42. J. Ferguson, E. R. Krausz, H. J. Guggenheim, *Mol. Phys.* **1975**, *29*, 1785.

43. J. Ferguson, H. U. Güdel, E. R. Krausz, H. J. Guggenheim, *Mol. Phys.* **1974**, *28*, 879.

44. C. J. Ballhausen, A. D. Liehr, *Mol. Phys.* **1959**, *2*, 23.

45. M. J. Harding, S. F. Mason, D. J. Robbins, A. J. Thomson, *Chem. Phys. Lett.* **1970**, *7*, 70.

46. E. I. Solomon, C. J. Ballhausen, *Mol. Phys.* **1975**, *29*, 279.

47. C. J. Ballhausen, *Introduction to Ligand–Field Theory, McGraw-Hill, New York,* **1962**.

48. D. Dollimore, D. Tinsley, *J. Chem. Soc. A* **1971**, 3043.

49. P. J. McCarthy, H. U. Güdel, *Coor. Chem. Rev.* **1988**, *88*, 69.

50. A. F. Schreiner, D. J. Hamm, *Inorg. Chem.* **1973**, *12*, 2037.

Chapter 7

Conclusions and Perspectives

Conclusions

The main aim of this work is to design polynuclear complexes using different polydentate ligand systems for molecular magnetism. Careful design of these polynuclear complexes has allowed us to isolate complexes with interesting geometries, and these results have led to valuable structural and magnetochemical insights. The main information and conclusions of this work are summarized below, and some future perspectives are offered.

Chapter 2

Tridentate *N*-methyldiethanolamine ligand acts as a backbone for the synthesis of the cluster complexes $Na^{I}_{2}Ni^{II}_{16}$ (**1**) and NaV^{IV}_{6} (**2**).

The structure of **1** is basically a tetramer of tetramer. The smaller tetramer subunits are connected to each other either by Na^{+} ions or by formate bridging groups. Interestingly no formate had been used during the syntheses, and only the use of the base NaOMe yielded **1** (other bases such as Et_3N, CH_3COO^{-}, NaOH did not yield **1**). Presumably the methoxide anion becomes oxidized to $HCOO^{-}$ during the reaction and the bridging formate does not originate from carbon dioxide of the air.

Complex **1** exhibits overall antiferromagnetic interaction. After a close examination of the structure we have considered only a tetranuclear unit during the magnetic simulation due to the symmetry of the molecule. There are two types of μ-oxo bridges in each tetranuclear unit. The observed *J*-values (+4.3 and -5.1 cm^{-1}) are in accord with those expected for the Ni–O(alkoxo)–Ni angles prevailing in the cluster: Ni(1)–O_{alk}–Ni(X) lying between 90 and 93°, whereas Ni–O_{alk}–Ni angles between the Ni(2), Ni(3) and Ni(4) centers are 132–134°. The strength of ferromagnetic coupling J_1 related to the angle 90–93° is relatively weak, presumably due to the additional presence of an acetate ligand in *syn–syn* mode.

The saturated magnetization value of 4.94 measured at 1.9 K and 7 T clearly indicates the participation of M_S = -4 or -5 Zeeman components. We conclude that the expected lowest energy state S_t = 4, 3, 2, 1 or zero (as the ground state for the tetranuclear

core with the evaluated positive and negative J values is $S_{core} = 1$) is not well isolated and the excited states with S values 4 or higher are within a few wave-numbers from the lowest lying state.

Complex **2** is an example of a ferromagnetically coupled hexa-nuclear wheel-shaped vanadium(IV) complex containing a Na^+ ion at the center of the wheel. Here the ClO_4^- ion is non-innocent and acts as an oxygen transfer agent.

Similar hexanuclear wheel shaped complexes are known with triethanolamine amine as a ligand. However, maximum cases solvothermal techniques have been used. We have used normal schlenck line techniques. All the coordination sites of N-methyldiethanolamine are coordinated to vanadium(IV) ion unlike triethanolamine where one $-CH_2-CH_2-OH$ group is always free.

Detailed analysis of the temperature dependent magnetic behavior at different magnetic fields (1, 0.1 and 0.01 T) demonstrates a ferromagnetic interaction is operative between the consecutive vanadium(IV) ions. However evaluation/simulation of the SQUID measurements led us to conclude that we can pin point the coupling constant in a certain range but not exactly.

Chapter 3

We have successfully prepared a single oximato-bridged $[Mn^{III}_2]_n$ in a facile way. As far as we are aware, the title complex is the first reported single oximato-bridged dinuclear Mn^{III} complex. Ferromagnetic Mn^{III}-Mn^{III} coupling stabilizes an $S_t = 4$ ground state and a negative axial zero-field-splitting parameter (D_{Mn}) has been observed. This work shows that the oximato-bridged Mn^{III} complexes should form an interesting basis for high-spin molecules.

Chapter 4

To study the spin polarization concept we have synthesized *N'N*-di(3,5-di-*tert*-butyl-salicylidene)-1,3-diaminobenzene (LH_2), using meta phenylenediamine as a linker. This ligand acts as a backbone for a diferric(III) complex: $[L_2Fe_2(NO_3)_2]$ **4**.

Detailed analysis of the temperature and field dependent magnetic moment behavior demonstrates a ferromagnetic interaction is operative between the two ferric(III) centers.

In this case the magnetic study alone was not enough to draw a conclusion about the magnetic ground state level as J is very small, even smaller than the zero-field splitting. Thus, the nature of the magnetic ground state of the dimer, **4**, was also investigated 'microscopically' by Mössbauer spectroscopy at liquid helium temperature with applied fields of 1 – 7 T. The hyperfine patterns show large magnetic splitting due to the presence of strong internal fields of about 51.6 T. The large splitting particularly rules out again anti-ferromagnetic spin coupling. Additionally, the persistent large splitting for all applied fields and the sharp lines with a clear quadrupole shift (difference between lines 1-2 and 5-6 Figure 4.16) indicate an 'easy axis' of magnetization.

The ferromagnetic nature of the coupling constant between the two ferric(III) ions has been also demonstrated by the DFT calculation. Unrestricted B3LYP DFT scheme shows that the spin densities at both iron atoms have the same sign, resulting in a net ferromagnetic exchange.

Finally, in this case the zero-field splitting parameter, D_{Fe}, for iron(III) in **4** is larger than the ferromagnetic exchange coupling constant *J* of the dimer. This means the competing zero-field and exchange interactions mix the total spin manifolds, and thus, S_{total} and $M_{s,\ total}$ are no longer good quantum numbers. Therefore we refrain from describing our system as having an $S_{total} = 5$ ground state.

Chapter 5

Complex **5** is a rare example of mixed valance V^{III}-V^{IV} complex and this complex is stable only in inert atmosphere. The preparation of **5** uses V(III) as starting material, so 50% of the vanadium ions are oxidized to +IV and a certain percentage of ligand converted to $C_6H_4(NH_2)_2$.

Magnetic susceptibility analysis shows that singlet and triplet states are very close to each other. EPR analysis suggest that it is necessary to consider the entire molecule during the simulations and triplet state is responsible for the multiple line spectrum.

Chapter 6

Here, 1-methylimidazole-2-aldoxime acts as backbone for the synthesis of a series of dinuclear complexes where Me_3Tacn acts as a capping ligand. Because of the isostructural nature these materials are unique and ideally suited for the study of intramolecular exchange interactions between the paramagnetic transition metal ions as a function of their respective d^n electronic configurations. Nine complexes were isolated and they are abbreviated as $Fe^{III}Ni^{II}$ (**6**), $Fe^{III}Zn^{II}$ (**7**), $Ga^{III}Ni^{II}$ (**8**), $Fe^{III}Mn^{II}$ (**9**), $Fe^{III}Fe^{II}$ (**10**), $Fe^{III}Cu^{II}$ (**11**), $Co^{III}Fe^{II}$ (**12**), $Cr^{III}Ni^{II}$ (**13**), $Cr^{III}Zn^{II}$ (**14**). Complexes have been characterized by elemental analysis, IR spectroscopy, ESI-MS, UV-vis spectroscopy, Mössbauer spectroscopy, SQUID, EPR together with X-ray structure analysis. All the complexes are isostructural.

The magnetic study confirms the essentially σ nature of the exchange interaction and applicability of the Goodenough-Kanamori rules in general to predict the nature of exchange interactions for different heterometal compounds containing the ferric ion in high-spin state. The strength of antiferromagnetic interaction decreases in the following order: $Fe^{III}Cu^{II} > Fe^{III}Ni^{II} > Fe^{III}Mn^{II}$, as is expected. Additionally, the strength of the antiferromagnetic interactions is lower in the present case compared to complexes with the pyridinealdoxime ligands. This may be because of the higher sigma donating ability of the pyridine-N relative to that of imidazole-N.

It is difficult to assign the low intense d-d transition as high intense CT bands are present in all the spectra. MCD is an important tool to avoid this kind of problem and hence these three complexes have been characterized MCD to assign the electronic transitions. Fe(III) h.s. and Ni(II) ions are antiferromagnetically coupled in complex **6**. Thus, **6** is an important complex to assign the electronic transition in MCD spectrum in a moderately coupled system.

Perspectives

A few ideas and perspectives, in the continuation of this work are outlined below:

1. Synthesis and magnetostructural characterization of Li^+, K^+, NH_4^+containing complex of *N*-methydiethanolamine ligand, isostructural with the complexes **1** and **2** need to be explored.

2. Alternating current (AC) susceptibility measurement of the $[Mn^{III}]_n$ complex (**3**), to check whether this complex can be a single molecule magnet (SMM).

3. HF-EPR measurement of the $[Mn^{III}]_n$ complex (**3**) to verify the ground state of the complex and for the precise determination of the sign and magnitudes of zero-field splitting parameter (*D*).

4. Synthesis and magnetostructural characterization of the $M_2L"_2$ (M = Mn^{III}, Ni^{II} and Cu^{II}) core congeners isostructural with **4**.

5. MCD properties of the $Fe^{III}Ni^{II}$ core with different exchange coupling constant and isostructural with **6** needs to be explored.

6. Synthesis and magnetostructural characterization of heterodinuclear $M_A{}^{III}M_B{}^{II}$ complex of derivatized imidazole-oxime ligands, isostructural with the complexes **6-14** need to be explored.

7. In traversing the literature of the magnetism of first-row d-block elements we have noticed that low valent paramagnetic Ti and V-complexes remain relatively unexplored, probably because of difficulties in synthesis and stability. Clearly, these aspects need to be further experimentally explored.

Appendices

1. Methods and Equipments

All the analyses were performed at the Max-Planck-Institut für Bioanorganische Chemie, Mülheim an der Ruhr, unless otherwise mentioned. Commercial grade chemicals were used for the synthetic purposes and solvents were distilled and dried before use.

Infrared Spectroscopy

Infrared spectra were measured from 400 to 4000 cm^{-1} as KBr pellets at room temperature on a '*Perkin-Elmer* FT-IR-Spectrophotometer 2000'.

NMR Spectroscopy

^{1}H- and ^{13}C- NMR spectra were measured using a '*Bruker* ARX 250, DRX 400 or DRX 500'. The spectra were referenced to TMS, using the ^{13}C or residual proton signals of the deuterated solvents as internal standards.

Mass Spectrometry

Mass spectra in the Electron Impact mode (EI; 70 eV) were recorded on a Finnigan MAT 8200 mass spectrometer. Only characteristic fragments are given with intensities. The spectra were normalized against the most intense peak having intensity 100. Electron Spray Ionization (ESI) mass spectra were recorded either on a Finnigan Mat 95 instrument or a Hewlett-Packard HP 5989 mass spectrometer. ESI- and EI-spectra were measured by the group of Dr. W. Schrader at the Max-Planck-Institute for Coal Research, Mülheim an der Ruhr.

Elemental Analysis

The determination of the C, H, N and metal content of the compounds was performed by the 'Mikroanalytischen Labor H. Kolbe', Mülheim an der Ruhr, Germany.

UV-VIS Spectroscopy

UV-VIS spectra were recorded on a '*Perkin-Elmer* UV-VIS Spectrophotometer Lambda 19'or on a Hewlett-Packard HP 8452A diode array spectrophotometer in the range 200-1200 nm. For UV-VIS spectro-electrochemical investigations the HP 8452A

diode array spectrophotometer was used, by employing a coulometry cuvette and Bu_4NPF_6 as supporting electrolyte.

Electrochemistry

Cyclic voltammetry, square wave voltammetry and linear sweep voltammetry exp.eriments were performed using an 'EG&G Potentiostat/Galvanostat 273A'. A standard three-electrode-cell was employed with a glass-carbon working electrode, a platinum-wire auxiliary electrode and Ag/AgCl (saturated LiCl in EtOH) reference electrode. Measurements were made under an inert atmosphere at room temperature. The potential of the reference electrode was determined using Fc^+/Fc as the internal standard.

Magnetic Susceptibility Measurements

The measurements of the temperature or field dependent magnetization of the sample were performed in the range 2 to 290 K at 1, 4 or 7 T on a '*Quantum Design* SQUID-Magnetometer MPMS'. The samples were encapsulated in gelatin capsules and the response functions were measured four times for each given temperature, yielding a total of 32 measured points. The resulting volume magnetization from the samples had its diamagnetic contribution compensated and was recalculated as volume susceptibility. Diamagnetic contributions were estimated for each compound by using Pascal's constants. The exp.erimental results were fitted with the program JULIUS calculating through full-matrix diagonalization of the Spin-Hamiltonian. The following Hamiltonian-operators were used:

$H_{ZE} = \mu_B \sum g_i \hat{S}_i .B$

$H_{HDVV} = -2 \sum J_{ij} \hat{S}_i . \hat{S}_j$

$H_{ZFS} = \sum D_i[\hat{S}_{iz}^2 - \{S_i(S_i+1)/3\} + E_i/D_i(\hat{S}_{ix}^2 - \hat{S}_{iy}^2)]$

Indexes i,j indicate individual spins. For the magnetic measurement the calculated g values obtained during simulation is the isotropic.

EPR Spectroscopy

First derivative X-Band EPR spectra of powdered or frozen solution samples were measured with a '*Bruker* ESP 300 Spectrometer' coupled to an '*Oxford Instruments* ESR 910-Cryostat'.

^{57}Fe-Mössbauer Spectroscopy

^{57}Fe-Mössbauer spectra were measured with an *Oxford Instruments* Mössbauer spectrometer in the constant acceleration mode. ^{57} Co/Rh was used as the radiation source. The minimum exp.erimental linewidths were 0.24 mm/s. The temperature of the sample was controlled by an '*Oxford Instruments* Variox Cryostat'. Isomer shifts were determined relative to α-iron at 300K. The measurements were carried out at 80K and 100K with solid samples containing the isotope ^{57}Fe.

Crystallography

X-ray diffraction data were collected on an '*Enraf-Nonius* CAD4 Diffractometer' or on a '*Siemens* Smart System'. Graphite-monochromatized Mo-Kα with $\lambda = 0.71073$ Å was employed. Data were collected by the 2θ-ω scan method ($3 \leq 2\theta \leq 50°$). The data were corrected for absorption and Lorenz polarization effects. The structures were solved by direct methods and subsequent Fourier-difference techniques, and refined anisotropically by full-matrix least-squares on F^2 with the program SHELXTL PLUS. Hydrogen atoms were included at calculated positions with $U < 0.08$ Å^2 in the last cycle of refinement.

GC / GC-MS Analysis

GC of the organic products were performed either on HP 6890 instruments using RTX-5 Amine 13.5 m S-63 columns respectively. GC-MS was performed using the above column coupled with a HP 5973 mass spectrometer with mass selective detector.

MCD Spectroscopy

Magnetic circular dichroism spectra were obtained on a home built instrument consisting of a JASCO J-715 spectropolarimeter and an Oxford Instruments SPECTROMAG magnetocryostat which is capable of generating magnetic fields up to 11T. Spectra were

taken for samples dissolved in butyronitrile which resulted in high quality glasses suitable for optical spectroscopy at low temperatures. Simultaneous gaussian resolution of absorption and MCD spectra were performed using Peakfit. All the measurements and VTVH-MCD fitting were done by Dr Sunita Salunke-Gawli of our group.

2. Crystallographic Data

Crystal Data and Structure Refinement for 1

Identification code	5580	
Empirical formula	$C_{108}\ H_{257}\ N_{15}\ Na_2\ Ni_{16}\ O_{89}$	
Formula weight	4175.63	
Temperature	100(2) K	
Wavelength	0.71073 Å	
Crystal system	Orthorhombic	
Space group	$P2_12_12_1$, No. 19	
Unit cell dimensions	a = 19.3308(6) Å	α = 90°
	b = 26.0589(8) Å	β = 90°
	c = 36.1281(12) Å	γ = 90°
Volume	18199.1(10) $Å^3$	
Z	4	
Density (calculated)	1.524 Mg/m^3	
Absorption coefficient	1.713 mm^{-1}	
F(000)	8768	
Crystal size	0.20x 0.08 x 0.04 mm^3	
Theta range for data collection	2.93 to 23.50°	
Index ranges	-21<=h<=21, -29<=k<=28, -40<=l<=40	
Reflections collected	136036	
Independent reflections	26843 [R(int) = 0.1330]	
Completeness to theta = 23.50°	99.5 %	
Absorption correction	Gaussian	
Max. and min. transmission	0.9342 and 0.7509	
Refinement method	Full-matrix least-squares on F^2	
Data / restraints / parameters	26843/ 81 / 2061	
Goodness-of-fit on F^2	1.131	
Final R indices [I>2sigma(I)]	R1 = 0.0798, wR2 = 0.1495	
R indices (all data)	R1 = 0.1066, wR2 = 0.1608	
Absolute structure parameter	0.029(15)	
Largest diff. peak and hole	0.972 and -0.657 e.$Å^{-3}$	

Crystal Data and Structure Refinement for 2

Identification code	5902	
Empirical formula	$C_{33}\ H_{74}\ Cl\ N_6\ Na\ O_{24}\ V_6$	
Formula weight	1291.05	
Temperature	100(2) K	
Wavelength	0.71073 Å	
Crystal system	Monoclinic	
Space group	Cc, No. 9	
Unit cell dimensions	a = 13.5049(12) Å	α = 90°.
	b = 23.205(2) Å	β = 90.623 (6)°
	c = 33.414(3) Å	γ = 90°.
Volume	10467.16) $Å^3$	
Z	8	
Density (calculated)	1.639 Mg/m^3	
Absorption coefficient	1.170 mm^{-1}	
F(000)	5328	
Crystal size	0.11x 0.10 x 0.02 mm^3	
Theta range for data collection	5.59 to 23.50°	
Index ranges	-15<=h<=15, -26<=k<=26, -37<=l<=37	
Reflections collected	39291	
Independent reflections	14982 [R(int) = 0.0972]	
Completeness to theta = 23.50°	97.6 %	
Absorption correction	Semi – empirical from equivalents	
Max. and min. transmission	0.9770 and 0.8821	
Refinement method	Full-matrix least-squares on F^2	
Data / restraints / parameters	14982/ 14 / 1282	
Goodness-of-fit on F^2	1.042	
Final R indices [I>2sigma(I)]	R1 = 0.0771, wR2 = 0.1869	
R indices (all data)	R1 = 0.1001, wR2 = 0.2032	
Absolute structure parameter	0.51(3)	
Largest diff. peak and hole	0.631 and -0.609 e.$Å^{-3}$	

Crystal Data and Structure Refinement for 3

Identification code	5270	
Empirical formula	C_{20} H_{22} Mn_2 N_{12} O_8	
Formula weight	668.38	
Temperature	100(2) K	
Wavelength	0.71073 Å	
Crystal system	Triclinic	
Space group	P-1, No.2	
Unit cell dimensions	a = 7.9237(5) Å	α = 94.011(5)°
	b = 8.8121(5) Å	β = 102.488(5)°
	c = 10.0035(6) Å	γ = 102.992(5)°
Volume	659.33(7) $Å^3$	
Z	1	
Density (calculated)	1.683 Mg/m^3	
Absorption coefficient	1.028 mm^{-1}	
F(000)	3160	
Crystal size	0.10 x 0.05 x 0.03 mm	
Theta range for data collection	2.98 to 27.50°	
Index ranges	-10<=h<=10, -11<=k<=11, -12<=l<=12	
Reflections collected	9729	
Independent reflections	3020 [R(int) = 0.0742]	
Completeness to theta = 27.50°	99.8 %	
Absorption correction	None	
Refinement method	Full-matrix least-squares on F^2	
Data / restraints / parameters	3020 / 0 / 193	
Goodness-of-fit on F^2	1.110	
Final R indices [I>2sigma(I)]	R1 = 0.0653, wR2 = 0.1598	
R indices (all data)	R1 = 0.0878, wR2 = 0.1738	
Largest diff. peak and hole	1.553 and -0.755 $e.Å^{-3}$	

Crystal Data and Structure Refinement for 4

Identification code	5695	
Empirical formula	$C_{79}\ H_{108}\ Cl_2\ Fe_2\ N_6\ O_{10}$	
Formula weight	1484.31	
Temperature	100(2) K	
Wavelength	0.71073 Å	
Crystal system	Monoclinic	
Space group	P2(1)/c	
Unit cell dimensions	a = 30.004(3) Å	α = 90°.
	b = 20.167(2) Å	β = 90.951(6)°
	c = 13.5983(9) Å	γ = 90°.
Volume	8227.1(13) $Å^3$	
Z	4	
Density (calculated)	1.198 Mg/m^3	
Absorption coefficient	0.474 mm^{-1}	
F(000)	3160	
Crystal size	0.04 x 0.03 x 0.02 mm^3	
Theta range for data collection	3.00 to 22.50°	
Index ranges	-32<=h<=32, -21<=k<=21, -14<=l<=14	
Reflections collected	82051	
Independent reflections	10735 [R(int) = 0.1418]	
Completeness to theta = 22.50°	99.7 %	
Absorption correction	None	
Refinement method	Full-matrix least-squares on F^2	
Data / restraints / parameters	10735 / 47 / 911	
Goodness-of-fit on F^2	1.067	
Final R indices [I>2sigma(I)]	R1 = 0.0754, wR2 = 0.1434	
R indices (all data)	R1 = 0.1517, wR2 = 0.1794	
Largest diff. peak and hole	0.505 and -0.688 e.$Å^{-3}$	

Crystal Data and Structure Refinement for 5

Identification code	6132	
Empirical formula	$C_{100}\ H_{155}\ Cl_{10}\ N_6\ O_{9.5}\ V_4$	
Formula weight	2151.58	
Temperature	100(2) K	
Wavelength	0.71073 Å	
Crystal system	Triclinic, P-1, No.2	
Space group	Cc, No. 9	
Unit cell dimensions	a = 15.0798(9) Å	α = 113.412(3)°
	b = 0.4731(13) Å	β = 96.194 (2)°
	c = 22.21243) Å	γ = 103.904(3)°
Volume	5947.3(6) $Å^3$	
Z	2	
Density (calculated)	1.203 Mg/m^3	
Absorption coefficient	0.580 mm^{-1}	
F(000)	2274	
Crystal size	0.2x 0.2 x 0.1 mm^3	
Theta range for data collection	2.76 to 25.00°	
Index ranges	-15<=h<=17, -24<=k<=24, -26<=l<=26	
Reflections collected	97715	
Independent reflections	20900 [R(int) = 0.1654]	
Completeness to theta = 25.00°	99.8 %	
Absorption correction	Semi – empirical from equivalents	
Max. and min. transmission	0.9348 and 0.8552	
Refinement method	Full-matrix least-squares on F^2	
Data / restraints / parameters	209000/ 226 / 1247	
Goodness-of-fit on F^2	1.011	
Final R indices [I>2sigma(I)]	R1 = 0.0685, wR2 = 0.1695	
R indices (all data)	R1 = 0.1300, wR2 = 0.2074	
Largest diff. peak and hole	1.369 and -0.836 e.$Å^{-3}$	

Crystal Data and Structure Refinement for 6

Identification code	5708	
Empirical formula	$C_{24}\ H_{39}\ Cl_2\ Fe\ N_{12}\ Ni\ O_{11}$	
Formula weight	857.13	
Temperature	100(2) K	
Wavelength	0.71073 Å	
Crystal system	Trigonal	
Space group	R – 2c, No. 167	
Unit cell dimensions	a = 12.3400(3) Å	α = 90°
	b = 12.3400(3) Å	β = 90°
	c = 78.516(3) Å	γ = 120°
Volume	10354.3(5) $Å^3$	
Z	12	
Density (calculated)	1.650 Mg/m^3	
Absorption coefficient	1.195 mm^{-1}	
F(000)	5316	
Crystal size	0.03x 0.26 x 0.08 mm^3	
Theta range for data collection	3.11 to 35.00°	
Index ranges	-19<=h<=19, -15<=k<=10, -100<=l<=125	
Reflections collected	31963	
Independent reflections	5035 [R(int) = 0.0393]	
Completeness to theta = 35.00°	99.0 %	
Absorption correction	Semi – empirical from equivalents	
Max. and min. transmission	0.7453 and 0.3757	
Refinement method	Full-matrix least-squares on F^2	
Data / restraints / parameters	5035/ 21 / 169	
Goodness-of-fit on F^2	1.036	
Final R indices [I>2sigma(I)]	R1 = 0.0383, wR2 = 0.1000	
R indices (all data)	R1 = 0.0496, wR2 = 0.1071	
Largest diff. peak and hole	0.977 and -0.995 $e.Å^{-3}$	

Crystal Data and Structure Refinement for 7

Identification code	5702	
Empirical formula	$C_{24}\ H_{39}\ Cl_2\ Fe\ N_{12}\ O_{11}\ Zn$	
Formula weight	863.79	
Temperature	100(2) K	
Wavelength	0.71073 Å	
Crystal system	Trigonal	
Space group	R – 3c, No.167	
Unit cell dimensions	a = 12.3961(3) Å	α = 90°
	b = 12.3961(3) Å	β = 90°
	c = 78.710(3) Å	γ = 120°
Volume	10474.4(5) $Å^3$	
Z	12	
Density (calculated)	1.643 Mg/m^3	
Absorption coefficient	1.329 mm^{-1}	
F(000)	5340	
Crystal size	0.10 x 0.07 x 0.02 mm	
Theta range for data collection	3.11 to 28.35°	
Index ranges	-16<=h<=16, -16<=k<=16, -104<=l<=104	
Reflections collected	76274	
Independent reflections	2917 [R(int) = 0.0662]	
Completeness to theta = 28.35°	99.7 %	
Absorption correction	Semi – empirical from equivalents	
Max. and min. transmission	0.7453 and 0.3757	
Refinement method	Full-matrix least-squares on F^2	
Data / restraints / parameters	2917 / 21 / 169	
Goodness-of-fit on F^2	1.044	
Final R indices [I>2sigma(I)]	R1 = 0.0397, wR2 = 0.1022	
R indices (all data)	R1 = 0.0528, wR2 = 0.1103	
Largest diff. peak and hole	0.822 and -0.696 $e.Å^{-3}$	

Crystal Data and Structure Refinement for 8

Identification code	5976	
Empirical formula	C_{24} H_{39} Cl_2 Ga N_{12} Ni O_{11}	
Formula weight	871.0	
Temperature	100(2) K	
Wavelength	0.71073 Å	
Crystal system	Trigonal	
Space group	R – 3C	
Unit cell dimensions	a = 12.3321(7) Å	α = 90°
	b = 12.3321(7) Å	β = 90°
	c = 78.163(7) Å	γ = 120°
Volume	10294.5(12) $Å^3$	
Z	12	
Density (calculated)	1.686 Mg/m^3	
Absorption coefficient	1.564 mm^{-1}	
F(000)	5376	
Crystal size	0.36 x 0.34 x 0.07 mm	
Theta range for data collection	3.13 to 33.22°	
Index ranges	-13<=h<=18, -18<=k<=18, -120<=l<=120	
Reflections collected	47599	
Independent reflections	4373 [R(int) = 0.0591]	
Completeness to theta = 33.22°	99.3 %	
Absorption correction	Semi – empirical from equivalents	
Max. and min. transmission	0.7444 and 0.4517	
Refinement method	Full-matrix least-squares on F^2	
Data / restraints / parameters	4373 / 21 / 169	
Goodness-of-fit on F^2	1.034	
Final R indices [I>2sigma(I)]	R1 = 0.0383, wR2 = 0.0998	
R indices (all data)	R1 = 0.0495, wR2 = 0.1065	
Largest diff. peak and hole	1.068 and -1.050 $e.Å^{-3}$	

Crystal Data and Structure Refinement for 9

Identification code	5728	
Empirical formula	$C_{27}H_{47}Cl_{2.50}FeMnN_{12.50}O_{13}$	
Formula weight	954.19	
Temperature	100(2) K	
Wavelength	0.71073 Å	
Unit cell dimensions	a = 26.7855(7) Å	α = 90°
	b = 14.5962(4) Å	β = 107.2°
	c = 22.2784(6) Å	γ = 120°
Volume	832221(4) $Å^3$	
Z	8	
Density (calculated)	1.523 Mg/m^3	
Absorption coefficient	1.073 mm^{-1}	
F(000)	3952	
Crystal size	0.06 x 0.24 x 0.30 mm	
Theta range for data collection	2.9 to 32.5°	
Index ranges	-40<=h<=38, -22<=k<=22, -33<=l<=33	
Reflections collected	113157	
Independent reflections	15040 [R(int) = 0.0517]	
Completeness to theta = 32.50°	99.8 %	
Absorption correction	0.89 mm^{-1}	
Max. and min. transmission	0.9488 and 0.7770	
Refinement method	Full-matrix least-squares on F^2	
Data / restraints / parameters	15040 / 72 / 586	
Goodness-of-fit on F^2	1.91	
Final R indices [I>2sigma(I)]	R1 = 0.0771, wR2 = 0.2522	
R indices (all data)	R1 = 0.0939, wR2 = 0.2607	
Largest diff. peak and hole	2.28 and -1.36 e.$Å^{-3}$	

Crystal Data and Structure Refinement for 10

Identification code	5725	
Empirical formula	$C_{24}\ H_{39}\ Cl_2\ Fe_2\ N_{12}\ O_{11}$	
Formula weight	854.27	
Temperature	100(2) K	
Wavelength	0.71073 Å	
Crystal system	Trigonal	
Space group	R 32, No.155	
Unit cell dimensions	a = 12.1963(11) Å	α = 90°
	b = 12.1963(11) Å	β = 90°
	c = 40.064(4) Å	γ = 120°
Volume	5161.1(8) $Å^3$	
Z	6	
Density (calculated)	1.649 Mg/m^3	
Absorption coefficient	1.073 mm^{-1}	
F(000)	2646	
Crystal size	0.055 x 0.040 x 0.034 mm	
Theta range for data collection	3.67 to 30.00°	
Index ranges	-17<=h<=17, -14<=k<=17, -56<=l<=52	
Reflections collected	16303	
Independent reflections	3276 [R(int) = 0.087]	
Completeness to theta = 30.00°	96.7 %	
Absorption correction	Semi – empirical from equivalents	
Max. and min. transmission	0.7453 and 0.3757	
Refinement method	Full-matrix least-squares on F^2	
Data / restraints / parameters	3276 / 21 / 164	
Goodness-of-fit on F^2	1.036	
Final R indices [I>2sigma(I)]	R1 = 0.0571, wR2 = 0.1117	
R indices (all data)	R1 = 0.0849, wR2 = 0.1226	
Absolute structure parameter	0.11(3)	
Largest diff. peak and hole	0.787 and -0.660 $e.Å^{-3}$	

Crystal Data and Structure Refinement for 11

Identification code	5762	
Empirical formula	C_{24} H_{39} Cl_2 Cu Fe N_{12} O_{11}	
Formula weight	861.96	
Temperature	100(2) K	
Wavelength	0.71073 Å	
Crystal system	Trigonal	
Space group	R – 3c, No.167	
Unit cell dimensions	a = 12.2693(5) Å	α = 90°
	b = 12.2693(5) Å	β = 90°
	c = 78.349(5) Å	γ = 120°
Volume	10214.2(8) $Å^3$	
Z	12	
Density (calculated)	1.682 Mg/m^3	
Absorption coefficient	1.283 mm^{-1}	
F(000)	5328	
Crystal size	0.36 x 0.34 x 0.07 mm	
Theta range for data collection	3.12 to 25.99°	
Index ranges	-15<=h<=15, -12<=k<=15, -96<=l<=96	
Reflections collected	44322	
Independent reflections	2239 [R(int) = 0.0957]	
Completeness to theta = 25.99°	99.8 %	
Absorption correction	Gaussian	
Max. and min. transmission	0.9006 and 0.6843	
Refinement method	Full-matrix least-squares on F^2	
Data / restraints / parameters	2239 / 21 / 169	
Goodness-of-fit on F^2	1.091	
Final R indices [I>2sigma(I)]	R1 = 0.0532, wR2 = 0.1240	
R indices (all data)	R1 = 0.0728, wR2 = 0.1341	
Largest diff. peak and hole	0.776 and -0.635 $e.Å^{-3}$	

Crystal Data and Structure Refinement for 12

Identification code	5832	
Empirical formula	C_{24} H_{39} Cl_2 Co Fe N_{12} O_{11}	
Formula weight	857.35	
Temperature	100(2) K	
Wavelength	0.71073 Å	
Crystal system	Trigonal	
Space group	R 32, No.155	
Unit cell dimensions	a = 12.1561(5) Å	α = 90°
	b = 12.1561(5) Å	β = 90°
	c = 39.878(2) Å	γ = 120°
Volume	5103.3(8) $Å^3$	
Z	6	
Density (calculated)	1.674 Mg/m^3	
Absorption coefficient	1.146 mm^{-1}	
F(000)	2652	
Crystal size	0.15 x 0.15 x 0.04 mm	
Theta range for data collection	3.90 to 32.49°	
Index ranges	-18<=h<=18, -17<=k<=17, -60<=l<=60	
Reflections collected	47102	
Independent reflections	4127 [R(int) = 0.087]	
Completeness to theta = 32.49°	99.7 %	
Absorption correction	None	
Refinement method	Full-matrix least-squares on F^2	
Data / restraints / parameters	4127 / 21 / 168	
Goodness-of-fit on F^2	1.086	
Final R indices [I>2sigma(I)]	R1 = 0.0720, wR2 = 0.1881	
R indices (all data)	R1 = 0.0835, wR2 = 0.1981	
Absolute structure parameter	0.06(4)	
Largest diff. peak and hole	1.020 and -1.339 e.$Å^{-3}$	

Crystal Data and Structure Refinement for 13

Identification code	5968	
Empirical formula	C_{24} H_{39} Cl_2 Cr N_{12} Ni O_{11}	
Formula weight	853.28	
Temperature	100(2) K	
Wavelength	0.71073 Å	
Crystal system	Trigonal	
Space group	R – 3c, No.167	
Unit cell dimensions	a = 12.3381(7) Å	α = 90°
	b = 12.3381(7) Å	β = 90°
	c = 78.347(6) Å	γ = 120°
Volume	10328.8(11) $Å^3$	
Z	12	
Density (calculated)	1.646 Mg/m^3	
Absorption coefficient	1.092 mm^{-1}	
F(000)	5292	
Crystal size	0.36 x 0.34 x 0.07 mm	
Theta range for data collection	3.12 to 34.28°	
Index ranges	-19<=h<=19, -18<=k<=18, -123<=l<=122	
Reflections collected	55757	
Independent reflections	3276 [R(int) = 0.087]	
Completeness to theta = 34.28°	97.8 %	
Absorption correction	Semi – empirical from equivalents	
Max. and min. transmission	0.9275 and 0.6946	
Refinement method	Full-matrix least-squares on F^2	
Data / restraints / parameters	4701 / 21 / 169	
Goodness-of-fit on F^2	1.041	
Final R indices [I>2sigma(I)]	R1 = 0.0470, wR2 = 0.1182	
R indices (all data)	R1 = 0.0642, wR2 = 0.1294	
Largest diff. peak and hole	0.908 and -0.842 $e.Å^{-3}$	

3. Magnetochemical Data

Complex $[Na^{I}_{2}\{Ni^{II}_{4}(HL)_3(OOCCH_3)_5(HCOO)_{0.5}\}_4]$ (1)

MW = 3672 g/mol, χ_{dia} = -1750.0 x 10^{-6} cm^3 mol^{-1}

m = 53.64 mg, H = 1.00 T

No	T(K)	μ_{eff}(exp.)	μ_{cal}(calc.)	χ_m·T(exp.)	χ_m·T(calc.)
1	2	6.21886	-	4.83574	-
2	5.03	6.75028	-	5.69751	-
3	10	7.49565	-	7.02522	-
4	15	8.19409	-	8.39542	-
5	20	8.66999	-	9.39893	-
6	29.99	9.18884	-	10.55754	-
7	40	9.49086	-	11.26295	-
8	50.01	9.72306	-	11.82081	-
9	60.03	9.92088	-	12.3067	-
10	70.05	10.101	-	12.75763	-
11	80.07	10.2687	-	13.18476	-
12	90.08	10.4167	-	13.56755	-
13	100.15	10.5587	-	13.93998	-
14	110.07	10.6779	-	14.2565	-
15	120.13	10.7937	-	14.56739	-
16	130.16	10.8896	-	14.8274	-
17	140.18	10.9856	-	15.08998	-
18	150.2	11.072	-	15.32828	-
19	160.19	11.1523	-	15.55142	-
20	170.23	11.2293	-	15.76691	-
21	180.23	11.2961	-	15.95505	-
22	190.24	11.362	-	16.14176	-
23	200.25	11.4195	-	16.30555	-
24	210.26	11.4753	-	16.46529	-
25	220.24	11.5291	-	16.62004	-
26	230.24	11.5757	-	16.75466	-
27	240.25	11.6208	-	16.88547	-
28	250.28	11.6534	-	16.98034	-
29	260.14	11.6809	-	17.06058	-
30	270.24	11.7236	-	17.18554	-
31	280.34	11.7656	-	17.3089	-
32	290.29	11.8086	-	17.43564	-

Complex $[Na^{I}_{2}\{Ni^{II}_{4}(HL)_3(OOCCH_3)_5(HCOO)_{0.5}\}_4]_{0.25}$ (1')**

MW = 918 g/mol. χ_{dia} = -437.0 x 10^{-6} cm^3 mol^{-1}

m = 53.64 mg, H = 1.00 T

No	T(K)	μ_{eff}(exp.)	μ_{cal}(calc.)	χ_m·T(exp.)	χ_m·T(calc.)
1	2	3.10943	2.95754	1.20893	1.09371
2	5.03	3.37514	3.09384	1.42438	1.19684
3	10	3.74782	3.59284	1.7563	1.61405
4	15	4.09704	4.06382	2.09885	2.06495
5	20	4.335	4.31335	2.34974	2.32633
6	29.99	4.59441	4.56862	2.63937	2.60982
7	40	4.74541	4.73611	2.81571	2.80469
8	50.01	4.86151	4.87373	2.95518	2.97005
9	60.03	4.96041	4.99227	3.07664	3.11629
10	70.05	5.05048	5.09499	3.18938	3.24585
11	80.07	5.13432	5.1844	3.29615	3.36077
12	90.08	5.20833	5.26218	3.39186	3.46236
13	100.15	5.27932	5.33055	3.48495	3.55292
14	110.07	5.3389	5.38964	3.56406	3.63212
15	120.13	5.39677	5.44239	3.64174	3.70357
16	130.16	5.44475	5.48898	3.70678	3.76725
17	140.18	5.49277	5.53031	3.77245	3.8242
18	150.2	5.53594	5.56721	3.83199	3.8754
19	160.19	5.57612	5.60028	3.88781	3.92158
20	170.23	5.6146	5.6302	3.94166	3.96359
21	180.23	5.64798	5.65718	3.98866	4.00167
22	190.24	5.68093	5.68171	4.03534	4.03645
23	200.25	5.7097	5.70409	4.07632	4.06831
24	210.26	5.73759	5.72459	4.11624	4.0976
25	220.24	5.76445	5.74334	4.15487	4.12449
26	230.24	5.78777	5.76065	4.18855	4.14939
27	240.25	5.81032	5.77665	4.22125	4.17247
28	250.28	5.82663	5.79151	4.24498	4.19397
29	260.14	5.84034	5.8051	4.26498	4.21367
30	270.24	5.86172	5.81804	4.29627	4.23248
31	280.34	5.88271	5.83009	4.32709	4.25003
32	290.29	5.90421	5.84123	4.35878	4.26628

During the simulation $1/4^{th}$ of **1 has been considered.

Complex $[NaL_6(V{=}O)_6]ClO_4$ (2)

MW = 1315.15 g/mol, χ_{dia} = -500.0 x 10^{-6} cm^3 mol^{-1}

m = 24.36 mg, H = 1.00 T

No	T(K)	μ_{eff}(exp.)	μ_{cal}(calc.)	χ_m·T(exp.)	χ_m·T(calc.)
1	2	5.99321	8.20704	4.49118	8.42198
2	25	6.59961	6.9366	5.446	6.01637
3	9.99	6.43951	6.41328	5.18498	5.14282
4	14.99	6.05282	6.03327	4.58096	4.55142
5	20.01	5.76082	5.74806	4.14963	4.13127
6	30	5.37336	5.37483	3.61021	3.61219
7	40	5.13784	5.14479	3.30067	3.30961
8	50.03	4.98246	4.98829	3.10405	3.11132
9	60.02	4.86711	4.87567	2.96199	2.97242
10	70.09	4.78301	4.78971	2.86051	2.86853
11	80.04	4.71836	4.72321	2.78371	2.78943
12	90.13	4.67091	4.66902	2.728	2.72579
13	100.18	4.62738	4.62471	2.67739	2.6743
14	110.19	4.59292	4.58783	2.63766	2.63182
15	120.01	4.56442	4.55709	2.60503	2.59667
16	130.13	4.53404	4.52993	2.57047	2.56581
17	140.18	4.51028	4.5065	2.5436	2.53933
18	150.21	4.49193	4.48606	2.52294	2.51635
19	160.2	4.474	4.46806	2.50284	2.4962
20	170.24	4.45959	4.452	2.48674	2.47829
21	180.23	4.4462	4.43769	2.47183	2.46238
22	190.26	4.43278	4.42476	2.45693	2.44805
23	200.25	4.42285	4.41308	2.44594	2.43514
24	210.24	4.4114	4.40247	2.43329	2.42345
25	220.24	4.40221	4.39279	2.42316	2.4128
26	230.14	4.3933	4.38399	2.41336	2.40315
27	240.28	4.38401	4.37568	2.40317	2.39404
28	250.26	4.37705	4.36815	2.39554	2.38581
29	260.3	4.36915	4.36114	2.3869	2.37816
30	270.21	4.36458	4.3547	2.38191	2.37114
31	280.29	4.36217	4.34861	2.37928	2.36452
32	290.33	4.3597	4.34295	2.37659	2.35836

Complex $[NaL_6(V{=}O)_6]ClO_4$ (2)

MW = 1315.15 g/mol, χ_{dia} = -500.0 x 10^{-6} cm^3 mol^{-1}

m = 24.36 mg, H = 0.10 T

No	T(K)	μ_{eff}(exp.)	μ_{cal}(calc.)	χ_m·T(exp.)	χ_m·T(calc.)
1	1.97	6.99811	8.0463	6.12354	8.09531
2	5.02	6.86846	6.88713	5.89875	5.93086
3	9.89	6.47501	6.4138	5.2423	5.14366
4	14.99	6.05107	6.03712	4.57831	4.55723
5	20	5.75119	5.75706	4.13577	4.14422
6	30	5.36303	5.38554	3.59635	3.6266
7	39.99	5.13054	5.15508	3.2913	3.32286
8	50.01	4.97839	4.99812	3.09898	3.12359
9	60.04	4.86789	4.88418	2.96294	2.9828
10	70.04	4.78378	4.79809	2.86143	2.87858
11	80.08	4.72293	4.73037	2.7891	2.7979
12	90.14	4.67333	4.67578	2.73083	2.73369
13	100.16	4.63465	4.6311	2.68581	2.6817
14	110.16	4.59817	4.59382	2.64369	2.63869
15	120.25	4.56632	4.56194	2.6072	2.6022
16	130.11	4.5333	4.53514	2.56963	2.57171
17	140.19	4.51156	4.51137	2.54504	2.54483
18	150.2	4.48957	4.49069	2.52029	2.52155
19	160.21	4.47252	4.47243	2.50118	2.50108
20	170.23	4.45664	4.45617	2.48346	2.48293
20	180.25	4.44193	4.44161	2.46709	2.46673
22	190.22	4.42958	4.42857	2.45339	2.45227
23	200.26	4.41723	4.41669	2.43973	2.43913
24	210.23	4.406	4.40594	2.42734	2.42727
25	220.26	4.39693	4.39607	2.41735	2.41641
26	230.26	4.38765	4.38706	2.40716	2.40651
27	240.27	4.38106	4.37877	2.39994	2.39743
28	250.28	4.372	4.3711	2.39002	2.38904
29	260.26	4.36063	4.36402	2.3776	2.3813
30	270.18	4.35665	4.35749	2.37327	2.37418
31	280.26	4.35216	4.3513	2.36838	2.36744
32	290.27	4.35497	4.34557	2.37144	2.36121

Complex $[NaL_6(V{=}O)_6]ClO_4$ (2)

MW = 1315.15 g/mol, χ_{dia} = -500.0 x 10^{-6} cm^3 mol^{-1}

m = 24.36 mg, H = 0.01 T

No	T(K)	μ_{eff}(exp.)	μ_{cal}(calc.)	χ_m·T(exp.)	χ_m·T(calc.)
1	1.88	6.98935	8.02428	6.10822	8.05107
2	4.97	6.84006	6.85918	5.85007	5.88282
3	9.85	6.42462	6.38254	5.16103	5.09364
4	14.99	6.02245	6.0001	4.53511	4.50151
5	20	5.72244	5.72094	4.09453	4.09238
6	30	5.33521	5.35421	3.55913	3.58453
7	40	5.10518	5.12779	3.25884	3.28777
8	50.01	4.95826	4.9742	3.07397	3.09377
9	60.06	4.84997	4.86285	2.94116	2.95681
10	70.06	4.75926	4.77893	2.83217	2.85563
11	80.07	4.70952	4.71311	2.77328	2.77751
12	90.11	4.66882	4.6601	2.72556	2.71539
13	100.09	4.61289	4.61679	2.66065	2.66515
14	109.97	4.57777	4.58095	2.62029	2.62393
15	120.06	4.54152	4.54992	2.57895	2.5885
16	130.16	4.51611	4.52326	2.55018	2.55826
17	140.19	4.49341	4.50034	2.5246	2.5324
18	150.2	4.47085	4.4803	2.49932	2.50989
19	160.2	4.45223	4.46261	2.47854	2.49011
20	170.24	4.44718	4.44684	2.47292	2.47254
21	180.07	4.42886	4.43301	2.45259	2.45719
22	190.22	5.31166	4.42013	3.52778	2.44293
23	200.26	4.40385	4.40863	2.42497	2.43024
24	210.25	4.41029	4.39822	2.43207	2.41877
25	220.25	4.38488	4.3887	2.40412	2.40831
26	230.27	4.38065	4.37998	2.39949	2.39875
27	240.29	4.36846	4.37193	2.38615	2.38994
28	250.28	4.36412	4.36453	2.38141	2.38186
29	260.29	4.37061	4.35766	2.3885	2.37437
30	270.31	4.36965	4.35129	2.38745	2.36743
31	280.24	4.3571	4.3454	2.37376	2.36103
32	290.26	4.34353	4.33985	2.35899	2.355

Complex $[Mn^{III}_2L_4(CH_3COO)_2]_n$ (3)

MW = 668.00 g/mol, χ_{dia} = -350.0 x 10^{-6} cm^3 mol^{-1}

m = 20.67 mg, H = 1.00 T

No	T(K)	μ_{eff}(exp.)	μ_{cal}(calc.)	χ_m·T(exp.)	χ_m·T(calc.)
1	2	3.99891	5.47513	1.99951	3.74826
2	5.01	5.71229	7.19143	4.08001	6.46654
3	10	7.04558	7.78359	6.2069	7.57532
4	15	7.56006	7.7681	7.14647	7.5452
5	20	7.65614	7.67363	7.32927	7.3628
6	30	7.53816	7.50795	7.10513	7.04829
7	40	7.41085	7.39567	6.86716	6.83906
8	50	7.31846	7.31827	6.697	6.69666
9	60.03	7.24599	7.26227	6.56503	6.59456
10	70.05	7.18987	7.22017	6.46373	6.51833
11	80.09	7.15525	7.18734	6.40163	6.45918
12	90.1	7.13207	7.16117	6.36022	6.41223
13	100.1	7.11078	7.13982	6.32231	6.37405
14	110.1	7.09753	7.12204	6.29877	6.34235
15	120.17	7.08669	7.10693	6.27954	6.31546
16	130.17	7.07773	7.09408	6.26367	6.29265
17	140.17	7.06818	7.08295	6.24678	6.27292
18	150.19	7.06425	7.0732	6.23984	6.25566
19	160.21	7.05906	7.06462	6.23067	6.24049
20	170.23	7.05616	7.05699	6.22555	6.22702
21	180.21	7.05197	7.0502	6.21816	6.21504
22	190.23	7.04676	7.04407	6.20898	6.20424
23	200.24	7.04583	7.03854	6.20734	6.1945
24	210.24	7.04357	7.0335	6.20336	6.18563
25	220.16	7.04033	7.02895	6.19765	6.17763
26	230.25	7.04183	7.02472	6.20029	6.1702
27	240.26	7.04019	7.02083	6.19741	6.16337
28	250.26	7.04262	7.01728	6.20168	6.15714
29	260.26	7.03901	7.01397	6.19533	6.15133
30	270.26	7.03751	7.0109	6.19269	6.14595
31	280.27	7.04425	7.00805	6.20456	6.14095
32	290.26	7.05599	7.00539	6.22525	6.13629

Complex $[L_2Fe_2(NO_3)_2]\cdot CH_2Cl_2\cdot$hexane (4)

MW = 1484.0 g/mol, χ_{dia} = -700.0 x 10^{-6} cm^3 mol^{-1}

m = 22.26 mg, H = 1.00 T

No	T(K)	μ_{eff}(exp.)	μ_{cal}(calc.)	χ_m·T(exp.)	χ_m·T(calc.)
1	2	8.02449	7.82004	8.0686	7.66269
2	5.01	9.09249	9.09523	10.35926	10.36551
3	9.99	8.94847	8.92176	10.03369	9.97388
4	14.99	8.77133	8.77066	9.64038	9.6389
5	20	8.68272	8.68098	9.44658	9.4428
6	30	8.58518	8.5837	9.23553	9.23235
7	39.99	8.53035	8.53234	9.11794	9.1222
8	50.01	8.49874	8.50064	9.05049	9.05454
9	60.02	8.47507	8.47918	9.00015	9.00888
10	70.03	8.45668	8.46373	8.96113	8.97608
11	80.06	8.44792	8.45201	8.94258	8.95124
12	90.09	8.44157	8.44285	8.92914	8.93185
13	100.12	8.43194	8.4355	8.90878	8.9163
14	110.09	8.42661	8.4295	8.89752	8.90362
15	120.16	8.42316	8.42443	8.89023	8.89292
16	130.16	8.41639	8.42017	8.87595	8.88392
17	140.18	8.40834	8.4165	8.85898	8.87618
18	150.12	8.4024	8.41333	8.84647	8.8695
19	160.2	8.39747	8.41053	8.83609	8.86359
20	170.21	8.39492	8.40807	8.83072	8.85841
21	180.24	8.39367	8.40586	8.82809	8.85375
22	190.23	8.3903	8.40391	8.82101	8.84965
23	200.24	8.39061	8.40214	8.82166	8.84592
24	210.25	8.38841	8.40053	8.81703	8.84253
25	220.25	8.38794	8.39908	8.81604	8.83948
26	230.25	8.38808	8.39775	8.81634	8.83668
27	240.26	8.38646	8.39653	8.81293	8.83411
28	250.26	8.38821	8.39541	8.81661	8.83175
29	260.27	8.38736	8.39437	8.81482	8.82957
30	270.25	8.38493	8.3934	8.80972	8.82752
31	280.24	8.3861	8.39251	8.81218	8.82565
32	290.23	8.38536	8.39169	8.81062	8.82393

Complex $[C_6H_4(NH_2)_2][L''_2V^{III}_2V^{IV}_2(\mu\text{-}Cl)_6(Cl)_4]$ (5)

MW = 1768.00 g/mol. $\chi_{dia} = -1100.0 \times 10^{-6}$ cm^3 mol^{-1}

m = 25.90 mg, H = 1.00 T

No	T(K)	μ_{eff}(exp.)	μ_{cal}(calc.)	χ_m·T(exp.)	χ_m·T(calc.)
1	1.99	1.60911	1.60203	0.32375	0.32091
2	4.94	2.16397	2.1443	0.58552	0.57493
3	9.92	2.23234	2.29997	0.62311	0.66143
4	14.97	2.25948	2.34646	0.63835	0.68844
5	20.01	2.29139	2.36857	0.65651	0.70148
6	30.01	2.38981	2.39755	0.71411	0.71875
7	40	2.51715	2.48603	0.79224	0.77278
8	50.01	2.64895	2.58361	0.87738	0.83463
9	60.07	2.77753	2.71486	0.96463	0.92159
10	70.04	2.89551	2.83154	1.04831	1.00251
11	80.06	3.00683	2.95091	1.13047	1.08881
12	90.12	3.1095	3.06381	1.20899	1.17372
13	99.97	3.20246	3.18296	1.28236	1.26679
14	109.98	3.28941	3.2917	1.35294	1.35482
15	119.88	3.36658	3.38729	1.41716	1.43465
16	130.2	3.44018	3.47523	1.4798	1.51011
17	140.23	3.50632	3.55053	1.53725	1.57626
18	150.24	3.56693	3.61705	1.59085	1.63588
19	160.26	3.62396	3.6761	1.64213	1.68972
20	170.3	3.67713	3.72875	1.69067	1.73847
21	180.28	3.72769	3.77547	1.73748	1.78231
22	190.32	3.77572	3.81765	1.78255	1.82236
23	200.3	3.82065	3.85541	1.82522	1.85858
24	210.32	3.86428	3.88968	1.86715	1.89177
25	220.35	3.90361	3.92079	1.90535	1.92215
26	230.35	3.94236	3.94906	1.94336	1.94997
27	240.26	3.97675	3.97466	1.97741	1.97534
28	250.41	4.01202	3.99869	2.01265	1.99929
29	260.38	4.04619	4.03036	2.04707	2.03109
30	270.42	4.07805	4.0505	2.07944	2.05144
31	280.43	4.10809	4.08907	2.11019	2.09069
32	290.41	4.13901	4.11624	2.14207	2.11857

Complex [L'$Fe^{III}Ni^{II}(^{Me}ImOx)_3](ClO_4)_2$ (6)

MW = 856.55 g/mol, χ_{dia} = -350.0 x 10^{-6} cm^3 mol^{-1}

m = 29.28 mg, H = 1.00 T

No	T(K)	μ_{eff}(exp.)	μ_{cal}(calc.)	χ_m·T(exp.)	χ_m·T(calc.)
1	1.95	2.54645	2.8896	0.8108	1.04404
2	5.19	3.26312	3.2341	1.3314	1.30782
3	9.86	3.49584	3.47332	1.52807	1.50845
4	14.99	3.61599	3.59983	1.63492	1.62034
5	20	3.66584	3.66005	1.68031	1.675
6	30	3.72248	3.71626	1.73263	1.72685
7	40	3.76631	3.75626	1.77367	1.76422
8	50.01	3.81932	3.80814	1.82395	1.81329
9	60.03	3.88839	3.87688	1.89052	1.87934
10	70.04	3.96838	3.95922	1.9691	1.96002
11	80.04	4.05634	4.05077	2.05736	2.05171
12	90.11	4.1531	4.14822	2.15668	2.15162
13	100.08	4.24849	4.24696	2.25689	2.25526
14	110.12	4.34976	4.34634	2.36577	2.36205
15	120.15	4.44768	4.44409	2.47348	2.46949
16	130.16	4.54081	4.53878	2.57815	2.57584
17	140.18	4.62879	4.63004	2.67902	2.68047
18	150.19	4.7135	4.71704	2.77797	2.78215
19	160.2	4.79378	4.79973	2.87341	2.88055
20	170.22	4.87016	4.87801	2.9657	2.97527
21	180.23	4.94226	4.9518	3.05416	3.06597
22	190.22	5.00975	5.02117	3.13815	3.15247
23	200.24	5.07753	5.08658	3.22364	3.23514
24	210.24	5.13979	5.14788	3.30318	3.31358
25	220.26	5.19951	5.20554	3.38038	3.38823
26	230.25	5.25711	5.25958	3.45569	3.45894
27	240.26	5.30913	5.31049	3.52442	3.52623
28	250.29	5.36078	5.35843	3.59333	3.59018
29	260.28	5.4082	5.40331	3.65718	3.65057
30	270.27	5.45243	5.44558	3.71725	3.70791
31	280.25	5.49659	5.48536	3.7777	3.76228
32	290.28	5.53816	5.52307	3.83506	3.81419

Complex [L'Fe^{III}Zn^{II}(^{Me}ImOx)$_3$](ClO$_4$)$_2$ (7)

MW = 863.00 g/mol, χ_{dia} = -350.0 x 10^{-6} cm^3 mol^{-1}

m = 33.78 mg, H = 1.00 T

No	T(K)	μ_{eff}(exp.)	μ_{cal}(calc.)	χ_m·T(exp.)	χ_m·T(calc.)
1	2	4.29471	4.29568	2.30626	2.30731
2	5.07	5.27022	5.13987	3.47295	3.30328
3	10	5.59429	5.55621	3.91319	3.8601
4	15	5.7008	5.70638	4.06362	4.07158
5	20	5.75056	5.77903	4.13487	4.17591
6	30	5.80139	5.84556	4.20829	4.27261
7	40	5.82808	5.87391	4.2471	4.31416
8	49.99	5.84344	5.88839	4.26951	4.33545
9	60.04	5.85388	5.89675	4.28478	4.34777
10	70.05	5.86191	5.90196	4.29655	4.35546
11	80.07	5.87122	5.90544	4.3102	4.36059
12	90.09	5.8788	5.90786	4.32134	4.36417
13	100.09	5.8839	5.90962	4.32884	4.36677
14	110.11	5.88875	5.91094	4.33598	4.36872
15	120.18	5.89546	5.91196	4.34587	4.37023
16	130.17	5.89451	5.91276	4.34447	4.37141
17	140.18	5.89848	5.9134	4.35032	4.37236
18	150.19	5.90346	5.91392	4.35767	4.37313
19	160.21	5.90694	5.91435	4.36281	4.37376
20	170.22	5.91229	5.91471	4.37072	4.3743
21	180.17	5.91416	5.915	4.37348	4.37472
22	190.24	5.91832	5.91527	4.37964	4.37512
23	200.25	5.93015	5.91549	4.39716	4.37545
24	210.24	5.92346	5.91569	4.38725	4.37574
25	220.28	5.92846	5.91586	4.39466	4.376
26	230.24	5.93006	5.91601	4.39703	4.37622
27	240.25	5.92309	5.91614	4.3867	4.37641
28	250.25	5.93545	5.91626	4.40503	4.37659
29	260.26	5.93525	5.91637	4.40473	4.37675
30	270.26	5.93828	5.91646	4.40923	4.37688
31	280.26	5.94166	5.91655	4.41425	4.37702
32	290.24	5.94651	5.91664	4.42146	4.37715

Complex [L'Fe^{III}Zn^{II}(^{Me}ImOx)$_3$](ClO$_4$)$_2$ (8)

MW = 870.00 g/mol, χ_{dia} = -350.0 x 10^{-6} cm^3 mol^{-1}

m = 29.19 mg, H = 1.00 T

No	T(K)	μ_{eff}(exp.)	μ_{cal}(calc.)	χ_m·T(exp.)	χ_m·T(calc.)
1	1.89	2.50785	2.40533	0.7864	0.72342
2	4.96	2.90269	2.89997	1.05352	1.05155
3	9.87	2.98032	2.98444	1.11062	1.1137
4	15	2.99709	3.00069	1.12316	1.12586
5	20	3.00346	3.00606	1.12794	1.12989
6	30	3.00851	3.00985	1.13173	1.13274
7	40.01	3.01079	3.01116	1.13345	1.13373
8	50.01	3.01215	3.01177	1.13447	1.13419
9	60.03	3.01052	3.01209	1.13325	1.13443
10	70.05	3.00989	3.01229	1.13277	1.13458
11	80.05	3.01094	3.01241	1.13356	1.13467
12	90.06	3.01132	3.01249	1.13385	1.13473
13	100.11	3.01293	3.01255	1.13506	1.13477
14	110.28	3.01385	3.01259	1.13575	1.13481
15	120.12	3.01193	3.01262	1.13431	1.13483
16	130.16	3.01033	3.01265	1.1331	1.13485
17	140.18	3.01011	3.01266	1.13294	1.13486
18	150.2	3.01064	3.01268	1.13334	1.13487
19	160.21	3.01042	3.01269	1.13317	1.13488
20	170.22	3.01127	3.0127	1.13381	1.13489
21	180.24	3.01074	3.0127	1.13341	1.13489
22	190.18	3.01063	3.01271	1.13333	1.1349
23	200.24	3.01116	3.01271	1.13373	1.1349
24	210.23	3.01097	3.01272	1.13358	1.1349
25	220.27	3.01214	3.01272	1.13447	1.1349
26	230.28	3.01228	3.01272	1.13457	1.1349
27	240.27	3.01343	3.01272	1.13544	1.1349
28	250.29	3.01454	3.01272	1.13627	1.1349
29	260.3	3.01576	3.01272	1.13719	1.1349
30	270.28	3.01754	3.01272	1.13854	1.1349
31	280.26	3.0201	3.01272	1.14047	1.1349
32	290.26	3.02318	3.01271	1.1428	1.1349

Complex [L'Fe^{III}Mn^{II}(^{Me}ImOx)$_3$](ClO$_4$)$_2$ (9)

MW = 852.00 g/mol, χ_{dia} = -400.0 x 10^{-6} cm^3 mol^{-1}

m = 30.73 mg, H = 1.00 T

No	T(K)	μ_{eff}(exp.)	μ_{cal}(calc.)	χ_m·T(exp.)	χ_m·T(calc.)
1	1.91	0.40389	0.01914	0.0204	0
2	5.06	0.90667	0.58741	0.10279	0.04339
3	10	1.67305	1.49754	0.34999	0.28201
4	14.98	2.19138	2.05158	0.60045	0.52927
5	20	2.60298	2.47521	0.84719	0.77042
6	30	3.26537	3.14725	1.33323	1.24556
7	39.99	3.80885	3.69682	1.81397	1.71854
8	49.99	4.27074	4.16923	2.28059	2.18582
9	60.04	4.66612	4.5829	2.72241	2.64109
10	70.04	5.00335	4.942	3.13013	3.07119
11	80.14	5.2952	5.25676	3.50595	3.47487
12	90.06	5.53837	5.52519	3.83535	3.83881
13	100.17	5.75495	5.76237	4.14118	4.17546
14	110.12	5.93569	5.96562	4.40538	4.47521
15	119.94	6.0952	6.14081	4.64534	4.74191
16	130.18	6.23523	6.30115	4.86123	4.99277
17	140.18	6.35895	6.43883	5.05606	5.21334
18	150.19	6.46708	6.5609	5.22947	5.41288
19	160.21	6.56513	6.66956	5.38924	5.59366
20	170.21	6.65306	6.76664	5.53457	5.75769
21	180.22	6.73078	6.85388	5.66464	5.90711
22	190.23	6.80317	6.93266	5.78714	6.04368
23	200.24	6.8664	7.004	5.89521	6.16871
24	210.26	6.9268	7.06892	5.99938	6.28359
25	220.26	6.9815	7.12808	6.09451	6.38921
26	230.21	7.02852	7.18205	6.17688	6.48632
27	240.28	7.0773	7.23223	6.26291	6.57728
28	250.25	7.11893	7.27803	6.33681	6.66085
29	260.3	7.15941	7.3207	6.40908	6.73918
30	270.27	7.19786	7.35998	6.4781	6.81169
31	280.28	7.23018	7.39662	6.53641	6.87968
32	290.23	7.26145	7.43053	6.59307	6.94291

Complex [L'Fe^{III}Fe^{II}(^{Me}ImOx)$_3$](ClO$_4$)$_2$ (10)

MW = 853.70 g/mol, χ_{dia} = -350.0 x 10^{-6} cm^3 mol^{-1}

m = 30.20 mg, H = 1.00 T

No	T(K)	μ_{eff}(exp.)	μ_{cal}(calc.)	χ_m·T(exp.)	χ_m·T(calc.)
1	2	4.8501	4.69298	2.94132	2.75384
2	5.04	5.62683	5.5486	3.95885	3.84953
3	10	5.79449	5.79423	4.19828	4.19791
4	15	5.83614	5.85642	4.25885	4.2885
5	20	5.85217	5.88059	4.28228	4.32397
6	30	5.86713	5.89895	4.3042	4.35102
7	40.01	5.87525	5.90567	4.31612	4.36093
8	50.01	5.88115	5.90886	4.3248	4.36565
9	60.03	5.88299	5.91062	4.3275	4.36825
10	70.04	5.88549	5.9117	4.33118	4.36984
11	80.05	5.89197	5.91241	4.34072	4.37089
12	90.09	5.89578	5.91291	4.34634	4.37163
13	100.14	5.90075	5.91327	4.35367	4.37217
14	110.12	5.90182	5.91355	4.35525	4.37258
15	120.14	5.90667	5.91377	4.36241	4.37291
16	130.17	5.90418	5.91394	4.35873	4.37316
17	140.19	5.90714	5.91408	4.36311	4.37336
18	150.19	5.90883	5.9142	4.3656	4.37354
19	160.13	5.91069	5.91431	4.36835	4.3737
20	170.21	5.91516	5.91439	4.37496	4.37382
21	180.23	5.91621	5.91448	4.37651	4.37396
22	190.24	5.91946	5.91454	4.38132	4.37404
23	200.25	5.92037	5.91461	4.38267	4.37415
24	210.24	5.92235	5.91467	4.3856	4.37424
25	220.25	5.92391	5.91473	4.38791	4.37432
26	230.25	5.92631	5.91477	4.39147	4.37438
27	240.27	5.93169	5.91481	4.39945	4.37444
28	250.21	5.93188	5.91487	4.39973	4.37453
29	260.26	5.9346	5.9149	4.40376	4.37458
30	270.27	5.93801	5.91495	4.40883	4.37465
31	280.27	5.94181	5.915	4.41447	4.37472
32	290.24	5.95272	5.91503	4.4307	4.37477

Complex [L'$Fe^{III}Cu^{II}(^{Me}ImOx)_3$]$(ClO_4)_2$ (11)

MW = 853.70 g/mol, χ_{dia} = -350.0 x 10^{-6} cm^3 mol^{-1}

m = 30.20 mg, H = 1.00 T

No	T(K)	μ_{eff}(exp.)	μ_{cal}(calc.)	χ_m·T(exp.)	χ_m·T(calc.)
1	2	3.74155	3.35621	1.75043	1.40844
2	5.05	4.42697	4.32217	2.4505	2.33585
3	10	4.64143	4.62316	2.69367	2.67251
4	15	4.70867	4.71725	2.77228	2.7824
5	20	4.73788	4.75844	2.80679	2.8312
6	29.98	4.76755	4.79228	2.84205	2.87161
7	40	4.78483	4.80665	2.86269	2.88886
8	50	4.79778	4.81821	2.87821	2.90277
9	60	4.81621	4.83392	2.90036	2.92173
10	70.04	4.84171	4.85697	2.93115	2.94966
11	80.05	4.87675	4.88764	2.97373	2.98703
12	90.12	4.91751	4.92522	3.02365	3.03314
13	100.15	4.96252	4.9676	3.07926	3.08556
14	110.04	5.01024	5.01247	3.13876	3.14156
15	119.98	5.05849	5.05902	3.19951	3.20018
16	130.17	5.10281	5.10698	3.25582	3.26114
17	140.19	5.14968	5.15342	3.3159	3.32072
18	150.19	5.193	5.19835	3.37192	3.37888
19	160.23	5.23785	5.24164	3.43042	3.43539
20	170.23	5.2778	5.28274	3.48295	3.48947
21	180.23	5.31661	5.32165	3.53436	3.54106
22	190.21	5.35239	5.35831	3.58209	3.59002
23	200.25	5.38593	5.39306	3.62713	3.63674
24	210.24	5.41873	5.42554	3.67144	3.68067
25	220.28	5.45001	5.45619	3.71395	3.72238
26	230.27	5.48074	5.48482	3.75595	3.76154
27	240.31	5.50887	5.51183	3.7946	3.79868
28	250.19	5.52936	5.53683	3.82288	3.83322
29	260.31	5.55623	5.56086	3.86013	3.86656
30	270.25	5.57369	5.58307	3.88443	3.89751
31	280.24	5.5919	5.60407	3.90985	3.92689
32	290.32	5.61264	5.62405	3.93891	3.95494

Complex [L'$Cr^{III}Ni^{II}(^{Me}ImOx)_3$]$(ClO_4)_2$ (13)

MW = 852.70 g/mol, χ_{dia} = -425.0 x 10^{-6} cm^3 mol^{-1}

m = 29.54 mg, H = 1.00 T

No	T(K)	μ_{eff}(exp.)	μ_{cal}(calc.)	χ_m·T(exp.)	χ_m·T(calc.)
1	1.93	1.38051	1.52487	0.2383	0.29074
2	4.95	1.79166	1.67672	0.40138	0.35153
3	9.88	2.28905	2.2066	0.65517	0.60882
4	14.99	2.79309	2.74137	0.97546	0.93967
5	20	3.16902	3.14109	1.25572	1.23368
6	29.99	3.64624	3.65128	1.66239	1.66698
7	40	3.92027	3.9397	1.92164	1.94074
8	49.99	4.10044	4.11796	2.10234	2.12034
9	60.05	4.2103	4.23786	2.2165	2.24561
10	70.05	4.29638	4.32262	2.30806	2.33634
11	80.02	4.35991	4.38562	2.37682	2.40493
12	90.09	4.41479	4.43466	2.43703	2.45902
13	100.15	4.45697	4.47358	2.48382	2.50237
14	110.02	4.49251	4.50461	2.52359	2.53721
15	120.16	4.52607	4.53102	2.56144	2.56704
16	130.18	4.54528	4.55294	2.58323	2.59194
17	140.18	4.56556	4.57161	2.60633	2.61324
18	150.21	4.58601	4.58778	2.62973	2.63176
19	160.23	4.60227	4.60184	2.64841	2.64792
20	170.22	4.61826	4.61416	2.66685	2.66211
21	180.24	4.6314	4.62512	2.68204	2.67477
22	190.26	4.6436	4.63489	2.69619	2.68609
23	200.24	4.65449	4.64362	2.70885	2.69622
24	210.18	4.66381	4.65148	2.71971	2.70535
25	220.24	4.67378	4.65868	2.73135	2.71373
26	230.22	4.68108	4.6652	2.73989	2.72133
27	240.27	4.68886	4.67119	2.74901	2.72833
28	250.27	4.69758	4.67667	2.75924	2.73473
29	260.27	4.70295	4.68174	2.76555	2.74066
30	270.25	4.70967	4.6864	2.77346	2.74612
31	280.25	4.71663	4.69073	2.78166	2.7512
32	290.32	4.72397	4.69478	2.79033	2.75595

Complex $[L'Cr^{III}Zn^{II}(^{Me}ImOx)_3](ClO_4)_2$ (14)

MW = 859.00 g/mol, χ_{dia} = -425.0 x 10^{-6} cm^3 mol^{-1}

m = 50.91 mg, H = 1.00 T

No	T(K)	μ_{eff}(exp.)	μ_{cal}(calc.)	χ_m·T(exp.)	χ_m·T(calc.)
1	2	3.53366	3.35898	1.56132	1.41077
2	5.01	3.69684	3.67336	1.70884	1.68721
3	9.9	3.73144	3.7309	1.74098	1.74048
4	15	3.73875	3.74256	1.74781	1.75137
5	20	3.74249	3.74655	1.75131	1.75511
6	30	3.74486	3.7494	1.75353	1.75778
7	40	3.74597	3.75041	1.75457	1.75873
8	50.01	3.7469	3.75087	1.75544	1.75916
9	60.01	3.74833	3.75112	1.75678	1.75939
10	70.1	3.74928	3.75127	1.75767	1.75953
11	80.14	3.7509	3.75137	1.75919	1.75963
12	90.1	3.75991	3.75144	1.76765	1.75969
13	99.98	3.75354	3.75148	1.76166	1.75973
14	110.05	3.7549	3.75152	1.76294	1.75977
15	119.99	3.75633	3.75155	1.76428	1.7598
16	130.18	3.75226	3.75156	1.76046	1.75981
17	140.18	3.75069	3.75159	1.75899	1.75983
18	150.21	3.75161	3.75159	1.75985	1.75983
19	160.23	3.75205	3.75161	1.76027	1.75985
20	170.21	3.75187	3.75161	1.7601	1.75985
21	180.23	3.75331	3.75162	1.76145	1.75986
22	190.26	3.75266	3.75162	1.76084	1.75986
23	200.26	3.75349	3.75163	1.76162	1.75987
24	210.24	3.75213	3.75163	1.76034	1.75987
25	220.27	3.75211	3.75164	1.76032	1.75988
26	230.23	3.75411	3.75164	1.7622	1.75988
27	240.35	3.75527	3.75164	1.76329	1.75988
28	250.29	3.7553	3.75164	1.76332	1.75988
29	260.28	3.75486	3.75164	1.7629	1.75988
30	270.19	3.75339	3.75165	1.76152	1.75989
31	280.28	3.7549	3.75165	1.76294	1.75989
32	290.24	3.756	3.75165	1.76397	1.75989

4. MCD Data

Table S1 Detailed Results for Concurrent Fits to the UV/Vis and MCD Spectra of Fe-Ni, **6**.

	Abs()* (nm)** (Fe/Ni)	MCD (Fe/Ni)	Assignment
1		11890(1085)(841)	$^3A_2 \rightarrow {}^3T_2(^3F)$, Ni
2		13238(1053)(755)	$^3A_2 \rightarrow {}^1E(^1D)$,Ni
3		14347(1312)(697)	
4		15895(1410)(629)	
5	16593(2206)(602)	17093(1203)(585)	
6	18537(2004)(539)	18040(1203)(554)	
7		18869(862)(529)	$^6A_1 \rightarrow {}^4T_1(^4G)$Fe
8		19501(1273)(512)	$^3A_2 \rightarrow {}^3T_1(^3F)$Ni
9	19988(1975)(500)	20335(1205)(491)	
10	21017(2258)(475)	21286(1222)(469)	
11	22246(1999)(449)	22027(1307)(453)	$^3A_2 \rightarrow {}^1T_2(^1D)$Ni
12	23509(1864)(425)	23959(1274)(417)	$^6A_1 \rightarrow {}^4T_2(^4G)$Fe
13	24757(1871)(403)	24546(1132)(407)	
14	25986(1655)(384)	26366(1488)(379)	$^6A_1 \rightarrow {}^4E_2(^4G)$ Fe
15	27185(1700)(367)	27218(1188)(367)	$^6A_1 \rightarrow {}^4A_2(^4G)$ Fe
16	28185(1805)(354)	27888(1111)(358)	
17		28532(1065)(350)	$^3A_2 \rightarrow {}^3T_1(^3P)$Ni
18	29092(1906)(343)	29289(1360)(341)	$^6A_1 \rightarrow {}^4T_2(^4D)$ Fe
19	30021(1820)(333)	30193(1261)(331)	$^6A_1 \rightarrow {}^4E(^4D)$ Fe
20	31142(2171)(321)	31682(1264)(315)	
21	32491(2112)(307) 32505	32551(1306)(307)	
22	33649(2225)(297)	33679(1232)(296)	$^6A_1 \rightarrow {}^4T_1(^4P)$ Fe
23	34896(2286)(286)	34594(1235)(289)	
24		35423(1145)(282)	

Table S2 Detailed Results for Concurrent Fits to the UV/Vis and MCD Spectra of Ga-Ni, **8**.

	Abs(Ga/Ni)	MCD (Ga/Ni)	Assignment
1	10183(2193)(982)		
2	11182(1576)(894)	11445(1349) (873)	$^3A_2 \rightarrow {}^3T_2(^3F)$
3	12320(1260)(811)	12116(1119)(825)	
4	13284(1353)(752)	13180(1142)(758)	$^3A_2 \rightarrow {}^1E(^1D)$
5	14433(1653)(692)		
6	15848(1886)(630)		
7	17359(1941)(576)		
8	18570(1844)(538)	18286(1044)(546)	
9	19624(1927)(509)	19410 (1060)(515)	
10		20033(1007)(499)	$^3A_2 \rightarrow {}^3T_1(^3F)$
11	20773(1889)(481)	20850(1007)(479)	$^3A_2 \rightarrow {}^1T_2(^1D)$
12		27452(10333)(364)	
13		28401(1182)(352), 28546(1177)(350)	$^3A_2 \rightarrow {}^3T_1(^3P)$
14		29299(1094)(341), 29536(1393)(338)	
15	31112(1785)(321)	31023(1066)(322)	
16	32545(1787)(307)	31990(1172)(312), 32852(1021)(304)	
17		33541(982)(298)	
18	34041(2020)293	34827(1210)(287)	
19	35546(2059)(281)	35628(1043)(280)	
20	36958(2058)(270)	37174(968)(269)	
21	38383(2066)(260)	38539(952)(259)	
22	39708(1938)(251)	39383(1274)(253)	
	41083(2309)(243)		

Table S3 Detailed Results for Concurrent Fits to the UV/Vis and MCD Spectra of Fe-Zn, **7**.

	Abs(Fe/Zn)	MCD(Fe/Zn)	Assignment
1	18337(2352)*(545)**	17862(889)*(559)**	$^6A_1 \rightarrow {}^4T_1(^4G)$Fe
2		18892(1000)(529)	
3	19594(2376)(510)		
4		20032(1315)(499)	
5	20672(2227)(483)	21137(973) (473)	
6	22190(2475)(450)	22275(1715) (448)	
7	23499(2086)(425)	23497 (1532)(425)	$^6A_1 \rightarrow {}^4T_2(^4G)$Fe
8	24719(2137)(404)	24556(1628) (407)	
9	25917(1985)(385)	25537(1620) (391)	$^6A_1 \rightarrow {}^4E_2(^4G)$ Fe
10	26943(1952)(371)	26575(1540) (376)	$^6A_1 \rightarrow {}^4A_2(^4G)$ Fe
11	27918(2122)(358)	27973 (1453)(357)	
12	28961(2109)(345)	28858(1335) (346)	$^6A_1 \rightarrow {}^4T_2(^4D)$ Fe
13	30186(2001)(331)	29465(1080) (339)	$^6A_1 \rightarrow {}^4E(^4D)$ Fe
14	31611(2341)(316)	31451(1904) (317)	
15	32850(2261)(304)	32381(1535) (308)	
16	33508(2152)(298)	33284(1404) (300)	$^6A_1 \rightarrow {}^4T_1(^4P)$ Fe
17	34774(1846)(287)	34329(1400)(291)	
18		35438(1489) (282)	
19	35941(1821)(278)		
20		37693(2066)(265)	
21			
		39906(1958)(250)	

*FWHM.
** values in nm.